Transport of nutrients from land to sea

Global modeling approaches and uncertainty analyses

Arthur Beusen

Transport of nutrients from land to sea:
Global modeling approaches
and uncertainty analyses

Transport van nutriënten van land naar zee:
mondiale modelleermethoden
en onzekerheidsanalyses
(met een samenvatting in het Nederlands)

Proefschrift

ter verkrijging van de graad van doctor
aan de Universiteit Utrecht
op gezag van de rector magnificus prof.dr. G.J. van der Zwaan,
ingevolge het besluit van het college voor promoties in het openbaar
te verdedigen op vrijdag 19 september 2014
des middags te 4.15 uur

door

Arthur Hendrikus Wilhelmus Beusen

geboren op 30 september 1965
te Heerlen

PROMOTOREN: prof. dr. A.F. Bouwman

prof. dr. J.J. Middelburg

Things should be as simple as possible, but no simpler.

(Albert Einstein)

aan Anneke, Bram, Sara en Simon

Contents

Chapter 1

Introduction and outline

1.1 General background

In the course of the 20th century, world population has increased by 400% from less than 1.7 billion in 1900 to more than 6.1 billion people in 2000 (Klein Goldewijk et al. 2010). To meet the increasing food demand for the growing population, crop production has increased by 350% and livestock production by 400% (Bouwman et al. 2013d). The dramatic increase in biomass production induced a growing demand for plant nutrients, and fertilizer nutrient use increased from negligible amounts in the beginning of the 20th century to more than 80 million tonnes of nitrogen (N) and 14 million tonnes of phosphorus (P) in 2000.

Phosphorus extraction from phosphate-rich rocks provides most of the P used in fertilizers (Van Vuuren et al. 2010). Nitrogen fertilizers are produced by fixing atmospheric molecular di-nitrogen (N_2) during the Haber-Bosch process (Smil 2001). Nitrogen is also fixed increasingly during fossil fuel combustion and during biological nitrogen fixation by leguminous crops (Galloway et al. 2004). The increasing demand for N and P fertilizers has led to an acceleration and an imbalance of the global nutrient cycles.

The acceleration of global nutrient cycles resulted in increasing nutrient emissions to air (for example, nitrous oxide, nitric oxide and ammonia) and water. Air emissions from agriculture and energy production are primarily re-deposited onto terrestrial ecosystems, but a small fraction reaches coastal and open ocean waters (Duce et al. 2008). Agricultural systems also leak nutrients to water through surface runoff, seepage, leaching and groundwater transport. Apart from emissions from agriculture, households and industries also discharge wastewater containing nutrients directly to surface water; these flows have been increasing rapidly during the 20th century as a result of population growth, urbanization, sewage connection and lagging wastewater treatment (Morée et al. 2013).

Not only have nutrient cycles accelerated, the global hydrological cycle has also changed during the 20th century as a result of climate change, expansion of agricultural land and deforestation (e.g., Vörösmarty et al. 2010). These and

other human activities caused the global water withdrawal to increase by 700% (Ghassemi and White 2007) and reservoir capacity by 600% (from 10 km^3 to 6000 km^3); this affected the magnitude and timing of runoff and river flow and increased the travel time of water in many rivers (Wisser et al. 2010).

These changes in N and P supply to waters and changes in the hydrological cycle have resulted in major changes in nutrient concentrations and transport. Eutrophication represents the ecosystem response to enrichment with nutrients. In aquatic systems, typical consequences of eutrophication include elevated primary production and respiration, and may ultimately lead to algal blooms, algal scum, enhanced benthic algal growth and massive growth of submersed and floating macrophytes (Vollenweider et al. 1992, Turner and Rabalais 1994, Hallegraeff 1993). After the algae die, the decay of organic material depletes the oxygen reserve of the water causing an array of secondary problems such as fish death (Diaz and Rosenberg 2008). Furthermore, the development of toxin-producing algae in marine environments is a threat to human health when accumulating in fish, particularly shellfish (Heisler et al. 2008). Eutrophication thus negatively affects several ecosystem services of rivers, lakes, and estuaries, such as recreation, fishing, hunting and the supply of drinking water.

Before reaching the coastal ocean, sediment, organic carbon (C) and nutrients from land transit through the continuum formed by soils, groundwater, riparian zones, floodplains, rivers, lakes and reservoirs. Biogeochemical processes in the aquatic continuum cause nutrient retention and thus reduce the absolute amount of nutrients reaching the ocean; in addition, these processes modify the ratio in which C, N, P and silicon (Si) are transferred, and the chemical form of each of these elements (Billen et al. 1991, Ensign and Doyle 2006, Reddy et al. 1999). For example, in aquatic ecosystems, Si retention is enhanced by increasing N and P inputs (Conley 2002). Because river networks link terrestrial landscapes to lakes and oceans, perturbations to river ecosystems can have large consequences for biogeochemical cycling at local, regional, and global scales.

Nutrient concentration data provide a measure of the eutrophication status of surface waters. Often, nutrient concentrations are determined for different nutrient forms (dissolved, inorganic and particulate). An important issue when interpreting measurement data is their representativeness, both in space and time. Whether or not a measurement or a series of measurements represents the nutrient regime in a river adequately does not only depend on the quality of the nutrient concentration measurement, but also on ancillary information necessary to estimate the load, such as location, discharge, water depth, day and time of the measurement, and number and frequency of sampling. For example, a large part of sediment transport may not be observed during monthly monitoring, because sediment transport often occurs during a few high discharge or flooding events.

Monitoring the nutrient status of a river allows for analyzing the variability, but long-term observations are not available for many rivers world-wide. Nutrient concentration data often cover a limited time period (year or less), and do not provide information on (i) the sources of the nutrients; (ii) the changes that have occurred as a result of major alterations in hydrology and nutrient delivery to

streams and rivers.

A common way to analyze and interpret river nutrient concentrations is by using models in which the real-world processes are represented in a simplified way. A range of models is available, each with its own purpose and spatial and temporal resolution. This thesis describes the development of different modeling approaches for assessing river nutrient transport and biogeochemistry. The objective is to improve our understanding of the interplay of changing nutrient sources, climate and hydrology as influenced by human activities and interventions, and biogeochemical processes along the land-river continuum; with a focus on uncertainties. Better knowledge on the processes is useful when developing strategies to reduce the negative effects of eutrophication.

1.2   Context: the Integrated Model to Assess the Global Environment (IMAGE)

The models that will be discussed in this thesis, are part of the Integrated Model to Assess the Global Environment (IMAGE). IMAGE has been developed since the mid 1980s at the National Institute for Public Health and the Environment (RIVM), and at the Netherlands Environmental Assessment Agency (Milieu en Natuur Planbureau, MNP, and Planbureau voor de Leefomgeving, PBL, at present) (Bouwman et al. 2006). IMAGE is an integrated assessment model, which is structured around the chain of key global sustainability problems (see Figure 1.1). Similar to other integrated assessment models, it contains two main subcomponents: i.e., 1) the human system, describing the long-term development of human activities relevant for sustainable development issues, and 2) the earth system, describing changes in the natural environment. The two systems are coupled in two directions: via the impact of human activities on the environmental system, and via the impacts of environmental change back on the human system.

Integrated assessment models, such as IMAGE, have established themselves as powerful tools to study future development of complex, large-scale environmental and sustainable development issues. There are at least two key reasons for this: 1) many of these issues are strongly interlinked and integrated models can capture important consequences of these linkages; and 2) substantial inertia is an inherent property of these problems, which can only be captured using long-term scenarios.

IMAGE has been set-up as an integrated assessment framework, i.e., some of the components are hard coupled, but others are connected through soft links (i.e., the models run independently with data exchange via data files). This architecture provides more flexibility to develop components separately and to perform sensitivity analyses, recognizing that feedbacks might not always be strong enough to warrant full integration.

The various submodels of the earth system module are fully coupled. Components of the human system such as the TIMER energy model, however, can also be run independently. The agro-economic models that are used as input for IMAGE do not form an official model component—but can still exchange infor-

mation on land supply, actual production levels and intensity. It should be noted that in addition to the core IMAGE 3.0 model, a larger IMAGE integrated assessment framework has been defined. The latter includes several PBL impact models that are soft-linked to the IMAGE model, such as the FAIR model (climate policy), GLOBIO (biodiversity), GLOFRIS (flood risks) and GISMO (human development).

The two main subsystems (human system and earth system) of the core model are specified in accordance with the key dynamics and diversity of the systems. The geographical resolution of IMAGE 3.0 is 26 socio-economic regions. These regions are selected given their relevance for global environmental problems and a relatively high degree of coherence within these regions. In the earth system, the key geographic scale is a $0.5° \times 0.5°$ (30×30 minutes) grid for plant growth, carbon and water cycles, while land-use is now allocated at a finer grid of 5×5 minutes.

In terms of temporal scale, both systems are run at annual time steps over the 1971–2100 period, focusing on long-term trends to capture important inertia aspects of global environmental problems. Within the earth system, much shorter time steps (for water, crop and vegetation modeling), but also five-year time steps (for slow processes such as climate change) are used. For many applications, the model is run up to 2050, depending on the questions. The IMAGE model deliberately also runs over the historical period 1971–2005 in order to test model dynamics against key historical trends.

Key inputs for the model are projections describing direct and indirect drivers of global environmental change. Most of these drivers (such as technology and lifestyle assumptions) are used as input in various subcomponents of IMAGE (Figure 1.1). Clearly, the exogenous assumptions made on these factors need to be consistent. To ensure this, so-called storylines are used, brief stories about how the future may unfold, that can be used to derive internally consistent assumptions for main driving forces. Important categories of scenario drivers include demographic factors, economic development, lifestyle, and technology change. Among these, population and economic development form a special category as they can be dealt with in quantitative sense as exogenous model drivers. Other drivers mostly concern assumptions in different subcomponents of IMAGE, for example both the yield assumptions in the crop growth model and the performance of solar power production in the energy model depend on a more generic description of the rate of technology change.

The IMAGE-Global Nutrient Model describes the fate of nitrogen (N) and phosphorus (P) emerging from concentrated point sources such as human settlements, and from dispersed or non-point sources such as agricultural and natural land. Through rivers and lakes, the nutrient surplus eventually enters coastal water bodies. Key drivers that determine the nutrient emissions from concentrated and point sources include the agricultural production with its fertilizer application, urban and rural population by sanitation system and level of wastewater treatment. For example, the model calculates the annual surface nitrogen balance from inputs such as biological nitrogen fixation, atmospheric nitrogen deposition and
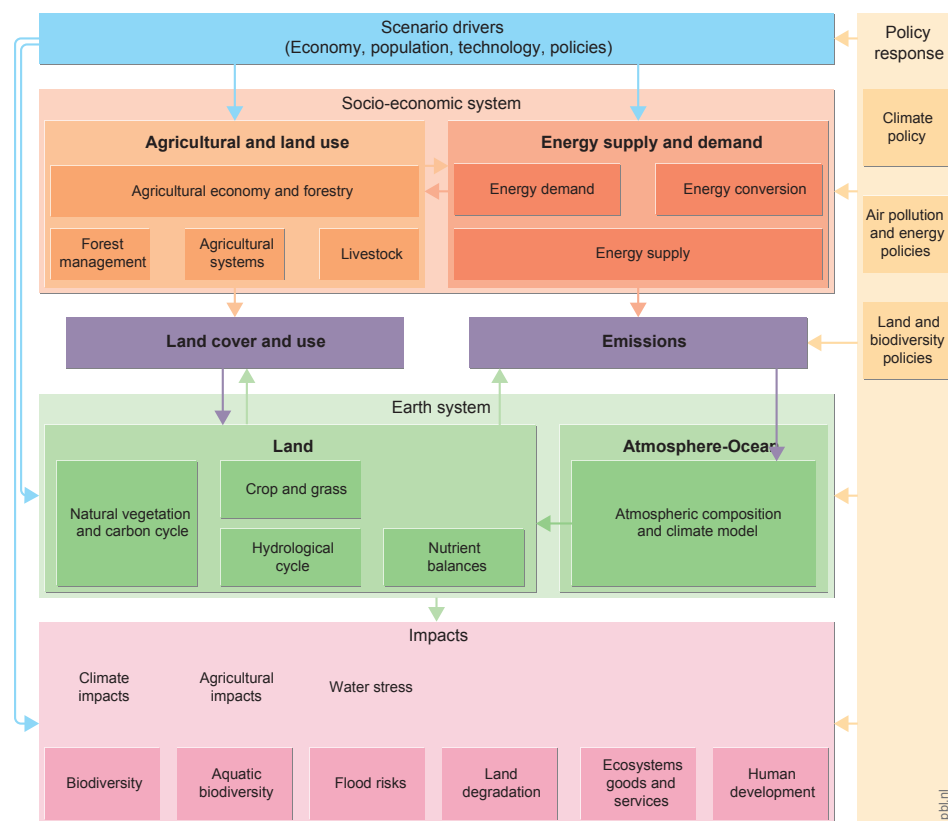
Figure 1.1: Schematic overview of the IMAGE 3.0 framework from Stehfest et al. (2014).

the application of synthetic nitrogen fertilizer and animal manure, and outputs such as nitrogen removal from the field by crop harvesting, hay and grass-cutting and grazing. The outflow of nutrients from the soil in combination with emissions from point sources and direct atmospheric deposition also determine the loading of nutrients to the surface water and its fate during transport via surface runoff, and transport in groundwater, riparian zones, lakes and reservoirs, and in-stream biogeochemical retention processes.

IMAGE 3.0 Global Nutrient Model includes three submodels:

The Wastewater model which generates nutrient flows in wastewater discharges; results of this model are included in the calculations presented in Chapter 5.

The Soil nutrient budget model describing all input and output of N and P in soil compartments (Figure 1.2); Chapter 3 presents the uncertainty analysis of this model.

The Nutrient environmental fate model which describes the fate of soil nutrient surpluses and wastewater nutrients in the aquatic environment (Figure 1.2), as discussed in Chapters 4 and 5.

The dissolved silica (DSi) model presented in Chapter 2 is part of the development of IMAGE-Global Nutrient Model, and aspects of it will be incorporated in the IMAGE 3.0 Global Nutrient Model in the near future.

1.3   Available model approaches

When modeling the transfer of nutrients from land to rivers, and nutrient transport by rivers to coastal seas, two fundamentally different modeling approaches exist (Bouwman et al. 2013c). The first model category uses lumped approaches, which combine all processes between the soil and the river mouth in a few parameters in simple, mostly statistical models. The second model category use distributed approaches, where the processes of nutrient delivery are described separately for all the landscape components, such as land surface, soil, groundwater, riparian zones, wetlands, streams and rivers and man-made reservoirs.

In lumped approaches, all processes between the soil and the river mouth are combined in a few parameters in simple, empirical models. Generally, lumped approaches assume limited a priori knowledge of biogeochemical processes, but provide empirical estimates of the aggregate supply and loss of nutrients through the use of conventional stream monitoring data, which are often readily available in large watersheds with mixed land use. Early examples include regressions of N export from large watersheds on population density (Peierls et al. 1991), net anthropogenic sources (Howarth et al. 1996), atmospheric deposition, and measures of per capita energy consumption by humans (Meybeck 1982). More recent examples are the Global Nutrient Export from WaterSheds (NEWS) models (Seitzinger et al. 2005, 2010, Mayorga et al. 2010). These models were developed in the framework of the Global NEWS project of United Nations Educational, Scientific and Cultural Organization (UNESCO)-Intergovernmental Oceanographic Committee
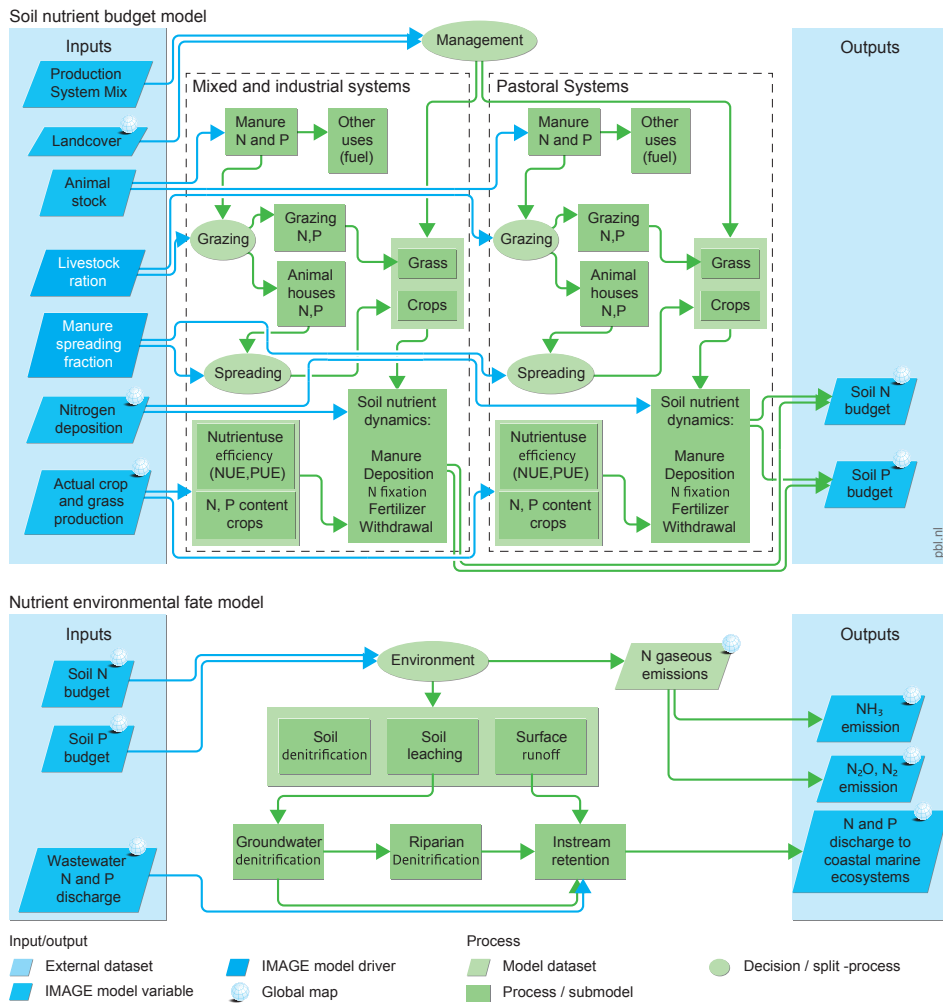
Figure 1.2: Schematic overview of the IMAGE-Global Nutrient Model adapted from Stehfest et al. (2014).

(IOC). Since most of the major rivers of the world cross at least one international border, eutrophication is a transboundary problem. International organizations like UNESCO, other UN organizations and OECD are interested in models that can be used to identify hot-spot regions across the world with problems of coastal eutrophication or where nutrient loads are rapidly increasing.

Global NEWS includes a group of regression models on a river-basin scale that can be used to explain historical river export and changes therein of dissolved and particulate nutrients, and to analyze scenarios to simulate future changes of these river loads. The Global NEWS system includes river-basin-scale models for predicting export at river mouths to the coastal zone of dissolved inorganic nitrogen and phosphorus (DIN, DIP), dissolved organic carbon, nitrogen and phosphorus (DOC, DON, DOP), total suspended solids (TSS), particulate organic carbon (POC), particulate nitrogen and phosphorus (PN and PP), and dissolved silica (DSi). The NEWS DSi model (Beusen et al. 2009) is one of the examples presented in this thesis.

Most distributed models are actually hybrid, i.e., they use a mixture of both modeling approaches. Part of the transfer of nutrients is lumped and other transfers are distributed. A recently developed hybrid approach (SPARROW; SPAtially Referenced Regression On Watershed attributes) (Smith et al. 1997) expands on conventional regression methods by using a mechanistic model structure in correlating measured nitrogen flux in streams with spatial data on nitrogen sources, landscape characteristics (e.g., soil permeability, temperature), and stream properties (e.g., discharge, travel time of water). The model, which separately estimates the quantities of nitrogen delivered to streams and the outlets of watersheds from point and diffuse sources, has been applied nationally in the United States (Smith et al. 1997) with separate studies of nitrogen flux in the Chesapeake Bay watershed (Preston and Brakebill 1999), the Mississippi River and its tributaries (Alexander et al. 2000, 2008), the watersheds of major U.S. estuaries (Alexander et al. 2001), and watersheds of New Zealand (McBride et al. 2000). By spatially referencing nitrogen sources and watershed attributes to surface water flow paths, defined according to a digital drainage network, and imposing mass-balance constraints, the model has been shown to improve the accuracy of predictions of stream export and the interpretability of model coefficients (Smith et al. 1997, Alexander et al. 2000, 2001).

In distributed approaches, components of landscapes in river basins are simulated separately with various nutrient transport pathways (atmospheric deposition, soil leaching, groundwater transport, riparian zones, and surface runoff, and direct discharge of waste water from human activities). Each pathway requires a different approach. The water flow, together with dissolved or particulate nutrients is modeled explicitly as a medium for transport and biogeochemical processing. The Riverstrahler model is an example of a distributed approach of a river systems model. It was first developed to study the Seine river basin (Billen and Garnier 2000), and later it was also applied to study other European (Mosel, Scheldt, Danube) and tropical rivers (Red river) (Garnier et al. 2000, Billen et al. 2005, Garnier et al. 2002, Quynh et al. 2005). Riverstrahler describes the nutrient in-

puts and the biological, microbiological and physical-chemical processes within segments of river systems.

1.4   This thesis: from lumped to distributed modeling of river nutrient transport

This thesis discusses examples of global models and focuses on approaches to analyze model sensitivity and uncertainty. The four examples presented are models developed to analyze either sources and transport of nutrients in rivers, or the biogeochemistry in the land-river continuum.

1.4.1   Lumped model for river dissolved silica export

The first example, presented in Chapter 2 is a lumped model, which was developed in the framework of the Global NEWS to calculate global DSi river export, with a strong focus on the uncertainty. DSi is, along with N and P, required for diatom growth. Diatoms are one of the most common phytoplankton types and are responsible for about half of the primary production in the world's oceans (Treguer and Pondaven 2000). The change in nutrient ratios ($N:Si$, $N:P$) in river discharge leads to the modification of phytoplankton species composition (Humborg et al. 2000, Conley et al. 1993) and changing DSi export to the sea will have an impact on aquatic food webs in coastal marine environments (Ittekot et al. 2006). To understand the role of DSi, N and P in coastal eutrophication, it is important to improve the quantification of DSi export to the coastal zone.

The NEWS DSi model is appropriate to estimate the nutrient river export at the mouth of the river. The parameters, which drive the models, are lumped on a river basin scale and are homogeneously distributed in space. The regression coefficients are global and constant in time and based on the year 2000. All processes which influence the river export at the river mouth are described by one or more regression coefficients. In contrast with most N and P export models, the NEWS DSi has no anthropogenic sources. DSi export to the ocean is influenced by large-scale alterations on land, such as river damming and climate change. Statistical approaches were used to identify the main drivers for river export of DSi with this lumped model. These drivers are fairly constant in time (except for precipitation).

The lumped regression models of the Global NEWS family were developed on the basis of river concentration and discharge data stemming from the mid-1990s or before. These models use both parameters describing natural processes (such as the DSi model) and anthropogenic factors. Examples include the NEWS model for estimating global river transport of sediments and associated particulate C, N, and P (Beusen et al. 2005) and using the fraction of wetland rice area in a river basin and the NEWS model for estimating river export of dissolved inorganic nitrogen (DIN) (Dumont et al. 2005), which uses fertilizer use as an input parameter.

In contrast to complex deterministic models, the lumped statistical methods have the advantage of being readily applied in large watersheds, and have been very useful as a first step towards identification of the sources of nutrient delivery to streams and rivers and their relative importance, and identifying regions where river nutrient export is high, or increasing rapidly. A number of important questions arise when applying these statistical models, particularly related to the validity of the regressions in situations with conditions differing from those prevailing in the period for which nutrient concentration measurements were used. Conditions may vary due to changes in agricultural production systems (fertilizer use was much less 50 years ago than today), nutrient delivery from new sources (e.g., aquaculture was a negligible source in 1950, contrary to its contemporary impact (Bouwman et al. 2013b, 2011b)), and climate change. A further reason why regression approaches may not be appropriate is that the behavior of processes may change in time. For example, the in-stream retention for N depends on the N concentration in the water column, and temperature. Furthermore, the simple regression models are limited in that they consider sources and sinks to be homogeneously distributed in space, do not separate terrestrial from in-stream retention processes, and rarely account for nonlinear interactions between sources and loss processes.

1.4.2   Distributed, spatially explicit models

Given these limitations of lumped regression models, I initiated a step-by-step development to arrive at a globally distributed, spatially explicit model, including model components for describing the soil nutrient budgets in natural ecosystems and agriculture, the transport and retention processes in different landscape components, and finally the transport and retention processes in streams and rivers.

Soil nutrient budget

The first step, which is the second example presented in Chapter 3, simulates the distribution of animal manure and fertilizer, as well as ammonia volatilization as one of the major components of soil N budgets. Soil nutrient budgets form the input to the distributed models presented in Chapters 4 and 5. The model presented in Chapter 3 is a distributed and spatially explicit model, which calculates the emissions of ammonia (NH_3) from global livestock production systems. The focus is the uncertainty of the simulated NH_3 emission and to the sensitivity in the drivers of NH_3 volatilization.

Nutrient delivery to streams and rivers

The third example is a distributed model for simulating the delivery of N to streams and rivers (see Figure 1.2). Chapter 4 addresses the possible change of terrestrial denitrification and nitrous oxide (N_2O) emissions from soils, groundwater and riparian zones under past and future climate change, increasing food and energy

production and agricultural intensification, using a simulation model. Like the previous chapters, there is a strong focus on the model sensitivity.

In-stream nutrient biogeochemistry

The last example in Chapter 5 presents the development of a model for describing both the N and P delivery to streams and rivers, but also the in-stream biogeochemical retention processes using the spiraling concept applied in a spatially explicit manner (see Figure 1.2). The spiraling concept (Stream Solute Workshop 1990) considers the spiral length, which consists of two parts: the uptake length, which is the distance travelled in dissolved form, and the turnover length, which is the distance traveled within the benthic compartment. Usually, uptake length is much longer than turnover length. Uptake length is generally evaluated empirically at the reach scale, with nutrient enrichment experiments, following nutrient decay downstream from a point-source, or with transport-based analysis (Ensign and Doyle 2006,various references in). Since the travel time of water and nutrients therein is essential to the spiraling concept, a coupling between the hydrological model PCR-GLOBWB (Van Beek et al. 2011) with an extended version of the nutrient delivery model described in Chapter 4 was performed. To address the uncertainties, this chapter includes an extensive sensitivity analysis, with a comparison of different time periods in the twentieth century.

Finally, this thesis concludes with a summary of the findings and suggestions for future research.

Chapter 2

Global patterns of dissolved silica export to the coastal zone: Results from a spatially explicit global model

A.H.W. Beusen, A.F. Bouwman, H.H. Dürr, A.L.M. Dekkers, and J. Hartmann, 2009.

Abstract

We present a multiple linear regression model developed for describing global river export of dissolved SiO_2 (DSi) to coastal zones. The model, with river-basin spatial scale and an annual temporal scale, is based on four variables with a significant influence on DSi yields (soil bulk density, precipitation, slope and area with volcanic lithology), for the pre-dam situation. Cross validation showed that the model is robust with respect to the selected model variables and coefficients. The calculated global river export of DSi is 380 Tg yr^{-1} (340–427 Tg yr^{-1}). Most of the DSi is exported by global rivers to the coastal zone of the Atlantic Ocean (41%), Pacific Ocean (36%) and Indian Ocean (14%). South America and Asia are the largest contributors (25% and 23%, respectively). DSi retention in reservoirs in global river basins may amount to 18–19%.

2.1   Introduction

Silicon (Si) clearly shows the link between rock and life. Silicon dioxide (SiO_2) or silica is the most abundant component of the earth's crust. It occurs as silicate minerals in igneous, metamorphic and sedimentary rocks. These minerals undergo physical and chemical weathering, which is the major natural source of dissolved silica (dissolved SiO_2, hereafter referred to as DSi) in aquatic ecosystems (Berner and Berner 1996). On its way through soils, aquifers, and riparian zones Si exerts control over the cycling and fate of carbon (C), nitrogen (N), phosphorus (P) and other nutrients (Ittekot et al. 2006).

Terrestrial plants take up a significant portion of the DSi produced during weathering (Bartoli 1983, Sommer et al. 2006). Amorphous silica (ASi) in phytoliths in many plants and soils is an important Si reservoir and may have an impact on the Si transfer from the terrestrial to the aquatic biosphere, due to its high dissolution rates compared to other particulate silica compartments in sediment fluxes (Bartoli 1983, Conley 1997, Van Cappellen 2003). ASi is produced and recycled on the land before its eventual transfer to the coastal areas through rivers. ASi may therefore make up an important contribution to total river Si loads (Conley 2002, Derry et al. 2005, Kurtz and Derry 2004).

Diatoms are the essential phytoplankton group that need Si as a major nutrient (Conley 2002). Marine diatoms in particular are often limited by Si (Kristiansen and Hoell 2002), while diatoms in river systems experience Si limitation occasionally, for example under high anthropogenic inputs of N and P (Billen and Garnier 2007). The Si for diatoms in coastal waters is delivered from rivers, from recycling within the water column at the sediment-water interface and from atmospheric deposition. The role of oceans in the global C cycle is coupled with the global Si cycle because diatoms comprise 50% of the biomass of today's ocean with a large contribution to C burial (Treguer and Pondaven 2000).

The silicate weathering process (desilication) consumes carbon dioxide (CO_2) (Gaillardet et al. 1999) and produces alkalinity. At the global scale, the magnitude of desilication is believed to depend primarily on lithology, runoff and erosion; weathering rates only showed a reasonable correlation with average temperature when large tropical rivers with abnormally low weathering rates were excluded (Gaillardet et al. 1999). Because of their geological and climatic settings, tropical river basins play a major role in chemical weathering and transfer of DSi and alkalinity to rivers and oceans (Jennerjahn et al. 2006). Because global warming is believed to be especially pronounced at high latitudes in the Northern hemisphere, a change in structure and cover of vegetation could rapidly alter the biogeochemistry of river systems and land-ocean interactions along the coasts of the Arctic Ocean (Humborg et al. 2006).

While riverine N loads have increased during the past decades (Bouwman et al. 2005b) and similar changes have occurred for P (Smith et al. 2003), Si loads have remained constant or even decreased in many rivers primarily as a result of Si retention in reservoirs and lakes through eutrophication and increased diatom productivity (Conley 2002, Ittekot et al. 2006). Settling diatom frustules accumu-

late rapidly in bottom sediments, because their specific gravity is far greater than that of nonsiliceous algae (Reynolds 1984). This has often altered the stoichiometric balance of N, P and Si (Rabalais 2002) which may not only affect the total production in freshwater and coastal marine systems, but also its quality. When diatom growth is compromised by Si limitation, non-diatoms may be competitively favored, with dominance of flagellated algae including noxious bloom-forming communities (Turner et al. 2003). Thus the biogeochemical cycling of C, N and P and food web dynamics leading to fisheries harvests are affected by shifts in the availability of Si (Billen and Garnier 2007, Ragueneau et al. 2006).

In this paper we describe, evaluate and apply a new model for predicting current global river loads of DSi to the world's coastal zones. This model was developed as part of an international interdisciplinary effort to model river export of multiple bioactive elements (C, N, P, and Si) and elemental forms (dissolved/particulate, inorganic/organic) called Global Nutrient Export from Watersheds (Global NEWS). We hereafter refer to our model as "NEWS-DSi".

A number of attempts have been made to estimate the current riverine DSi export to coastal zones. Many used simple extrapolation schemes based on data mostly from large rivers. For example, Clarke (1924) and Livingstone (1963) used data for a few large temperate rivers. Meybeck (1979) used a biome typology and included data for 60 rivers. Treguer et al. (1995) estimated a global river export of 0.34 Pg yr^{-1} of dissolved SiO_2 using data from Meybeck and Ragu (1995). Lacking a global representative data set for ASi river export, our study focuses on DSi.

Apart from current DSi loads in rivers, it is important to know how and where these loads will change in the future under changing land use, dam construction and climate change. Statistical methods using multiple regression are useful for analyzing the relationships between river nutrient export and controlling factors, and have been successfully applied to estimate river export of the various compounds of C, N and P (Seitzinger et al. 2005).

NEWS-DSi is also based on a regression approach to analyze a large data set of DSi measurements representing the pre-dam situation. The aim of this work is to analyze the controls of DSi. Because NEWS-DSi was developed as part of a larger system of models with consistent input data sets and formulation, its output can be directly compared with output from other NEWS models (Seitzinger et al. 2005). NEWS-DSi also represents the first spatially explicit, global estimate of river DSi export to the oceans with an uncertainty range, based on a statistical, lumped river-basin scale model.

2.2 Data and methods

2.2.1 River DSi loads and ancillary data

We used data on DSi load or concentration measured at or close to the river mouth. DSi annual load data were converted to annual DSi yield (DSiY, in ton SiO_2

$km^{-2} yr^{-1}$) using the basin area estimates from Fekete et al. (2002). The data set includes DSiY data for 208 rivers representing the "pre-dam", natural or pristine situation (Figure 2.1 and SI S2.1). The DSiY data cover the period between the 1920s and 1990s. Hence, instead of a fixed base-year, the criterion of selection was the absence of dams and reservoirs or human impact. The DSiY data are generally multi-year averages from (1) Meybeck and Ragu (1995) (selecting the "pre-dam" situation), (2) data on pristine rivers with data from numerous reports on river chemistry prior 1950/60, i.e., before the main development of large reservoirs in world rivers (Vörösmarty et al. 1997), and (3) recent analyses in regions with limited human impacts like Alaska and Canada, Amazon and Orinoco basins, Patagonia, and West and South Africa. References and more details on the data selection are in Dürr et al. (2009).

There are some uncertainties associated with the DSi data. The main sources of uncertainty are inconsistent measurement techniques and insufficient sampling frequency. Considerable bias may be caused by variation in the hydrology, concentration-discharge relationships and sampling frequency (Stelzer and Likens 2006). Regarding the computation of the annual DSi load, Meybeck and Ragu (1995) note that the various reports used are not always clear about how average annual values were obtained. It is therefore not possible to provide accurate uncertainty estimates for our data, but in general best available discharge-weighted data were used and the Meybeck and Ragu (1995) database is currently still the most frequently used data set at global scale Moatar and Meybeck (2007) estimated the uncertainty induced by the frequency of regular river measuring campaigns to result in errors around 10% for major ions, expressed by the electrical conductivity.

Table 2.1: River-basin characteristics included in the regression analysis

	Dimension	Reference
A. General		
River basin id	-	Vörösmarty and Fekete (2000), Fekete et al. (2002)
DSi export	10^6g SiO_2 yr^{-1} km^{-2}	Meybeck and Ragu (1995) as summarized in Dürr et al. (2009)
Area covered by ice	%	FAO (1991)
Area covered by glaciers/land ice	%	FAO (1991)
Area covered by lakes, wetlands	%	Lehner and Döll (2004)
River basin area[a]	km^2	Fekete et al. (2002)
Maximum elevation within river basin	m	National Geophysical Data Center (2002)
B. Climate		
Dominant climate grouping based on Agro-Ecological Zones	Climate group	De Pauw et al. (1996)
Dominant climate grouping based on Holdridge classification	Climate group	Leemans (1989), Leemans (1990)
Mean annual temperature and square of temperature[b]	°C	New et al. (1999)

(Continued on next page . . .)

Table 2.1: (Continued)

	Dimension	Reference
Annual runoff[b]	mm	Fekete et al. (2002)
Fournier runoff based on river-basin discharge[b]	mm	Fekete et al. (2002)
Fournier runoff based on grid runoff[b]	mm	Fekete et al. (2002)
Annual mean precipitation and natural logarithm	mm day^{-1}	Fekete et al. (2002)
Fournier precipitation[b]	mm day^{-1}	Fekete et al. (2002)

C. Land use

	Dimension	Reference
Area of natural ecosystems, arable land and grassland in extensive and intensive systems, area of marginal and semi-natural grassland, total grassland, wetland rice, arable land excluding wetland rice	%	Bouwman et al. (2006)
Area of irrigated land	%	Siebert and Döll (2001)

D. Parent material

	Dimension	Reference
Dominant lithology[c]	-	Amiotte Suchet et al. (2003)
Lithology[d]	-	Dürr et al. (2005)
Mechanical erodibility index of parent material[e]	-	Amiotte Suchet et al. (2003)

E. Soil conditions

	Dimension	Reference
River-basin average soil content of silt, sand, clay and soil organic carbon	%	Batjes (1997, 2002)
River-basin average soil water holding capacity	mm	Batjes (1997, 2002)
Fraction of river-basin area with texture class (very fine, fine, medium, coarse, organic)	Fraction	Batjes (1997, 2002)
River-basin average topsoil bulk density	10^6g m^{-3}	Batjes (1997, 2002)

F. Relief

	Dimension	Reference
Average slope based on 5 by 5 minutes digital elevation map (DEM)[f]	m km^{-1}	National Geophysical Data Center (2002)
Average slope (based on FAO)[f]	m km^{-1}	FAO (1991)
Average slope (based on Global Agro-Ecological Zones)[g]	m km^{-1}	FAO/IIASA (2000a)
Maximum slope (based on FAO)	m km^{-1}	FAO (1991)

(Continued on next page ...)

Table 2.1: (Continued)

	Dimension	Reference
Fournier slope based on DEM[h]	m km^{-1}	National Geophysical Data Center (2002)

For model development and extrapolation, we used ancillary information at the river basin scale, such as river basin area, climate, elevation, lithology, soil properties and relief (Table 2.1). We also included data from different sources representing the same variable (see for example, relief and climate-related variables). Due to lack of reliable maps for land use for the first part and middle part of the 20th century, we included data on current land use, assuming that the broad patterns of regional agricultural areas including large areas suitable for irrigation

---

[a]79 river basins from Fekete et al. (2002) had to be excluded because of conflicts with our delineation of land areas, and 5342 river basins representing 89% of the global land area were included in our analysis.

[b]For mean annual precipitation we assumed a minimum value of 0.01 mm day^{-1} for three river basins with less rainfall. We excluded all river basins with annual runoff less than 3 mm yr^{-1} (660 rivers out of 6292) and glaciated river basins (211). The "Fournier" expression of precipitation and runoff is calculated as the sum of the square values for all months divided by the annual sum. These expressions provide a representation of the variability within a year (seasonal variation).

[c]Classes for lithology include 1, sand/sandstone; 2, carbonate rock; 3, shales; 4, plutonic/metamorphic; 5, gabbros; 6, acid volcanic rock; 7, basalt; 8, ice. Ice and gabbros do not occur in the data set of 124 river basins.

[d]Classes according to Dürr et al. (2005) (1 = Major Water bodies, 2 = Ice + Glaciers, 3 = Plutonic basic, 4 = Plutonic acid, 5 = Volcanic basic, 6 = Volcanic acid, 7 = Precambrian Basement, 8 = Metamorphic Rocks, 9 = Complex lithology, 10 = Siliciclastic consolidated sedimentary, 11 = Mixed consolidated sedimentary, 12 = Carbonated consolidated sedimentary, 13 = Evaporites, 14 = Semi- to unconsolidated sedimentary, 15 = Alluvial deposits, 16 = Loess, 17 = Dunes and shifting sand) were regrouped as follows: 1 = Water and ice (classes 1 and 2); 2 = Plutonic & metamorphic rocks (classes 3, 4, 7, and 8), 3 = Volcanic (classes 5 and 6 and 50% of class 9); 4 = Siliciclastic sediment (classes 10 and 50% of class 9); 5 = Carbonated Sediment (classes 11 and 12); 6 = unconsolidated sediments (classes 14 and 15); 7 = Quarternary sediments (classes 13, 16, and 17); 8 = all no data classes.

[e]Mechanical erodibility ranges from 1 to 40 with 1, plutonic and metamorphic rocks; 2, volcanic rocks; 4, consolidated sedimentary rocks; 10, different rock types in folded zones; 32, nonconsolidated sedimentary rocks; 40, recent alluvial.

[f]In the DEM there are 36 cells with 5 by 5 minute resolution within one cell of 0.5 degree, our working resolution. The slope is the absolute height difference between two midpoints of 5 by 5 minute cells in the latitudinal direction divided by the arclength. The same is done for the longitudinal direction. Slopes are calculated for land cells only. Average slope is sum of all values divided by the number of values (normally 72 if all 5 by 5 minute grid cells are land).

[g]The fractional distribution within each 0.5 degree grid cell of the classes in the Global Agroecological Zones (GAEZ) map (1 = 0–2%, 2 = 2–5%, 3 = 5–8%, 4 = 8–16%, 5 = 16–30%, 6 = 30–45%, 7 = > 45%) were recalculated to a mean slope: 1% (class 1), 3.5% (class 2), 6.5% (class 3), 12% (class 4), 23% (class 5), 37.5% (class 6) and 50% (class 7).

[h]The Fournier slope for each 0.5 by 0.5 degree grid cell is calculated as the sum of the squares of the average slope of each 5 by 5 minute resolution grid cell in each direction divided by the number of values (72 or less).
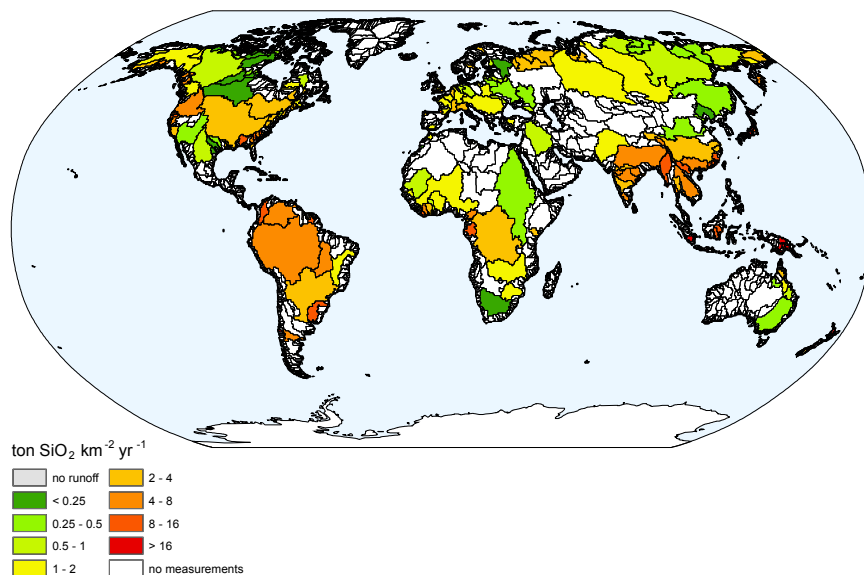
Figure 2.1: Coverage of river basins with DSiY data (ton SiO_2 $km^{-2}yr^{-1}$) used in this study. Together these river basins cover 68 Mkm^2 which is about 58% of the global land area.

have been similar during the period covered by the DSi load measurements. The error caused by this assumption on the global scale is limited, because the global agricultural area has increased by only 11% between 1960 and 2000 (FAO 2008). In addition, the DSi data for river DSi export cover a long period ($\approx$ 1920–1990), so there is not one single year for land cover that matches all observations. Furthermore, we included current climate data, assuming that the recent changes in climate are insignificant compared to recent anthropogenic modifications of the hydrologic cycle such as dam construction (Vörösmarty et al. 2000). We recognize that in specific regions where rapid land use or climate changes have occurred, there may be a mismatch between the period represented by the DSi measurements and the land use, climate and hydrological data.

We made plots of the various variables and the DSiY to inspect if other relationships yield a better fit with the data than linear ones. We thus added ln(precipitation) and temperature[2] as variables to include in the regression analysis.

2.2.2   Multiple regression of DSiY

We assessed the influence of a range of independent variables listed in Table 2.1, without a priori selection. The influence of these variables on DSiY was analyzed with S-PLUS (Insightful 2005) in three steps to develop and validate a statistical

model: (1) Stepwise regression and identification of outliers to select the important variables which explain the variance in the behavior of TDSiY and obtain the best linear regression model based on the full dataset; (2) Cross-validation of the model using randomly selected subsets of the data containing 75% of the rivers in the full dataset, to analyze the robustness and the uncertainty of the model predictions; (3) Testing and validation of the fitted regression model and Monte Carlo simulation to obtain the distribution and confidence interval of the model coefficients. Steps (1) to (3) are based on the dataset of rivers with measurements. The three steps will be elaborated below (Sections 2.2.3–2.2.5).

2.2.3   Stepwise regression

Multiple linear regression requires the observations to be normally distributed. We used the Box-Cox procedure (Box and Cox 1964) for transforming the DSiY data into a normal shape using an appropriate exponential lambda (λ) according to:

$$\text{TDSiY} \;=\; \frac{(\text{DSiY}^{\lambda} - 1)}{\lambda} \tag{2.1}$$

The relevant independent variables for the multiple regression were selected with the S-PLUS function "step". This function uses forward selection. In forward selection the model is either acceptable or otherwise the most significant variable that is not yet included in the model, is added. The best model in the function step is that with the lowest Akaike's Information Criterion (AIC), which is the log-likelihood of the model plus a penalty for the number of variables included (Akaike 1974). This penalty is used to include only those variables in the model for which the likelihood decreases sufficiently to gain accuracy.

After each run we checked for the presence of outliers. Potential outliers were identified on the basis of a combination of (1) the highest Cook's distance (Cook 1977) of all rivers, and (2) the distribution of the residuals; that is, if the regression model is adequate, the residuals are normally distributed. When the residuals are plotted against the quantiles of a standard normal distribution, the residuals should be on a straight line. Outliers are visible by their large deviation from the straight line. A potential outlier was actually excluded if there was also a clear effect on the multiple regression coefficient ($> 1\%$). Outliers were excluded and the stepwise regression with the same initial model was repeated.

Models thus developed have the following form:

$$\text{E[TDSiY]} \;=\; \sum \beta_i X_i \tag{2.2}$$

where E[TDSiY] is the expectation of the transformed prediction based on the independent variables X_i and the estimated regression coefficients β_i.

2.2.4   Cross-validation

To investigate the robustness of the model in equation 2.2, we cross-validated the outcome using two approaches. The first one was used to analyze whether the

variables X_i are the same for subsets of the measurement data. This robustness of the selected model variable X_i was tested by constructing 5000 models similar to the standard model. However, in this part of the cross-validation we based the 5000 models on a subset of $\approx 75\%$ of the complete set of rivers with TDSiY data, excluding a randomly selected subset of $\approx 25\%$.

The second approach is used to determine the robustness of the regression coefficients β_i and to obtain the distribution and confidence interval of the model coefficients. This is done by estimating β_i values on the basis of a randomly selected subset of 75% of the data (training set) and testing predictions against the remaining 25% (validation set). This step was repeated 5000 times.

2.2.5   Testing and validation

The transformed prediction for each river with known X_i values is obtained from equation (2.2). The uncertainty of the model was assessed with the estimated regression coefficients from step (2) having a multinormal distribution with known mean and covariance. We used Monte Carlo simulation to draw 5000 equally probable sets of β_i. Each set was used to predict the TDSiY based on the known X_i values.

2.2.6   Extrapolation

Subsequently, we used the model developed for extrapolation to all global rivers, including those for which no measurements are available, to estimate the global DSi river export, and analyzed the effects of dams. We used the DSi load instead of DSiY to present predicted river export of DSi. First TDSiY predictions are back-transformed and DSi load is then calculated as the product of DSiY and basin area. By calculating the global sum of the DSi river export using the sets of equally probable β_i from step (3) of the multiple regression, we obtained 5000 estimates representing the complete distribution of the global DSi river export. We used the mean and the 2.5 and 97.5 percentiles of this distribution for our uncertainty estimates of the global DSi river export.

We also calculated the effect of dam construction on the retention of DSi in river basins. Where the water residence time is increased by dam construction, the growth of diatoms is increased causing a reduction of the river DSi load. Sedimentation of the diatoms in the form of suspended phytoliths (Reynolds 1984) is closely related to sedimentation of suspended solids (Conley 2002). Furthermore, diatom and non-diatom phytoplankton growth depends on the $N : P : Si$ element ratios (Conley 2002, 2000) and conditions like temperature, light and water turbidity influencing photosynthesis and respiration. Lacking a globally applicable approach for estimating DSi retention, here we use two methods as a first order estimate. The first one is the retention of dissolved inorganic phosphate (PR) estimated by Harrison et al. (2005) for all global river basins (Fekete et al. 2002), assuming that retention of dissolved inorganic phosphate and DSi are similar, although this will probably change with photosynthesis:respiration (P:R) ratios and

Table 2.2: Results of stepwise linear regression[a]

Variable	Dimension	β	Standard error	t	$\Pr(> |t|)$[b]
Intercept	-	2.5612	0.55	4.6	6.5E−06
ln(Precipitation)	mm day^{-1}	1.6077	0.08	21.2	0
Lith. Volcanic	-	1.6916	0.30	5.5	8.5E−08
Bulk density	Mg m^{-3}	−2.5959	0.38	−6.8	<1.0E−10
GAEZ slope	m km^{-1}	0.0310	0.01	4.8	2.4E−06

[a] The selected independent variables with the estimated coefficients, standard errors, t-statistic and p-values ($\Pr(> |t|)$) for the standard model.
[b] The p-values show that all variables are highly significant ($p \ll 0.05$).

may only be true for high P:R ratios. The second one is the sediment trapping efficiency (SR) for all global rivers (Fekete et al. 2002) proposed by Vörösmarty et al. (2003), based on the idea that sedimentation rates of suspended solids and diatom frustules are similar.

2.3 Results and discussion

2.3.1 Multiple linear regression model for DSiY

Using the Box-Cox transformation procedure, we found that for $\lambda = 0.0686$ the distribution of our TDSiY data is as close to a normal distribution as possible. We found four rivers to be consistent outliers, i.e., the Rio Negro (Argentina), Neva (Russia), Sous (Morocco) and Inguri (Georgia) (Table S2.1). These four rivers were excluded from the model development, leaving 204 rivers with DSiY data for all further steps. Together these 204 river basins cover 68 Mkm^2 which is about 58% of the global ice-free land area connected to the oceans (i.e., exorheic).

The stepwise regression resulted in the selection of four variables with a significant influence on TDSiY. These variables are the natural logarithm of annual precipitation, topsoil bulk density, the fraction of the river basin area covered by volcanic rocks, and terrain slope (Table 2.2). The multiple regression coefficient (R^2) for this model is 0.80. The predicted and observed values of TDSiY are presented in Figure 2.2.

The natural logarithm of annual precipitation has the strongest correlation with TDSiY and is first added to the regression model, followed by the aerial fraction covered by volcanic rock. The model is further enhanced by the soil bulk density. The terrain slope is the last variable added to the model, and exerts the smallest influence on TDSiY (Table 2.2). There are no anthropogenic variables with significant effect on TDSiY. These model variables are the large-scale controls of TDSiY in this lumped multiple regression approach at the scale of river basins. The model variables should therefore not be regarded as process parameters.

The logarithm of annual precipitation is highly significant and important. The
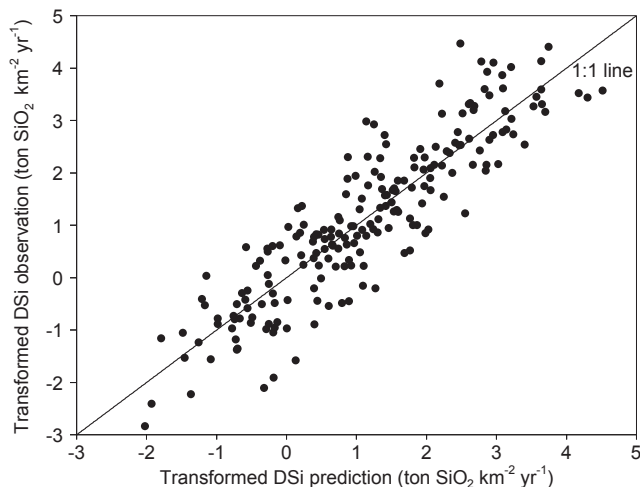
Figure 2.2: Predicted versus observed TDSiY for 204 rivers in the data set.

river yield of DSi is higher in river basins with high annual precipitation than in rivers with dry climates. The amount of water percolating through the soil, subsoil and parent material is a major variable determining rock weathering rates (Gaillardet et al. 1999, Kump et al. 2000, Hilley and Porder 2008).

A potential role of vegetation is confirmed by the factor bulk density of the top-soil, which has a negative influence on river DSi yields (Table 2.2). Generally soils with low bulk density are more developed, have more soil organic matter (including phytoliths) and stable aggregate structure than soils with high bulk density (Brady 1990). This also reflects the development of the ecosystem. Moreover, soils with low bulk density have a high porosity, and thus minerals and phytoliths are more easily accessible for dissolution and uptake by the vegetation.

Terrain slope is the third variable with significant influence on DSi yields (Table 2.2). Relief is one of the major determinants of natural erosion rates within one climate zone (Schumm 1977). Erosion is generally more severe in landscapes with steep slopes compared to gently sloping or flat terrain. In addition, Allison (1973) reported that eroded material contains more organic matter than the soil remaining. Therefore, in sloping areas erosion should stimulate the transport of soil organic matter containing phytoliths, and subsequent dissolution and transport of DSi (Conley 2002). In addition, erosion or physical denudation is intimately coupled to chemical weathering. The physical removal of soil material sustains chemical weathering by continuously refreshing mineral surfaces and by precluding the development of thick soils (Dupré et al. 2003, Gaillardet et al. 1999).

Finally, the occurrence of volcanic rock has a positive influence on DSi yield (Table 2.2), similar to results for Japan (Hartmann et al. 2008). The important

influence of volcanic material is due to the fast desilication of poorly ordered aluminosilicates such as allophane (Bolt and Bruggenwert 1976).

In summary, the overall importance of precipitation and occurrence of volcanic rocks point to the role of weathering as the ultimate source of DSi. The results also support the important biological control of the global silicon cycle (Bartoli 1983, Conley 2002), mainly through the factor bulk density (indicator for soil and ecosystem development). Precipitation and slope probably influence erosion, transport and dissolution of DSi from both the mineral and biological components.

2.3.2   Cross validation

The robustness of the multiple regression model, evaluated by developing 5000 models based on randomly selected subsets of the rivers with DSiY data, is discussed on the basis of the significant model variables and the predictions for the β values.

To test the robustness of the selected model variable X_i, we made 5000 models based on the measurements with a randomly selected subset of 50 measurements excluded. In all 5000 models both the natural logarithm of annual precipitation and bulk density are significant variables. In 99% of the models the occurrence of volcanic rock is significant. Overall, slope is significant in 92% of the models, although in 65% of the models this is based on the information from the GAEZ data, and in 27% of the models the slope data are from the FAO (Table 2.1). There were 121 models with only 3 parameters. The combination of the natural logarithm of annual precipitation, bulk density and the occurrence of volcanic rock were found in 100 out of these 121 models. The slope (GAEZ) instead of the occurrence of volcanic rock was found in 21 models. Precipitation and temperature (both without transformation) were found in none of the 5000 models.

The robustness of our model is also illustrated by the fact that 58% out of the 5000 models have exactly the same model variables as the standard model, while 83% models are similar to the standard model, the only difference being the source of information for slope (GAEZ or FAO, see Table 2.1).

Temperature squared (not temperature as such) is a significant variable in only 11 out of 5000 models, always in combination with the four variables of the standard model. The lack of a temperature effect may be due to the influence of a small number of tropical lowland rivers such as the Amazon and Congo (Gaillardet et al. 1999). These large catchments are covered by thick, highly weathered soils (Driessen and Dudal 1990) with low chemical weathering fluxes of silicates (Dupré et al. 2003). Close to 50% of the DSi in the Amazon originates in the Andes region, with extensive volcanic deposits (Mortatti and Probst 2003).

Temperature determines the rates of chemical and biological processes at all levels (Bolt and Bruggenwert 1976, Garnier et al. 2006). However, we find that temperature is not an important control of DSi river export at the global scale. We therefore specifically investigated the effect of temperature by a number of data analyses: excluding the Amazon, Nile and Congo, excluding all river basins with temperatures > 15 degrees, and excluding all temperatures > 20 degrees.

Table 2.3: Minimum and maximum values of regression coefficients (β) obtained with 5000 simulations and the value for the standard model[a]

Variable	Minimum	Standard model	Maximum
Intercept	1.3708	2.5612	3.9699
ln(Precipitation)	1.4418	1.6077	1.7643
Lith. volcanic	0.8864	1.6916	2.3965
Bulk density	−3.5644	−2.5959	−1.7805
GAEZ slope	0.0145	0.0310	0.0456

[a] See Table 2.2.

In a further analysis we excluded all river basins with warm humid tropical and warm seasonal tropical dry climates (according to GAEZ, see Table 2.1), and finally we excluded only warm humid tropical climate. None of these experiments yielded temperature as a significant variable. In fact, all the resulting models confirm the above cross validation. The lack of a temperature influence confirms the conclusions of Kump et al. (2000). They showed that laboratory studies reveal a strong dependence of mineral dissolution on temperature, but at larger spatial scales this is often obscured by other environmental factors that co-vary with temperature. This is also in agreement with Gaillardet et al. (1999) who studied silicate weathering rates and found a weak correlation of weathering rates with temperature only when excluding some large tropical rivers such as the Amazon and Congo.

To assess the robustness of the model regression coefficients (β_i) we estimated β_i values on the basis of a randomly selected subset of 75% of the data (training set) and made predictions for the remaining 25% (validation set). The minimum and maximum values of each estimated β_i are not fixed but change for random selections of 75% of the 204 rivers with DSiY measurement data. The coefficients obtained with the 5000 selections of rivers generally range within an acceptable factor of two around the value of the standard model (Table 2.3).

2.3.3   Testing and validation

Another approach for testing the model is a comparison between the modeled DSi load (note that this is back-transformed from TDSiY and multiplied by the river basin area) with that based on the measurements. We use the Bland-Altman test (Bland and Altman 1996), which involves comparison of the residuals (difference between observed and predicted DSi load) with the mean of the predicted and observed DSi load. This test showed that there is no systematic relation between the residuals and the mean of the predicted and observed DSi load.

The relationship between observed and predicted river DSi loads is presented in Figure 2.3. Figure 2.4 shows the DSi yield of the standard model for all global rivers. We can now use the full DSi model to predict DSi load (i.e., the back-

Table 2.4: Area covered, DSi river export from the standard model, and 2.5 and 97.5 percentiles obtained with 5000 Monte Carlo simulations

Number of river basins[a]	Area covered	Predicted DSi export	Monte Carlo	
			2.5 perc.	97.5 perc.
	Mkm^2	$Tg\ SiO_2\ yr^{-1}$	$Tg\ SiO_2\ yr^{-1}$	$Tg\ SiO_2\ yr^{-1}$
204 river basins included in the TSS data set	68	190^b	173	212
3840 river basins within range	111	346	315	386

[a] For the 204 rivers included in the DSi data set, and for all 3840 rivers for which the variables are within the range of the DSi data set (Table 2.5).
[b] The estimate based on the DSi observations in the data set is 194 $Tg\ SiO_2\ yr^{-1}$.

transformed value of DSiY times the river basin area for the river considered) for the 204 rivers with DSiY measurement data (Figure 2.1). The estimated value with the standard model of 190 Tg yr^{-1} is slightly lower than the total observed DSi load of 194 Tg yr^{-1} for the same rivers (Table S2.1). The 95% confidence interval based on Monte Carlo simulation is (173, 212) (Table 2.4). Together these 204 river basins cover 68 Mkm^2 (Table 2.4; Table S2.1) which is about 58% of the global ice-free exorheic, i.e., connected to the oceans, land area (118 Mkm^2).

2.3.4   Extrapolation

The estimated global DSi export from the total of 5342 river basins is 380 Tg SiO_2 yr^{-1} (Figure 2.4) with a 95% confidence interval of (340, 427). In our global prediction we avoided using values of variables outside the validity range of the model, which are minimum and maximum values of the 208 rivers with DSiY data in our dataset listed in Table 2.5. The model estimate for those river basins (3840 out of 5342) with all model variables within the validity range is 346 Tg SiO_2 yr^{-1} with a 95% confidence interval of (315, 386) (Table 2.4). This represents an area of 111 Mkm^2 or 94% of the global exorheicland area.

For 1502 out of 5342 river basins covering 6% of the global exorheicland area at least one model variable is outside the validity range (Table 2.5). If these values are restricted to the minimum and maximum values of the model (Table 2.5), we obtain an additional load of 33 Tg yr^{-1} with a range of 25 to 41 Tg yr^{-1}.

Turning to individual rivers, we see that the global DSi river export is dominated by only a small number of rivers. For example, the DSi load of the Amazon is 42 Tg SiO_2 yr^{-1}, or 11% of global DSi river export, for 5% of the exorheic landmass. The Zaire has the second largest DSi river export with 16 Tg SiO_2 yr^{-1}, or 4% of global DSi river export, for 3% of the exorheic landmass. There are 8 rivers covering 15% of the global exorheic land area (Amazon, Orinoco, Parana and Magdalena in South America, Chang Jiang, Ganges-Brahmaputra and Mekong in Southeast Asia and Zaire in Africa) that together contribute 25% to the global
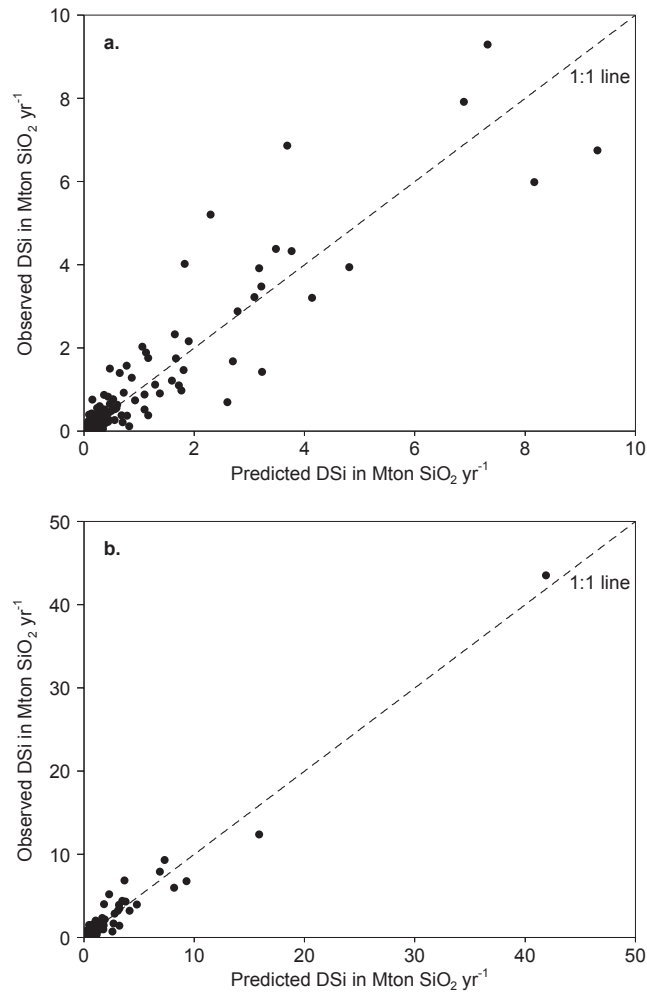
Figure 2.3: Predicted versus observed DSi river load for 204 rivers in the data set for (top) the range 0–10 Mton SiO_2 yr^{-1} and (bottom) the full data set.

Table 2.5: Minimum and maximum values of variables in the DSi data set of observations, minimum and maximum for all global river basins, and the number of river basins outside the range of values for rivers included in the DSi data set

Variable	Unit	Range of values for rivers included in the DSi data set		Range of values for all river basins[a]		Number of river basins outside the range in the DSi data set
		Min.	Max.	Min.	Max.	
ln(Precipitation)	mm day^{-1}	-0.65	2.40	-2.46	3.02	825
Bulkdensity	Mg m^{-3}	0.94	1.65	0.31	1.78	210
Lith. volcanic	-	0	0.76	0.00	1.00	125
GAEZ slope	m km^{-1}	1.96	41.98	0.00	50.00	342

[a] 5342 rivers within the 0.5° by 0.5° river network of Fekete et al. (2002) which are included in this study.

DSi river export.

Most of the pre-dam DSi is exported by global rivers to coastal zones of the Atlantic Ocean (41%, with a dominant contribution of about one quarter from the Amazon), Pacific Ocean (36%) and Indian Ocean (14%) (Table 2.6). South America and Asia are the largest contributors (25% and 23%, respectively) (Table 2.7). Oceania, with a total basin area of only 3 Mkm^2, contributes 18% of global DSi river export, which is similar to that from South Asia with a total basin area of 18 Mkm^2 and a contribution of 17%.

2.3.5 Effect of dams

We recognize that the two methods (PR, representing the retention of inorganic phosphate, and SR, which represents sediment trapping) for estimating Si retention may not correctly describe DSi retention. Also, they differ on the river basin, regional and continental scale, although the global average DSi retention is similar (retention of 18% for PR approach and 19% for SR) (Table 2.6 and 2.7). The largest differences are found for Africa (26% based on the PR approach and 35% for SR, which results in a global DSi river export difference of 4 Tg SiO$_2$ yr^{-1} (Table 2.7) and the Arctic Ocean (17% for PR and 9% for SR). However, a smaller difference in estimated retention for the Atlantic Ocean, the largest global recipient of DSi, of 2% has large consequences for the global DSi retention (a global DSi river export difference of 3 Tg SiO$_2$ yr^{-1}).

The DSi retention of 18–19% causes a reduction of global DSi river export from 380 to 307–312 Tg SiO$_2$ yr^{-1}. Our global estimate of river DSi export accounting for DSi retention is 9% lower than the 336 Tg SiO$_2$ yr^{-1} estimated by Treguer et al. (1995).

Table 2.6: Predicted river export of DSi to the world's oceans for the pre-dam situation and retention in global reservoirs based on two methods

Ocean	Area	Pre-dam DSi river export	Contribution to global DSi river export	DSi retention with PR[a]	DSi retention with SR[a]
	(Mkm^2)	$(Tg\ yr^{-1})$	(%)	(%)	(%)
Arctic Ocean	18	18	5	17	9
Atlantic Ocean	43	155	41	23	25
Indian Ocean	17	51	14	11	11
Land	14	8	2	18	17
Mediterranean & Black Sea	8	11	3	40	46
Pacific Ocean	19	137	36	13	15
World	118	380	100	18	19

[a] PR is the phosphate retention from Harrison et al. (2005); SR is sediment retention from Vörösmarty et al. (2003).

Table 2.7: Predicted river export of DSi from the world's continents for the pre-dam situation and retention in global reservoirs based on two methods

Continent	Area	Pre-dam DSi river export	Contribution to global DSi river export	DSi retention with PR[a]	DSi retention with SR[a]
	(Mkm^2)	$(Tg\ yr^{-1})$	(%)	(%)	(%)
Africa	23	49	13	26	35
Australia	5	4	1	7	8
Europe	10	20	5	15	19
North America	22	57	15	22	21
North Asia[b]	19	20	5	17	10
Oceania	3	68	18	1	1
South America	17	95	25	24	21
South Asia[b]	18	66	17	19	25
World	118	380	100	18	19

[a] PR is the phosphate retention from Harrison et al. (2005); SR is sediment retention from Vörösmarty et al. (2003).
[b] Asia is divided in North Asia (North of 45°N) and South Asia (South of 45°N) based on the location of the river mouth.
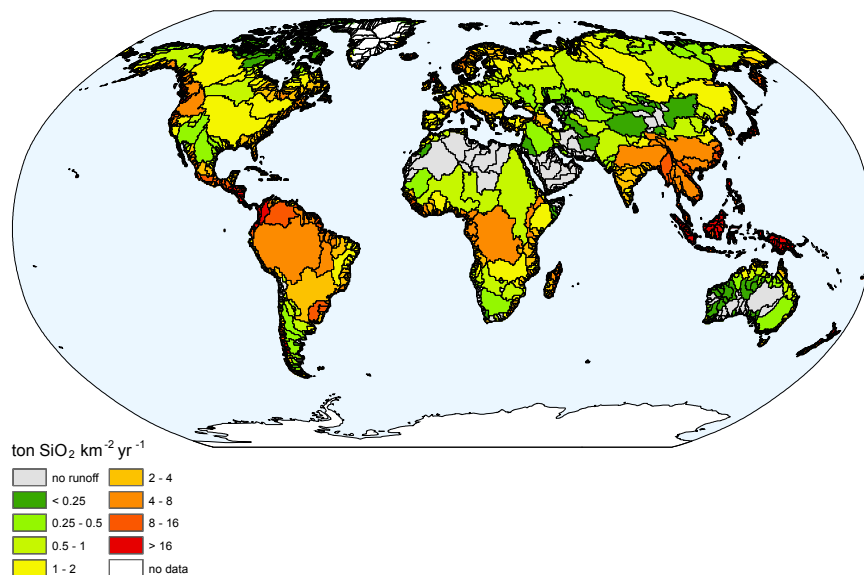
Figure 2.4: Predicted DSiY values (ton SiO_2 km^{-2} yr^{-1}) for all global river basins using the NEWS-DSi model.

2.3.6   Uncertainties

NEWS-DSi explains $\approx 80\%$ of the variability in the transformed TDSiY, leaving 20% of the variability unexplained. We recognize that the multiple regression coefficient is not a proper indicator of the uncertainty. A better way to express the behaviour of the model is to show that predictions for DSiY (ton km^{-2} yr^{-1}) are within a factor of 1.5 of the observations for 50% of the river basins in the data set used (204 rivers) (Figure 2.5). This relative error of 1.5 and a fraction of the rivers of 0.5 means that for 50% of the rivers with DSiY data the following statement is valid: $1/1.5 < $ (prediction/observation) < 1.5. DSiY predictions are within a factor of 2 for 70% and within a factor of 3 for 90% of the 204 rivers with observations (Figure 2.5).

The NEWS-DSi model is robust with respect to the available data. By using Monte Carlo simulations to obtain a range of predictions, and not just one, we have tried to account for model uncertainty. The NEWS-DSi model prediction for the total DSi load for 3840 rivers is 346 Tg yr^{-1}. The 97.5% upper bound is 386 Tg yr^{-1}, which exceeds the mean by only 11%.

Apart from the model uncertainty, there are other uncertainties related to the DSiY data and the ancillary basin data. Uncertainty associated with available DSiY data are discussed in detail elsewhere (Stelzer and Likens 2006). The main sources of uncertainty are: (1) inconsistent measurement techniques; (2) varying and often low sampling frequency. The potential bias caused by these uncertain-
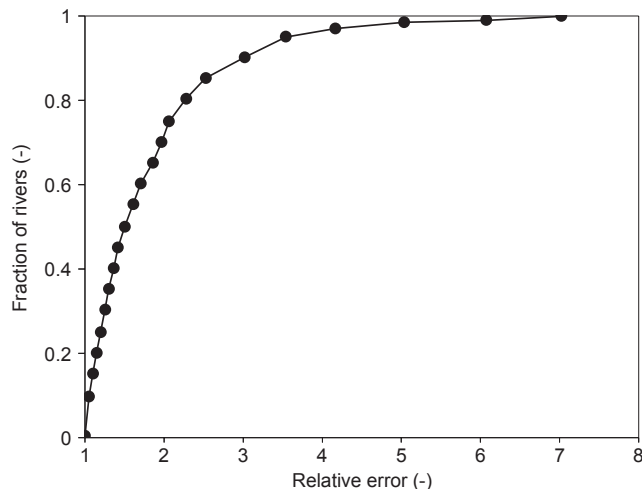
Figure 2.5: Fraction of rivers with observations DSiY versus the relative error (calculated as prediction : observation for cases where prediction > observation, or observation : prediction for all other cases). For example, the relative error of 3 and a fraction of the rivers of 0.9 means that for 90% of the observed rivers the following statement is valid: $1/3 <$ (prediction/observation) < 3.

ties in the data is recognized, but due to lack of information provided in the measurement reports this bias can not be quantified.

Regarding the ancillary basin data, there are two major uncertainties. Firstly, we use river-basin averages for most basin characteristics. Averages may not reflect the influence of a factor such as temperature or precipitation for large river basins occurring in different climate zones. Also, the effect of seasonal variation in climate, runoff, vegetation and land cover, and agricultural and forestry management is not reflected in our approach. For other factors such as slope or soil properties the variability may be lost by averaging. Our global model should therefore not be used to predict DSiY for individual river basins, or within river basins, but rather for regional to continental scale applications.

We found land use not be significant. This does not mean that differences in agricultural land use versus natural vegetation are not important. For example, Conley et al. (2008) showed that deforestation causes increasing DSi river export. For proper analysis of the effects of changing land use, time series would be needed to relate land use changes to TDSiY. Similarly, we have not analyzed the importance of DSi in wastewater flows, which may contribute perhaps 8% in densely populated river basins (Sferratore et al. 2006), but have been estimated to be < 2% at global scale for total additional human DSi additions (Van Dokkum et al. 2004).

There is also uncertainty in the river basin data per se. One example of uncer-

tainty in the ancillary data is that in the river basin area estimates. Comparison of data provided by Meybeck and Ragu (1995) and Fekete et al. (2002) show significant disagreement in some river basins. This has important repercussions for the calculation of DSiY.

Finally, globally applicable estimates for DSi retention in reservoirs are not available, so that the uncertainty in our estimates for the actual DSi load may be larger than that for the pre-dam load.

2.4   Conclusions

We developed a robust lumped model for DSiY at the scale of river basins and with an annual temporal scale. The model was cross-validated by using training and validation data sets. Our model predictions realistically describe the information in the measurement data set. Our approach provides new insights in the main drivers of river export of DSi at the scale of river basins on the basis of the limited data set of DSi river export available to us. The cross validation of the regression model gives strong indications that the DSi yield depends on the natural logarithm of annual precipitation, bulk density and the occurrence of volcanic rock. Terrain slope has a smaller but significant influence on DSi export than the other variables, but is still robust (more than 90% of the models found this variable significant). Temperature is not found as a significant variable, even when we focused on river basins in extra-tropical climates.

The overall importance of precipitation and occurrence of volcanic rocks point to the role of weathering as the ultimate source of DSi. The results also support the important biological control of the global silicon cycle proposed earlier by Bartoli (1983), mainly through the factor bulk density (indicator for soil and ecosystem development). Precipitation and slope probably influence dissolution of DSi from both the mineral and biological components.

Our regression approach is not the only way to model DSi river export. Other approaches such as process-based models (Billen and Garnier 2000, Garnier et al. 2002, Sferratore et al. 2005) require far more knowledge and data on processes and their controls in the DSi cycle at the river basin scale than our approach. Such data and knowledge is currently still lacking for global-scale application of process-based models.

There are multiple scale problems related to our lumped model approach. Our model should therefore not be used to predict the DSi load for individual rivers; it is more appropriate to estimate the regional, continental or global DSi river export to the coastal zone, and changes therein as a result of climate change and dam construction (e.g., Syvitski et al. 2003).

Inevitably there is considerable uncertainty associated with our predictions. Nonetheless, as the first attempt to develop a robust, internally consistent, and spatially-explicit global model of DSi river export, NEWS-DSi constitutes a significant advance in its own right. With the NEWS-DSi model now available, it is possible to analyze the exported ratios of N, P and Si in all different forms (Billen

and Garnier 2007, Seitzinger et al. 2005), also including information on the effect of dam construction.

Acknowledgments

Supporting information

S2.1   Regression data

We used data on DSi load or concentration measured at or close to the river mouth. DSi annual load data were converted to annual DSi yield (DSiY, in ton SiO_2 km^{-2} yr^{-1}) using the basin area estimates from Fekete et al. (2002). The data set includes DSiY data for 208 rivers representing the "pre-dam", natural or pristine situation. The DSiY data cover the period between the 1920s and 1990s. Hence, instead of a fixed base-year, the criterion of selection was the absence of dams and reservoirs or human impact. The DSiY data are generally multi-year averages from (i) Meybeck and Ragu (1995) (selecting the "pre-dam" situation), (ii) data on pristine rivers with data from numerous reports on river chemistry prior 1950/60, i.e., before the main development of large reservoirs in world rivers (Vörösmarty et al. 1997), and (iii) recent analyses in regions with limited human impacts like Alaska and Canada, Amazon and Orinoco basins, Patagonia, and West and South Africa. References and more details on the data selection are in Dürr et al. (2009).

We developed the NEWS-DSi model and used the factors given in Table S2.1.

Table S2.1: River-basin characteristics included in the regression analysis

Name[a]	River id[a]	Basin area[a]	Runoff[a]	DSi[b]	Prec[c]	Bulk[d]	Volcan[e]	Slope[f]
Amazon	1	5829300	6202.91	7.44	1.75	1.36	0.05	6.37
Nile	2	3812400	445.67	0.37	0.43	1.48	0.06	10.57
Congo	3	3682700	2290.42	3.36	1.43	1.39	0.00	8.41
Mississippi	4	3206700	274.09	2.15	0.71	1.5	0.01	10.13
Ob	5	3040300	226.56	1.72	0.18	1.36	0.09	8.46
Parana	6	2657600	632.95	3.49	1.13	1.45	0.11	7.79
Yenisey	7	2591900	306.4	1.52	0.23	1.39	0.18	18.8
Lena	8	2455900	200.8	0.89	0.04	1.36	0.04	19.19
Niger	9	2231900	403.9	1.8	0.59	1.51	0.01	6.22
Chang Jiang	11	1792300	455.12	3.34	1.02	1.41	0.12	27.5
Amur	12	1760500	136.34	0.4	0.41	1.4	0.15	17.74

Table S2.1: (Continued)

Name[a]	River id[a]	Basin area[a]	Runoff[a]	DSi[b]	Prec[c]	Bulk[d]	Volcan[e]	Slope[f]
Arctic Red	13	1704600	106.29	0.65	0.06	1.19	0.06	10.99
Ganges-Brahmaputra	14	1625600	914.21	4.86	1.23	1.43	0.03	20.33
Zambezi	17	1358700	323.19	1.23	0.93	1.45	0.01	12.68
Indus	20	1142200	62.03	1.38	0.1	1.48	0.03	22.3
Nelson	21	1144000	60.29	0.1	0.29	1.36	0.01	5.37
Saint Lawrence	24	1056200	405.69	2.22	0.77	1.39	0.02	7.61
Orinoco	25	1034900	1550.78	6.5	1.85	1.38	0.07	9.71
Murray	26	1030700	11.7	0.4	0.19	1.58	0.07	4.19
Shatt el Arab	27	989790	68.44	0.58	−0.32	1.47	0.07	15.72
Orange	28	942030	1.09	0.19	−0.15	1.52	0.06	14.47
Huang He	29	893910	13.35	0.42	0.18	1.4	0.02	20.17
Yukon	30	861260	66.17	1.63	−0.3	1.27	0.18	21.01
Senegal	31	844470	59.88	0.66	0.00	1.54	0.05	4.92
Colorado (Ari)	34	807760	1.83	0.37	−0.19	1.53	0.19	20.14
Rio Grande (US)	35	803880	0.77	0.6	−0.1	1.51	0.21	15.09
Danube	36	790020	168.74	1.24	0.77	1.42	0.08	19
Tocantins	37	765600	911.34	5.7	1.53	1.41	0.02	6.33
Mekong	38	756290	446.82	5.2	1.4	1.4	0.08	21.17
Columbia	40	733760	128.55	4.76	0.54	1.4	0.55	27.52
Kolyma	43	670070	61.39	0.78	−0.19	1.41	0.13	20.37
Sao Francisco	45	612860	170.6	1.43	1	1.47	0.00	7.87
Dnepr	47	510730	25.99	0.36	0.48	1.47	0.00	6.44
Don	49	424450	11.03	0.29	0.31	1.56	0.00	8.66
Limpopo	51	419330	0.08	1.05	0.29	1.52	0.13	14.58
Zhujiang	54	407620	152.56	7.06	1.36	1.42	0.13	25.11
Irrawaddy	55	404990	418.6	10.67	1.67	1.39	0.04	22.53
Volta	56	396470	94.35	1.59	1.05	1.54	0.01	5.54
Khatanga	58	373110	87.06	0.74	−0.08	1.3	0.2	13.29
N. Dvina	59	363110	64.25	2.3	0.51	1.31	0.00	6.36
Uruguay	60	355110	105.87	9.06	1.39	1.44	0.57	10.46
Indigirka	63	336420	36.9	0.47	−0.27	1.41	0.09	20.46
Pechora	66	316380	64.18	2.43	0.41	1.15	0.02	8.46
Godavari	67	310650	71.48	6.06	1.06	1.55	0.46	10.28
Churchill (Hud)	68	304970	24.67	0.19	0.24	1.13	0.01	3.96
Kazan	69	305390	45.86	0.09	−0.24	1.42	0.03	2.78
Neva	72	286150	49.45	0.03	0.53	1.29	0.00	5.74
Liao	74	274560	3.4	0.13	0.28	1.51	0.19	12.96
Magdalena	77	250660	209.57	12.71	1.67	1.33	0.35	22.86
Krishna	78	250830	9.91	2.09	0.79	1.54	0.42	9.61
Fraser	83	238450	56.28	1.59	0.75	1.45	0.52	26.27
Anadyr	87	227350	41.71	2.65	−0.01	1.37	0.41	17.76
Yana	88	226560	11.65	0.45	−0.29	1.46	0.00	22.9
Olenek	89	224820	46.69	0.44	−0.21	1.32	0.03	13.22

Table S2.1: (Continued)

Name[a]	River id[a]	Basin area[a]	Runoff[a]	DSi[b]	Prec[c]	Bulk[d]	Volcan[e]	Slope[f]
Ogooue	93	209220	221.81	8.38	1.63	1.37	0.00	5.94
Negro (Arg)	99	197740	14.64	4.96	−0.27	1.47	0.23	14.46
Wisla	106	181260	14.11	1.38	0.57	1.45	0.00	8.51
Hong	108	170480	78.26	10.25	1.34	1.41	0.17	36.14
Rhine	110	165600	56.2	1.61	0.92	1.39	0.04	17.67
Koksoak	120	150860	85.1	0.82	0.66	1.32	0.02	5.39
Elbe	121	149080	15.6	0.64	0.54	1.35	0.12	10.74
Chao Phrya	126	141360	51.16	3.94	1.25	1.39	0.02	16.86
Mahanadi	127	140820	63.63	6.18	1.26	1.52	0.01	10.75
Fitzroy East	128	138170	0.11	0.6	0.56	1.58	0.08	5.25
Sanaga	131	128650	197.59	7.15	1.57	1.37	0.02	8.9
Brazos (Tex)	135	124970	0.18	0.4	0.64	1.56	0.00	6.98
Mobile/Alabama	137	124100	27.26	12.13	1.34	1.4	0.00	10
Burdekin	140	120880	0.09	1.25	0.42	1.57	0.14	5.09
Colorado (Tex)	141	121080	0.00	0.24	0.43	1.61	0.00	6.87
Loire	143	118600	18.15	1.86	0.75	1.4	0.09	11.37
Kuskokwim	145	116500	19.57	3.7	0.08	1.16	0.03	16.04
Narmada	147	113800	50.46	3.7	1.04	1.57	0.54	10.92
Flinders	150	110020	0.03	0.27	0.14	1.62	0.06	1.96
San Joaquin	153	109490	10.22	3.54	0.35	1.49	0.11	22.74
Back	154	109400	11.35	0.07	−0.46	1.48	0.00	2.62
Bandama	161	103650	30.55	2.18	1.29	1.45	0.00	4.76
Po	163	102420	68.89	2.63	1.18	1.43	0.12	27.28
Rhone	165	99537	52.17	2.49	1.08	1.43	0.03	26.28
Anabar	166	99688	22.47	0.45	−0.26	1.23	0.04	10.52
La Grande	167	99362	41.13	1.44	0.67	1.3	0.00	4.06
Tana (Ken)	168	98453	15.88	2.26	0.89	1.47	0.16	9.45
Nemanus	172	97469	13.12	0.41	0.54	1.59	0.00	6.03
Saguenay	179	92374	42.31	2.58	0.97	1.33	0.00	8.66
Pur	187	86720	25.93	2.24	0.31	1.05	0.00	3.38
Penzhina	190	86487	15.21	1.72	0.17	1.31	0.42	19.8
Daugava	193	83810	11.18	0.65	0.55	1.62	0.00	5.56
Comoe	197	82067	24.83	0.63	1.23	1.48	0.01	5.64
Peel	199	80918	4.26	1.04	−0.43	1.42	0.02	21.04
Cauweri	203	78371	24.46	4.51	1.09	1.5	0.04	12.19
Sepik	206	76709	118.01	19.06	2.08	1.28	0.21	18.63
Sassandra	208	76300	41.35	5.02	1.5	1.4	0.00	6.75
Mezen	211	76159	19.67	2.13	0.47	1.21	0.00	6.9
Barito	213	73824	141.72	12.23	2.1	1.27	0.17	9.88
Seine	216	73701	10.39	1.27	0.67	1.43	0.00	10.11
Gambia	219	71918	20.73	1.26	1.05	1.48	0.11	10.9
Susquehanna	220	72244	17.99	2.45	0.93	1.33	0.00	20.35
Dnestr	221	72212	3.95	0.61	0.49	1.53	0.00	14.29

(Continued on next page . . .)

Table **S2.1**: (Continued)

Name[a]	River id[a]	Basin area[a]	Runoff[a]	DSi[b]	Prec[c]	Bulk[d]	Volcan[e]	Slope[f]
Mitchell	224	70915	12.22	2.88	1.06	1.48	0.12	4.54
Mahakam	225	70775	134.31	15.72	2.12	1.31	0.16	11.42
Fuchun Jiang	240	67131	45.24	3.24	1.34	1.44	0.48	24.17
Tapti	242	66150	10.46	4.43	0.85	1.58	0.75	10.06
Menjiang	243	66129	49.38	11.2	1.5	1.4	0.32	32.94
Maroni	248	64502	108.91	10.03	1.85	1.39	0.00	7.09
Kuban	251	64027	17.39	0.61	0.88	1.5	0.08	19.22
Fly	261	61149	137.87	19.7	2.34	1.29	0.2	11.45
Sacramento	271	58975	16.5	6.88	0.9	1.43	0.59	21.18
Musi	273	58368	79.21	34.74	1.97	1.25	0.31	6.28
Skeena	275	58650	36.76	4.84	1.01	1.4	0.29	32.56
Seal	279	58361	11.39	0.34	0.13	1.17	0.00	2.22
Garonne	281	58095	9.83	1.25	0.87	1.4	0.06	21.38
Nadym	283	58176	16.68	2.43	0.33	0.99	0.00	3.72
Onega	284	58033	13.19	2.05	0.59	1.24	0.04	5.7
Sakarya	286	57112	1.82	1.25	0.33	1.45	0.28	21.58
Anderson	288	56978	5.39	0.2	−0.65	1.23	0.00	7.06
Guadalquivir	300	53752	1.76	1.95	0.44	1.44	0.07	23.57
Saint John	303	53167	29.31	1.66	1.06	1.25	0.18	14.45
Coppermine	308	52398	4.98	0.34	−0.48	1.34	0.04	4.76
Nueces	312	51369	0.00	0.24	0.44	1.62	0.00	7.53
Stikine	313	51580	17.42	5.72	0.65	1.42	0.43	33.13
Kamchatka	318	50842	29.98	7.46	0.76	0.97	0.52	22.9
Luan	333	46560	0.00	0.37	0.24	1.5	0.17	21.25
Weser	340	45807	10.13	0.99	0.69	1.36	0.01	10.43
Susitna	341	45860	10.78	5.9	0.18	1.25	0.25	27.67
Meuse	353	43488	22.4	3.05	0.91	1.39	0.02	9.37
Hudson	356	43324	19.81	0.81	0.99	1.32	0.00	17.81
Kobuk	362	42755	4.74	1.77	−0.47	1.18	0.07	18.54
Altamaha	367	41557	2.93	4.18	1.23	1.43	0.00	8.07
Eastmain	368	41630	17.12	1.86	0.79	1.2	0.00	4.16
Santee	370	40585	9.31	4.47	1.24	1.39	0.05	13.14
Potomac	380	38452	6.85	2.18	0.97	1.38	0.00	18.68
Sebou	381	38392	1.2	1.71	0.48	1.47	0.02	32.41
Kymijoki	395	36151	4.39	0.58	0.45	1.12	0.00	7.1
Savannah	396	35894	9.77	10.47	1.32	1.4	0.00	12.63
Tornionjoki	404	34884	11.44	2.13	0.33	1.12	0.05	11.96
Dongjiang	411	33852	23.79	10.31	1.58	1.43	0.24	22.21
Purari	415	33628	47.45	37.97	2.1	1.28	0.12	26.21
Mae Klong	419	32794	51.08	6.73	1.89	1.42	0.07	25.44
Klamath	426	32246	4.47	9.32	0.81	1.4	0.7	28.13
Connecticut	430	31594	13.88	3.44	1.03	1.28	0.02	21.12
Dalalven	451	30076	8.48	2.93	0.59	1.09	0.13	12.94

Table S2.1: (Continued)

Name[a]	River id[a]	Basin area[a]	Runoff[a]	DSi[b]	Prec[c]	Bulk[d]	Volcan[e]	Slope[f]
Sabine	467	28917	4.28	1.4	1.16	1.42	0.00	5.58
Hayes (Arctic)	477	28184	5.29	0.3	−0.51	1.48	0.07	6.34
Pee Dee	484	27735	5.77	14.36	1.14	1.4	0.11	10.15
Hanjiang	528	25309	15.96	12.72	1.46	1.43	0.27	25.55
Nyong	537	24576	47.49	2.28	1.72	1.4	0.00	9.17
Cavally	542	24495	21.55	8.42	1.78	1.39	0.00	5.32
Tauy	544	24659	6.73	1.91	0.17	1.34	0.56	22.09
Suwannee	558	23900	2.87	2.31	1.31	1.33	0.00	2.99
Amguema	577	22671	7.2	1.82	0.01	1.44	0.56	28.09
James	583	22042	3.73	6.62	0.99	1.4	0.19	13.51
Suriname	598	21473	25.8	5.98	1.85	1.4	0.00	5.09
Kikori	603	21411	51.28	24.37	2.4	1.24	0.38	22.08
Moisie	614	21278	11.35	2.42	0.99	1.34	0.00	13.09
Neches	616	21177	1.83	2.59	1.19	1.42	0.00	5.32
Delaware	624	20978	6.13	5.26	1.01	1.34	0.00	14.91
Kennebec	650	19726	12.09	3.87	1.1	1.27	0.23	16.01
Ellice	657	19683	2.72	0.04	−0.53	1.48	0.00	3.39
Bio Bio	658	19548	11.76	20.03	0.89	1.05	0.29	28.07
Waikato	659	19482	18.17	24.74	1.6	0.94	0.28	14.79
Penobscot	662	19479	9.96	2.63	1.03	1.24	0.27	13.02
Sous	677	18646	0.00	0.14	−0.19	1.48	0.25	34.5
Minho	703	18281	8.47	2.43	1.2	1.35	0.11	27.62
Tone	738	17407	15.08	10.4	1.34	1.08	0.5	20.97
Thames	743	17395	5.2	2.55	0.68	1.45	0.00	4.5
Trent	754	17036	5.18	1.83	0.63	1.46	0.00	3.99
Lielupe	787	15620	2.21	0.46	0.47	1.51	0.00	4.09
Brantas	812	15261	12.23	49.16	1.57	1.44	0.5	9.19
Konkoure	821	15138	14.78	7.46	1.86	1.32	0.03	15.31
Clutha	822	15231	6.17	2.96	0.95	1.38	0.3	23.73
Kiso	829	15085	18.59	17.71	1.6	1.25	0.21	28.18
Ban Pakong	835	14970	11.06	5.06	1.61	1.38	0.00	6.82
Shinano	843	14818	13.06	22.16	1.49	1.19	0.49	28.06
Eel	871	14223	7.43	7.35	1.25	1.36	0.11	32.09
Jiulong	883	13984	7.94	16.99	1.39	1.43	0.11	30.38
Adour	902	13479	3.4	8.48	1	1.44	0.00	14.6
Waitaki	911	13313	17.04	9.41	1.56	1.34	0.13	30.83
Cape Fear	930	12652	1.97	2.69	1.18	1.42	0.14	5.88
Ameca	1021	11540	2.28	7.53	1.16	1.34	0.62	32.76
Rogue	1039	11370	3.99	11.43	1.09	1.33	0.42	33.77
Ishikari	1045	11242	3.76	22.65	1.24	1.22	0.53	19.98
Matanuska	1082	10540	2.78	8.5	0.35	1.24	0.25	27.17
Thjorsa	1146	9462	7.85	25.2	1.11	1.14	0.7	13.44
Kola	1160	9330	4.39	0.85	0.57	1.16	0.11	14.57

Table S2.1: (Continued)

Name[a]	River id[a]	Basin area[a]	Runoff[a]	DSi[b]	Prec[c]	Bulk[d]	Volcan[e]	Slope[f]
Citarum	1184	9170	10.16	24.86	1.78	1.35	0.25	15.66
Cimanuk	1189	9164	14.26	23.41	2	1.18	0.48	21.22
Serayu	1195	9157	19.55	46.94	2.23	1.31	0.28	17.05
Rioni	1209	9150	5.28	4.33	1.33	1.28	0.1	22.56
Umpqua	1236	9005	4.14	12.13	1.07	1.3	0.6	32.6
Venta	1310	8561	2.55	0.55	0.62	1.65	0.00	5.41
Gauja	1331	8313	1.45	0.74	0.49	1.59	0.00	4.96
Olfusa	1348	8061	4.15	32.28	0.95	1.1	0.62	13.06
Escambia	1357	7921	1.72	4.95	1.44	1.45	0.00	8.2
Yodo	1394	7604	5.35	9.68	1.41	1.33	0.03	15.61
Neuse	1398	7573	2.99	3.57	1.26	1.29	0.00	3.48
Tenryu	1401	7573	9.21	13.24	1.55	1.23	0.21	29.88
Mogami	1441	7255	7.52	30.88	1.5	1.29	0.45	22.11
Kitakami	1452	7188	6.41	18.01	1.32	1.04	0.02	20.96
Tokachi	1490	6804	5.75	37.12	1.24	1.05	0.17	27.08
Inguri	1492	6804	3.91	0.78	1.17	1.38	0.23	39.98
Teshio	1510	6600	4.9	27.03	1.25	1.32	0.3	17.33
Humptulips	1533	6371	6.62	37.83	1.54	1.25	0.27	17.13
Approuague	1602	6140	12.59	17.06	2.11	1.39	0.00	5.26
Kelantan	1623	6127	10.38	19.13	2.07	1.4	0.00	13.81
Citanduy	1647	6104	12.19	19.8	2.12	1.44	0.03	9.77
Manavgat	2088	4907	0.62	15.06	0.62	1.44	0.00	41.98
Agano	2094	4891	5.08	17.54	1.5	1.18	0.57	26.24
Waimakariri	2213	4493	1.77	8.31	0.95	1.28	0.00	18.13
Quinault	4362	2085	5.6	21.9	2.22	1.2	0.3	25.14

[a]Data on river basin characteristics are from Fekete et al. (2002) and Vörösmarty et al. (2003, 2000).

[b]DSi: Observed dissolved silica export at the mouth of the river basin (Mg km^{-2}).

[c]Prec: Natural logarithm of precipitation (mm day^{-1}) (New et al. 1999).

[d]Bulk: Bulk density (Mg m^{-3}). Soil data from Batjes (2002).

[e]Volcan: Fraction volcanic rock (-). Fraction of the river basin area with volcanic material based on Dürr et al. (2005).

[f]Slope: GAEZ slope (m km^{-1}) from FAO/IIASA (2000b). The fractional distribution within each 0.5° grid cell of the classes in the Global Agroecological Zones (GAEZ) map (1 = 0–2%, 2 = 2–5%, 3 = 5–8%, 4 = 8–16%, 5 = 16–30%, 6 = 30–45%, 7 = >45%) were recalculated to a mean slope: 1% (class 1), 3.5% (class 2), 6.5% (class 3), 12% (class 4), 23% (class 5), 37.5% (class 6) and 50% (class 7).

Chapter 3

Bottom-up uncertainty estimates of global ammonia emissions from global agricultural production systems

A.H.W. Beusen, A.F. Bouwman, P.S.C. Heuberger, G. Van Drecht, and
K.W. Van Der Hoek, 2008.
Atmospheric Environment **42**: 6067–6077.

Abstract

Here we present an uncertainty analysis of NH_3 emissions from agricultural production systems based on a global NH_3 emission inventory with a 5 by 5 minute resolution. Of all results the mean is given with a range (10% and 90% percentile). The uncertainty range for the global NH_3 emission from agricultural systems is 27–38 (with a mean of 32) Tg NH_3-N yr^{-1}, N fertilizer use contributing 10–12 (11) Tg yr^{-1} and livestock production 16–27 (21) Tg yr^{-1}. Most of the emissions from livestock production come from animal houses and storage systems (31–55%); smaller contributions come from the spreading of animal manure (23–38%) and grazing animals (17–37%). This uncertainty analysis allows for identifying and improving those input parameters with a major influence on the results. The most important determinants of the uncertainty related to the global agricultural NH_3 emission comprise four parameters (N excretion rates, NH_3 emission rates for manure in animal houses and storage, the fraction of

the time that ruminants graze and the fraction of non-agricultural use of manure) specific to mixed and landless systems, and total animal stocks. Nitrogen excretion rates and NH$_3$ emission rates from animal houses and storage systems are shown consistently to be the most important parameters in most parts of the world. Input parameters for pastoral systems are less relevant. However, there are clear differences between world regions and individual countries, reflecting the differences in livestock production systems.

3.1   Introduction

Ammonia is an important atmospheric pollutant with a wide variety of impacts. A large portion of atmospheric aerosols, acting as cloud condensation nuclei, consists of sulfate neutralized to various extents by NH$_3$ (Graedel and Crutzen 1993). Essentially, all emitted NH$_3$ is returned to the surface by deposition, which is known to be one of the causes of soil acidification (Van Breemen et al. 1982), eutrophication of natural ecosystems and loss of biodiversity (Bouwman et al. 2002c, Millennium Ecosystem Assessment 2006).

At present the annual global use of synthetic nitrogen (N) fertilizers is about 80 Tg (Tg = teragram; 1 Tg = 10^{12} g); an even larger amount of animal manure N is produced in livestock production systems. The use of N fertilizer and the production of animal wastes are expected to increase in the coming decades, particularly in developing countries (Bruinsma 2003).

One of the major pathways of N loss from agricultural systems is ammonia (NH$_3$) volatilization. Ammonia is constantly formed in soils from biological degradation of organic compounds and from ammonium (NH$_4^+$) yielding synthetic and organic fertilizers. Since NH$_3$ is a gas, any of it present in the soil, water or fertilizer can volatilize to the atmosphere; its reactions in water are fundamental in regulating the rate of loss. After NH$_3$ is applied to the soil, the NH$_4^+$ can be retained on the exchange sites, nitrified to nitrate (NO$_3^-$), or decomposed to NH$_3$, depending on soil and environmental conditions.

Ammonia volatilization may be responsible for the loss of 10–30% of the N fertilizer applied and the N excreted by animals, and is the major anthropogenic source of atmospheric NH$_3$(Bouwman et al. 2002a). In agricultural production systems there are several technical options to reduce NH$_3$ emissions, such as reduction of the N input, increase of the efficiency of N use in both crop and livestock production systems, for example by reducing NH$_3$ loss from the system (Van Egmond et al. 2002). Given the concern about the environmental impacts of NH$_3$, several industrialized countries have policies to reduce NH$_3$ emissions. Most of the policies in Europe and the U.S.A. intend to decrease human and plant exposure to S and N pollutants and ecosystem loads. European countries therefore agreed on significant reductions of NH$_3$ emissions by signing different protocols developed under the Convention on Long Range Transboundary Air Pollution (CLRTAP) (UN-ECE 1999).

Here we present a global inventory of NH$_3$ emissions associated with livestock

production and fertilizer use. We updated the $1°$ by $1°$ resolution inventory for agricultural NH_3 emission for the year 1990, as presented by Bouwman et al. (1997), with data for the year 2000 and implemented several other improvements. Here we analyze the uncertainties of calculated NH_3 emissions in the updated inventory for agricultural systems resulting from uncertainty in the input parameters. This allows for identifying and improving those input parameters with a major influence on the results.

The issue of scaling of emissions has been addressed by many authors, see for example Bouwman (1999). Ammonia inventories are available at the global, continental, national and finer scales (Asman et al. 1998). At the global scale the distributions are based on country data mainly. However, within grids the emissions show variability that is not captured at the scale of global emission inventories (Bouwman and Asman 1997). For example, Dragosits et al. (2002) investigated the variability of emissions, deposition and impacts of NH_3 within a 5 by 5 km grid cell (comparable in size to our grid cells) of the national inventory for the U.K. Their results indicated that the most extreme local variability is linked to housing and storage systems similar to findings in other countries (Bouwman and Asman 1997).

The purpose of this model-based inventory is to provide input for global atmospheric chemistry transport models (CTM) (see Dentener et al. 2006). Since wet and dry deposition is modeled by the different CTMs in different ways, the emission fields in the inventory described in this paper, represent the potential or gross flux of NH_3 to the atmosphere. The potential flux does not account for the difference between ambient NH_3 concentrations and the compensation concentrations regulating the exchange of NH_3 between the surface and the atmosphere. Hence, local deposition is not accounted for in our inventory. Emission fields can provide input for modeling the role of NH_3 in global cycles of S species and radiative forcing of climate through aerosol formation. Investigation of subgrid variability is therefore not within the scope of this study, in view of the purpose of our inventory.

In this paper we describe differences in the uncertainty of NH_3 emissions from agriculture and the major factors determining the uncertainty between countries and world regions, i.e., the U.S.A., the India and China regions, Western Europe and the Netherlands as well as differences within the U.S.A.

3.2   Data and methods

3.2.1   Ammonia emission inventory

We updated the $1°$ by $1°$ resolution NH_3 emission inventory for the year 1990, as presented by Bouwman et al. (1997), with data for the year 2000 and implemented several improvements: (i) more detailed spatial land-use information (5 by 5 min, or about 8 by 8 km at the equator, which is an increase in resolution by a factor of 144), (ii) different livestock production systems, (iii) recent estimates for animal

Table 3.1: Global area of cropland and grassland in mixed and pastoral systems

Area	Mha
Cropland in mixed systems	1370
Cropland in pastoral systems	125
Grassland in mixed systems	725
Grassland in pastoral systems	2625

N excretion rates, and (iv) improved NH_3 emission calculations for the spreading of manure and N fertilizer, (v) emission factors representing the lumped effect of housing, grazing and spreading were replaced by a mass-flow approach, where at each stage of manure management a proportion of N is lost (mainly as NH_3) and the remainder is passed on the next stage. This also allows for assessing the consequences of abatement at one stage of manure management on NH_3 losses at later stages of manure management.

The global 5 by 5 minute resolution land-cover distribution used in this study is based on a combination of two data sets from different satellite sensors, i.e., the IGBP-DisCover and the GLC2000 data set (Klein Goldewijk and Van Drecht 2006). Our land-cover data set includes agricultural areas for cropland and grassland that are consistent with statistical information from FAO (2007) on the country scale and for some large countries at the state (U.S.A.) or provincial (China) level.

Two livestock production systems are distinguished, i.e., pastoral systems, and mixed and landless systems. A grid cell is assumed to be covered by mixed and landless systems where cropland covers more than 25%. Otherwise the grid cell is considered to be dominated by pastoral production systems. This approach is similar to the approaches of Bouwman et al. (2005a) and Kruska et al. (2003). Although there may be a large variation between countries, this assumption yields a rough distinction between pastoral, and mixed and landless systems (Table 3.1).

It should be noted that areas designated for parks, nature reserves or protected areas may or maybe not included in the definition of permanent pastures of FAO (2007) in some countries. For example, national Australian reports (National Land and Water Resources Audit 2001) indicate that the area of permanent pastures from FAO (2007) for Australia includes a range of land tenures, and many of these are actually located in the "wilderness areas" that we excluded from the available area for allocation.

We used data from FAO (2007) for animal stocks for 10 animal categories (beef cattle, dairy cattle, buffalo, pigs, poultry, sheep and goats, along with the category of small ruminants, asses, mules, horses and camels). Associated N excretion rates (specified for Western Europe, North America, rest of the industrialized countries and developing countries) were taken from Van Der Hoek (1998). Within a country, excretion rates are assumed to be the same in mixed and landless, and pastoral

systems.

First, the livestock production for each animal category is divided into mixed and landless, and pastoral systems on the basis of Seré and Steinfeld (1996) and Bouwman et al. (2005a). For each system, the manure is distributed over grazing and animal houses, and storage systems. Stored manure can be applied to crops and grassland. In a number of countries stored manure is used either for other purposes (mainly fuel and building materials) or is not used (Figure 3.1). We assume that this part of the manure ends outside the agricultural system, and is excluded from our analysis. The fraction of grazing animals or the fraction of the time spent by ruminants in the meadows is derived from the ratio of grass to total feed in the ration of each animal category, as presented by Bouwman et al. (2005a). For the states in the U.S.A. we used estimates from US-EPA (2006). The fraction of manure N that ends outside the agricultural system is based on data presented by Mosier et al. (1998) and assumptions for India given by Bouwman et al. (2005c).

In a small number of countries the a priori estimates of the distribution over pastoral and mixed and landless systems, and within each system over grazing and animal houses and storage, lead to unrealistic (excessive) annual input rates. In such cases, the manure is redistributed iteratively until annual input rates are less than or close to pre-defined maximum rates, which come to 250 kg ha^{-1} yr^{-1} of N in mixed and landless systems, and 125 kg ha^{-1} yr^{-1} in pastoral systems. In mixed cropland this occurs in 9 minor countries, city-states and islands, and in Egypt. In grassland systems this occurs in 22 (mostly minor) countries, all having small areas of grassland, small areas of grassland in mixed systems compared to pastoral grassland or no grassland at all. We recognize that the maximum manure N rates are not based on nutrient requirements or production figures. However, given the uncertainty in the area estimates for cropland and grassland (particularly for small developing countries, islands and city-states), livestock numbers, and grass production, we consider these assumptions to be acceptable.

In a few countries manure allocation to grazing or storage and application is not possible with the above criteria, and corrections are needed by moving manure pools within pastoral or mixed systems between cropland and grassland, or by moving manure between pastoral and mixed systems. Re-distribution of manure from one pool to another one has many consequences. For example, when manure is moved from mixed to pastoral systems or vice versa, all flows including grazing, storage and spreading and associated NH$_3$ volatilization rates need to be re-calculated.

We used data on total fertilizer from FAO (2007) on the use of different fertilizer types from IFA (2003) and fertilizer use in grassland from IFA/IFDC/FAO (2003). The difference between total use and application to grassland was assumed to be applied to cropland and evenly spread over the area of total cropland. We used sub-national data on N fertilizer use for the U.S.A. (AAPFCO/TFI 2006), and China (China National Bureau of Statistics 2006a,b, USDA 2006).

Ammonia volatilization rates for animal houses and grazing systems are taken from Bouwman et al. (1997). Volatilization from spreading of animal manure and
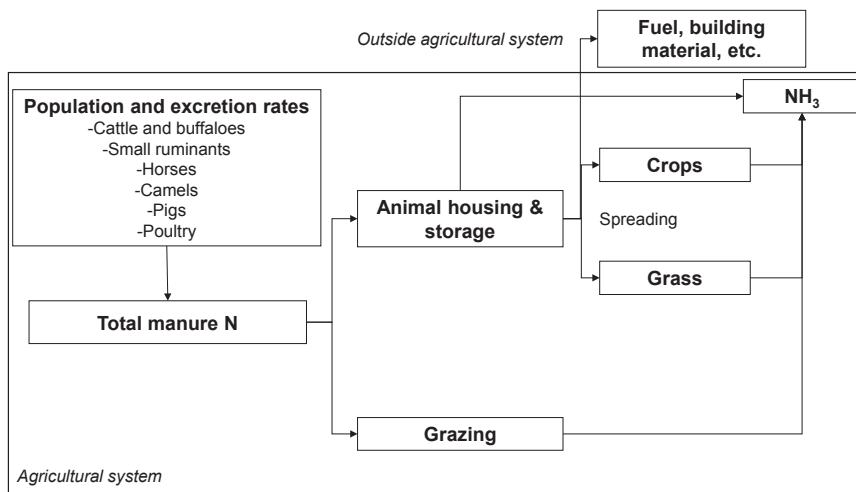
Figure 3.1: Distribution of manure over different animal manure management systems. This is done in pastoral, and mixed and landless systems.

N fertilizers is calculated with the empirical residual maximum likelihood (REML) model based on crop type, manure or fertilizer application mode, soil CEC, soil pH and climate (presented by Bouwman et al. 2002a). Fertilizer type (including animal manure) is used as a model factor for calculating NH_3 volatilization from applied fertilizers.

For manure spreading we assume that all manure is incorporated in soils in cropland and broadcast in grassland. In the model, soil incorporation of manure leads to reductions in NH_3 loss of up to 50% compared to broadcasting (Bouwman et al. 2002a). We recognize that these assumptions may not be realistic in all countries. The effectiveness of incorporation to reduce NH_3 volatilization depends on the timing of spreading and incorporation and the technique used for incorporation (Bussink and Oenema 1998).

3.2.2   Uncertainty analysis

For assessing uncertainty in the agricultural NH_3 emissions, we used ranges for all input parameters used directly in the emission inventory for calculating NH_3 volatilization (Table 3.2). Land cover is assumed to be non-varying. For animal stocks and N fertilizer use we employed a range for the input data between 90% and 110% of the default country data from FAO (2007); this is the uncertainty in the statistical data according to Bouwman et al. (1997). None of the other input parameters is based on statistical data, but inferred from various literature sources or derived from so-called "expert" estimates, as described in Bouwman et al. (2005c) and Bouwman et al. (2005d). For input parameters representing

Table 3.2: Selected parameters showing method and assumption for uncertainty analysis

Parameter description	(Abbreviation used)	Method[a]	R^a
Animal stocks	(STOCKS)	A	0.10
N fertilizer use	(FERTILIZER)	A	0.10
Maximum manure application rate	(MAX_APPLICATION_RATE)	A	0.25
Excretion in mixed and landless systems	(EXCRETION_MIXED)	A	0.25
Excretion in pastoral systems	(EXCRETION_PAST)	A	0.25
Fraction NH_3 volatilization from grazing animals in mixed and landless systems	(NH3_GRAZING_MIXED)	A	0.50
Fraction NH_3 volatilization from grazing animals in pastoral systems	(NH3_GRAZING_PAST)	A	0.50
Fraction NH_3 volatilization from housing and storage in mixed and landless systems	(NH3_STOR_MIXED)	A	0.50
Fraction NH_3 volatilization from housing and storage in pastoral systems	(NH3_STOR_PAST)	A	0.50
Fraction production in mixed and landless systems	(FR_PROD_MIXED)	B	0.25
Fraction grazing in mixed and landless systems	(FR_GRAZING_MIXED)	B	0.25
Fraction grazing in pastoral systems	(FR_GRAZING_PAST)	B	0.25
Fraction manure ending outside the agricultural system in mixed and landless systems	(FR_OUTSIDE_MIXED)	B	0.25
Fraction manure ending outside the agricultural system in pastoral systems	(FR_OUTSIDE_PASTORAL)	B	0.25
Fraction stored manure applied to grassland in mixed and landless systems	(FR_STOR_TO_GRASS_MIXED)	B	0.25
Fraction stored manure applied to grassland in pastoral systems	(FR_STOR_TO_GRASS_PAST)	B	0.25

[a] A, the range around the default value X is calculated as $[(1.0 - R)X, (1.0 + R)X]$;
B, the range around the default value X is calculated as $[\max(0.0, (X - R)), \min(1.0, (X + R))]$.

rates or volumes (e.g., excretion rates), we assume a variation in the input data of between 75% and 125% of the default value for each country, province or state. We used a range of 50% to 150% of the default for the emission factors (NH_3 volatilization from animal houses and storage systems, and from grazing animals in both pastoral and mixed and landless) For other input parameters that indicated a fraction, we established a large variation of ± 0.25 around the default value, with a minimum value of 0 and a maximum of 1 (Table 3.2).

We recognize that these ranges are debatable. However, they reflect the confidence we have in the values of the various input parameters. Parameters with narrow ranges are assumed for data obtained from statistics, and wider ranges for expert estimates. We also note that not all the parameters are independent. For example, the fraction of the livestock production in mixed and landless systems
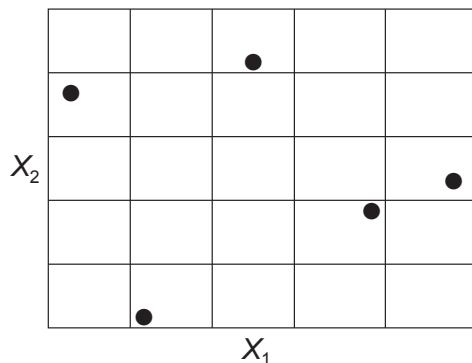
Figure 3.2: Example of a Latin hypercube with two parameters, X_1 and X_2 ($k = 2$) and $N = 5$.

influences the amount of manure in housing and storage systems. This is because there is a more common type of manure management in mixed and landless than in pastoral systems.

In our analysis the N application rates are varied in response of changing animal N excretion, amount of manure N available for spreading and fertilizer application rates. Grid-specific ammonia volatilization from manure spreading and fertilizer application are generated by the Bouwman et al. (2002a) regression model. This model predicts the fraction of N lost as NH_3 based on soil, climate and management conditions. Here we use the uncertainty of the regression model determined by Bouwman et al. (2002a).

In order to limit computational load we used the Latin Hypercube Sampling (LHS) technique (Saltelli et al. 2000). LHS offers a stratified sampling method for the separate input parameters, based on subdividing the range of each of the k parameters into disjunct equiprobable intervals based on a uniform distribution. By sampling one value in each of the N intervals according to the associated uniform distribution in this interval, we obtained N sampled values for each parameter.

The sampled values for the first model parameter are randomly paired to the samples of the second parameter, and these pairs are subsequently randomly combined with the samples of the third source, etc. Hence, within each country, province or state we apply the same set of samples (Table 3.2). This results in an LHS consisting of N combinations of k parameters (Figure 3.2). The parameter space is thus representatively sampled with a limited number of samples. Although a ratio of $N/k > 4/3$ is generally considered to be sufficient (Iman and Helton 1985), we used a ratio of 30. In this paper we use $N = 500$ and 16 input parameters ($k = 16$).

LHS can be used in combination with linear regression to quantify the uncertainty contributions of the input parameters to the model outputs (Saltelli et al. 2000, 2004). The output Y (NH_3 volatilization for any spatial unit, in this paper
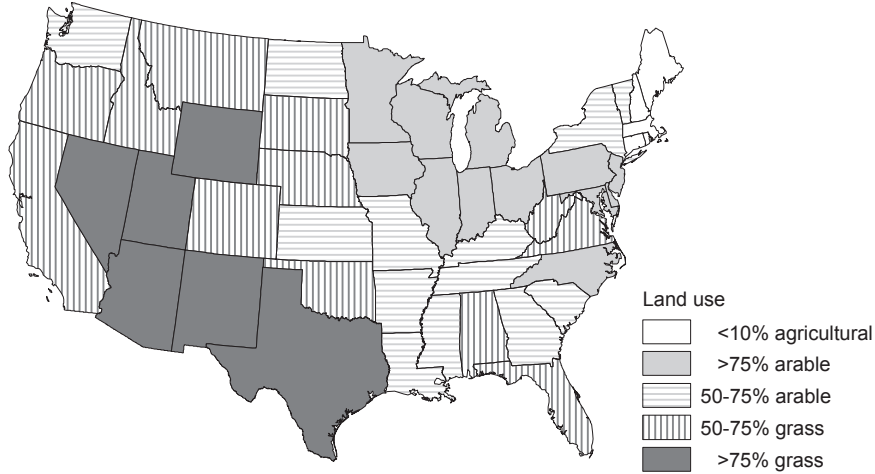
Figure 3.3: Grouping of U.S. states on the basis of land use.

country or world region) is approximated by a linear function of the parameters X_i (Table 3.2) expressed by

$$Y \quad = \quad \beta_0 + \beta_1 X_1 + \beta_2 X_2 + \cdots + \beta_n X_n + \epsilon \qquad (3.1)$$

where β_i is the so-called ordinary regression coefficient and ϵ is the error of the approximation. The quality of the regression model is expressed by the coefficient of determination (R^2), representing the amount of variation Y explained by $Y - \epsilon$. Since β_i depends on the scale and dimension of X_i, we used the standardized regression coefficient (SRC_i), which is a relative sensitivity measure obtained by rescaling the regression equation on the basis of the standard deviations σ_Y and σ_{X_i}:

$$SRC_i \quad = \quad \beta_i \frac{\sigma_{X_i}}{\sigma_Y} \qquad (3.2)$$

SRC_i can take values in the interval $[-1, 1]$. SRC_i is the relative change $\Delta Y / \sigma_Y$ of Y due to the relative change $\Delta X_i / \sigma_{X_i}$ of the parameter X_i considered (both with respect to their standard deviation σ). Hence, SRC_i is independent of the units, scale and size of the parameters, and thus sensitivity analysis comes close to an uncertainty analysis. A positive SRC_i value indicates that increasing a parameter value will cause an increase in the calculated NH_3 emission, while a negative value indicates a decrease in the emission caused by a parameter increase.

Testing for the statistical significance of SRC is done with the student t-statistic (Saltelli et al. 2000). SRC is significantly different from zero if the absolute value of the student t-statistic exceeds a value of 2.

For a given spatial unit (in this paper country or world region) the sum of squares of SRC_i values of all parameters equals the coefficient of determination

(R^2), which for a perfect fit equals 1. Hence, $SRC_i{}^2/R^2$ yields the contribution of parameter X_i to the NH$_3$ emission (Y). For example, a parameter X_i with $SRC_i = 0.1$ adds 0.01 or 1% to Y in case R^2 equals 1.

We discuss only those input parameters with an absolute SRC_i value exceeding 0.2 (contributing more than 4%) provided that their SRC_i is significant. It should be noted that this may vary between countries, with low SRC_i values for a parameter in one region, and high values for the same parameter in another country, depending on the characteristics of the agricultural system.

Although we can analyze the uncertainty of NH$_3$ emissions for any spatial unit, the aggregated results are presented here for the world as a whole, the U.S.A. and a grouping of states on the basis of land use (Figure 3.3), the India region (Afghanistan, Bangladesh, Bhutan, India, Nepal, Pakistan and Sri Lanka), the China region (China, Mongolia, Taiwan), Western Europe (Austria, Belgium, Denmark, Finland, France, Germany, Gibraltar, Greece, Iceland, Ireland, Italy, Luxembourg, the Netherlands, Norway, Portugal, Spain, Sweden, Switzerland and United Kingdom) and the Netherlands. This enables us to illustrate differences between various parts of the world, and large and small regions, with a wide variation in the characteristics of livestock and crop production systems.

3.3   Results and discussion

We will first discuss the N flows and NH$_3$ emissions, and their uncertainty. Subsequently, we will discuss the uncertainty caused by the individual input parameters. Of all results the mean is given with a range (10% and 90% percentile). All N flows and NH$_3$ emissions are expressed in units of N.

3.3.1   Uncertainty of the N flows and NH$_3$ emissions

The global N excretion by the ten animal categories amounts to 112 Tg yr^{-1} (Table 3.3) with a range of 93–132 Tg yr^{-1}. The spatial distribution of animal manure production and use thus reflects the distribution of the production of meat and milk in two broad production systems. This is presented by Bouwman et al. (2005a) on the basis of Seré and Steinfeld (1996) (Figure 3.4). According to our results, about 14% (5–26%) of the total amount of animal manure ends outside the agricultural system. This includes animal manure that is not used, or manure used as fuel, building materials, animals feed or for other purposes. Most of the total manure (66% (55–77%)) is generated in mixed and landless systems, and 20% (13–27%) in pastoral systems.

Within the mixed and landless systems, 62% (50–73%) of the manure is collected in animal houses and storage systems, and 38% (27–50%) is excreted in pastures. For the pastoral systems 94% (86–99%) is excreted in pastures. A total amount of manure N (46 (33–62) Tg yr^{-1}), collected in animal houses and storage systems in mixed and landless systems is applied primarily to croplands. Storage of manure is much less important in pastoral systems (1 Tg of N per year with a

Table 3.3: Global estimates of manure excretion in animal houses and storage systems and excretion during grazing, spreading of stored manure in cropland and grassland, and fertilizer use in cropland and grassland for the year 2000

Agricultural system	Manure/fertilizer N			
	Mean[a]	Range	Mean[a]	Range
	Gg yr^{-1}		% of total	
Distribution of manure N				
Mixed and landless systems	74 020	58 450– 92 500	66	55–77
Housing and storage	45 876	33 007– 61 799	41	31–52
Grazing	28 160	18 434– 39 040	25	17–33
Pastoral systems	22 291	14 600– 31 000	20	13–27
Housing and storage	1 378	215– 3 097	1	0– 3
Grazing	20 880	13 574– 29 718	19	12–26
Outside agricultural system	15 708	5 958– 29 155	14	5–26
Total	112 228	92 807–132 272	100	
Spreading of manure (excluding NH$_3$ loss from animal houses and storage)				
Cropland in mixed systems	30 825	21 423– 42 371	82	76–89
Grassland in mixed systems	5 874	2 454– 11 020	16	10–20
Cropland in pastoral systems	872	144– 1 917	2	1– 3
Grassland in pastoral systems	234	16– 670	1	0– 1
Total	37 805	26 320– 51 687	100	
N Fertilizer use				
Cropland	79 095	72 760– 85 416	97	-[b]
Grassland	2 787	2 564– 3 010	3	-[b]
Total	81 882	75 324– 88 426	100	

[a] The mean is given with a range (10% and 90% percentile) of all results.
[b] No range for the percentage of total N fertilizer, because fertilizer use in cropland and grassland were varied in the same way in each calculation.

Table 3.4: Global NH$_3$ emission from storage, grazing and spreading of manure in mixed and pastoral systems, and emission due to N fertilizer use in cropland and grassland for the year 2000

Source	NH$_3$-N emission (Gg yr^{-1})		Emission factor (%)	
	Mean[a]	Range	Mean[a]	Range
Housing and storage in mixed systems	9 177	5 057–13 949	20	12–28
Housing and storage in pastoral systems	272	46– 629	20	12–28
Grazing in mixed systems	2 960	1 598– 4 542	11	6–15
Grazing in pastoral systems	2 527	1 305– 4 115	12	7–17
Spreading in cropland	4 794	3 325– 6 560	15	11–20 [b,c]
Spreading in grassland	1 388	578– 2 536	23	16–30 [b]
Total animal manure	21 119	15 576–26 855	19	15–23
N fertilizer use in cropland	11 020	10 137–11 900	14	10–18 [b]
N fertilizer use in grassland	163	150– 176	6	4– 8 [b]
Total fertilizer use	11 182	10 300–12 100	14	10–18 [b]

[a] The mean is given with a range (10% and 90% percentile) of all results.

[b] Based on the uncertainty range presented by Bouwman et al. (2002a).

[c] Our estimate of the mean emission rate for manure application to crops is lower than in the original publication, because here we assumed that incorporation was the application mode for all manure instead of broadcasting.

range of 0–3 Tg).

The global NH$_3$-N emission from animal manure is about 21 (16–27) Tg yr^{-1} (Table 3.4); 44% (31–55%) of this comes from animal houses and storage systems, 27% (17–37) from grazing animals and 30% (23–38%) from spreading of animal manure. NH$_3$-N volatilization from N fertilizer use is 11 (10–12) Tg yr^{-1}, bringing the total NH$_3$-N loss for agricultural systems to 32 (27–38) Tg yr^{-1}.

Comparison of our inventory with data for 17 European countries reported to the United Nations Economic Commission for Europe (UNECE) (UNECE 2003, Vestreng 2003, Vestreng et al. 2005) shows good agreement (Figure 3.5). Our estimates tend to be somewhat lower than the reported values indicated by the total NH$_3$ emission for these countries (2412 Gg NH$_3$-N yr^{-1} in our inventory and 9% lower than the reported 2662 Gg NH$_3$-N yr^{-1}). Our estimate for the U.S.A. of 2117 Gg yr^{-1} for NH$_3$-N emission from livestock operations only (including manure spreading and excluding fertilizer use) exceeds the estimate of 1869 Gg NH$_3$-N yr^{-1} from USEPA (2005) by 13% for the year 2002.

It is clear that the uncertainty in the estimates used for this comparison include large uncertainties as well. For example, the USEPA estimate in the 1999 national emission inventory (using a different methodology) was 2954 Gg NH$_3$-N yr^{-1}, which is 58% more than the estimate for 2002, while animal populations for most animal categories increased considerably between 1999 and 2002.
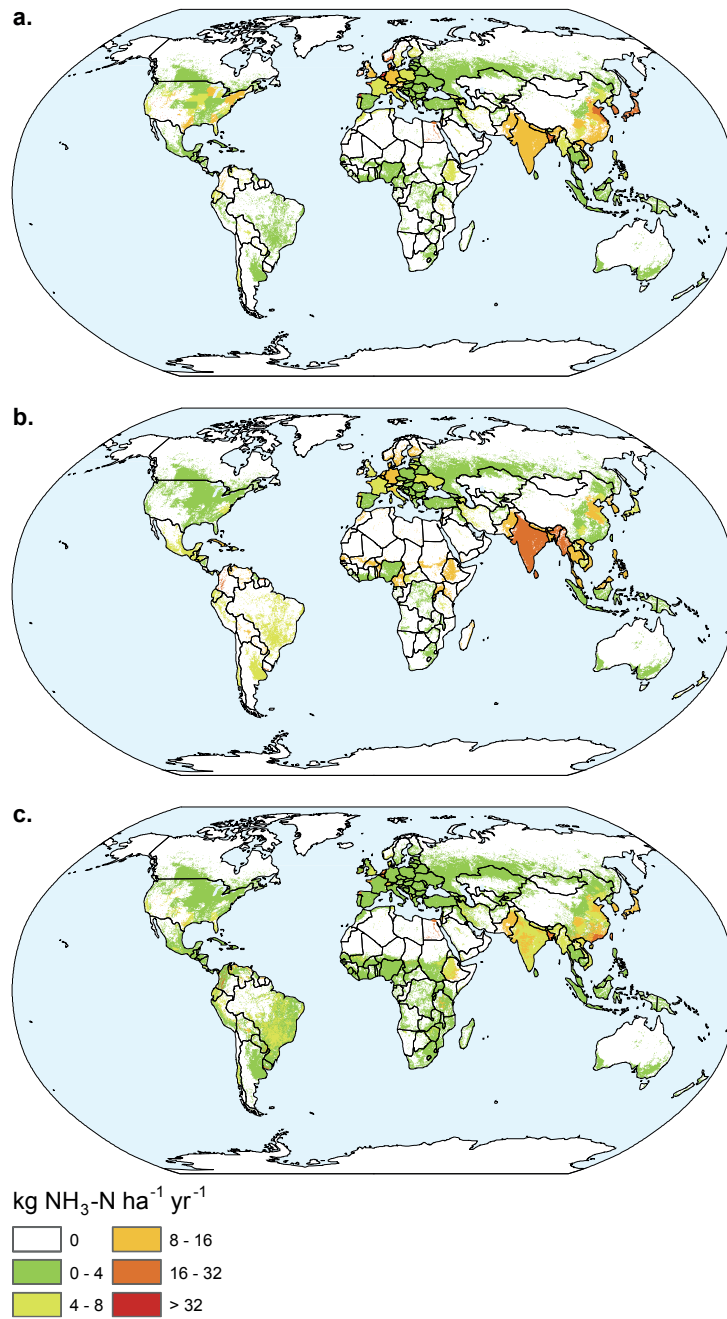
Figure 3.4: NH₃ emissions from housing, storage (top panel) and grazing (middle panel) in mixed and landless systems, and emissions due to the spreading of manure in cropping systems (bottom panel).
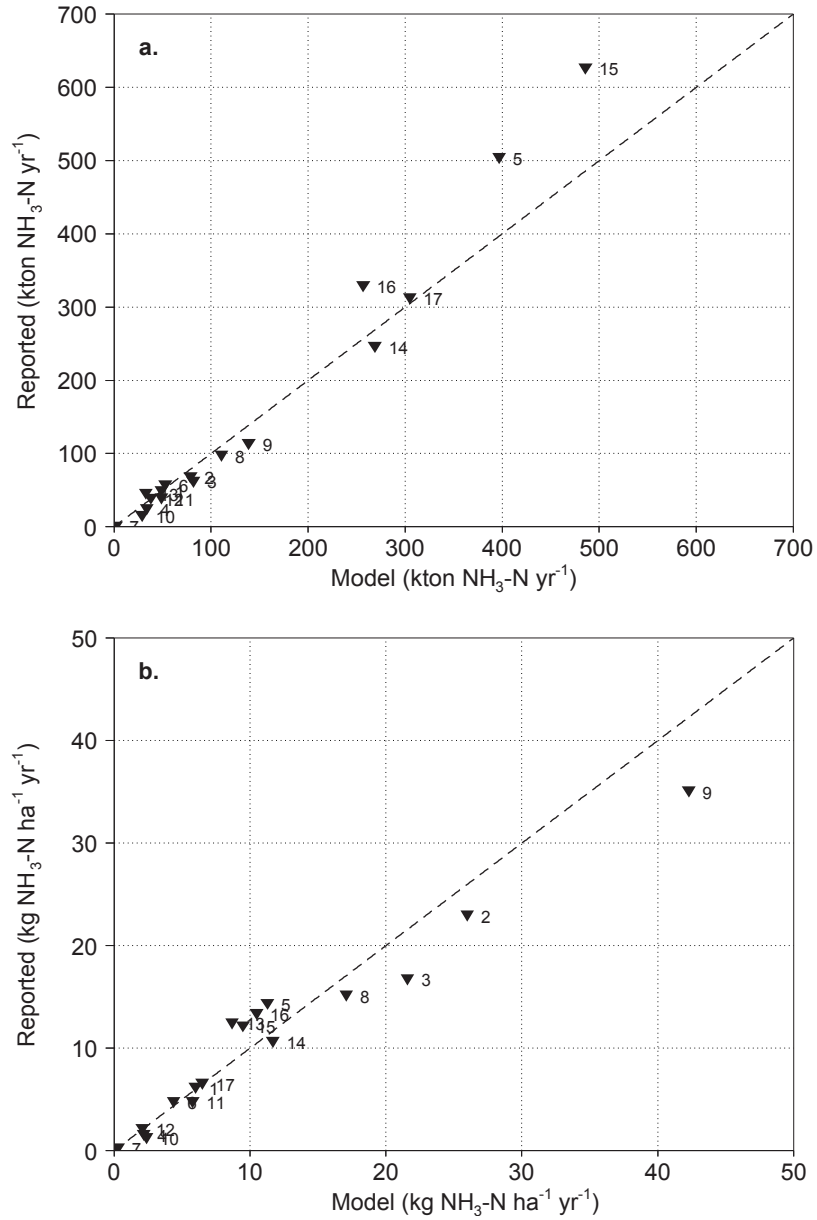
Figure 3.5: Comparison of our inventory with reported data (UNECE 2003, Vestreng 2003, Vestreng et al. 2005) for 17 European countries for a) total emission and b) emission per hectare of agricultural land. Labels indicate: 1=Austria, 2=Belgium, 3=Denmark, 4=Finland, 5=Germany, 6=Greece, 7=Iceland, 8=Ireland, 9=Netherlands, 10=Norway, 11=Portugal, 12=Sweden, 13=Switzerland, 14=UK, 15=France, 16=Italy, 17=Spain.

3.3.2   Uncertainty caused by input parameters

We will first discuss the parameters for the global-scale NH_3 emissions. The absolute SRC values calculated for the 16 parameters (Table 3.2) for the global-scale NH_3 emission results show five of them to exceed 0.2 with a significant influence (absolute value of t-statistic > 2); this is in absolute values of SRC. These are N excretion rates in mixed and landless systems ($SRC = 0.51$); NH_3 emission rates from animal houses and storage in mixed and landless systems (0.49); the fraction of manure ending outside the agricultural system in mixed and landless systems (-0.40); the fraction of grazing in mixed and landless systems (-0.32) and animal stocks (0.27) (Figure 3.6). On the global scale the contribution of each of the other parameters is less than 4%.

It is clear that the uncertainty caused by variation of excretion rates and NH_3 volatilization from animal houses and manure storage (both in mixed and landless systems) are similar, both parameters having high positive SRC values. Animal stocks have a somewhat lower positive SRC value, and the fraction of grazing in mixed and landless systems a somewhat lower, but negative, SRC value. This reflects lower NH_3 emission rates for grazing versus the cascade of confinement with NH_3 emissions from animal houses, and subsequent spreading of the stored manure with associated NH_3 emissions. The large negative SRC for the fraction of manure ending outside the agricultural system in mixed and landless systems reflects lower NH_3 emissions where more manure is excluded from the agricultural system.

The R^2 values for the linear regression models for the different regions are of the same order of magnitude (0.93–0.95 for the larger regions). Hence, we can compare the SRC values between regions (Figure 3.6). Smaller countries have a low R^2 (e.g., 0.90 for the Netherlands), so that the SRC value cannot be compared with that of other regions. This is due to the intensity of agricultural production systems and the small agricultural area in the Netherlands; changes in input parameters can cause major (nonlinear) shifts in the distribution of animal manure and N fertilizer, leading to lower R^2 values than in large regions.

The major parameters on global scale with a positive effect on agricultural NH_3 emissions are also the most important ones, with a positive effect on NH_3 emissions in all regions and countries analyzed, although in a somewhat different order. For China and India the NH_3 emission rates from animal houses and storage in mixed and landless systems is consistently the most important parameter; the N excretion rate in mixed and landless livestock production systems is the second-most important. The SRC values for animal stocks are similar in all regions (0.23–0.26, and globally 0.27).

Turning to the other parameters we see more striking differences. For example, in India the fraction of the manure ending up outside the agricultural system (mainly fuel use) is quite important, as indicated by SRC values of -0.60 for mixed and landless systems and -0.25 for pastoral systems.

The fraction of the time spent by animals grazing in meadows versus confinement in mixed and landless systems is a more important and significant deter-

Figure 3.6: *SRC* values for the 16 input parameters for the world and world regions (left), the U.S.A. as a whole and 5 groups of states in the U.S.A. (right) according to the grouping shown in Figure 3.3. Values are sorted on the information of the first column. Input parameters with *SRC* values between -0.2 and 0.2 have only a small contribution ($< 4\%$) on the total NH_3 emissions.

minant of NH_3 emission in Western Europe ($SRC = -0.52$) than on the global scale (with $SRC = -0.32$), the U.S.A. (-0.35), China (-0.31) and the Netherlands (-0.37). Finally, the fertilizer use, has an important effect ($SRC = 0.23$) in China, compared with the other regions and the world. This reflects the relatively large contribution of N fertilizer use to NH_3 emission in China (Chinese N fertilizer use come to about 25% of the global total), and dominant use of N fertilizers such as urea and ammonium bicarbonate in wetland rice systems, which leads to high NH_3 losses (Bouwman et al. 2002a).

The SRC values for most other factors reflect the characteristics of the livestock production system in each country or world region, with varying importance of red meat (mainly beef) and white meat (pork, poultry) production, and differences in the importance of pastoral systems relative to the mixed and landless systems (Figure 3.6). White meat production systems are generally landless, with typically high NH_3 emissions due to higher degrees of confinement and storage, and more manure spreading. For example, in the Netherlands the contribution of pigs and poultry to total manure N production is close to 40%, while it is only 20% in the U.S.A. This is one of the main reasons that the SRC (0.62) for NH_3 emission rates from animal houses and storage in mixed and landless systems in the Netherlands is larger than in the U.S.A. (0.55).

The SRC values portray a similar pattern for the groups of states within the U.S.A. compared to the U.S.A. as a whole (Figure 3.6). Excretion in mixed and landless systems is the major factor for the states with more grassland than arable land (SRC of 0.51–0.58). For the other states within the U.S.A., the SRC values for NH_3 volatilization from animal houses and storage systems in mixed and landless systems is the major factor (0.48–0.63). High values for storage and housing emissions indicate that both white meat production, and the confined milk and meat production, are more important in parts of the U.S.A. than on the global scale ($SRC = 0.49$). The SRC values for animal stocks range from 0.23 to 0.26 in the U.S.A., which are similar to the values calculated for the global scale and the other regions. One striking difference between the different parts of the U.S.A. is that the fraction of the production taking place in mixed and landless systems is an important factor in those states with 50–75% and with > 75% grassland coverage within their agricultural area (SRC 0.26–0.35, respectively). For the U.S.A. as a whole, this factor was not important ($SRC = 0.15$) and not significant. In these states most of the cattle are raised in pastoral systems; increasing the production of mixed and landless systems; deceasing production in pastoral systems leads to a large and significant increase in NH_3 emission.

Unfortunately there are no analyses of uncertainty of NH_3 emissions at the global scale. We therefore selected two examples of such analyses using model-based emission inventories, one for the UK and one for Canada. Our results are in agreement with a study on UK ammonia emissions using a mass-flow model (Webb and Misselbrook 2004) similar to our approach for estimating N flows and NH_3 emissions. Webb and Misselbrook (2004) found that their model was most sensitive to the length of the housing period for cattle. At the global scale and all regions included in our analysis we consistently find this to be among the most

important parameters, excretion rates logically determining the overall N flow through the agricultural system.

A Canadian study on the sensitivity of the full livestock NH_3 emission inventory (Sheppard et al. 2007) found excretion rates for cattle and pigs to be dominant. The main conclusion was that while emission factors for NH_3 volatilization were not well-characterized for Canadian conditions, it is at least as important to concentrate future research efforts to improving approaches to estimate N excretion rates. This supports our finding that N excretion rates are the first priority for improvements in global-scale NH_3 inventories.

The uncertainty caused by animal stocks can be reduced by improving the quality of data on the stocks, preferably by age class, with consistency in terms of the time of the year or season of the census. The uncertainty caused by variation in the N excretion rates shows that it is important to distinguish between pastoral, mixed and landless systems. An improvement may be achieved by using the animal productivity (milk and meat) within each system, and the feed rations and protein contents, and by using different subclasses within the animal categories based on age as a basis for calculating N excretion rates, instead of using default mean excretion rates for the animal population as a whole as done in this study. It is also important to include animal traction (for the large ruminants) in calculating the energy intake of animals.

The estimates of the NH_3 emission from animal houses and storage systems can be improved by collecting data on the type of animal housing and storage system, storage duration, temperatures as determining fermentation and changes in total ammoniacal nitrogen content, ventilation rate and exchange, manure management practices, in relation to NH_3 volatilization rates. Such systems and the corresponding NH_3 losses vary widely in different parts of the world. For example, in parts of Africa animals are kept in confined open areas during the night, while in other parts of the world animals are kept in closed stables, with varying degrees of emission reduction measures and farm management.

While we have explored the uncertainties of our emission inventory approach, there are other major uncertainties in the upscaling approach in our inventory. Some uncertainties are caused by the scarcity of data on the spatial and temporal distribution of application of synthetic fertilizers and animal manure by crop, and the prevailing management conditions. These uncertainties can be reduced in several ways. Firstly, field measurements are required, particularly in tropical agro-ecosystems; these are still under-represented in the available data from the literature. Secondly, the upscaling can be improved significantly by using subnational data on agricultural practices and management. Thirdly, studies are needed on spatial scales of fields to explore the variability of emissions, deposition and impacts within landscapes, particularly outside Europe where such data are not available. Fourthly, similar to Bouwman et al. (1997) the results of our emission inventory could be used in an atmospheric transport model to validate modeled with measured deposition rates to improve the relationships and emission factors used.

3.4   Conclusions

We have explored the uncertainties of our emission inventory. This allows for identifying and improving those input parameters with a major influence on the NH_3 emissions. Our analysis yields two major conclusions, one relating to quantification of the uncertainty and the second concerning the contribution of the various input parameters to the NH_3 emission from agricultural systems. With respect to uncertainty, we calculated a range of 27–38 (with a mean of 32) Tg yr^{-1} for the global NH_3-N emission from agricultural systems. The contribution from N fertilizer use is 10–12 (11) Tg yr^{-1} of NH_3-N (29–41%), while the contribution from livestock production to the global agricultural NH_3-N emission is 59–71% (16–27 Tg yr^{-1} with a mean of 21 Tg yr^{-1}); 31–55% of this latter emission comes from animal houses and storage systems, 17–37% from grazing animals and 23–38% from the spreading of animal manure.

We identified five parameters with an important contribution to the global NH_3 emission. Four of them relate to mixed and landless production systems (N excretion rates, NH_3 emission rates from animal houses and storage, the grazing fraction and the fraction of manure ending outside the agricultural system). The fifth parameter is the total animal stock. The N excretion rate in mixed and landless livestock production systems remains consistently the dominant parameter in the large world regions. However, in countries where landless white meat and confined milk and beef production systems make a major contribution to total manure N, the contribution of animal houses and storage systems to total agricultural NH_3 emission exceeds that of animal N excretion. Future inventories, both on the global and country scales, should focus on these factors.

Chapter 4

Global trends and uncertainties in terrestrial denitrification and N$_2$O emissions

A.F. Bouwman, A.H.W. Beusen, J. Griffioen, J.W. Van Groenigen,
M.M. Hefting, O. Oenema, P.J.T.M. Van Puijenbroek, S. Seitzinger,
C.P. Slomp, and E. Stehfest, 2013.

Abstract

Soil nitrogen (N) budgets are used in a global, distributed flow-path model with 0.5° by 0.5° resolution, representing denitrification and N$_2$O emissions from soils, groundwater and riparian zones for the period 1900 to 2000 and scenarios for the period 2000–2050 based on the Millennium Ecosystem Assessment. Total agricultural and natural N inputs from N fertilisers, animal manure, biological N$_2$ fixation and atmospheric N deposition increased from 155 to 345 Tg N yr^{-1} (Tg = teragram; 1 Tg = 10^{12}g) between 1900 and 2000. Depending on the scenario, inputs are estimated to further increase to 408 to 510 Tg N yr^{-1} by 2050. In the period 1900–2000, the soil N budget surplus (inputs minus withdrawal by plants) increased from 118 to 202 Tg yr^{-1}, and this may remain stable or further increase to 275 Tg per year by 2050, depending on the scenario. N$_2$ production from denitrification increased from 52 to 96 Tg yr^{-1} between 1900 and 2000, and N$_2$O-N emissions from 10 to 12 Tg N yr^{-1}. The scenarios foresee a further increase to 142 Tg N$_2$-N and 16 Tg N$_2$O-N yr^{-1} by 2050. Our results

indicate that riparian buffer zones are an important source of N$_2$O contributing an estimated 0.9 Tg N$_2$O-N yr^{-1} in 2000. Soils are key sites for denitrification and are much more important than groundwater and riparian zones in controlling the N flow to rivers and the oceans.

4.1   Introduction

The global nitrogen (N) cycle is driven by the fixation of inert atmospheric molecular nitrogen (N$_2$) and the formation of reactive bio-available N compounds, such as nitrate (NO$_3^-$), ammonium (NH$_4^+$) and N oxides. Humans have accelerated this cycle through fertiliser production and use, and fossil fuel combustion (Galloway et al. 2004). Denitrification is the microbial process that removes NO$_3^-$, anaerobically reducing it to nitrite (NO$_2^-$), nitric oxide (NO), the greenhouse gas nitrous oxide (N$_2$O) and N$_2$. In agricultural soils, NO$_3^-$ mainly originates from fertilisers, animal manure, crop residues and soil organic matter. The organic substrates have to be mineralized first to ammonium by heterotrophic micro-organisms, while nitrifying bacteria subsequently oxidize the NH$_4^+$ to NO$_2^-$ and NO$_3^-$. In natural ecosystems the main N sources are biological N$_2$ fixation and atmospheric deposition. In terrestrial ecosystems, denitrification occurs mainly in soils, groundwater and riparian zones. Other human-managed systems where denitrification occurs include manure storage systems, wastewater treatment plants, bioreactors and constructed or reclaimed wetlands.

Denitrification is an important process because it leads to significant N losses from agricultural systems, while, by converting NO$_3^-$ and NO$_2^-$ into gaseous N$_2$, N$_2$O and NO$_x$, denitrification reduces the problem of a global N overload on the hydrological system. In doing so, denitrification transfers this overload to the atmosphere, where N$_2$O and NO$_x$ can have negative environmental impacts.

Since denitrification is an anaerobic process, oxygen (O$_2$) is the most important regulator (Tiedje 1988). Nitrate is the electron acceptor and source of N, and C serves as the electron donor and energy source for heterotrophic denitrifying bacteria. Soil pH has a marked effect on denitrification, with lower rates under acid than under slightly alkaline conditions (Yamulki et al. 1997). Denitrification has an optimum temperature range of 25–30°C (Saad and Conrad 1993). Temperature also controls decomposition and nitrification rates (Tiedje 1988), and therefore regulates the availability of O$_2$, NO$_3^-$ and organic C. Soil denitrification and N$_2$O production and consumption are extremely variable in time and space (McClain et al. 2003) due to variability of the major regulators.

Groundwater discharge to surface waters generally consists of a mixture of water from different parts of the aquifer, characterized by a wide range of travel times. The NO$_3^-$ concentration in groundwater depends on the time of infiltration into the saturated zone, the NO$_3^-$ concentration of that water and the denitrification loss during its transport (Böhlke et al. 2002). As O$_2$ becomes limiting in the saturated zone, heterotrophic micro-organisms increasingly switch to NO$_3^-$ as an electron acceptor for the oxidation of organic C. This organic C may be present

in either dissolved form or as part of the sediment matrix. If pyrite is present in subsurface sediments, denitrification coupled to pyrite oxidation may become the dominant removal process (Zhang et al. 2009). Pyrite is a common iron disulphide mineral, and is often found in association with unconsolidated marine deposits in the terrestrial subsurface and in association with coal and shale deposits.

Riparian areas are wetlands located at the interface between the terrestrial and aquatic components of the landscape, which, due to their position, contribute to the control of nutrient and energy fluxes towards surface waters. Riparian denitrification is an important mechanism to remove N in subsurface runoff and shallow groundwater moving from uplands towards streams (Mayer et al. 2007). Similar to soils, N_2O emission from riparian zones is caused by an imbalance between N_2O production and consumption. These imbalances increase at high concentrations of O_2 and NO_3^- in the soil and at low pH (Van Den Heuvel et al. 2011). Although limited in surface area, riparian zones have been identified as hot spots for denitrification and N_2O emission especially along lower order streams (Groffman et al. 1998).

Both rates of denitrification and N_2O emissions (Bouwman et al. 2011a) have changed as a result of human intervention in the global N cycle. Future population growth and economic development may lead to further acceleration of the global N cycle. Quantifying where, when and how much denitrification occurs on the basis of measurements alone is virtually impossible (Boyer et al. 2006a). Models have therefore become essential tools. In this paper we address the possible change of terrestrial denitrification and N_2O emissions from soils, groundwater and riparian zones under past and future climate change, increasing food and energy production and agricultural intensification, using a simulation model. The term denitrification is used to indicate total nitrate reduction to N_2, N_2O and NO. Details on the data, models and scenarios used and part of the results are provided in SI 4.5.

4.2   Estimating global terrestrial denitrification and N_2O emissions

4.2.1   Data used

Spatially explicit soil budgets at 0.5° by 0.5° resolution were used for 1900, 1950, 1970 and 2000 (Bouwman et al. 2011a). Projections for the period 2000–2050 (Bouwman et al. 2009) were based on the four Millennium Ecosystem Assessment (MEA) scenarios implemented with the spatially explicit Integrated Model for the Assessment of the Global Environment (IMAGE) (Bouwman et al. 2006) (SI S4.1–S4.3). All data, including land use, soil N budgets (Bouwman et al. 2009), climate and the spatial runoff data developed for the MEA scenarios (Fekete et al. 2011) form the basis of the calculations presented here.

The four MEA scenarios are Global Orchestration (GO), Order from Strength (OS), Technogarden (TG) and Adapting Mosaic (AM). They differ in the assumed population growth, economic and industrial development, human diets, leading to

Table 4.1: N input and output terms for agricultural (agr.) and natural (nat.) ecosystems for 1900, 1950, 1970, 2000 (Bouwman et al. 2011a), and for 2030 and 2050 for the four Millennium Ecosystem Assessment scenarios (Bouwman et al. 2009)

	Agriculture							
	Fertil-iser	Man-ure[a]	Biolog-ical fixation	Depo-sition	Total N in-puts	N with-drawal	NH$_3$-N emis-sion	Soil N budget agr.
	N_{fert}	N_{man}	N_{fix}	N_{dep}		N_{withdr}	N_{vol}	N_{budget}
Year-scenario	N (10^{12}g yr^{-1})							
1900	1	36	14	6	56	34	6	16
1950	4	52	23	13	93	52	10	30
1970	29	76	30	26	161	78	18	66
2000	83	101	39	36	258	112	33	113
2050-GO	119	190	55	49	412	202	59	152
2050-TG	98	155	57	33	343	182	48	113
2050-AM	75	144	55	44	318	169	42	108
2050-OS	109	163	56	51	378	179	51	147

	Natural ecosystems			
	Biolog-ical fixation	Depo-sition		Soil N budget
	N_{fix}	N_{dep}		N_{budget}
Year-scenario	N (10^{12}g yr^{-1})			
1900	75	24		99
1950	63	23		86
1970	57	31		88
2000	53	33		86
2050-GO	52	46		98
2050-TG	46	26		72
2050-AM	51	39		90
2050-OS	49	39		88

[a] Excluding manure N that ends outside the agricultural system, such as manure stored in lagoons or used as fuel or building material (in 2000 this was 11 Tg N).

varying greenhouse gas emission pathways and climate change. GO portrays a globally connected society that focuses on global trade and economic liberalization and takes a reactive approach to ecosystem problems, but also takes strong steps to reduce poverty and inequality and to invest in public goods, such as infrastructure and education. In contrast, OS is a regionalized and fragmented world, concerned with security and protection, emphasising regional markets, paying little attention to public goods, and taking a reactive approach to ecosystem problems. TG is a globally connected world relying strongly on environmentally sound technology, using managed or engineered ecosystems to deliver ecosystem services, and taking a proactive approach to environmental problems. In AM, regional ecosystems are the focus, and local, proactive management of ecosystems is based on simple technologies. More details on the scenarios including the assumptions on N management in agriculture are provided in SI S4.3 and Table S4.1.

The annual soil N budget includes the N inputs and outputs for $0.5°$ by $0.5°$ grid cells for agricultural and natural land. N inputs include biological N_2 fixation (N_{fix}), atmospheric N deposition (N_{dep}), application of synthetic N fertiliser (N_{fert}) and animal manure (N_{man}). Outputs in the soil N budget include ammonia (NH_3) volatilisation (N_{vol}), N removal from the field through crop harvesting, hay and grass cutting, and grass consumed by grazing animals (N_{withdr}). The soil N budget (N_{budget}) was calculated as follows:

$$N_{budget} \quad = \quad N_{fix} + N_{dep} + N_{fert} + N_{man} - N_{withdr} - N_{vol} \qquad (4.1)$$

The soil N budget ignores N accumulation in soil organic matter where there is a positive budget (surplus), and also ignores N supply from soil organic matter decomposition in case of a negative budget (deficit). With no accumulation, N surpluses therefore represent a potential loss (by denitrification, surface runoff and leaching). Table 4.1 lists the global N input and output terms for agricultural land and land under natural vegetation for the different years and scenarios.

Compared with earlier work (Bouwman et al. 2009) we assumed lower biological N_2 fixation rates in natural ecosystems, based on Vitousek et al. (2013), who estimated that N_2 fixation was only 58 Tg yr^{-1} (Tg = teragram; 1 Tg = 10^{12} g) in pre-industrial times. The estimates used to calculate N fixation in natural ecosystems are based on the medium estimate for area coverage of leguminous plants and free-living N fixing bacteria (Cleveland et al. 1999). Here, we used the low estimate for the areal coverage, and this reduces global N fixation for the year 1900 from 143 to 75 Tg N yr^{-1} and for the year 2000 from 101 to 53 Tg N yr^{-1}.

4.2.2   Computing denitrification

The model used to simulate N flows from the soil via leaching through groundwater systems and riparian zones, and via surface runoff to surface water is a modification of the conceptual model of Van Drecht et al. (2003). Details on the model are given in SI S4.4–S4.8. Here a brief summary is provided.

Annual soil denitrification is calculated as a fraction of the surplus of the soil N budget corrected for surface runoff (equations S4.8, S4.9), based on temperature,
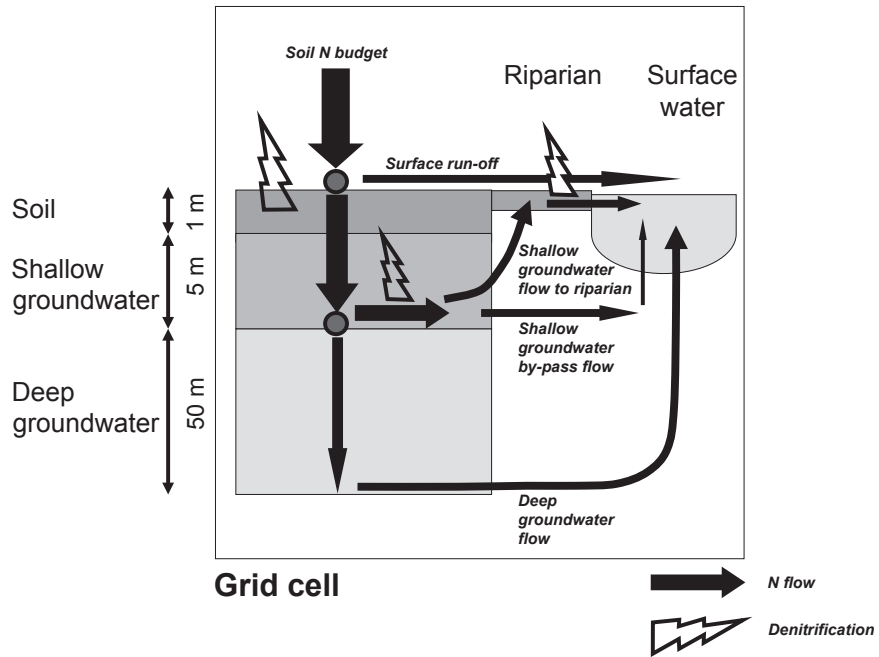
Figure 4.1: Global model with 0.5° by 0.5° resolution applied in this study, representing denitrification in soils, groundwater and riparian zones. Not all grid cells include all compartments, depending on the presence of shallow groundwater, deep groundwater and surface water.

the residence time of water and NO_3^- in the soil, soil texture, soil drainage and soil organic C. Leaching of NO_3^- from the root zone (1 m thick) to groundwater is the soil N budget minus soil denitrification and surface runoff (equation S4.14).

Two groundwater subsystems are distinguished (Figure 4.1). The shallow groundwater system represents the upper metres of the saturated zone (typically 5 m) and is characterized by short residence times before water enters local surface water at short distances, or infiltrates the deep groundwater system.

A deep system with a thickness of 50 m is defined where a deeper groundwater flow is present (SI S4.7). This deep groundwater system has longer residence times than the shallow system, as water flows to greater depths and drains to larger rivers at greater distances. We assume that denitrification is negligible in the deep groundwater system, and the modelled NO_3^- outflow from deep groundwater is thus a maximum estimate.

Riparian zones generally represent a small area of the drainage basin. However, they are critical control points for groundwater N fluxes within the watershed (Vidon and Hill 2006). In our approach all shallow groundwater (if present) in a grid cell flows towards streams (Figure 4.1). As small streams have the largest riparian ecotone length within drainage networks, these riparian zones are considered more important for groundwater N processing than those bordering larger water bodies. We ignored surface water bodies, such as lakes or larger streams, where shallow groundwater by-passes riparian zones or riparian zones are less reactive. The calculation of denitrification in riparian zones is similar to that in soils with two differences. Firstly, a biologically active layer with a thickness of 0.3 m is assumed, as riparian zones show strong vertical gradients. Denitrification rates are high in this topsoil due to the high organic matter contents. Secondly, we included the effect of pH on denitrification rates and the gaseous end-products (Figure S4.1a).

4.2.3   Computing N_2O emissions

Nitrous oxide emission from soils under natural vegetation and from agricultural land are calculated with regression models (see SI S4.6). N_2O production in groundwater is calculated using the IPCC emission factor (0.25% of the N leached from the root zone) (IPCC 2006).

Our approach for riparian areas (SI S4.8) includes corrections for the observed inhibition of denitrification at low soil pH, and for high N_2O fractions when denitrification is inhibited (Van Den Heuvel et al. 2011). With this conceptual approach, the fraction of N_2O in total denitrification is high when conditions limit denitrification, and low when conditions are optimal (Figure S4.1b). Field measurements show a wide range of N_2O emissions from riparian areas indicating that these can be both sources and sinks for N_2O. In general, fluxes from riparian areas are low compared with those from agricultural soils. Fractions of N_2O relative to the total denitrification end product (N_2+N_2O) range from 0.3 up to 73% (Table S4.4).

4.2.4 Sensitivity analysis

The sensitivity of the model was investigated using Latin Hypercube Sampling, with uncertainty ranges for 17 parameters, and expressed using the standardized regression coefficient (SRC), to compare model output of 10 variables (Table S4.5) (more details are in SI S4.10).

4.3 Results

4.3.1 Period 1900–2000

The global soil N budget has increased from 118 to 202 Tg yr^{-1} between 1900 and 2000. Hereafter, we exclude arid regions, where denitrification is assumed to be negligible (SI S4.5). Between 1900 and 2000, the global N budget thus calculated increased from 100 to 183 Tg yr^{-1} (Figure 4.2a). This increase is primarily the result of an increasing agricultural N budget, from 16 to 114 Tg yr^{-1}, and a decreasing N budget for soils under natural vegetation (from 99 to 86 Tg yr^{-1}), caused by land-use change. There are large differences between different countries. Soil N budgets increased rapidly after 1950 for industrialized countries, while rapid increases in developing countries like China and India started only from the 1970s. Small positive or even negative soil N budgets were recorded for many developing countries in Africa, Asia and South America.

Between 1900 and 2000 there has been an increase of global N fertiliser use from practically zero to more than 80 Tg yr^{-1}, N excretion by animals (from 36 to 101 Tg yr^{-1}) and biological N_2 fixation in agriculture (14 to 39 Tg N yr^{-1}). These changes in agriculture led to increasing emissions of NH_3 (6–33 Tg N yr^{-1}). Together with increasing NO_x emissions (from 7 to 38 Tg yr^{-1} according to Representative Concentration Pathways, RCP, http://www.iiasa.ac.at/web-apps/tnt/RcpDb) due to expanding fossil fuel use and industrial production, this caused rapidly increasing atmospheric N deposition (from 6 to 36 Tg yr^{-1} for agricultural land, and from 24 to 33 Tg yr^{-1} for natural ecosystems) between 1900 and 2000 (Table 4.1).

Soil denitrification largely follows the trend in the N budgets. Annual global soil denitrification increased from 45 to 79 Tg N yr^{-1} between 1900 and 2000 (Figure 4.2a), which is the result of a rapid increase in denitrification in agricultural soils (from 9 to 51 Tg N yr^{-1}), and a decrease in denitrification in soils under natural vegetation (from 36 to 28 Tg N yr^{-1}) as a result of forest conversion to agriculture. Spatial variability is large (Figure 4.3).

Between 1900 and 2000 the calculated transfer of N from soils to groundwater (51–54% of the soil N budget surplus), and denitrification in groundwater (23–24% of the N load from soil leaching) and riparian zones (11–13% of N load from shallow groundwater) were all relatively stable. The river N load increased from 38 to 65 Tg N yr^{-1} between 1900 and 2000. Long-term storage of N in groundwater increased from 0 to 10 Tg N yr^{-1} between 1900 and 2000 (Figure 4.4) and cumulative N storage in deep groundwater between 1900 and 2000 amounted to around 376 Tg. This has long-lasting effects. A calculation with zero N inputs after 2000 yields
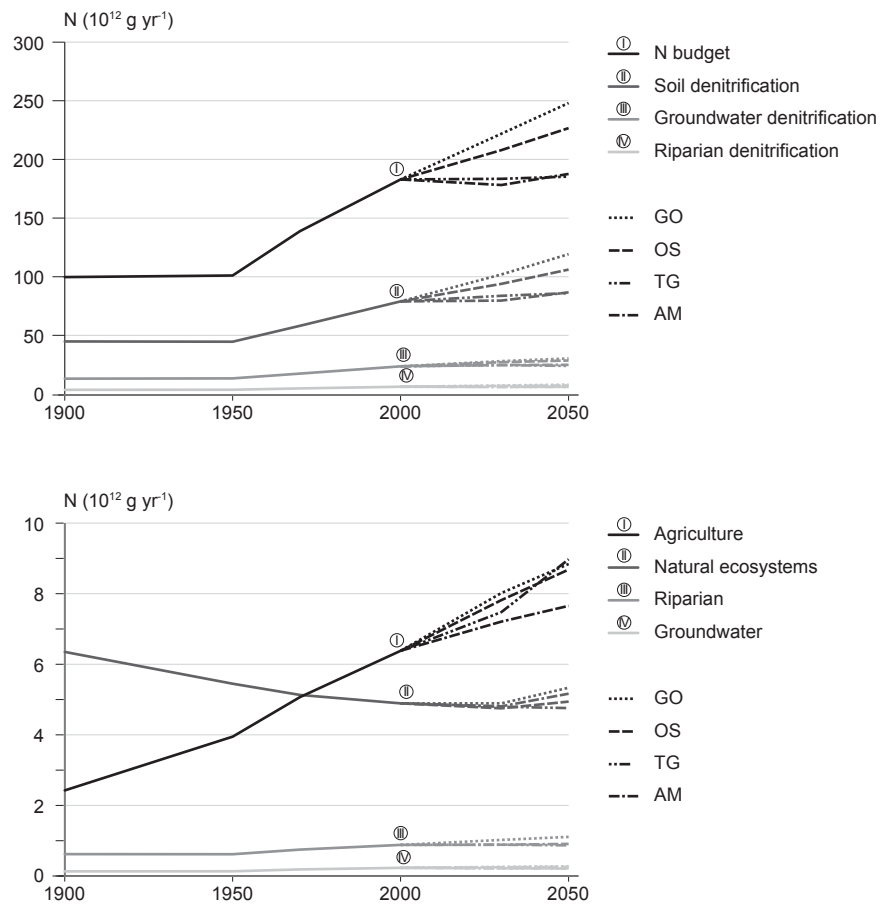
Figure 4.2: Global soil N budget (excluding arid regions) and (a) denitrification (N_2, NO and N_2O) and (b) N_2O emission for soils, groundwater and riparian zones for 1900–2000, and for 2000–2050 for the four MEA scenarios.
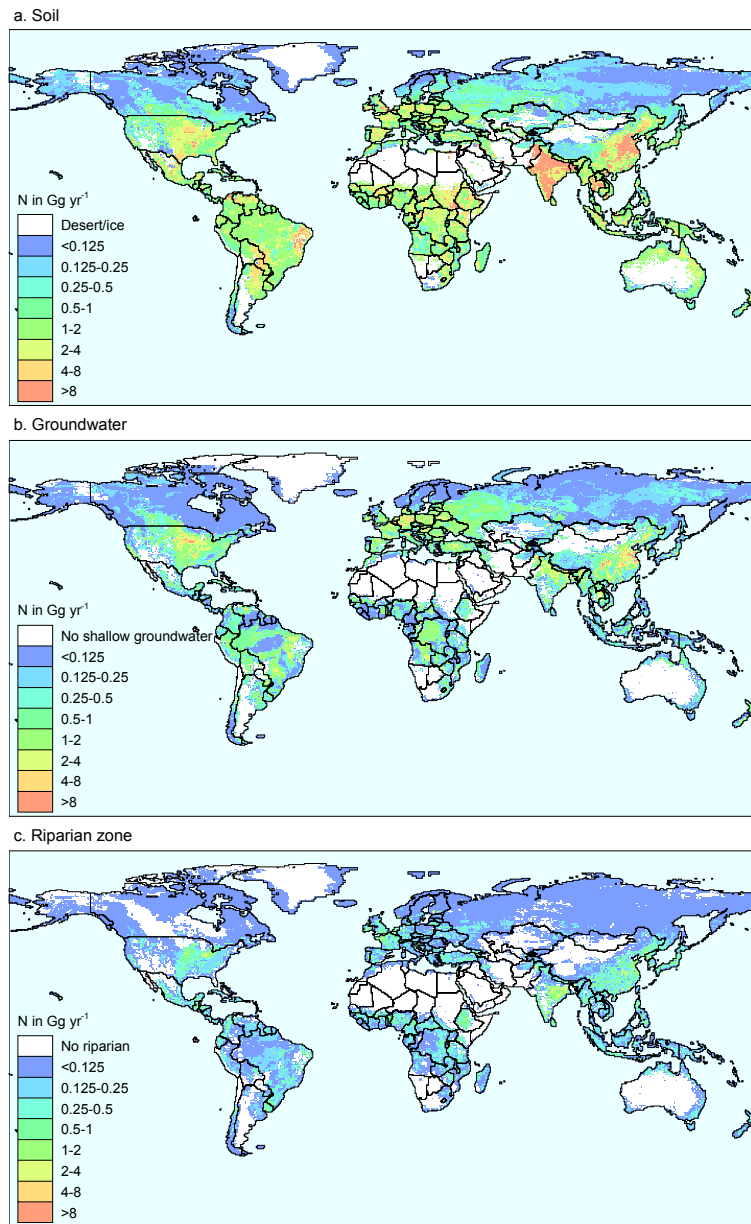
a. Soil

b. Groundwater

c. Riparian zone

Figure 4.3: Denitrification (N$_2$, NO and N$_2$O) computed for the year 2000 for (a) soils excluding arid regions, (b) groundwater, and (c) riparian zones. Denitrification is denoted as total N in Gg (10^9 g) per grid cell, because the location of outgassing for groundwater and riparian zones is not known.

an outflow from deep and shallow groundwater of 5.6 Tg N yr^{-1} in 2030 and 2.5 Tg N yr^{-1} in 2050 using climate and land cover data for the GO scenario.

Between 1900 and 2000, N_2O emissions from soils under natural vegetation decreased (from 6.3 to 4.9 Tg N_2O-N yr^{-1}), while N_2O emissions from agricultural fields rapidly increased (from 2.4 to 6.4 Tg N_2O-N yr^{-1}) (Figure 4.2b). Emissions from groundwater and riparian zone changed accordingly. The overall spatial distributions of N_2O emissions from groundwater and riparian areas are similar (Figure S4.2).

Global annual N_2O emissions from all sources (including indirect emissions from N deposition in natural ecosystems, industry and energy-related emissions, biomass burning and oceans) increased from around 13 to 17 Tg N_2O-N yr^{-1} between 1900 and 2000 (Table S4.7).

4.3.2   Period 2000–2050

The four MEA scenarios portray different futures, with the annual global N budget increasing from 202 Tg yr^{-1} in 2000 to 275 Tg yr^{-1} in 2050 in the GO scenario and to 251 Tg yr^{-1} in the OS scenario. The environment-oriented scenarios (TG and AM) show slightly decreasing trends in N budgets (Figure 4.2b). The N budget for land under natural vegetation reflects the result of forest conversion to agricultural land, particularly in the TG scenario, and increasing N inputs from atmospheric deposition (especially in the GO scenario) (Table 4.1).

The scenarios GO and OS show a rapid increase in soil denitrification, primarily due to increasing denitrification in agricultural soils with large N surpluses. The TG and AM scenarios predict a stabilisation, which reflects the balance between an increase of denitrification in agriculture and a decrease in natural ecosystems.

The transfer of N from soils to groundwater is expected to decrease from 51% to 44% by 2050, groundwater denitrification will increase from 25% to 27–29% of N leaching, while riparian denitrification will stabilize at 13% of the N inflow from groundwater in the GO scenario between 2000 and 2050. The overall N retention of the terrestrial system shows a slight increase, from 51–54% to 57% of the soil N budget in 2050, for the GO scenario, primarily due to the increase in soil denitrification. With the rapid increase of the global soil N budget, the annual N flow to rivers is therefore increasing rapidly, from 64 Tg N yr^{-1} in 2000 to 84 Tg N yr^{-1} in 2050 (GO scenario) (Figure 4.4).

The trends in groundwater and soil denitrification differ (Figure 4.2a). For example, in the GO scenario, soil denitrification increases by 51% between 2000 and 2050, while groundwater denitrification increases by 29%. In the OS scenario there is also a difference (34% increase in soil and 21% increase in groundwater denitrification). The TG and AM scenarios show a small increase of soil and groundwater denitrification after 2000 (Figure 4.2a). Long-term storage of N in groundwater ranges from 3 under AM and TG to 7 Tg N yr^{-1} under the GO scenario in 2050 (not shown).

Similar to the trends in soil and groundwater denitrification, the TG and AM scenarios predict a slight increase in riparian denitrification, while a larger increase

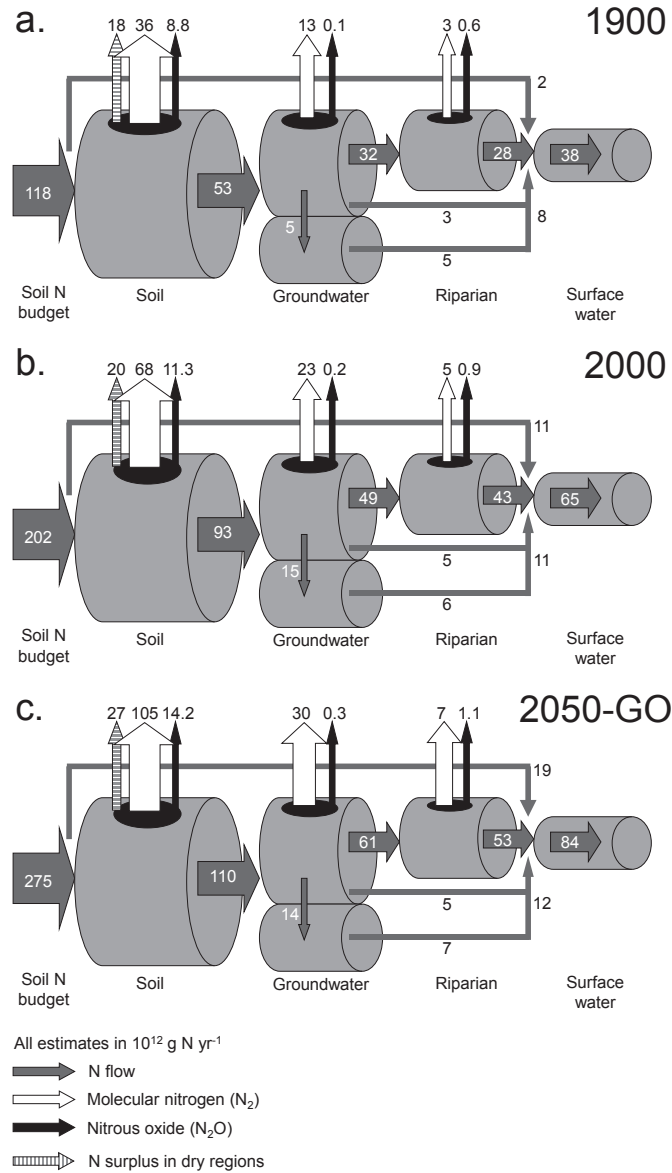**Figure 4.4**: Scheme presenting the global N flows for 1900, 2000 and 2050 for the Global Orchestration (GO) scenario through global soils, groundwater, riparian zones to surface water, and associated N$_2$ and N$_2$O production in each compartment. The sum of N$_2$ and N$_2$O equals total denitrification. The imbalance between deep groundwater inflow and outflow is caused by (temporary) storage.

is expected under the GO and OS scenarios (8 Tg N yr^{-1} in 2050) (Figure 4.2a).

The scenarios show increases in global N_2O emissions from agricultural soils from 6.4 Tg N_2O-N yr^{-1} in 2000 to 7.7 (AM scenario) and 9.0 Tg N_2O-N yr^{-1} (TG, with large areas of energy crops, see Table S4.2) (Figure 4.2b). Global N_2O emissions from all sources increase from 16.5 Tg N_2O-N yr^{-1} in 2000 to 18.0 (AM) and 19.7 (GO) Tg N_2O-N yr^{-1} in 2050 (Table S4.7).

4.3.3   Model sensitivity

Here, we discuss the standardized regression coefficient (SRC) (Table S4.6), concentrating on SRC values exceeding 0.2 (i.e., a contribution of $0.2^2 = 0.04$ or about 4% to the variation of global results). Results for a similar analysis on the regional or smaller scale or different year would yield different results, depending on the N balances and hydrological and geographical setting including climate.

Temperature, net precipitation (or runoff) and the soil N budget for natural ecosystems, cropland and grassland are important determinants for almost all global model variables, including the outflow to the rivers. The direction of the effect is variable, e.g., precipitation increase reduces soil denitrification, while temperature has a positive effect. N in surface runoff is most strongly determined by the various parameters that determine runoff and the N therein, with a strong effect of land use. For global soil denitrification, the N budget in cropland ($SRC = 0.60$) has the largest contribution, followed by the N budget in natural ecosystems (0.47) and temperature (0.50). N leaching has a similar sensitivity, but here the N budget in natural ecosystem (0.67) has the largest influence on variation, followed by N budget in cropland (0.54), and temperature (-0.43).

The outflow from shallow groundwater is most sensitive to variation of the thickness of the shallow layer ($SRC = -0.65$), the N budget in natural ecosystems ($SRC = 0.50$), net precipitation (0.31), and the N budget of cropland (0.25). The outflow from the deep groundwater system is sensitive to the half-life of nitrate (0.66), the thickness of the deep layer (-0.46), the water partitioning to the deep layer (0.27). The N inflow and bypass flow for riparian zones have sensitivities comparable to those of the N outflow from shallow groundwater.

4.4   Discussion

Our results indicate that soil denitrification is the major terrestrial N removal process, thus confirming results from other studies (e.g., Seitzinger et al. 2006). Denitrification in groundwater (23–25% of the N leaching from soils) and riparian areas (11–13% of N inflow from groundwater) is here estimated to be much less than in soils (42–45% of the soil N budget). This is because the denitrification potential in groundwater is strongly limited by the availability of electron donors. The denitrification potential in riparian areas is limited by their relatively small area, by the geohydrological setting, that determines the residence time and contact with organic–rich riparian soils.

Table 4.2: Global estimates of terrestrial denitrification

	Total N (Tg yr^{-1})	Soil	Ground-water	Riparian zone
Total				
Emery et al. (1955)	69			
Gruber and Sarmiento (1997)	175–202			
Codispoti et al. (2001)	255–450			
Soderlund and Svensson (1976)		108–160		
Tiedje (1988)[a]		105–185		
Van Drecht et al. (2003)		124	44	
Seitzinger et al. (2006)		124	44	
Canfield et al. (2010)	100			
Galloway et al. (2004)[a] (year ≈2000)	125			
Galloway et al. (2004)[a] (year 2050)	173			
This study (year 2000)[b]	109 (101–118)	79 (72–85)	24 (19–29)	6 (5–9)
This study (year 2050)[c]	110–158	80–119	24–30	6–8
Agriculture				
Hofstra and Bouwman (2005)		22–87		
This study (year 2000)		51		

[a] As estimates are based on mass balance considerations, these numbers represent total terrestrial denitrification.
[b] Standard model and range from sensitivity analysis (Tables S4.5 and S4.6).
[c] Lowest (TG) and highest (GO) scenario.

Our global soil denitrification estimates (58–79 Tg N yr^{-1} for 1970–2000) are at the low end of the range of estimates from literature (Table 4.2). The main reasons for our low estimate are the revised estimates for biological N$_2$ fixation in natural ecosystems (see Section 4.2.1), and the arid regions, where we calculated a N surplus of about 20 Tg N yr^{-1} due to our estimation of minimal denitrification under these conditions (Figure 4.4; SI S4.5).

Modelled long-term storage of N in deep groundwater systems is consistent with observations in intensively managed agricultural land in, for example, China and France (Ju et al. 2004, Ducharne et al. 2007). More generally, contamination of groundwater with nitrate is a wide-spread phenomenon (Griffioen et al. 2005) indicating that the removal rate of reactive N via denitrification has not kept pace with accelerated N cycling during the last decades.

Any global estimate of N$_2$O emissions is fraught with potential errors, and the global estimates based on different methods for croplands range from 2.1 to 3.2 Tg N$_2$O-N yr^{-1}. The estimates presented in this study are within the range of uncertainty of the various models used (Table S4.7). The results of our model indicate that riparian areas may be an important global source of N$_2$O, but to our knowledge no other global estimates for riparian zones are available for comparison. Regarding the N$_2$O fraction of the N inflow, our estimate of 0.02 is within the range of estimates in the literature (Table S4.4).

We discuss some aspects of the uncertainties in our soil N budgets, denitrification in soil, groundwater and riparian zones, and N$_2$O emissions. Comparison of different datasets on global spatially explicit soil N budgets showed that there are important differences in the spatial allocation of biological N$_2$ fixation, atmospheric N deposition, and the output terms crop N withdrawal and NH$_3$ volatilisation (Van Drecht et al. 2005). Furthermore, uncertainty analysis within the agricultural system showed that livestock N excretion rates and NH$_3$ emission rates from animal houses and storage systems are consistently the most important parameters in most parts of the world (Beusen et al. 2008).

The assumption of a static soil N pool is important in all landscape components, as illustrated by the sensitivity to variation in the N budget (Table S4.6). Accounting for the current N release from soil organic matter loss of 25 Tg yr^{-1} due to deforestation (Bodirsky et al. 2012) would increase the estimated global N budget and thus total denitrification by 12%.

One of the largest uncertainties in estimating the N cycle is the amount of reactive N that is converted to N$_2$ in the process of denitrification (Galloway et al. 2004). As the concentration of N$_2$, the largest component of the atmosphere, cannot be used to derive N$_2$ emissions in a top down approach, the only methods to estimate global denitrification are the upscaling of field measurements and the application of denitrification models. Most field methods for determining denitrification rates have serious potential flaws, and measured denitrification rates are therefore only proxies for actual denitrification rates (Groffman et al. 2006) (SI S4.1). Available methods have various problems; they change substrate availability or disturb the physical conditions of the process, lack sensitivity, or are time consuming and expensive. The measurement of denitrification is also difficult due

to the high spatial and temporal variations in terrestrial environments. Mass balance and stoichiometric approaches seem most suitable to constrain denitrification estimates at larger spatial scales (Groffman et al. 2006).

Models for estimating soil denitrification range from the scale of micro-sites and microbial dynamics to simplified factorial approaches used at global scales (Heinen 2006, Boyer et al. 2006a). Not surprisingly, model comparison reveals strong differences in the results, indicating considerable shortcomings in current knowledge of scaling effects on soil denitrification and its controlling variables in models.

Compared with other soil denitrification models (Heinen 2006), the model applied in this paper is simple, computing denitrification based on soil N budgets as a function of temperature, soil water, organic matter, texture and drainage. Apart from uncertainties in soil N budgets, the soil denitrification model is most sensitive to the N availability (soil N budget), water flux and temperature (Table S4.6).

In groundwater, the continued availability of electron donors for denitrification will depend on its source. If dissolved organic carbon (DOC) leaches from soils in significant amounts, there will be a continuous supply of electron donors with the incoming NO_3^-. The importance of DOC as an electron donor in aquifers depends on the subsurface setting (Rivett et al. 2008). Where solid phase components, such as organic matter and pyrite in the aquifer matrix are dominant (Postma et al. 1991) the electron donors are not replenished and can gradually be depleted with time (Zhang et al. 2009). Recent studies confirm the important role of pyrite for NO_3^- removal in groundwater (Rivett et al. 2008).

Due to lack of information on the availability of organic matter and pyrite, the conceptual model approach used in this paper applies lithology as a proxy for denitrification potential in groundwater, represented by the half-life of NO_3^-. The travel time determines the disappearance of NO_3^- and the outflow to surface water or riparian areas. The model assumption of no denitrification in deep groundwater may be incorrect if NO_3^- moves to deep groundwater in sedimentary deposits containing reactive organic matter and pyrite. However, the sensitivity of modelled river loading due to variation of the half-life of nitrate in deep groundwater is relatively small (Table S4.6).

Riparian processing is a spatially explicit phenomenon based on the interaction of NO_3^- in groundwater with the biologically active zone of the riparian area (Hill 1996). There are large uncertainties in our estimates of the by-pass flow (which can occur when groundwater intersects with the ground surface and emerges as a "seep"), and deep flow below the microbially active portion of soil that emerges below the river, i.e., underflow. By-pass flow through highly permeable coarse grained sediments such as gravel and sand can also significantly reduce the denitrification capacity due to shorter residence time and low organic matter contents. Effective nitrate removal in riparian zones of $> 90\%$ is predominantly found in glaciated areas where permeable surface soils are underlain with by an impermeable layer at a depth of 1–4 m (Hill 1996).

Modelling riparian processes requires spatial information on their hydrogeological conditions. Even detailed maps (1:10000 to 1:20000) to determine the topog-

raphy of riparian areas have limitations (Vidon and Hill 2006) and it is impossible to know the location of riparian areas at the 0.5° by 0.5° resolution of this study. With all the simplifications in the simulation of the N inflow to riparian areas and denitrification, the model results are a first attempt to quantify denitrification and N_2O emissions, showing strong sensitivity to total water flow, soil N budget, and N inflow from shallow aquifers (Table S4.6).

Turning to N_2O emissions, we see several causes of uncertainty. The fraction of N lost as N_2O from nitrification, nitrifier denitrification or denitrification often shows a strong non-linear relationship with the controlling factors, which makes upscaling difficult. In order to estimate direct N_2O emissions, measurement data at the field scale have been used to derive relationships between controlling factors and N_2O emissions with statistical techniques (Stehfest and Bouwman 2006, Bouwman et al. 2002b), neural networks (Ryan et al. 2004), or using process-based models (Farquharson and Baldock 2008). Contrary to N_2, the emissions of N_2O at larger scales can be evaluated with top-down (inverse) modelling of N_2O emissions (Corazza et al. 2011).

The statistical approach used here to estimate N_2O emission from soils (Bouwman et al. 2002b) has a model uncertainty of -40 to $+70\%$. This uncertainty does not include the potential errors related to the upscaling and the spatial data used that are difficult to quantify. Our estimate for N_2O emissions from groundwater under agricultural soils is lower than that based on the IPCC method (IPCC 2006), primarily because our simulated N leaching of N inputs for 2000 is smaller (24%) than that proposed by IPCC (30%). The IPCC emission factor approach represents the combined emission from groundwater and riparian zones, although recent studies (e.g., Vilain et al. (2011)) suggest that the N_2O production in groundwater alone may be close to the IPCC value. In addition, the IPCC approach represents the N_2O emission from N during its travel time in groundwater; this is not consistent with the denitrification and N_2O emission estimates for soil and riparian zones, which represent a specific year. However, with half-life values of 2–5 years, and assuming that the year-to-year change of the N inflow to groundwater is small, this error is acceptable when compared with all other uncertainties.

Predictions of N_2O emissions from riparian zones are complex, as denitrification controls both the production and the consumption of this greenhouse gas. Uncertainty exists on how N_2O transported by shallow groundwater through the subsoil contributes to the surface N_2O emissions from riparian zones. As groundwater comes to the soil surface in these zones, outgassing of N_2O can be significant. However, soil conditions in riparian zones can be favourable for denitrifier activity, and significant N_2O consumption may occur in the topsoil (DeSimone et al. 2010). N_2O can also result from nitrification or nitrifier denitrification (Wrage et al. 2001), particularly at the upland edges of the riparian zones where soil conditions are oxic and ammonium concentrations high due to direct agricultural inputs. Furthermore, soil acidification from nitrifier activity may lead to an increase in N_2O emission by reducing denitrifier N_2O consumption.

4.5 Concluding remarks

Despite large uncertainties in our model approach, we conclude that N removal by denitrification as a fraction of the N inflow has not changed in the continuum formed by soil-groundwater-riparian zones during the 20$^{\text{th}}$ century. This implies that the transfer of N from land to surface water has increased roughly at the same rate as the increase in the N budget.

In terrestrial systems, denitrification in soils is the primary N removal process, followed by groundwater and riparian zones. Our model shows that the removal of reactive N via denitrification from terrestrial and aquatic systems has not kept pace with accelerated N inputs into agriculture.

Our attempt to simulate riparian denitrification and N$_2$O emission is the first ever done, and indicates that riparian zones may be an important landscape element for N removal at the global level; given the conditions in many riparian areas, with incomplete denitrification accompanied by high fractional N$_2$O production, global N$_2$O emissions from riparian areas may exceed those from groundwater.

The scenarios indicate that the gradual increase of reactive N transfer to surface waters and the atmosphere will continue in the coming decades, unless drastic improvements in agricultural management occur. This may have important consequences for biogeochemistry in river networks and coastal seas, inducing a series of processes, such as stimulation of plant growth, algal blooms, decomposition, burial, and hypoxia.
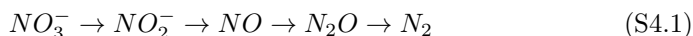
Acknowledgments

Supporting information

S4.1   Denitrification and N$_2$O flux measurements

Denitrification is mainly a microbiological process in which nitrate (NO$_3^-$) is anaerobically reduced to nitrite (NO$_2^-$), nitric oxide (NO), the greenhouse gas nitrous oxide (N$_2$O) and dinitrogen (N$_2$):

$$NO_3^- \rightarrow NO_2^- \rightarrow NO \rightarrow N_2O \rightarrow N_2 \tag{S4.1}$$

Soil denitrification rates are generally estimated using indirect methods, because of the near impossibility to measure accurately the increase in N$_2$ concentration produced by denitrification relative to the high ambient atmospheric N$_2$ concentration. The conventional method is the measurement of NO$_3^-$ disappearance, assuming that this removal is exclusively through denitrification. This is not correct when other loss pathways play a role, for example leaching or NH$_3$ volatilisation. A second common procedure is the acetylene inhibition technique (Ryden et al. 1978), in which acetylene inhibits the final step in denitrification, and denitrification is assumed to be equivalent to N$_2$O production. However, this technique can both significantly underestimate (Bollmann and Conrad 1997) or overestimate (Schmidt et al. 2001, Wrage et al. 2004) denitrification rates. A third method makes use of ^{15}N labelled NO$_3^-$ and the measurement of ^{15}N$_2$O and ^{15}N$_2$. Under controlled conditions, measurements can be made of the increase of N$_2$O and N$_2$ following the replacement of the soil atmosphere by helium. A fourth approach is the N-balance method, where the N inputs and outputs for a given area can be measured and, generally, denitrification is the unaccounted for part of the balance. The N balance method generally comprises a prolonged period (for example, a complete growing season). Hofstra and Bouwman (2005) showed that the N balance approach generally yields higher denitrification estimates than other techniques. The uncertainty in the determination of each of the terms in the N balance is high and the overall result of the balance is sensitive to minor variation in inputs or outputs, and not always all sources and sinks are taken into account. Finally, under controlled conditions in the laboratory, the end products of denitrification, including N$_2$, can be measured directly, following replacement of the ambient N$_2$-rich air in incubation vials with helium (He). However, the results of such controlled-condition experiments are difficult to translate to practical conditions in the field (Qin et al. 2012).

Generally, the concentration of excess N$_2$ produced by denitrification in groundwater is estimated by comparing the measured concentrations of Argon (Ar) and N$_2$ with those expected from atmospheric equilibrium, assuming that Ar is a stable component (Blicher-Mathiesen et al. 1998, Böhlke et al. 2002). Measuring excess N$_2$ is complicated by variations in recharge temperatures and the entrapment of air bubbles near the groundwater surface, leading to varying background concentrations of dissolved N$_2$ in groundwater due to contact of the water with atmospheric air (Böhlke et al. 2002) or losses by degassing (Blicher-Mathiesen et al. 1998). Local fluxes of N$_2$O are often measured in vented, closed chambers (Hutchinson and Livingston 2001, Levy et al. 2011) using a gas chromatograph with ECD detector or with an infrared gas analyser (IRGA) (Paul et al. 2012, Alluvione et al. 2010, Velthof et al. 1996). If the flux chambers are attached to pre-installed, permanent frames this will minimize disturbance of the soil structure and reduce errors due to soil compaction and forced diffusion.

S4.2   The IMAGE model

The objective of the Integrated Model for the Assessment of the Global Environment (IMAGE) version 2.4 model (Bouwman et al. 2006) is to explore the long-term dynamics of global environmental change. The model consists of several modules. General economic and demographic trends for 24 world regions drive human activities. Regional energy consumption, energy efficiency improvement, fuel substitution, supply and trade of fossil fuels and renewable energy technologies are simulated with the The IMAGE Energy Regional Model (TIMER) model (Van Vuuren et al. 2006) to calculate energy production, energy use, industrial production, emissions of greenhouse gases, ozone precursors and sulphur. Ecosystem, crop and land-use models are used to compute land use on the basis of regional consumption, technological developments, production and trading of food, animal feed, fodder, grass and timber, and local climatic and terrain properties.

Greenhouse gas emissions from land-use change, natural ecosystems and agricultural production systems are computed as well as the biosphere-atmosphere exchange of carbon dioxide (CO$_2$). The atmospheric and ocean models calculate changes in atmospheric composition by employing the emissions and by taking oceanic CO$_2$ uptake and atmospheric chemistry into consideration. Subsequently, changes in climate are computed by resolving oceanic heat transport and changes in radiative forcing by greenhouse gases and aerosols. The ecosystem and crop growth models of IMAGE account for feedbacks of climate change and rising atmospheric CO$_2$.

Although IMAGE 2.4 is global in application (with data and scenarios at the scale of world regions), it performs many of its calculations on a terrestrial 0.5° by 0.5° resolution (crop yields and crop distribution, land cover, land-use emissions, nutrient surface balances and C cycle). Data from many different sources are used to calibrate the energy, climate and land-use variables over the 1970–2000 period.

Contrary to the original Millennium Ecosystem Assessment (MEA) scenarios

described in Alcamo et al. (2006) where IMAGE version 2.2 was used (IMAGE-team 2001), here we use an update (version 2.4) of the IMAGE model for simulating land use and nutrient distributions (Bouwman et al. 2006). The major improvements relevant to this study, compared to IMAGE 2.2, include the new land-cover inventory (Klein Goldewijk et al. 2006), the base year which was updated to the year 2000 (1995 in IMAGE 2.2), the modeling of land-use changes based on a larger number of world regions, an improved description of livestock production systems and the calculation of surface nutrient balances (Bouwman et al. 2006).

S4.3   Scenarios

The four scenarios of the Millennium Ecosystem Assessment (MEA) (Alcamo et al. 2006) describe contrasting pathways for the future development of human society and ecosystems. The MEA scenarios are therefore a good basis for expanding them with scenarios for future agricultural nutrient inputs and outputs and nutrient cycling in natural ecosystems. The scenarios are described in comprehensive datasets including greenhouse gas emissions, climate, land use, etc. Climate data were used by Fekete et al. (2011) to compute the runoff fields that, together with land use and climate, form the basis of the calculations in this study.

The Millennium Ecosystem Assessment used four scenarios: Global Orchestration (GO), Order from Strength (OS), Technogarden (TG) and Adapting Mosaic (AM). GO portrays a globally connected society that focuses on global trade and economic liberalisation and takes a reactive approach to ecosystem problems, but also takes strong steps to reduce poverty and inequality and to invest in public goods, such as infrastructure and education.

In contrast, OS is a regionalised and fragmented world, concerned with security and protection, with the emphasis primarily on regional markets, paying little attention to public goods, and taking a reactive approach to ecosystem problems.

TG is a globally connected world relying strongly on environmentally sound technology, using highly managed, often engineered, ecosystems to deliver ecosystem services, and taking a proactive approach to the management of ecosystems in an effort to avoid problems.

In AM, the fourth scenario, regional watershed-scale ecosystems are the focus of political and economic activity. Local institutions are strengthened and local ecosystem management strategies are common; societies develop a strongly proactive approach to the management of ecosystems based on simple technologies. The major drivers relevant to land use and agriculture are discussed below.

Based on the scenario storylines and attitude towards the environment, the regional scenarios for the use of N fertilisers are based on efficiency of N use in crop production (Table S4.1). This efficiency is the ratio of harvested crop dry matter production to N inputs (Bouwman et al. 2009). For constructing the regional scenarios for fertiliser use, we distinguish countries with a current nutrient surplus (industrialised countries and a number of developing countries like China

Table S4.1: Main drivers of ecosystem change for the Millennium Ecosystem Assessment scenarios from Alcamo et al. (2006) and assumptions for agricultural nutrient management

	Global Orchestration (GO)	Order from Strength (OS)	Technogarden (TG)	Adapting Mosaic (AM)
Brief description				
	Globalisation, economic development, reactive approach to environmental problems	Regionalisation, fragmentation security, reactive approach to environmental problems	Globalisation, environmental technology, proactive approach to environmental problems	Regionalisation, local ecological management with simple technology, proactive approach to environmental problems
General trends				
World population (billion)	Low 2000: 6.1 2030: 7.7 2050: 8.2	High 2000: 6.1 2030: 8.6 2050: 9.7	Medium 2000: 6.1 2030: 8.2 2050: 8.9	High 2000: 6.1 2030: 8.5 2050: 9.6
Income (annual per capita GDP growth rate)	High 2000–2030: 2.6% 2030–2050: 3.0%	Low 2000–2030: 1.6% 2030–2050: 1.3%	High 2000–2030: 2.1% 2030–2050: 2.6%	Medium 2000–2030: 1.8% 2030–2050: 2.2%
Global GHG emissions (Gt C-eq yr^{-1})	High 2000: 9.8 2050: 25.6	High 2000: 9.8 2050: 20.3	Low 2000: 9.8 2050: 7.1	Medium 2000: 9.8 2050: 18.0
Global mean temperature increase (°C)	High 2000: 0.6 2030: 1.4 2050: 2.0	High 2000: 0.6 2030: 1.3 2050: 1.7	Low 2000: 0.6 2030: 1.3 2050: 1.5	Medium 2000: 0.6 2030: 1.4 2050: 1.9
Per capita food consumption	High, high meat	Low	High, low meat	Low, low meat
Agricultural trends[a]				
Productivity increase	High	Low	Medium-high	Medium
Energy crops	4% of cropland area in 2050	1% of cropland area in 2050	28% of cropland area in 2050	2% of cropland area in 2050
Fertiliser use and efficiency	No change in countries with a surplus; rapid increase in N and P fertiliser use in countries with soil nutrient depletion (deficit)	No change in countries with a surplus; slow increase in N and P fertiliser use in countries with soil nutrient depletion (deficit)	Rapid increase in countries with a surplus; rapid increase in N and P fertiliser use in countries with soil nutrient depletion (deficit)	Moderate increase in countries with a surplus; slow increase in N and P fertiliser use in countries with soil nutrient depletion (deficit); better integration of animal manure and re-cycling of human N and P from households with improved sanitation but lacking a sewage connection.

[a] Scenarios on the scale of 24 world regions of the IMAGE model; a downscaling procedure is used to construct spatially explicit scenarios with 0.5° by 0.5° resolution. When aggregated to the country scale, estimates for fertiliser use and livestock production reflect differences between countries in FAO's Agriculture Towards 2030 (Bruinsma 2003); the scenario outcomes vary around the FAO values.

and India), and countries with a deficit, i.e., the crop uptake exceeds the inputs leading to degradation of soil fertility.

Fertiliser use efficiency is assumed to increase to a varying degree in industrialised countries, China and India, while in most developing countries fertiliser use will increase (with an apparent decrease in fertiliser use efficiency, similar to developments in industrialised countries in the period 1950–1980 (Dobermann and Cassman 2005, Table S4.1)).

We used regional data from the FAO Agriculture Towards 2030 study (Bruinsma 2003) as a guide. Increasing fertiliser use efficiency in industrialised countries is most rapid in the Technogarden and Adapting Mosaic scenarios, based on the attitude towards environmental issues. Also, increasing fertiliser use to avoid soil degradation in developing countries is more important in the Technogarden and Adapting Mosaic scenarios.

The scenarios assume, depending on the economic growth, a gradual increase of livestock production in mixed and industrial systems relative to pastoral systems, leading to increasing amounts of manure stored in animal houses and storage systems.

The scenarios differ in the relative importance of pork and poultry versus ruminant meat, mixed and industrial production, and grazing versus the concentrated feed-dependent production of ruminants. Apart from the impact of such changes on the productivity, the milk and meat production per animal is also assumed to increase; consequently, the excretion per unit of product will decrease. These changes are most rapid in the Global Orchestration and Technogarden scenarios. Improved manure recycling in the total agricultural system is assumed to play an important role in the Adapting Mosaic scenario. Lower meat and milk consumption is a typical feature of the Technogarden scenario compared to the Global Orchestration scenario.

S4.4   Hydrology

Total runoff is divided into surface runoff and excess water flow:

$$Q_{\text{tot}} = Q_{\text{sro}} + Q_{\text{eff}} \tag{S4.2}$$

where Q_{sro} is surface runoff (m yr^{-1}), Q_{eff} is the excess water flow from the soil (m yr^{-1}). Surface runoff is a large part of total runoff in steep areas or in flat terrain with sealed surfaces (e.g., urban areas) or in areas covered with an impermeable topsoil. In our model this is reflected by a slope dependent runoff factor ($f_{\text{Qsro}}(slope)$, no dimension), which is fitted to the slope-runoff classification for unconsolidated sediments according to Bogena et al. (2005):

$$f_{\text{Qsro}}(S) = 1 - e^{-0.00617 \max[1, S]} \tag{S4.3}$$

where S is the slope in m km^{-1}, $f_{\text{Qsro}}(S)$ (no dimension) is the median value within each 0.5° grid cell; median value is obtained from 90 by 90 m resolution

digital elevation map. Factors that reduce surface runoff are land use and soil texture (Velthof et al. 2009, 2007). Apart from slope, surface runoff is influenced by soil texture and land use ($f_{\text{Qsro}}(texture)$ and $f_{\text{Qsro}}(landuse)$, respectively, both dimensionless):

$$f_{\text{Qsro}} \;\; = \;\; f_{\text{Qsro}}(slope)\, f_{\text{Qsro}}(texture)\, f_{\text{Qsro}}(landuse) \tag{S4.4}$$

$$Q_{\text{sro}} \;\; = \;\; f_{\text{Qsro}}\, Q_{\text{tot}} \tag{S4.5}$$

Surface runoff reduction is smallest (10%) in soils with very fine topsoil texture ($f_{\text{Qsro}}(texture) = 0.9$), somewhat larger (25%) for loam and sandy loam ($f_{\text{Qsro}}(texture) = 0.75$), and largest (75%) for coarse sand and peat ($f_{\text{Qsro}}(texture) = 0.25$). Furthermore, surface runoff is not limited in arable land ($f_{\text{Qsro}}(landuse) = 1.0$), reduced by 75% in grassland ($f_{\text{Qsro}}(landuse) = 0.25$) and 87.5% in natural vegetation ($f_{\text{Qsro}}(landuse) = 0.125$).

After infiltration, groundwater flows laterally to ditches and streams or vertically to deeper groundwater layers. This process is described by distinguishing two groundwater subsystems, similar to Van Drecht et al. (2003), De Wit and Pebesma (2001) and De Wit (2001). The shallow groundwater system represents the upper 5 metres of the saturated zone and is characterised by short residence times before water enters local surface water at short distances or infiltrates the deep groundwater system.

A deep system with a thickness of 50 m (Meinardi 1994) is defined where a deeper ground water flow is present. Deep groundwater is assumed to be absent (i) in areas with non-permeable, consolidated rocks; (ii) in the presence of surface water (rivers, lakes, wetlands, reservoirs); (iii) in coastal lowlands (< 5 m above sea level), where we assumed (artificial) drainage or high groundwater levels. This deep groundwater system has longer residence times than the shallow system, as water flows to greater depths and drains to larger rivers at greater distances.

The excess water flow Q_{eff} is divided into interflow (shallow system) and groundwater runoff (deep system):

$$Q_{\text{eff}} \;\; = \;\; Q_{\text{tot}} - Q_{\text{sro}} \;\; = \;\; Q_{\text{int}} + Q_{\text{gwb}} \tag{S4.6}$$

where Q_{int} is interflow through the shallow system (m yr^{-1}), and Q_{gwb} is the groundwater runoff through the deep system (m yr^{-1}). Q_{gwb} is calculated from the fraction f_{Qgwb} of Q_{eff} that flows towards the deep system:

$$Q_{\text{gwb}} \;\; = \;\; f_{\text{Qgwb}}(p)\, Q_{\text{eff}} \tag{S4.7}$$

where p is the effective porosity (-) (Table S4.2). We assume that the deep layer (if present) has the same soil characteristics as the surface layer.

S4.5   Soil denitrification

For positive values of the N budget (equation 4.1), denitrification in the top 1 m of soil (or less for shallow soils) is calculated as a fraction $f_{\text{den,soil}}$ (Van Drecht

Table S4.2: Porosity (p), the fraction of excess water flowing to deep groundwater ($f_{\mathrm{Qgwb}}(p)$), and the half life of NO_3^- in groundwater ($dt50_{\mathrm{den}}$) for different lithological classes

Lithological class[a]	Porosity (p) ($\mathrm{m^3\ m^{-3}}$)	$f_{\mathrm{Qgwb}}(p)$ [b] (-)	$dt50_{\mathrm{den}}$ (year)
1. Alluvial deposits	0.15	0.50	2
2. Loess	0.20	0.67	5
3. Dunes and shifting sands	0.30	1.00	5
4. Non-Semiconsolidated sedimentary	0.30	1.00	5
5. Evaporites	0.20	0.67	5
6. Carbonated consolidated sedimentary	0.10	0.33	5
7. Mixed consolidated sedimentary	0.10	0.33	5
8. Silici-clastic consolidated sediment[c]	0.10	0.33	1
9. Volcanic basic	0.05	0.17	5
10. Plutonic basic	0.05	0.17	5
11. Volcanic acid	0.05	0.17	5
12. Complex lithology	0.02	0.07	5
13. Plutonic acid	0.02	0.07	5
14. Metamorphic rock	0.02	0.07	5
15. Precambrian basement	0.02	0.07	5

[a] Lithological classes as defined by Dürr et al. (2005).
[b] $f_{\mathrm{Qgwb}}(p) = p/0.3$, 0.3 being maximum porosity.
[c] Weathered shales containing pyrite.

Table S4.3: Denitrification fractions for soil texture, soil organic carbon and soil drainage. Source: Van Drecht et al. (2003)

Soil texture class	f_{text} (-)	Soil drainage	f_{drain} (-)	Soil organic carbon content	f_{SOC} (-)
Coarse	0.0	Excessively-well drained	0.0	$< 1\%$	0
Medium	0.1	Moderate well drained	0.1	$1 - 3\%$	0.1
Fine	0.2	Imperfectly drained	0.2	$3 - 6\%$	0.2
Very fine	0.3	Poorly drained	0.3	$6 - 50\%$	0.3
Organic	0.0	Very poorly drained	0.4	Organic	0.3

et al. 2003):

$$N_{\text{den,soil}} = f_{\text{den,soil}} \max(0, N_{\text{budget}} - N_{\text{sro}}) \tag{S4.8}$$

where N_{sro} is the N loss by surface runoff, calculated on the basis of slope using the approach of Bogena et al. (2005), and further modified by land use and soil texture, i.e., factors that reduce surface runoff according to Velthof et al. (2009, 2007):

$$N_{\text{sro}} = f_{\text{Qsro}} C_{\text{sro}} N_{\text{inp}} \tag{S4.9}$$

where N_{sro} is the N in surface runoff (kg km^{-2} yr^{-1}), N_{inp} is the N input from fertiliser and animal manure including spreading and grazing, biological N$_2$ fixation by leguminous crops, atmospheric deposition (kg km^{-2} yr^{-1}) and f_{Qsro} is the overall runoff fraction (equation S4.4). C_{sro} (no dimension) is a calibration constant (0.5) so that N_{sro} results match the model of Velthof et al. (2009, 2007).

$$f_{\text{den,soil}} = \min\left[(f_{\text{climate}} + f_{\text{text}} + f_{\text{drain}} + f_{\text{soc}}), 1\right] \tag{S4.10}$$

where f_{climate} (-) represents the effect of climate on denitrification rates, combining the effects of temperature and residence time of water and NO$_3^-$ in the root zone; f_{text}, f_{drain}, and f_{soc} (-) (Table S4.3) are factors representing the effects of soil texture, soil drainage and soil organic C content, respectively. The factor f_{climate} is calculated as:

$$f_{\text{climate}} = f_{\text{K}} T_{\text{r,so}} \tag{S4.11}$$

where f_{K} (-) is the temperature effect on denitrification, $T_{\text{r,so}}$ (yr) is the mean annual residence time of water and NO$_3^-$ in the root zone.

The temperature effect f_{K} is calculated according to the Arrhenius equation (Firestone 1982, Shaffer et al. 1991, Kragt et al. 1990):

$$f_{\text{K}} = 7.94 \cdot 10^{12} \exp\left(\frac{-e_{\text{a}}}{R K}\right) \tag{S4.12}$$

where e_{a} is the activation energy (74830 J mol^{-1}), K the mean annual temperature (Kelvin) and R is the molar gas constant (8.3144 J mol^{-1} K^{-1}). The mean annual

residence time of water in the root zone is given by:

$$T_{\mathrm{r,so}} \;=\; \frac{tawc}{Q_{\mathrm{eff}}} \tag{S4.13}$$

where *tawc* (m) is the soil total available water capacity for the top 1 m (or less if soils are shallower) and Q_{eff} is defined in equation S4.6. We assume that the residence time of NO$_3^-$ equals that of water based on the high mobility of NO$_3^-$ in soils. For agricultural soils under crops in dry regions we assume a minimum value for $T_{\mathrm{r,so}}$ of 1.0; in dry regions agricultural crops can not grow without irrigation, and this is represented by assuming a total water supply equal to the soil water capacity.

This formulation implies that in arid regions residence time is long, resulting in values of f_{climate} and $f_{\mathrm{den,soil}}$ equal to one, suggesting that 100% of the N surplus is removed by denitrification. In arid regions this is not realistic, since there are various fates of N, including accumulation of nitrate in the vadose zone below the root zone (Walvoord et al. 2003), surface runoff, ammonia-N volatilisation, nitrification, denitrification (Peterjohn and Schlesinger 1990). It is not possible to quantify the relative contribution of each process (Peterjohn and Schlesinger 1990), but it is clear that only a negligible part of N surpluses in arid climates is lost by denitrification. We therefore assume that the fate of the N surplus is determined by other processes than denitrification in soils under natural vegetation and grassland and with annual precipitation < 3 mm. The global amount of this N surplus in the 3100 Mha of arid lands was 20 Tg in the year 2000 (Figure 4.4).

The factors for f_{text}, f_{drain}, and f_{soc} account for the soil water and O$_2$ status (Table S4.3). Anaerobic conditions favouring denitrification may be more easily reached and maintained for longer periods in fine-textured soils than in coarse-textured ones. This is because fine-textured soils have more capillary pores and hold water more tightly than sandy soils do. The factor f_{drain} accounts for soil aeration, and denitrification rates are generally higher in poorly drained than in well-drained soils (Bouwman et al. 1993). The soil O$_2$ status is also influenced by root respiration and microbial activity. Oxygen consumption by microorganisms is driven by temperature, supply of C, and water availability. Temperature and soil water are represented in f_{climate}; we therefore use soil organic C content as a proxy for the C supply. The values used for f_{text}, f_{drain}, and f_{soc} are given in Table S4.3.

S4.6   Computing N$_2$O emissions from soils

Nitrous oxide emission from soils under natural vegetation is calculated with the regression model presented by Bouwman et al. (1993). N$_2$O emission from fertiliser application and spreading of animal manure in agricultural land are calculated with a regression model based on 846 series of measurements in agricultural fields (Bouwman et al. 2002b). The model is based on environmental (climate, soil organic C content, soil texture, drainage and soil pH) and management-related factors (N application rate, fertiliser type, crop type).

S4.7   Groundwater transport and denitrification

The role of urbanised areas is neglected, because the total area of urbanised land is about 0.3% of the total land area of countries (Angel et al. 2005). We note that loss of N to the environment can be substantial in urbanised areas, where sewerage systems are either well-developed or absent (e.g., Foppen 2002, Wakida and Lerner 2005, Van Den Brink et al. 2007, Nyenje et al. 2010). The role of natural NH$_4^+$ in groundwater is also neglected, which is justified by the observation that the median NH$_4^+$ concentration in groundwater of 25 European aquifers is 0.15 mg l^{-1} (Shand and Edmunds 2008), which is low (0.7–1.2%) compared to present-day agricultural contamination of groundwater with nitrate, for example in Europe (EEA 2013).

The difference between the soil N budget, N in surface runoff and denitrification leaches from the root zone to groundwater (if present):

$$N_{\text{leach}} \quad = \quad N_{\text{budget}} - N_{\text{sro}} - N_{\text{den,soil}} \qquad \text{(S4.14)}$$

The NO$_3^-$ concentration in the excess water leaching from the root zone is calculated from the leached N and the excess water flow (Q_{eff}, equation S4.6):

$$C_{\text{in}}(0) \quad = \quad \frac{N_{\text{leach}}}{Q_{\text{eff}}} \qquad \text{(S4.15)}$$

After infiltration, groundwater flows laterally to ditches and streams or vertically to deeper groundwater layers. The shallow groundwater system represents the upper metres of the saturated zone (typically 5 m) and is characterised by short residence times before water enters local surface water at short distances or infiltrates the deep groundwater system.

We assume that no denitrification occurs in the deep groundwater system. We note that some denitrification could be expected with sedimentary organic matter and pyrite, but also that a bias exists in the literature for sites with rapid denitrification (Green et al. 2008), which makes assessment at the global scale difficult.

The NO$_3^-$ concentration in groundwater depends on the historical year of infiltration into the saturated zone and the denitrification loss during its transport (Böhlke et al. 2002, Van Drecht et al. 2003). Outflow concentrations of N compounds depend on reaction progress. Therefore the time available for denitrification needs to be known. Since we use a time step of one year, seasonal changes in groundwater level are ignored, and mean travel time $T_{\text{r,aq}}$ depends on the ratio between specific groundwater volume and water recharge:

$$T_{\text{r,aq}}(t) \quad = \quad \min\left(\frac{p\,D}{Q_{\text{inflow}}(t)}, 1000\right) \qquad \text{(S4.16)}$$

where p is the effective porosity (m^3 m^{-3}), D is aquifer depth (m) (Table S4.2) and Q_{inflow} is the water recharge of shallow groundwater, Q_{int}, or recharge of deep groundwater, Q_{gwb} (m y^{-1}). Effective porosity is estimated based on the

lithological class (Table S4.2). The deep system is fed by a vertically draining shallow system (Figure 4.1). The travel time distribution for vertical flow in the shallow system is uniform so travel time equals mean travel time. For lateral flow to surface water, travel times are highly variable. Meinardi (1994) describes travel time distribution for lateral flow in a vertical cross section as follows:

$$g_{\text{age}}(z) \;\; = \;\; -T_{\text{r,aq}} \ln \left(1 - \frac{z}{D} \right) \tag{S4.17}$$

where z is the depth (m; $z = 0$ at the top and and $z = D$ at the bottom of the aquifer), g_{age} is the age of groundwater at depth z (yr), and $T_{\text{r,aq}}$ is the mean travel time over the thickness of the aquifer (yr). For shallow groundwater (sgrw) we assume $D_{\text{sgrw}} = 5$ m, and for the deep groundwater (dgrw) layer (if present) $D_{\text{dgrw}} = 50$ m (Meinardi 1994).

Denitrification during transport in the shallow system along each flow path in a homogeneous and isotropic aquifer, drained by parallel rivers or streams, is described by a first order degradation process. At time t and at depth z the outflow concentration is:

$$C(t, z) \;\; = \;\; C_0(t - g_{\text{age}}(z)) \, e^{-k \, g_{\text{age}}(z)} \tag{S4.18}$$

where the decay rate k is:

$$k \;\; = \;\; \frac{\ln(2)}{dt50_{\text{den}}} \tag{S4.19}$$

The NO$_3^-$ concentration in the inflow to deep groundwater ($C_0(t)$) is the outflow from the shallow groundwater system. The half-life of NO$_3^-$ in the shallow system $dt50_{\text{den}}$ depends on the lithological class (Dürr et al. 2005), with low values (1 year) for silici-clastic material, 2 years for alluvial material, and, 5 years for all other lithological classes. For $dt50_{\text{den}} = 2$ and a travel time of 50 years, the NO$_3^-$ concentration will be reduced by $e^{-k(t-50)}$ which is close to $3 \cdot 10^{-8}$.

S4.8   Denitrification and N$_2$O emission from riparian areas

For riparian areas, pH is one of the key parameters controlling denitrification rates (Simek and Cooper 2002, Knowles 1982), next to to temperature, water saturation, NO$_3^-$ availability and soil organic carbon availability. Under controlled conditions using pure cultures, denitrification activities have been shown to have an optimum at pH 6.5 to 7.5, and decrease at both low (below 4) and high (above 10) pH values.

Our model is based on observed inhibition of denitrification at low soil pH, and the high N$_2$O fractions when denitrification is inhibited (Van Cleemput 1998, Van Den Heuvel et al. 2011). Hence, the fraction N$_2$O of total riparian denitrification is high when conditions limit denitrification, and low for optimal conditions for denitrification. Field measurements show a wide range of N$_2$O emissions from riparian areas (Table S4.4) indicating that these areas can be both sources and sinks for N$_2$O. In general, however, fluxes from riparian areas are found to be low compared

Table S4.4: Riparian zone N_2O emission and emission fractions

Reference	N_2O emission (kg N ha^{-1} y^{-1})	Fraction ($N_2O/(N_2+N_2O)$) (-)	Fraction (N_2O/N input) (-)
Schipper et al. (1993)	6390		
Weller et al. (1994)	0.04–0.35		
Jordan et al. (1998)	0.016–1.5		0.055
Jacinthe et al. (1998)	0.66–11.0		0.0002
Walker et al. (2002)	24.2		
Dhondt et al. (2004)	−1.8–1.5		
Hefting et al. (2003, 2006a,b)	2–20	0.08–0.73	0.028–0.058
Oehler et al. (2007)	51.6	0.6	
Mander et al. (2008)	0.44–7.8		
Hopfensperger et al. (2009)	0.079		0.03
Soosaar et al. (2011)	0.4–0.7	0.019–0.03	0.003
Beaulieu et al. (2011)		0.0–0.5	
Vilain et al. (2011)	0.5		

with agricultural soils. Fractions of N_2O relative to the total denitrification end product (N_2+N_2O) range from 0.3 up to 73% (Table S4.4).

The denitrification potential in riparian zones is based on the characteristics of the groundwater flow, soil, and climate. Denitrification in riparian zones is calculated using the same approach as discussed for soil denitrification; in addition, we assume that heterotrophic denitrification is dominant and is highest at pH > 7 (Figure S4.1a). A dimensionless denitrification pH reduction factor $f_{denpH,rip}$ is commonly included in denitrification models. This factor assumes a value of 1 at pH > 7 and values of 0 at pH < 3.

$$N_{den,rip} = f_{den,rip} N_{in} \tag{S4.20}$$

$$f_{den,rip} = \min[(f_{climate} + f_{text} + f_{drain} + f_{soc}), 1] f_{denpH,rip} \tag{S4.21}$$

The N_{in} entering the riparian zone is the residual in the shallow groundwater layer after denitrification has been accounted for. The factor $f_{climate}$ includes the temperature effect f_K (equation S4.12) and the travel time $T_{r,rip}$ of water and NO_3^- through the riparian zone. $T_{r,rip}$ is calculated as follows:

$$T_{r,rip} = \frac{D_{rip}\, tawc}{Q_{int}} \tag{S4.22}$$

where $tawc$ is the available water capacity for the top 1 m, and D_{rip} is the thickness of the riparian zone ($D_{rip} = 0.3$ m of soil, or less for shallow soils), and Q_{int} is the interflow leaving the shallow groundwater system and flowing through riparian areas. Thus, $T_{r,rip}$ is short where the water flux is large or where the soil layer is thin.
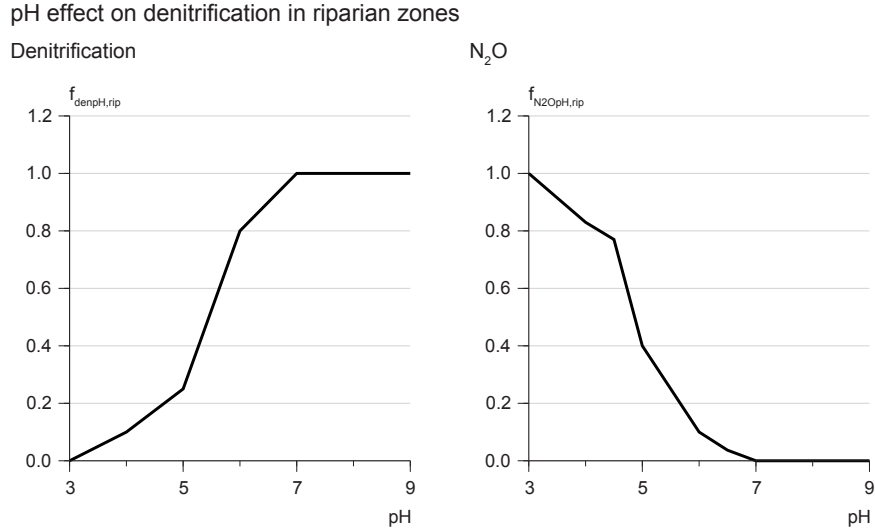
pH effect on denitrification in riparian zones

Denitrification N_2O

Figure S4.1: (a) Reduction fraction ($f_{denpH,rip}$) of riparian denitrification as a function of soil pH and (b) the fraction N_2O of total denitrification as a function of soil pH ($f_{N2OpH,rip}$).

All interflow (if present) in a grid cell is assumed to flow towards streams through riparian zones (Figure 4.1), except in (fractions of) grid cells with surface water bodies, such as wetlands, lakes or larger streams, where shallow groundwater by-passes riparian zones.

N_2O emission is calculated from the denitrification rate and local soil pH:

$$N_2O_{rip} \;\; = \;\; f_{den,rip} \left(1 - f_{den,rip}\right) f_{N2OpH,rip} \, N_{in} \qquad (S4.23)$$

where $f_{N2OpH,rip}$ is the fraction N_2O fraction of total denitrification as a function of soil pH (Figure S4.1b).

S4.9   Other land based human-managed denitrification

Additional land-based denitrification occurs in manure storage systems, wastewater treatment plants and wetlands. Reliable data on manure storage conditions are not available, particularly for the early 20th century. We assumed that in 1900 all stored animal manure was solid manure, although a fraction of the liquids (urine) may have seeped into the soil. In 2000 and 2050 we assumed that 50% of the stored manure for cattle was solid, and for pigs 20%. This may underestimate the amount of slurries in European countries and other industrialised countries.
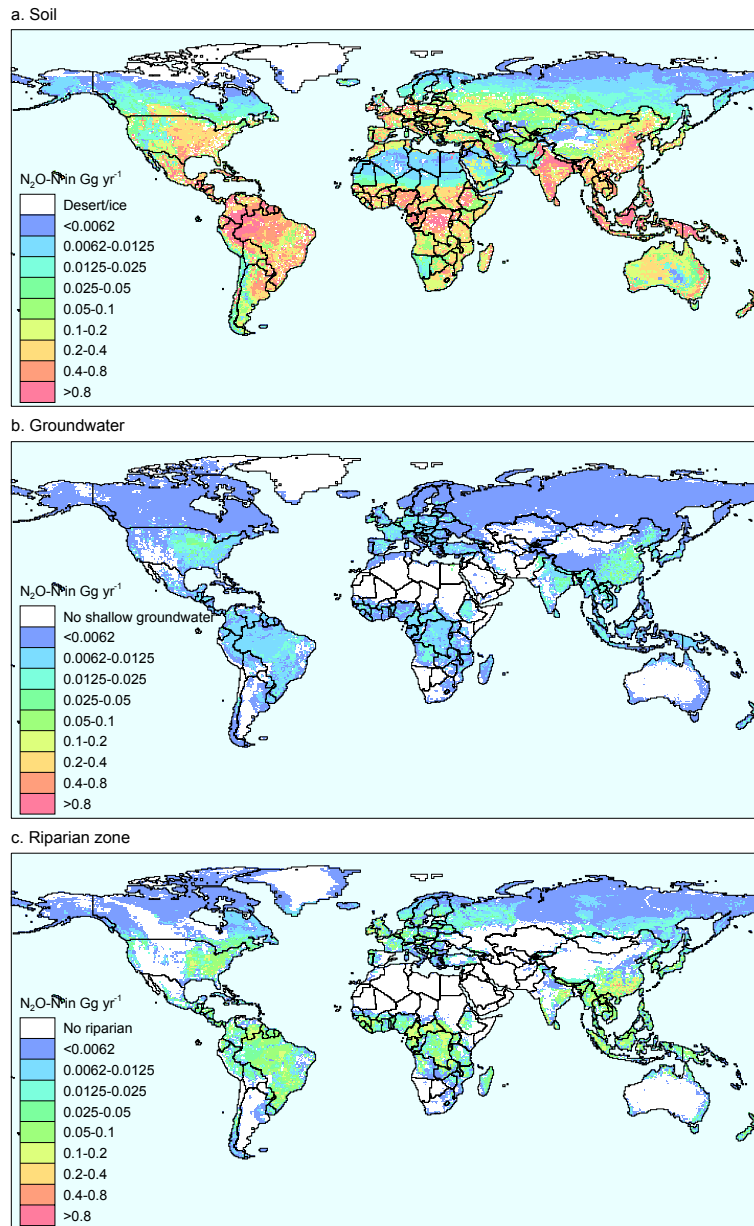
a. Soil

b. Groundwater

c. Riparian zone

Figure S4.2: Nitrous oxide emission computed for the year 2000 for (a) soils, (b) groundwater and (c) riparian zones. Emissions are denoted in N$_2$O-N per grid cell, because the location of out gassing for groundwater and riparian zones is not known.
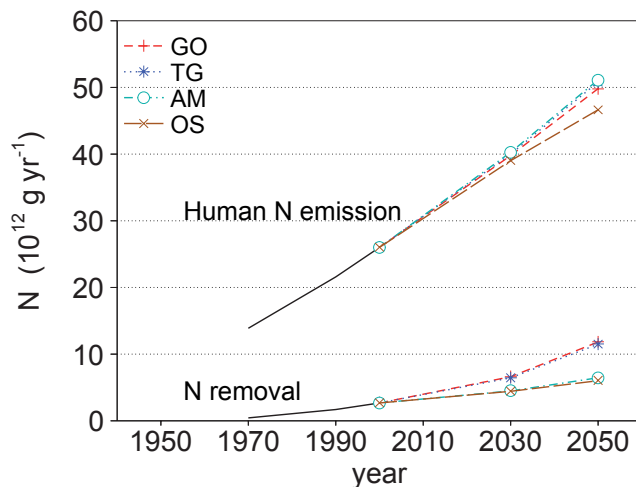
Figure S4.3: Global human N excretion and N removal in wastewater treatment systems for 1970–2000, and 2000–2050 for the four Millennium Ecosystem Assessment scenarios. Based on Van Drecht et al. (2003).

Denitrification is calculated as 20% of the N in solid manure, accounting for NH_3 losses. Denitrification in manure storage systems thus calculated increased from 2.5 Tg N yr^{-1} in 1900 to 5 Tg N yr^{-1} in 2000, and will further increase to up to 10 Tg N yr^{-1} under the Global Orchestration scenario in 2050.

For wastewater treatment systems we used data from Van Drecht et al. (2009) for the period 1970–2050 (Figure S4.3). Assuming that all N removal is by denitrification, denitrification during wastewater treatment amounted to 2.7 Tg N yr^{-1} in 2000, and this may increase to up to 12 Tg N yr^{-1} in 2050 under the Global Orchestration scenario. It is not currently possible for us to estimate denitrification in human-managed wetlands due to a lack of information on how much N is involved.

S4.10   Sensitivity analysis

The sensitivity of the model to 17 model parameters was investigated for nine output variables representing global results for river N delivery the year 2000 (Table S4.5). In order to limit computational load in the sensitivity analysis, the Latin Hypercube Sampling (LHS) technique (Saltelli et al. 2000) was used. LHS offers a stratified sampling method for the separate input parameters, based on subdividing the range of each of the k parameters into disjunct equiprobable intervals based on a uniform distribution. By sampling one value in each of the N intervals according to the associated distribution in this interval, we obtained N sampled values for each parameter. The number of runs N was 400.

Table S4.5: Model parameters included in the sensitivity analysis, their symbol and description, equation where they are used, and the standard, minimum, mode and maximum value considered for the sampling procedure

Symbol	Description	Equation	Distribution[a]	Standard	Min.	Mode	Max.
Q_{tot}	Runoff (total)	S4.2	U1	1.0	0.9		1.1
$Temp$	Mean annual air temperature	S4.12	U2	0.0	−1.0		1.0
$N_{budget,grass}$	N budget in grasslands	4.1	U1	1.0	0.9		1.1
$N_{budget,crops}$	N budgets in croplands	4.1	U1	1.0	0.9		1.1
$N_{budget,nat}$	N budget in natural ecosystems	4.1	U1	1.0	0.9		1.1
f_{Qsro}	Overall runoff fraction	S4.4	U1	1.0	0.9		1.1
f_{Qgwb}	Fraction of Q_{eff} that flows towards the deep system	S4.7	U1	1.0	0.9		1.1
C_{sro}	Calibration constant for N in surface runoff	S4.9	U3	0.5	0.4		0.6
$f_{Qsro}(grass)$	Land-use effect on surface runoff for soils under grassland	S4.4	T1	0.25	0.0	0.25	0.5
$f_{Qsro}(crops)$	Land-use effect on surface runoff for soils under crops	S4.4	T2	1.0	0.75	0.995	1.0
$f_{Qsro}(nat)$	Land-use effect on surface runoff for soils in natural ecosystems	S4.4	T3	0.125	−0.05	0.125	0.3
D_{rip}	Thickness of riparian zone	S4.22	T2	0.3	0.2	0.3	1.0
D_{sgrw}	Thickness of shallow groundwater system	S4.17	U3	5.0	3.0		7.0
D_{dgrw}	Thickness of deep groundwater system	S4.17	U3	50.0	30.0		70.0
p	Porosity of aquifer material	S4.7, S4.16	U1	1.0	0.9		1.1
$dt50_{den,sgrw}$	Half-life of nitrate in shallow groundwater	S4.19	U1	1.0	0.8		1.2
$dt50_{den,dgrw}$	Half-life of nitrate in deep groundwater	S4.19	T4	∞	0.0	20.0	40.0

[a] Samples values are applied to all grid cells. For sampling, either uniform of triangular distributions are used. A triangular distribution is a continuous probability distribution with lower limit a, upper limit b and mode c, where $a \leq c \leq b$. The probability to sample a point depends on the skewness of the triangle. In the case of $dt50_{den,dgrw}$, $a\,c = b\,c$, and probability to sample a point on the left and right hand side of c is the same. In other cases, for example $f_{Qsro}(crops)$ is a fraction [0,1], with standard value of 1.0. To achieve a high probability to sample close to 1.0, the triangle is designed with $b = 1$ and c is close to 1. For some of the above distributions the expected value is not equal to the standard. Since the calculated R^2 for all output parameters exceeds 0.99, this approach for analyzing the sensitivity is still valid. The distributions used are:

U1. Uniform; values are multipliers for standard values on a grid cell basis.

U2. Uniform; values are added to the standard values on a grid cell basis.

U3. Uniform; values are used as such.

T1. Triangular; values range between 0.125 and 0.5.

T2. Triangular.

T3. Triangular; values range between 0.1 and 0.3.

T4. Triangular; default value represents the mode. Values range between 3 and 40. These values are used to multiply with the standard values of $dt50_{den,sgrw}$ (because we assume there is no denitrification in deep groundwater in the standard case).

The sampled values for the first model parameter are randomly paired to the samples of the second parameter, and these pairs are subsequently randomly combined with the samples of the third source, etc. This results in an LHS consisting of N combinations of k parameters. The parameter space is thus representatively sampled with a limited number of samples.

LHS can be used in combination with linear regression to quantify the uncertainty contributions of the input parameters to the model outputs (Saltelli et al. 2000, 2004). The output Y considered (see columns in Table S4.6) is approximated by a linear function of the parameters X_i expressed by

$$Y \;=\; \beta_0 + \beta_1 X_1 + \beta_2 X_2 + \cdots + \beta_n X_n + \epsilon \tag{S4.24}$$

where β_i is the so-called ordinary regression coefficient and ϵ is the error of the approximation. The quality of the regression model is expressed by the coefficient of determination (R^2), representing the amount of variation Y explained by $Y - \epsilon$. Since β_i depends on the scale and dimension of X_i, we used the standardised regression coefficient (SRC_i), which is a relative sensitivity measure obtained by rescaling the regression equation on the basis of the standard deviations σ_Y and σ_{X_i}:

$$SRC_i \;=\; \beta_i \, \frac{\sigma_{X_i}}{\sigma_Y} \tag{S4.25}$$

SRC_i can take values in the interval $[-1, 1]$. SRC is the relative change $\Delta Y / \sigma_Y$ of Y due to the relative change $\Delta X_i / \sigma_{X_i}$ of the parameter X_i considered (both with respect to their standard deviation σ). Hence, SRC_i is independent of the units, scale and size of the parameters, and thus sensitivity analysis comes close to an uncertainty analysis. A positive SRC_i value indicates that increasing a parameter value will cause an increase in the calculated model output, while a negative value indicates a decrease in the output considered caused by a parameter increase.

The sum of squares of SRC_i values of all parameters equals the coefficient of determination (R^2), which for a perfect fit equals 1. Hence, SRC_i^2 / R^2 yields the contribution of parameter X_i to Y. For example, a parameter X_i with $SRC_i = 0.1$ adds 0.01 or 1% to Y in case R^2 equals 1.

Table S4.6: Standardized regression coefficient (SRC)^a values representing the relative sensitivity of 9 model variables representing global model results (columns) to variation in 17 parameters (rows, see Table S4.5)

Parameter	N_{budget}	N_{sro}	$N_{\text{den,soil}}$	N_{leach}	$N_{\text{out,sgrw}}$	$N_{\text{out,dgrw}}$	$N_{\text{in,rip}}$	$N_{\text{bypass,rip}}$	$N_{\text{out,river}}$
Q_{tot}			−0.22	0.24	0.31	0.19	0.30	0.31	0.32
$Temp$			0.50	−0.43	−0.19		−0.19	−0.21	−0.18
$N_{\text{budget,grass}}$	0.33	0.02	0.30	0.21	0.14		0.15	0.10	0.14
$N_{\text{budget,crops}}$	0.65	0.17	0.60	0.54	0.25	0.04	0.25	0.25	0.30
$N_{\text{budget,nat}}$	0.73	0.03	0.47	0.67	0.50	0.14	0.51	0.44	0.50
f_{Qsro}		0.39	−0.05	−0.11	−0.08		−0.09	−0.03	0.11
f_{Qgwb}					−0.12	0.27	−0.12	−0.10	−0.05
C_{sro}		0.78	−0.14	−0.20	−0.14		−0.14	−0.06	0.25
$f_{\text{Qsro}}(grass)$		0.35	−0.06	−0.10	−0.07		−0.08	−0.03	0.10
$f_{\text{Qsro}}(crops)$		0.31	−0.04	−0.09	−0.07		−0.08	−0.03	0.08
$f_{\text{Qsro}}(nat)$		0.19	−0.01	−0.07	−0.06		−0.07	−0.03	0.03
D_{rip}						0.04			−0.20
D_{sgrw}					−0.65	−0.14	−0.64	−0.71	−0.57
D_{dgrw}						−0.46			−0.09
p					−0.17	−0.14	−0.16	−0.18	−0.16
$dt50_{\text{den,sgrw}}$					0.31	0.08	0.31	0.34	0.27
$dt50_{\text{den,dgrw}}$		−0.01		0.00	0.01	0.66	0.01	0.01	0

^{a} Cells in with no values represent insignificant SRC values; cells with values show significant SRC, gray colours indicate values −0.2 < SRC < 0.2; dark gray colours indicate values exceeding +0.2 and −0.2, respectively. An SRC value of 0.2 indicates that the parameter concerned has an influence of $0.2^2 = 0.04$ (4%) on the model variable considered.

Table S4.7: Nitrous oxide emissions for 1900–2000 (Bouwman et al. 2011a) and 2030 and 2050 for the four Millennium Ecosystem Assessment scenarios (Bouwman et al. 2009) according to the IMAGE model for the sources A: Natural systems, B: Agriculture, C: Groundwater, D: Riparian, E: Energy, F: Industry, G: Biomass burning, H: Rivers, I: Oceans

Year-scenario	A	B	C	D	E	F	G	H	I	Total
1900	6.3	2.4	0.1	0.6	n.d.[a]	n.d.	n.d.	0.1	3.0	12.6
1950	5.4	4.0	0.1	0.6	n.d.	n.d.	n.d.	0.1	3.0	13.2
1970	5.1	5.1	0.2	0.7	0.1	0.7	0.1	0.1	3.0	15.2
2000	4.9	6.4	0.2	0.9	0.2	0.4	0.3	0.2	3.0	16.5
2050-GO	5.3	8.8	0.3	1.1	0.5	0.3	0.2	0.2	3.0	19.7
2050-TG	4.8	9.0	0.2	0.9	0.1	0.1	0.1	0.2	3.0	18.4
2050-AM	5.2	7.7	0.2	0.9	0.4	0.3	0.2	0.2	3.0	18.0
2050-OS	4.9	8.7	0.3	1.0	0.5	0.4	0.2	0.2	3.0	19.1

[a] n.d. = no data. Nitrous oxide emissions expressed as Tg N yr^{-1}.

Table S4.8: Global estimates of N_2O emission from soils under cropland, grassland and natural vegetation[a]

Reference	Cropland	Grassland	Natural ecosystems	Inventory year/ model
	N_2O-N in Tg yr^{-1}			
Bouwman et al. (2002b)	2.7 (1.6–5.1)			1995/statistical
Stehfest (2006)	2.1			1998/DAYCENT
Stehfest and Bouwman (2006)	3.4 (1.6–6.9)			1995/statistical
Berdanier and Conant (2011)	2.3 (1.6–3.2)			1995/statistical
This study	3.2^b	2.7	4.9	2000/statistical

[a] Excluding N_2O emission of 0.5 Tg N_2O-N yr^{-1} from animal houses and manure storage systems.

[b] Estimates based on IPCC (2006) are not included; IPCC considers the fertiliser-induced emission (emission from fertilised plots minus that from unfertilised control plots) and not the total emissions.

Chapter 5

Exploring changes in nitrogen and phosphorus biogeochemistry in global rivers in the twentieth century

A.H.W. Beusen, L.P.H. Van Beek, A.F. Bouwman, and J.J. Middelburg, 2014.
In preparation.

Abstract

This paper presents the first global spatially explicit modeling approach based on coupled hydrology – nitrogen (N) and phosphorus (P) delivery to surface water – in-stream retention. Model results are consistent with time series of total N and P concentrations for a selection of rivers. We portray dramatic changes that occurred during the 20th century in both delivery and in-stream retention due to expanding agriculture, increasing wastewater discharge, and construction of dams and formation of reservoirs. Global delivery to streams increased from 34 to 65 Tg yr^{-1} of N and 5 to 9 Tg yr^{-1} of P. Global nutrient retention did not keep up with the delivery. Model results indicate a rapid increase of reservoir retention (globally from almost zero to 10% for N and 12% for P) due to dam construction. However, this intervention in the hydrologic system leads to less flooding and a decrease of the retention downstream of the dam from 32 to 23% for N and 44 to 36% for P. As a result of the more rapid increase in delivery compared to retention, river export to coastal seas increased

from 19 to 37 Tg yr^{-1} of N and 2 to 4 Tg yr^{-1} of P. The model revealed important differences in N : P ratios in river export in different parts of the world resulting from the interplay of multiple processes and economic activities in different river basins. River export showed a world-wide increase in the molar N : P ratio during recent decades.

5.1   Introduction

Nutrients, sediment, and organic carbon (C) are transported from land to sea through the continuum formed by soils, groundwater, riparian zones, rivers, lakes, and reservoirs. The hydrology, ecology and biogeochemical processing in each of these components of the landscape are strongly coupled and result in retention of a significant fraction of the nutrients (Billen et al. 1991).

Retention along the aquatic continuum affects the absolute amount of nutrients reaching the ocean. In addition, retention processes change the ratio in which C, nitrogen (N), phosphorus (P) and silicon (Si) are transferred, and the chemical form of each of these elements. Because river networks link terrestrial landscapes to lakes and oceans, perturbations to river ecosystems can have large consequences for biogeochemical cycling at local, regional, and global scales.

During the past century, human activities have been rapidly changing, leading to an increase in energy and food production, forest clearing for agricultural expansion, intensification of agricultural production, including the use of fertilizer and animal manure production, atmospheric deposition of nutrients, and wastewater flows (Stumm 1973, Galloway et al. 1995, Van Drecht et al. 2009, Bouwman et al. 2013d). Deforestation and expanding agricultural land use have caused increasing sediment, C and nutrient transport through river systems (Seitzinger et al. 2010), which can influence photosynthetic and heterotrophic production and cause dramatic changes in aquatic ecosystems (Vollenweider et al. 1992, Cloern 1996, Dodds 2002). Climate change, dam construction, irrigation, and consumptive water use affect the hydrology and biogeochemistry of aquatic ecosystems. Changing nutrient loads affect the biogeochemical nutrient retention in rivers (e.g., Mulholland et al. 2008, Soetaert et al. 2006).

Currently, eutrophication accounts for the foremost aquatic ecosystem management problem in rivers, lakes, and estuaries worldwide. Eutrophication resulting from nutrient loading was first evident in lakes and rivers from excessive growth of macrophytes and floating algal scums (Butcher 1947). In its most serious manifestations, eutrophication of surface waters leads to turbid waters with decreased oxygen concentrations (hypoxia), production of toxins by algae and bacteria, and fish kills (Diaz and Rosenberg 2008).

The impact of multiple disturbances on nutrient retention on a global scale is poorly understood (Stanley et al. 2010). Models are essential tools to analyze the biogeochemical nutrient retention processes in rivers in a changing world.

For analyzing the global impact of multiple changes and disturbances, distributed approaches are needed, where the delivery of nutrients is described for the land, groundwater, riparian zones and river compartments. In this paper we

present such a distributed approach to analyze the changes during the past century (1900–2000). This period encompasses dramatic changes in human population and economic human activities that have resulted in global changes, such as climate change, land-use change, changes in the hydrology by dam construction, irrigation, and consumptive water use (Wisser et al. 2010).

Our main objective is to include in-stream nutrient retention in a global-scale spatially explicit model and to infer its importance, spatial variability and trends during the 20$^{\text{th}}$ century. Several model approaches exist for describing in-stream biogeochemistry, ranging from lumped statistical to mechanistic approaches (see review by Bouwman et al. 2013c). Here, we use the first-order nutrient spiraling ecological concept (Newbold et al. 1981) to describe in-stream biogeochemistry of total N and total P. This reach-lumped formulation of stream nutrient retention ignores the detailed biogeochemical transformations and is sufficient for describing the nutrient balance of aquatic systems at the watershed to global scale.

Retention processes for N and P differ. Denitrification, here used for sum of microbial denitrification and anammox, is responsible for most N losses from surface water (Boyer et al. 2006a), while sedimentation and sorption by sediments are responsible for the removal of P from the water column (Reddy et al. 1999). Despite the fact that nutrient form (particulate, dissolved, organic, inorganic) has an important impact on these retention processes, the spiraling concept is based on biological factors controlling removal (spiral length) and hydrologic conditions, and hence is appropriate to describe these processes at large scales as demonstrated by Marcé and Armengol (2009) and Wollheim et al. (2008a). We focus on the flows of total N and total P, because of the importance of the ratios between these two elements for biogeochemistry and the functioning of downstream aquatic ecosystems. The N and P river export including the N and P delivery to surface water is available on request.

5.2   Data and methods

We coupled the hydrological model PCR-GLOBWB (Van Beek et al. 2011) with the nutrient delivery model of the Integrated Model to Assess the Global Environment (IMAGE) (Bouwman et al. 2006) (SI S5.1). The delivery model used to simulate N flows from soils via leaching through groundwater and riparian systems, and via surface runoff to surface water has been presented recently (Bouwman et al. 2013a). Here, we extend the approach by including P flows, and retention in freshwater systems based on the spiraling concept (Figure 5.1). All calculations presented have a yearly time scale, and refer to total N and total P (total of all chemical forms). Section 5.2.1 presents the hydrological model, 5.2.2 the nutrient delivery model, and 5.2.3 the in-stream nutrient retention model. The sensitivity analysis is discussed in Section 5.2.4.
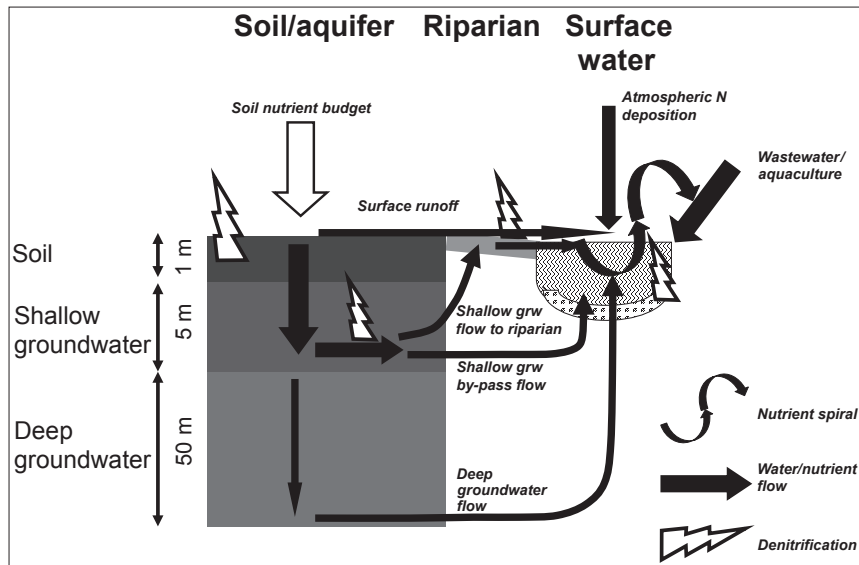
Grid cell

Figure 5.1: Scheme of the coupled hydrology – nutrient delivery – in-stream nutrient retention.

5.2.1   Hydrology

The grid-based global hydrological model PCR-GLOBWB (Van Beek et al. 2011) representing the terrestrial part of the hydrological cycle is used to quantify water stores and fluxes. For this study it is implemented with a daily time step and a spatial resolution of $0.5°$ by $0.5°$ output for the 20th century simulations is available with a monthly and yearly time step. All further calculations refer to the annual aggregated results.

The land surface in PCR-GLOBWB is represented by a topsoil (0.3 m thick or less) and a subsoil (1.2 m thick or less). The soil layers contain a partly unsaturated zone. Precipitation falls as rain if air temperature exceeds 0 °C, and as snow otherwise. Snow accumulates on the surface, and melt is temperature controlled. Potential evapotranspiration is broken down into canopy transpiration and bare soil evaporation, which are reduced to an actual evapotranspiration rate based on soil moisture availability. Vertical transport in the soil column arises from percolation or capillary rise, depending on the vertical hydraulic gradient present between these layers.

Water is delivered as specific runoff to the drainage network, consisting of direct runoff, interflow and base flow according to the approach presented elsewhere (Bouwman et al. 2013a). See SI S5.2- S5.3 for more details on the water balance model, drainage network and handling of soil and vegetation.

Twentieth century monthly precipitation and temperature are from New et al. (2000) and downscaled to daily values using the ERA-40 reanalysis (Uppala et al. 2005). Precipitation and temperature were fed directly into the model whereas secondary variables (vapor pressure, wind speed, cloud cover, temperature) were used to compute reference potential evapotranspiration using the Penman-Monteith equation according to FAO guidelines (Allen et al. 1998). For the overlapping period 1960–2001 the actual sequence of ERA-40 years was used, which was repeated for the preceding period 1901–1959.

Drainage density is computed from the Hydro1k dataset (Verdin and Greenlee 1996). The drainage network is based on the DDM30 flow direction map of (Döll and Lehner 2002) and the lake characteristics taken from the GLWD1 product (Lehner and Döll 2004). Reservoirs are from the GRaND dataset (Lehner et al. 2011) and introduced dynamically on the basis of the reported construction year.

The specific runoff accumulates along the drainage network and the resulting flood wave is simulated using the kinematic wave approximation with the resistance depending on the channel and floodplain characteristics and the channel gradient. Where the storage exceeds the channel capacity, flooding occurs, water depth and extent depending on the elevation distribution within a $0.5°$ by $0.5°$ grid cell. The river channels can be interrupted by lakes and reservoirs for which the outflow is controlled by a storage-outflow relationship for lakes and by the requested downstream demand in the case of reservoirs (further details in S5.2.2).

A mask of water bodies is combined with the DDM30 flow direction map to create a continuous watershed that drains towards the lake or reservoir outlet to ensure proper hydrological routing; this mask comprises all lakes and reservoirs. At

any time, a grid cell can function either as a river lake or reservoir. Endorheic lakes have no outlet point. The channel dimensions are parameterized on the basis of the Leopold and Woolhiser relationships for bank full discharge and the overbank storage capacity based on the Hydro1k dataset (more details in Winsemius et al. 2013, Van Beek and Bierkens 2009).

Each water body is specified by a volume and surface area, and thus depth. The water level in lakes is constant, as the through flow will increase with increasing discharge. The water travel time is determined by the discharge and the volume of the water body. Assuming that the flooding volume is refreshed every year with the discharge, and the rest of the river discharge follows the main channel, the travel time in a river with floodplains is determined as follows:

$$\tau = \frac{V}{Q - V_{\mathrm{f}}} \tag{5.1}$$

where τ is the travel time (year), V is the volume of the water body (including river bed) (m^3), Q is the discharge (m^3 yr^{-1}) and V_{f} is the volume of the flooded area per year (m^3 yr^{-1}). While the simulated discharge includes the regulating effect of reservoirs, consumptive water use has not been included as it is difficult to identify its source (groundwater, surface water) and to quantify its spatial distribution with certainty.

5.2.2 Nutrient delivery

This section describes all processes and pathways of N and P delivery to surface water. For N, the model components have been presented in detail elsewhere (Bouwman et al. 2013a); this paper gives a brief presentation, with more details in the supporting information (SI).

Soil N and P budgets

We use annual soil N and P budgets for agricultural systems calculated with the IMAGE model by Bouwman et al. (2013d) for the years 1900, 1950, 1960, 1970, 1980, 1990, 1995, and 2000 for 0.5° by 0.5° grid cells for agricultural and natural land. Soil N budgets have the input terms fertilizer, manure, biological N$_2$ fixation and atmospheric deposition; P inputs are fertilizer and manure; N and P outputs include crop and grass harvest and grazing. The soil N budget also accounts for ammonia volatilization (for more details see SI S5.4).

Soil N and P loss by surface runoff

Our model distinguishes two nutrient loss pathways; i.e., losses from recent nutrient applications in the form of fertilizer, manure or organic matter ($N_{\mathrm{sro,rec}}, P_{\mathrm{sro,rec}}$) (Hart et al. 2004), and a "memory" effect ($N_{\mathrm{sro,mem}}, P_{\mathrm{sro,mem}}$) related to long-term historical changes in soil nutrient inventories (McDowell and Sharpley 2001,

Tarkalson and Mikkelsen 2004):

$$N_{\text{sro,rec}} \quad = \quad N_{\text{sro,rec}} + N_{\text{sro,mem}} \tag{5.2}$$

Estimates of soil erosion losses from Cerdan et al. (2010) were used as a basis for calculating $P_{\text{sro,mem}}$ and $N_{\text{sro,mem}}$. The approach presented by Cerdan et al. (2010) based on slope, soil texture and land cover type were used to estimate country aggregated soil-loss rates for arable land, grassland and natural vegetation. Soil loss from peat soils was assumed to be low (equal to fine texture). These estimates were then calibrated to obtain the mean erosion loss estimates for Europe (360 ton kg of soil per km^2 for arable fields, 40 ton per km^2 for grassland and 15 ton per km^2 for natural vegetation). The model with these calibration factors was then applied to all grid cells of the world.

As the model keeps track of all inputs and outputs in the soil P budget, the actual P content can be calculated. The initial P stock for the year 1900 in the top 30 cm is taken from Yang et al. (2010). All inputs and outputs of the soil balance are assumed to occur in the top 30 cm; the model replaces P enriched or depleted soil material lost at the surface by erosion with fresh soil material (with the initial soil P content) at the bottom. For N we use the soil organic C content, which is assumed to be constant over time, as a basis to calculate N in eroded soil material using land-use specific C:N ratios (soil C:N for arable land 12, for grassland 14 and for soils under natural vegetation 14) (based on Batjes 1996, Guo and Gifford 2002, McLauchlan 2006, Brady 1990).

$P_{\text{sro,rec}}$ and $N_{\text{sro,rec}}$ are calculated from the N and P input terms (SI S5.4, equation S5.4) on the basis of f_{qsro}, which depends on slope (using the approach of Bogena et al. (2005)) and further modified by land use and soil texture, i.e., factors that reduce surface runoff according to Velthof et al. (2009, 2007) (see SI S5.2.1). For N, the equation is:

$$N_{\text{sro,rec}} \quad = \quad f_{\text{cal}}\, f_{\text{qsro}}\, N_{\text{inp}}(landuse) \tag{5.3}$$

where f_{cal} is a calibration factor of 0.3 to match the N runoff results of Miterra (Velthof et al. 2009, 2007).

Subsurface N transport and loss

The model used to simulate N flows from the soil via leaching through groundwater systems and riparian zones, and via surface runoff to surface water is a modification of the conceptual model of Van Drecht et al. (2003). Details on the model are given in SI S5.5–S5.6. Here, a brief summary is provided.

Annual soil N leaching is calculated as a fraction of the surplus of the soil N budget corrected for surface runoff (equation S5.5), based on temperature, the residence time of water and NO_3^- in the soil, soil texture, soil drainage and soil organic C. Denitrification in shallow groundwater is a function of the travel time and the half-life of nitrate. The travel time distribution is calculated over the thickness of 5 m, with a maximum travel time of 100 years within a grid cell.

The mean travel time is a function of the aquifer thickness, porosity and the inflow. Porosity and the half-life of nitrate depend on the lithology. We assume that denitrification is negligible in the deep groundwater system, and the modeled NO_3^- outflow from deep groundwater is thus a maximum estimate.

The calculation of denitrification in riparian zones is similar to that in soils with two differences. Firstly, a biologically active layer with a thickness of 0.3 m is assumed, as riparian zones show strong vertical gradients. Denitrification rates are high in this topsoil due to the high organic matter contents. Secondly, we included the effect of pH on denitrification rates (SI S5.7).

Allochtonous inputs of organic matter

Recent estimates suggest that allochtonous organic matter inputs to surface water is an important flux in the global C cycle (Cole et al. 2007). So far, the impact of this process as a nutrient source has not been investigated globally. Here, we use estimates of NPP from IMAGE for wetlands and floodplains. Part of annual NPP is assumed to be deposited in the water during this flooding, and where flooding is temporary, the litter from preceding periods is assumed to be available for transport in the flood water. The ratio of litter to belowground inputs of organic matter ranges from $30 : 70$ to $70 : 30$ (Trumbore et al. 1995, Vogt et al. 1986); here we assume that 50% of total NPP ends in the surface water. N and P inputs to the water are estimated based on a $C : N$ ratio of 100 and a $C : P$ ratio of 1200 (Vitousek 1984, Vitousek et al. 1988).

Other nutrient sources

Other nutrient sources distinguished include P release from weathering of parent rock according to Hartmann et al. (2014), N and P in wastewater (from Morée et al. (2013), N and P release from aquaculture (from Bouwman et al. (2013b) and Bouwman et al. (2011b)) and atmospheric N deposition to surface water (see SI S5.8).

5.2.3　In-stream nutrient retention

Three processes contribute to N retention: denitrification, sedimentation and uptake by aquatic autotrophs. Denitrification is generally the major component of N retention (Saunders and Kalff 2001). For P the processes are sedimentation and sorption by sediment (Reddy et al. 1999).

Retention in a grid cell is calculated as a first order approximation according to:

$$R \;=\; 1 - \exp\left(\frac{-v_{f,E}}{H_L}\right) \tag{5.4}$$

where R is the retention (-), $v_{f,E}$ is the net uptake velocity (m yr^{-1}) for the nutrient E considered (N or P), and H_L is the hydraulic load (m yr^{-1}) obtained from:

$$H_L \;=\; \frac{D}{\tau} \tag{5.5}$$

where D is the depth of the water body (m) and τ is the residence time (yr). τ is calculated from the volume V (m³) of the water body and the discharge Q (m³ yr⁻¹):

$$\tau \;\; = \;\; \frac{V}{Q} \tag{5.6}$$

for all water bodies except for river channels and floodplains where the discharge Q is reduced by the water volume in the floodplains (see equation 5.1). In this approach hydrological (defined by H_{L}) and biological factors (defined by v_{f}) controlling removal are isolated, assuming first order kinetics is applicable.

Net uptake velocity is different for each element E (N or P). For N, the basic value for all water body types of 35 m yr⁻¹ taken from Wollheim et al. (2008b, 2006) is modified based on temperature and N concentration:

$$v_{\mathrm{f,N}} \;\; = \;\; 35 f(t)\, f(C_{\mathrm{N}}) \tag{5.7}$$

where t is annual mean temperature (°C) and C_{N} is the N concentration in the water. $f(C_{\mathrm{N}})$ describes the effect of concentration on denitrification as a result of electron donor limitation in the case of high N loads; $f(C_{\mathrm{N}})$ decreases from a value of 7.2 at $C_{\mathrm{N}} = 0.0001$ mg l⁻¹ to 1 for $C_{\mathrm{N}} = 1$ mg l⁻¹ and decreasing to 0.37 for $C_{\mathrm{N}} = 100$ mg l⁻¹ and constant at higher concentrations.

The temperature effect $f(t)$ is calculated as:

$$f(t) \;\; = \;\; \alpha^{(t-20)} \tag{5.8}$$

where $\alpha = 1.0717$ for N (following Wollheim et al. (2008a) and references therein) and $\alpha = 1.06$ for P (following Marcé and Armengol (2009)).

For P, the basic value for v_{f} of 44.5 m yr⁻¹ taken from Marcé and Armengol (2009) is used for all water body types, with a modification based on temperature:

$$v_{\mathrm{f,P}} \;\; = \;\; 44.5\, f(t) \tag{5.9}$$

The drainage network of PCR-GLOBWB represents streams and rivers of Strahler order (Strahler 1957) six and higher. The parameterization of lower order streams follows the approach presented by Wollheim et al. (2008a) (see SI S5.12).

5.2.4   Sensitivity analysis

The sensitivity of the model was investigated using Latin Hypercube Sampling, with uncertainty ranges for 48 parameters for the N and 34 for the P model results for delivery, retention and river export, and expressed using the standardized regression coefficient (SRC), to compare model output of 9 variables (Table S5.3). Details on this analysis are in SI S5.9.

5.3   Results and discussion

The results are presented for rivers draining into the Pacific Ocean, Arctic Ocean, Atlantic Ocean, Indian Ocean, and the combined Mediterranean Sea and Black

Sea basins. Subsequently we present a comparison of simulated total N and P concentrations with monitoring time series for selected rivers (section 5.3.1), model sensitivity analysis (5.3.2), results for the N and P delivery to surface water (5.3.3), N and P retention in rivers, lakes and reservoirs (5.3.4), and the N and P export to coastal marine ecosystems (5.3.5).

5.3.1   Comparison with monitoring data for selected rivers

Our model integrates submodels for hydrology, spatially explicit nutrient delivery patterns and in-stream retention, each of which has been parameterized independently. We therefore deliberately did not calibrate our model results, since that would not lead to a better understanding of the behavior of the model and lacunae in the data used. Here we simply compare the modeled concentrations with time-series of measurements for the rivers Rhine, Meuse, Mississippi, and a large number of monitoring stations in Europe. Furthermore, we compare various results of the model with selected rivers worldwide.

The uncalibrated model shows good agreement for the period 1970–2000 with concentration data for the Rhine (both total N and total P) (Figure 5.2). Modeled total P concentrations in both Meuse (1970–2000) and Mississippi (1974/75–2000) are slightly lower than observation, while simulated total N concentrations exceed measurements by less than about a factor of two. Moreover, the model not only reproduces actual concentrations, but also captures quite well the long-term trends during the monitoring period.

Another performance test involves a direct comparison between aggregated data and model results for a large number of European rivers (European Environment Agency 2013). This dataset includes 125 rivers, 49 for N and 76 for P. Results show a reasonable coefficients of determination (R^2) of 0.6 for P ($n = 981$) and N ($n = 709$). The average of all measurements for N and P is slightly lower than the simulated concentrations (0.16 versus 0.23 mg P l^{-1} and 1.25 versus 1.40 mg N l^{-1}). The mean of observations and model values over the monitoring period for each station showed good agreement. There is also good agreement between model and data for the mean for all stations for each year (SI S5.11 and Figure S5.2).

Our model results also show a much better agreement with the validation dataset for the early 1990's for total N collected by Van Drecht et al. (2003) with smaller residuals than the earlier model versions without in-stream nutrient processing (see Figure S5.3). Modeled total N concentrations for the Amazon for the early to mid-1980's (0.7–0.9 mg l^{-1}) are close to the measured values (0.4–0.5), and results for total P (0.07 mg l^{-1}) are close to observations (0.06 mg l^{-1}) (Meybeck and Ragu 1995, Forsberg et al. 1988).

5.3.2   Model sensitivity and uncertainties

Various factors may cause model errors, for example the simulated hydrology, delivery, and climate. The influence of a range of factors on simulated concentra-
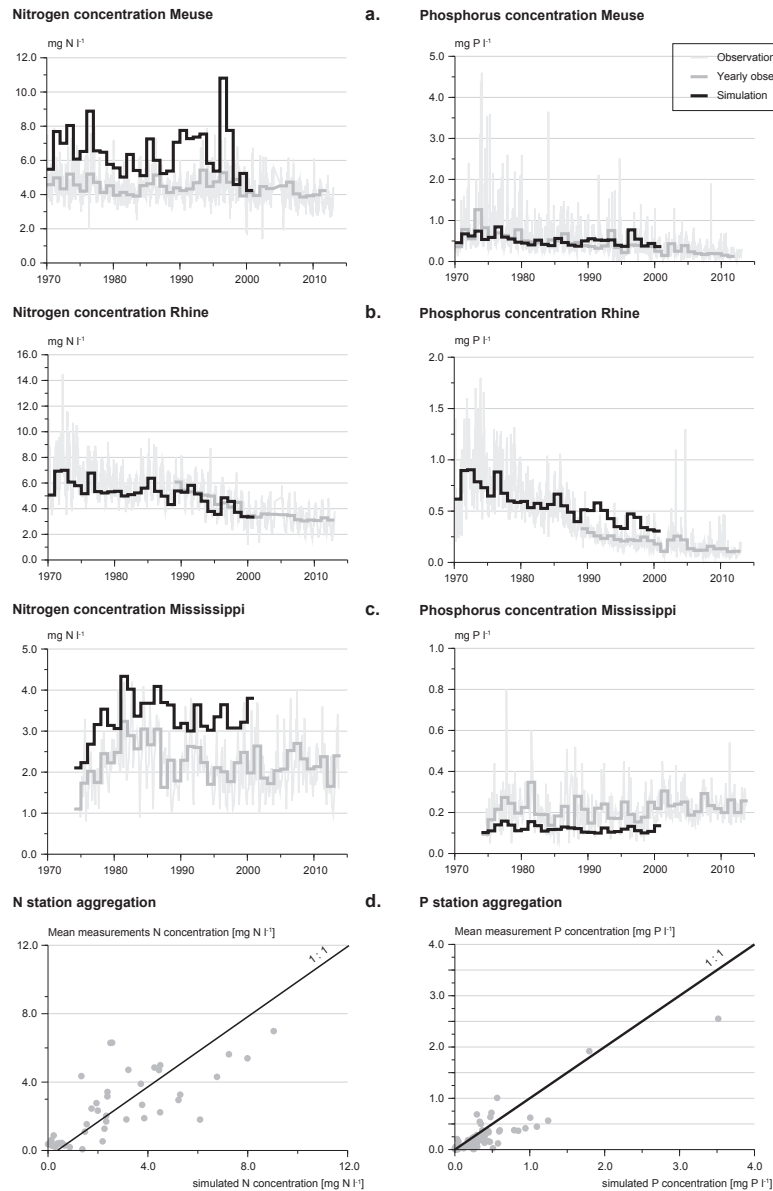
Figure 5.2: Comparison of modeled (black line) and measured (light grey, and aggregated yearly values in dark grey) concentrations of total N (left) and P (right) in the rivers Meuse (a), Rhine (b), Mississippi (c) and mean of observations and model values over the monitoring period for each station for a set of European rivers (d) (See S5.11 for a description of monitoring data). Yearly mean discharge-weighed concentrations have been calculated for those years with available discharge data.

tions was investigated in the sensitivity analysis for the years 1900, 1950 and 2000. Results presented in Tables S5.4 and S5.5 show that the sensitivity of modeled delivery, retention, and river export of N differs from that of P in many aspects. Total runoff (q_{tot}) is more important for delivery, retention, and river export of P than for N because it is also driving weathering of P.

The soil N budget is an important factor in natural ecosystems. For crop systems, the soil N budget is important for N delivery and river export in 2000. For P the budgets are less important, because soil P governs P runoff and not the budget. The reduction fraction of N leaching in natural ecosystems (equation S5.6) is an important factor for N delivery to streams, and is only important for river N export in 1900.

Our model results suggest that allochtonous organic matter input to stream is an important but uncertain nutrient source. The factors determining the allochtonous organic matter input of N and P to streams and rivers (flooded area, litterfall, its reduction factor for litterfall, and its $C:N$ and $C:P$ ratio) are similarly important for the delivery and river export of N in 1900, 1950, and 2000. For P delivery, these factors are important in 1900, and allochtonous organic matter inputs are less important for P than for N.

The P weathering source is significant for delivery in 1900 and 1950, and for river P export in 1900. In later years, the anthropogenic sources become increasingly dominant.

For the modelling of river retention, the sensitivity analysis for a range of parameters shows that net uptake velocity and mean length ratio (ratio of mean length of nth order river divided by the mean length of $(n-1)$ order river) are important for retention and river export for both N and P. For nitrogen, the assumption that N retention depends on concentration is significant in all years for the retention and river export. Temperature is important for retention of P for all years, and for retention and river export of N for all years.

Results of the sensitivity analysis differ from previous studies (e.g., Bouwman et al. 2013a), primarily because the current model includes additional sources (allochtonous inputs) and changes in the model for surface runoff and leaching.

5.3.3   N and P delivery to surface water

Agricultural budgets (Bouwman et al. 2013d) and total N budget (Bouwman et al. 2013a) have been discussed elsewhere. The total soil N and P budgets, including the increase in soil P, are briefly discussed in SI S5.10. Global N delivery to surface water increased from 34 to 64 Tg yr^{-1} (Figure 5.3), i.e., a $\approx 90\%$ increase; global P delivery increased from 5 to 9 Tg yr^{-1} (Figure 5.4). Similar to the soil N budgets, the increase has been most rapid for the Pacific Ocean, Indian Ocean and Mediterranean Sea and Black Sea; the Indian Ocean is close to the global average ($\approx 90\%$ increase), and the Arctic and Atlantic and endorheic rivers are less than the global average (Figure 5.3). For P, the increase rates in the delivery show similar differences between oceans, but the increase rates have been less rapid (globally 81%, Pacific 143%, Mediterranean Sea and Black Sea 92%, Indian Ocean
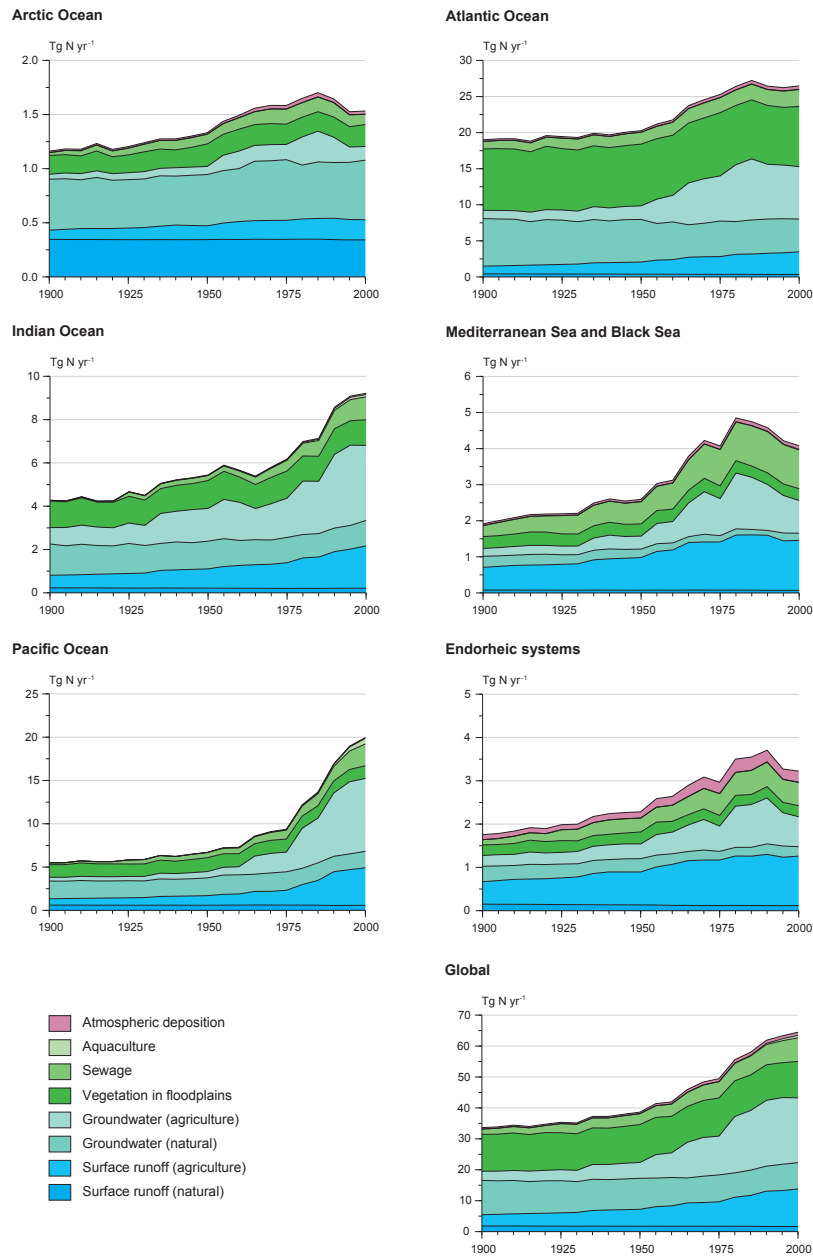
Figure 5.3: N delivered to surface water from different sources (surface runoff from natural ecosystems and agriculture, groundwater, wastewater, atmospheric deposition and aquaculture) for rivers discharging in the Arctic ocean, Atlantic Ocean, Indian Ocean, Mediterranean Sea and Black Sea, Pacific Ocean, endorheic systems, and global for the 20th century.
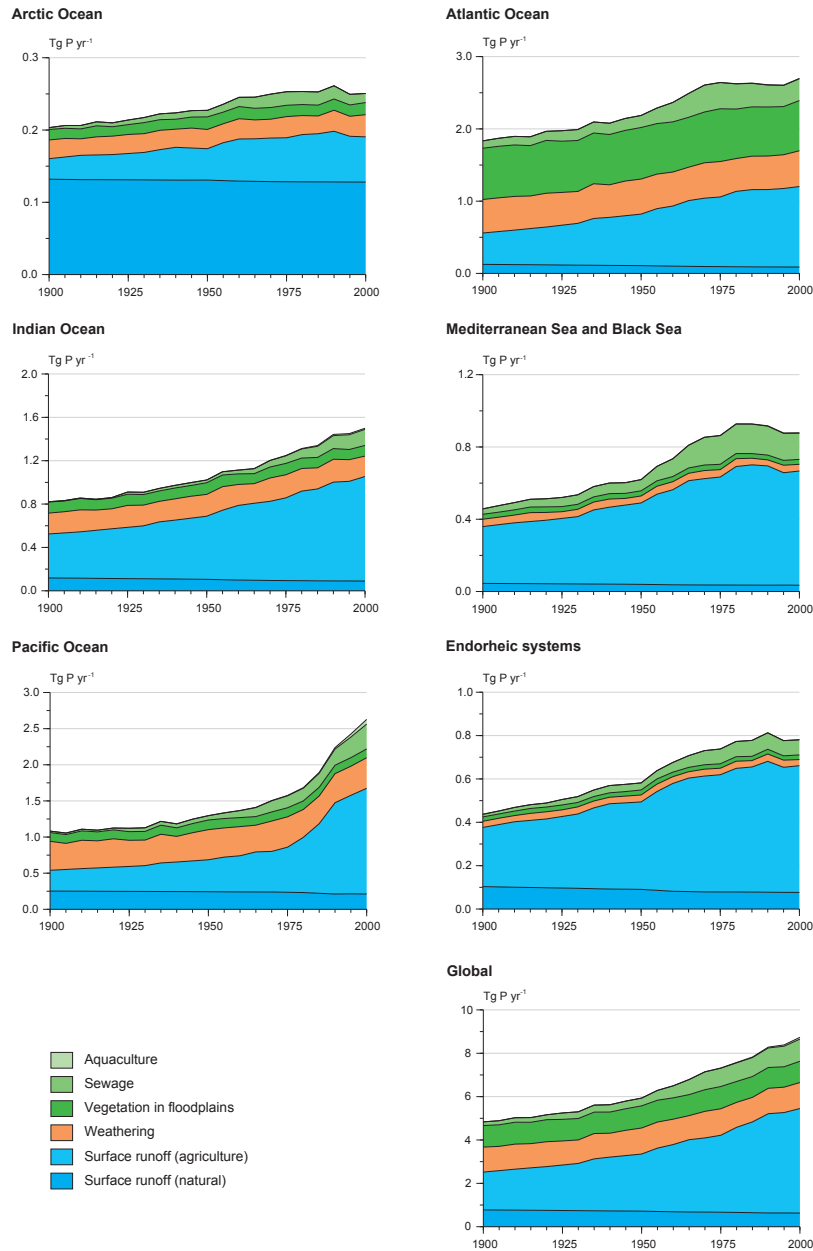
Figure 5.4: P delivered to surface water from different sources (surface runoff from natural ecosystems and agriculture, wastewater, aquaculture and weathering) for rivers discharging in the Arctic ocean, Atlantic Ocean, Indian Ocean, Mediterranean Sea and Black Sea, Pacific Ocean, endorheic systems, and global for the 20th century.

82%, endorheic rivers 79%, Arctic 23%, Atlantic 47%) (Figure 5.4).

The contribution of the various sources to the delivery to surface water (Figure 5.3 and 5.4) varies from place to place. Globally, the contribution of natural vegetation in floodplains is large and almost constant, and its relative share decreased due to increases in other sources. In absolute terms, most increases came from the total of diffuse sources, i.e., globally from 32 to 55 Tg N yr^{-1} and from 5 to 8 Tg P yr^{-1}. The delivery by diffuse sources to rivers discharging in the Pacific (30% for N, 29% for P) and Atlantic (43% for N and for 31% P) both contributed a large share to global diffuse delivery in 2000. Globally, the relative increase was more rapid for N (75%) than for P (64%), and more rapid for rivers draining into the Pacific Ocean (217% for N and 109% for P) than for all other rivers. Rivers draining into the Atlantic showed a slower increase (33% for N, 38% for P) than the global average, and the Indian Ocean and Mediterranean Sea and Black Sea increased similarly as the global average.

The contribution of agriculture (surface runoff, groundwater) increased most in the Pacific and Indian regions. Agriculture also increased rapidly in the Mediterranean region between 1950 and 1980, and started to decrease afterwards. The Atlantic region is dominated by large rivers such as the Amazon and Congo. Comparison with the continental aggregated results (not shown) shows that trends in Europe as a whole are similar to those of the Mediterranean region. Surface runoff is a very large source of P in the Mediterranean, Indian and Pacific region, and less so in the Atlantic.

Smaller absolute but spectacular relative increases came from the point sources. The delivery by point sources increased globally from 2 to 8 Tg N yr^{-1} (+340%) and from 0.2 to 1 Tg P yr^{-1} (+500%) between 1900 and 2000. The increase was slightly less than the global average in most rivers, but for the Pacific Ocean (factor of 12 for N and 17 for P) and Indian Ocean (factor of 39 for N and 50 for P) the increase is much more rapid.

Delivery of N and P by aquaculture also showed a dramatic increase after 1950, but remains small compared to the diffuse and natural sources. Atmospheric deposition also increased, but its contribution also remains small. Locally, however, aquaculture and atmospheric N deposition may be important and even dominant.

The molar N : P ratio of total nutrient delivery showed small variations in the course of time in most parts of the world (globally 14–17; Arctic 12–15; Atlantic 20–23; Indian 11–14; Mediterranean Sea and Black Sea 9–12; endorheic rivers 9–10) (Figure 5.5). However, the changes were much larger in the Pacific (increase from 11 to 17 between 1900 and 2000). The patterns of change varied, with a decrease in N : P ratio for the Atlantic rivers in the first part of the century, and an increase in the last part of the century, while the N : P ratio in the nutrients delivered to rivers draining into the Pacific Ocean and Indian Ocean did not show a trend in the first part of the century, and show an increase after 1950 and a decrease after 1980/1990.
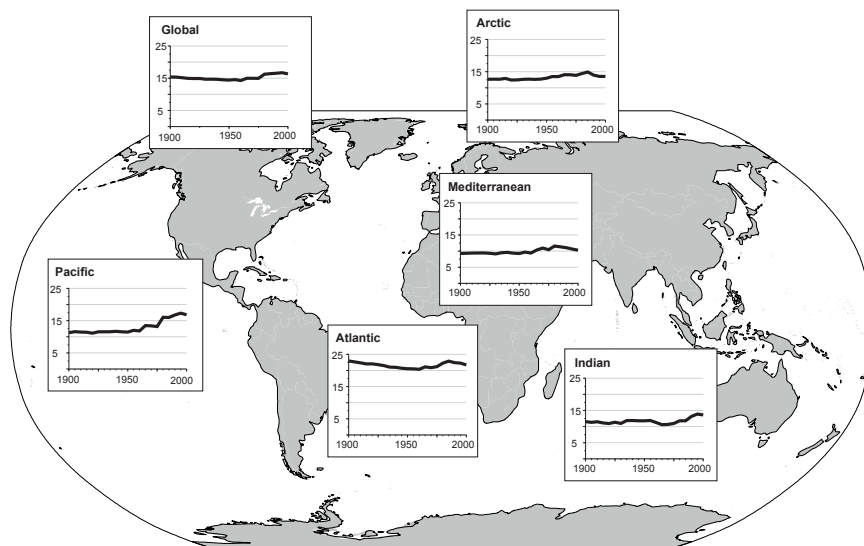
Figure 5.5: Molar N : P ratio of water delivered to surface water for rivers discharging in the Arctic ocean, Atlantic Ocean, Indian Ocean, Pacific Ocean and Mediterranean Sea and Black Sea for the 20th century.

5.3.4   N and P retention in rivers

Global nutrient retention was rather constant (41–44% for N, and 53–58% for P) during the 20th century, with minor variations from year to year and an increase by a few percent in the last three decades (Figure 5.6). There are, however, large differences in the total retention between Mediterranean Sea and Black Sea (44–52%), Indian Ocean (37–53%), Pacific (27–32%), Atlantic (38–44%), with an increase in Atlantic and Indian in the last decades, and a gradual decrease in the Pacific Ocean. The P retention is largest in the Indian Ocean (54–66%, with a gradual increase with time). P retention is smaller in the Arctic Ocean and Mediterranean Sea and Black Sea (both 50–60%), Atlantic (48–55%), and Pacific (37–42%), and in these regions there are no clear trends in the period 1900–1970, and an increase in the last three decades.

Total retention is the net result of changes in the retention in the streams and rivers, lakes and reservoirs. N and P retention in streams and rivers has the largest contribution to total retention in all parts of the world, except endorheic systems. River and lake retention decreased, and reservoir retention increased, in some cases at the cost of lake retention where dams have been constructed in a lake area. In 1900, rivers contributed 75% to total N retention and 82% for P, and lakes about 25% for N and 18% for P, and this changed rapidly in rivers 53% for N and 63% for P and lakes (22% for N and 15% for P), respectively, in the year 2000, the complement being retention in reservoirs (25% for N and 22% for P).
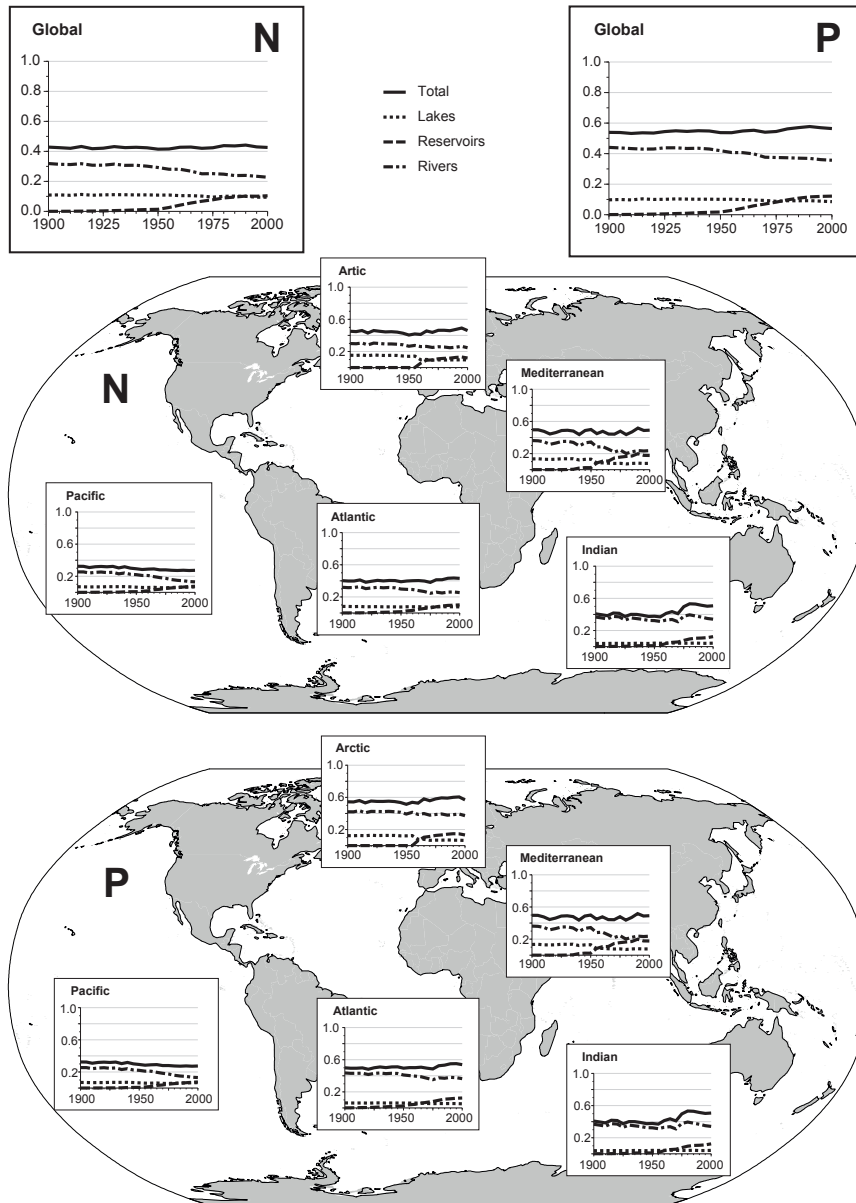
Figure 5.6: Retention (fraction retained) of N and P in water delivered to surface water for rivers discharging in the Arctic ocean, Atlantic Ocean, Indian Ocean, Pacific Ocean and Mediterranean Sea and Black Sea for the 20th century.

Rivers draining into the Mediterranean Sea and Black Sea retain more N and P than the global average due to the importance of reservoir retention. The share of reservoirs in total N retention is around 25% globally, except in rivers draining into the Mediterranean Sea and Black Sea, where it is 36% for N and 29% for P for the year 2000. This is related to the construction of the Aswan Dam between 1960 and 1970, and the Iron Gate dams in the Danube river between 1972 and 1984.

Total N and P retention in rivers draining into the Pacific Ocean is less than the global average. In this part of the world reservoirs play a smaller part, and also rivers and lakes retain less nutrients than elsewhere; N retention slowly decreased due to the effect of increasing N concentrations in surface water, while P retention was more or less constant, due to increasing retention in reservoirs balancing the decreasing river retention due to regulation of the discharge.

Our model for N retention based on the spiraling concept is more sophisticated than earlier versions with a fixed retention rate of 30% (Van Drecht et al. 2003). Our global average N retention (43%) is larger, mainly due to the implementation of sub-grid retention in lower order streams. Moreover, our model accounts for heterogeneity due to hydrology, climate and N concentration. Our calculated retention is less than the 53% computed globally by Wollheim et al. (2008a). This may have several causes, the major ones being differences in hydrology, input and its spatial distribution. It is difficult to compare retention among models, since it depends on the nutrient delivery to surface water, and Hejzlar et al. (2009) found in a model comparison that the simulated N and P retention showed larger differences among the models than among rivers. To our knowledge, there is no global model for P river transport that includes in-stream processing, available for comparison.

Simulated P retention reflects sorption of P in the sediments of reservoirs, lakes and streams and rivers. The model does not describe desorption processes in the case of exchange between the water column and P-saturated sediment material (Richardson and Qian 1999, Reddy et al. 1999).

5.3.5   N and P export to coastal marine ecosystems

In the 20th century the global river export of N (19 to 37 Tg yr^{-1}, or +93%) showed a more rapid increase than that of P (3 to 4 Tg yr^{-1}, or +71%). The increase in N export by rivers draining into the Pacific Ocean (+290% for N) and Mediterranean Sea and Black Sea (+115%) is much faster than in other parts of the world (Figure 5.7). The increase in P export was largest in the Pacific (+142%) and Mediterranean Sea and Black Sea (77%), and smaller than that of N in all parts of the world.

The differential increase of N and P explains the increase in the N:P ratio in rivers draining into the Pacific (13 to 21), Indian Ocean (14 to 20), Mediterranean Sea and Black Sea (10 to 14) and no clear increase for the Atlantic Ocean (Figure 5.8). Similar to the nutrient delivery to surface water, the rivers draining into the Pacific and Indian Oceans showed no trend in the first half of the century,
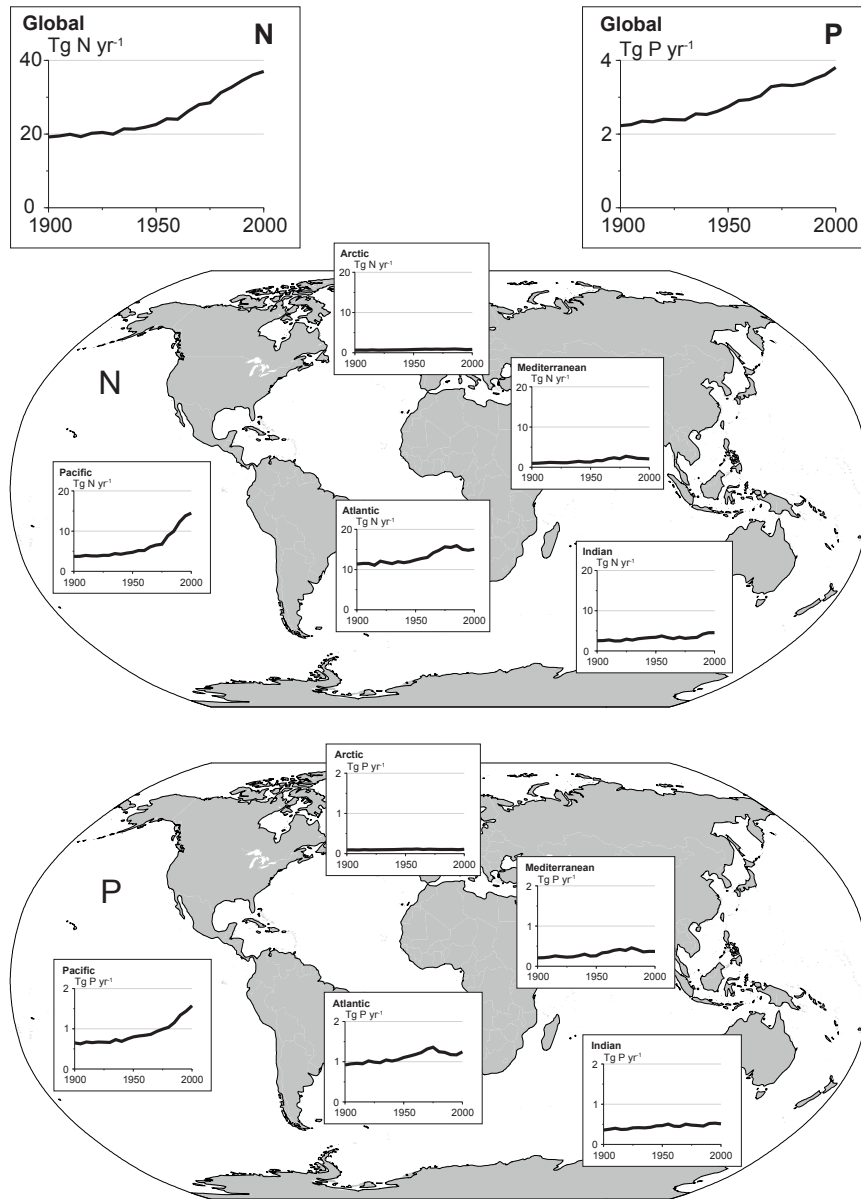
Figure 5.7: River export of N and P to coastal marine ecosystems for rivers discharging in the Arctic ocean, Atlantic Ocean, Indian Ocean, Pacific Ocean and Mediterranean Sea and Black Sea for the 20th century.

Figure 5.8: Molar N : P ratio of water exported to coastal marine ecosystems for rivers discharging in the Arctic ocean, Atlantic Ocean, Indian Ocean, Pacific Ocean and Mediterranean Sea and Black Sea for the 20th century.
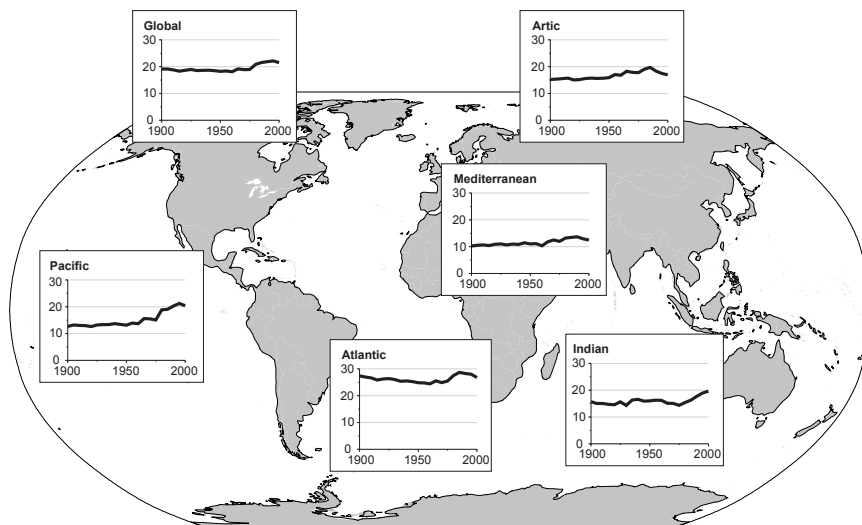
and began to increase in the last 3–4 decades, while in the Atlantic the N : P ratio showed a decreasing trend in the first half, an increase after 1950/1960 and a decrease again after 1980/1990.

Global estimates of current river N export vary widely, ranging from close to 60 Tg N yr^{-1} (Boyer et al. 2006b, Seitzinger et al. 2005) to close to 40 Tg N yr^{-1} (Green et al. 2004). A previous version of our model with a constant global export coefficient yielded estimates of 54 Tg N yr^{-1} (Van Drecht et al. 2003) and 46 (Bouwman et al. 2005b). Our global river N export for 2000 is on the low end of the range of estimates. Our global estimate for river export for total N is close to the Global NEWS model estimate of 43 Tg yr^{-1}, while simulated P export is much less than the estimate of 8.6 Tg P yr^{-1} (Seitzinger et al. 2010).

Our simulated river P export is much smaller than the estimate of 22 Tg P yr^{-1}, which includes 20 Tg yr^{-1} of particulate P (Meybeck 1982). The latter estimate was based on five extrapolation methods using data for a limited number rivers. Our model results suggest that given the strength of each of the sources and range of uncertainty in each of them, global estimates for river P export exceeding 10 Tg yr^{-1} seem unrealistic.

5.4   Concluding remarks

This paper presents the first global spatially explicit approach based on coupled hydrology – N and P delivery to surface water – in-stream retention. Model results without specific calibration are in fair agreement with time series of concentration measurements for a selection of large and smaller rivers. As such our model is similarly useful as the more empirical models in use; however, in addition to estimating of river nutrient export, our model can also be used to explore changes in various processes and interactions between them during the 20th century. We portray the dramatic changes that occurred during the 20th century in both delivery and in-stream retention due to expanding agriculture, increasing wastewater discharge, and construction of dams and formation of reservoirs.

Model results indicate a rapid increase of reservoir retention due to the construction of dams; at the same time, this intervention in the hydrologic system reduces the monthly variation in river discharge, with less flooding and a decrease of the retention downstream of the dam. However, the model also suggests that there has been a world-wide increase of nutrient delivery during the 20th century that is much larger than the increase in retention induced by reservoir development with the consequence that river transport of nutrients to the ocean increased.

The model results indicate important differences in N : P ratios in river export in different parts of the world resulting from the interplay of many processes and economic activities in different river basins. River export shows a world-wide increase in the molar N : P ratio during recent decades, primarily as a result of the stagnating P fertilizer and ever increasing N fertilizer use.

Increasing river export is responsible for eutrophication of coastal marine ecosystems leading to phenomena such as increased production and hypoxia; changing nutrient stoichiometry may lead to phenomena such as harmful algal blooms. Analysis of what the impacts of nutrients have been in the past, and how eutrophication effects will change in future scenarios, requires coupling our model to coastal biogeochemistry models.

Our results indicate that the estimated global river P export was largely overestimated by Meybeck (1982) who based his estimate on C : P ratios for small number of rivers; our sensitivity analysis shows that any estimated global river export > 10 Tg P yr^{-1} is unrealistic.

Separate uncoupled models can be used for in-stream processing of N and P, as different processes are responsible for N and P retention, i.e., denitrification and chemical sorption. Only in case of plant uptake and decomposition and mineralization there is a close coupling of N and P (and C and Si). Particularly small streams are known to play an important role in nutrient retention (Wollheim et al. 2008a, Ensign and Doyle 2006). The hydrology model lacks first-order to fifth order streams; therefore it was necessary to describe the biogeochemistry with a simple a priori parameterization of sub-grid spiraling. This parameterization shows that improving the resolution to 5 by 5 minutes will not result in a better representation of lower-order streams.

A first simple improvement of the in-stream model is by adding the process

of P saturation of sediments and desorption in case of decreasing river P loads. A next, larger step is the incorporation of a mechanistic model for describing in-stream processes. This allows us to analyze the individual processes and their interplay (plant uptake, sedimentation, diagenetic processes, denitrification), and also to simulate the different nutrient forms, which is important when studying impacts such as harmful algal blooms, blue-green algae and hypoxia.

Acknowledgments

Supporting information

S5.1   The IMAGE model

The objective of the Integrated Model for the Assessment of the Global Environment (IMAGE) version 2.4 model (Bouwman et al. 2006) is to explore the long-term dynamics of global environmental change. The model consists of several modules. General economic and demographic trends for 24 world regions drive human activities. Regional energy consumption, energy efficiency improvement, fuel substitution, supply and trade of fossil fuels and renewable energy technologies are simulated with The IMAGE Energy Regional Model (TIMER) (Van Vuuren et al. 2006) to calculate energy production, energy use, industrial production, emissions of greenhouse gases, ozone precursors and sulfur. Ecosystem, crop and land-use models are used to compute land use on the basis of regional consumption, technological developments, production and trading of food, animal feed, fodder, grass and timber, and local climatic and terrain properties.

Greenhouse gas emissions from land-use change, natural ecosystems and agricultural production systems are computed as well as the biosphere-atmosphere exchange of carbon dioxide (CO_2). The atmospheric and ocean models calculate changes in atmospheric composition by employing the emissions and by taking oceanic CO_2 uptake and atmospheric chemistry into consideration. Subsequently, changes in climate are computed by resolving oceanic heat transport and changes in radiative forcing by greenhouse gases and aerosols. The ecosystem and crop growth models of IMAGE account for feedbacks of climate change and rising atmospheric CO_2.

Although IMAGE 2.4 is global in application (with data and scenarios at the scale of world regions), it performs many of its calculations on a terrestrial $0.5°$ by $0.5°$ resolution (crop yields and crop distribution, land cover, land-use emissions, nutrient surface balances and carbon (C) cycle). Data from many different sources are used to calibrate the energy, climate and land-use variables over the 1970–2000 period.

S5.2   Hydrology

S5.2.1   Water balance

Each grid cell represents varying fractions of contiguous land and fresh water surfaces. The fresh water surface represents the drainage network of laterally connected channels, lakes and reservoirs along which the locally generated specific runoff is accumulated and routed to obtain the river discharge. Land cover is either natural vegetation, cropland or grassland.

Water drains from the soil column and is delivered as specific runoff to the drainage network, consisting of direct runoff, interflow and base flow. PCR-GLOBWB was used here to simulate the runoff and convert it into regulated discharge (i.e., with inclusion of reservoirs but without water abstraction) and this was used to simulate waterborne nutrient transport. First, total runoff q_{tot} (m yr^{-1}) is divided into surface runoff and excess water flow:

$$q_{\text{tot}} \;=\; q_{\text{sro}} + q_{\text{eff}} \;=\; f_{\text{qsro}}\, q_{\text{tot}} + q_{\text{eff}} \qquad (\text{S5.1})$$

where q_{sro} is surface runoff (m yr^{-1}) and q_{eff} is the excess water flow to the soil (m yr^{-1}). Surface runoff is a large part of total runoff in steep areas or in flat terrain with sealed surfaces (e.g., urban areas) or in areas covered with an impermeable topsoil. In our model this is reflected by a slope dependent runoff factor, which is fitted to the slope-runoff classification for unconsolidated sediments according to Bogena et al. (2005):

$$f_{\text{qsro}}(slope) \;=\; 1 - e^{-0.00617\, \max[1,S]} \qquad (\text{S5.2})$$

where S is the slope in m km^{-1}. Since this function is non-linear, $f_{\text{qsro}}(slope)$ is the median value of all 90 by 90 m cells within each grid cell. Factors that reduce surface runoff are land use and soil texture (Velthof et al. 2009, 2007):

$$f_{\text{qsro}} \;=\; f_{\text{qsro}}(slope)\, f_{\text{qsro}}(texture)\, f_{\text{qsro}}(landuse) \qquad (\text{S5.3})$$

We assume that surface runoff is not limited ($f_{\text{qsro}}(texture) = 1.0$) in soils with very fine topsoil texture; $f_{\text{qsro}}(texture) = 0.75$ for loam and sandy loam, and 0.25 for coarse sand and peat.

Water stagnation may occur in flat land (slope < 20 m km^{-1}) where soils are saturated based on the Improved Arno Scheme (Todini 1996, Hageman and Gates 2003). Soils that are (semi-)permanently saturated are identified as poorly drained areas and are associated with the occurrence of bogs and peat lands. Also, where percolation at the interface between soil and groundwater reservoir is impeded (e.g., in the case of permafrost), water can stagnate and drain as topographically driven saturated interflow.

After infiltration, groundwater flows laterally to ditches and streams or vertically to groundwater. Two groundwater subsystems are distinguished (main text, Figure 1). The shallow groundwater system represents the upper 5 meters of the saturated zone and is characterized by short residence times before water enters

Table S5.1: Porosity (p), the fraction of excess water flowing to deep groundwater ($f_{\text{qgwb}}(p)$), half life of nitrate in groundwater ($dt50_{\text{den}}$), activation energy ($E_{a,w}$) and background P concentration (C_{PWeath}) for various lithological classes

Lithological class[a]	Porosity (p)[b] $(\text{m}^3\ \text{m}^{-3})$	$f_{\text{Qgwb}}(p)$ (-)	$dt50_{\text{den}}$ (yr)	$E_{a,w}$ (kJ mol^{-1})	C_{PWeath}[c] (g m^{-3})
1. Alluvial deposits	0.15	0.50	2	50	0.0516
2. Loess	0.20	0.67	5	50	0.0256
3. Dunes and shifting sands	0.30	1.00	5	50	0.0790
4. Non-Semiconsolidated sedimentary	0.30	1.00	5	60	0.0248
5. Evaporites	0.20	0.67	5	0	0.0000
6. Carbonated consolidated sedimentary	0.10	0.33	5	0	0.0708
7. Mixed consolidated sedimentary	0.10	0.33	5	60	0.1032
8. Silici-clastic consolidated sediment[d]	0.10	0.33	1	60	0.0568
9. Volcanic basic	0.05	0.17	5	50	0.0896
10. Plutonic basic	0.05	0.17	5	50	0.0896
11. Volcanic acid	0.05	0.17	5	60	0.0116
12. Complex lithology	0.02	0.07	5	60	0.0645
13. Plutonic acid	0.02	0.07	5	60	0.0224
14. Metamorphic rock	0.02	0.07	5	60	0.0336
15. Precambrian basement	0.02	0.07	5	60	0.0224

[a] Lithological classes as defined by Dürr et al. (2005).
[b] $f_{\text{Qgwb}}(p) = p/0.3$, 0.3 being maximum porosity.
[c] Background P concentrations (C_{PWeath}) were calculated on the basis of Hartmann et al. (2014).
[d] Weathered shales containing pyrite.

local surface water at short distances (< 1 km) or infiltrates the deep groundwater system. A deep system with a thickness of 50 m (Meinardi 1994) is defined where a deeper groundwater flow is present (SI S5.2.4) and contributes substantially to the runoff. This deep groundwater system has longer residence times than the shallow system, as water flows to greater depths and drains to larger rivers at greater distances (> 1 km).

The partitioning of the excess water flow q_{eff} between interflow (shallow system) and groundwater runoff (deep system) is based on the effective porosity of the parent material (SI S5.5, Table S5.1).

All interflow (if present) in a grid cell is assumed to flow towards streams through riparian zones (Figure 5.1), except in (fractions of) grid cells with surface water bodies, such as wetlands, lakes or larger streams, where shallow groundwater by-passes riparian zones.

Although riparian zones generally represent a small area of the drainage basin, they are critical control points for groundwater fluxes and dissolved N within many watersheds (Vidon and Hill 2006). Riparian zones along small streams have long ecotone lengths within drainage networks, and are considered more important for groundwater N processing than those bordering larger water bodies.

S5.2.2   Vegetation and land cover

Vegetation effects are taken into account by partitioning the land surface by fraction into different types. Similarly, spatial variations in soil properties can be accounted for by considering effective values for each of these vegetation types.

Soil characteristics are assumed to be constant under changing land cover, except for soil total available water capacity (*tawc*); the relative distribution of *tawc* varies with changing root depth distributions based on Canadell et al. (1996). All other soil parameters are from the FAO Digital Soil Map of the World (FAO 1991) and ISRIC Wise data (Batjes 1997, 2002). Lithological properties (such as hydraulic conductivity) are derived from a global lithological map (Dürr et al. 2005).

Similar to earlier implementations of PCR-GLOBWB, vegetation parameters are taken from the Olson classification of the GLCC dataset with a resolution of 30 arc seconds and values assigned using the parameter dataset of Hagemann et al. (1999). The parameterization is adjusted to the reconstruction of agricultural land cover for 1900–2000 with 5-year time steps derived from the IMAGE model (Bouwman et al. 2013d) based on historical data (Klein Goldewijk et al. 2011) in order to achieve consistency between the simulated hydrology and imposed land use (SI S5.3).

S5.2.3   Drainage network

Water bodies such as lakes and reservoirs can extend over several $0.5°$ by $0.5°$ grid cells and are included if their volume exceeds that of the channel within a cell. Where more than one reservoir is located within the same grid cell, they are merged and the combined storage and volume assigned to the dominant reservoir. At the start of the simulation, in 1901, 107 out of a total of 132 reservoirs of the GRaND is included as 88 spatially individual water bodies, corresponding to 78% of the reported total volume of 16.4 km^3. For 2000, 5595 out of a total of 6369 reservoirs are included as 3507 spatially individual water bodies, corresponding to 98% of the reported total volume of 5848.4 km^3. No demand is imposed on the reservoirs and by default they are assigned the purpose of hydropower generation. In absence of pricing generation at the global scale (Haddeland et al. 2006, Adam and Lettenmaier 2008), this results in an operation that maximizes the available potential energy. In this case, this conforms with 75% of the maximum storage capacity in absence of detailed global data. The remaining 25% are reserved to buffer inflow for flood control purposes. Reservoir release is linearly scaled to storage when reservoir storage falls below 30% of the available capacity. This reduced

outflow also results in a realistic, gradual filling of reservoirs after completion of dam construction.

S5.2.4   Occurrence of deep groundwater

Deep groundwater is assumed to be absent (i) in areas with non-permeable, consolidated rocks; (ii) in the presence of surface water (rivers, lakes, wetlands, reservoirs); and (iii) in coastal lowlands (< 5 m above sea level), where we assumed (artificial) drainage or high groundwater levels.

S5.3   Linking IMAGE and PCR-GLOBWB land cover

The land cover reconstruction for the 20th century specifies the fractions of arable land and grassland within each $0.5°$ by $0.5°$ grid cell. To combine this information with the Olson classification, three separate maps at the original resolution of 30 arc seconds were created, including (i) Olson classes that were assumed to represent semi-natural vegetation and that were spatially extrapolated per Holdridge Life Zone (Holdridge 1967); (ii) Olson classes representing cropland; and (iii) Olson classes representing grassland.

For the reconstructed land cover under the two agriculturally managed conditions, i.e., crops and pasture, all 30 arc seconds cells within a $0.5°$ by $0.5°$ cell are ranked in order of decreasing suitability from 0 to 1. This is achieved by first delineating their current extent in the GLCC and ranking on the basis of slope, computed from the Hydro1k database (Verdin and Greenlee 1996). Next, the adjoining cells are ranked on the basis of the slope parallel distance starting from the delineated areas. These rank orders are then normalized, values near zero indicating the most suitable locations, one indicating the poorest locations, and used to match the IMAGE derived fractions for each $0.5°$ by $0.5°$ cells. In this procedure, cropland has priority, followed by grassland. Any remaining areas are subsequently filled with semi-natural vegetation types. On the basis of the resulting patched land cover, the land cover parameterization for PCR-GLOBWB was then derived.

S5.4   Soil nutrient budgets

The soil N budget (N_{budget}) was calculated as follows:

$$N_{\text{budget}} = N_{\text{fix}} + N_{\text{dep}} + N_{\text{fert}} + N_{\text{man}} - N_{\text{withdr}} - N_{\text{vol}} \qquad \text{(S5.4)}$$

where N_{fix} is biological N fixation, N_{dep} is atmospheric N deposition, N_{fert} is application of synthetic N fertilizer, N_{man} is animal manure, N_{withdr} is N withdrawal from the field through crop harvesting, hay and grass cutting, and grass consumed

Table S5.2: Denitrification fractions for soil texture, soil organic carbon and soil drainage. Source: Van Drecht et al. (2003)

Soil texture class	f_{text} (-)	Soil drainage	f_{drain} (-)	Soil organic carbon content	f_{SOC} (-)
Coarse	0.0	Excessively-well drained	0.0	$< 1\%$	0
Medium	0.1	Moderate well drained	0.1	1–3%	0.1
Fine	0.2	Imperfectly drained	0.2	3–6%	0.2
Very fine	0.3	Poorly drained	0.3	6–50%	0.3
Organic	0.0	Very poorly drained	0.4	Organic	0.3

by grazing animals, N_{vol} is ammonia (NH$_3$) volatilization. The P budget is calculated in a similar way, P inputs being from fertilizer and animal manure, and output being crop withdrawal.

The estimates for biological N fixation rates in natural ecosystems are based on Vitousek et al. (2013). They estimated that N fixation was only 58 Tg yr^{-1} in pre-industrial times. Here, we used the low estimate for the areal coverage of leguminous plants from Cleveland et al. (1999) as discussed by Bouwman et al. (2013a), and this yields an estimated global N fixation for 1900 of 75 Tg N yr^{-1} and of 53 Tg N yr^{-1} in 2000.

For 1900–1930 we assume constant soil budgets, 1935–1945 budgets are equal to those in 1950, and soil budgets for 1965 and 1975 are equal to 1970, and 1985 is equal to 1980.

For P, the model accounts for changes in soil P content due to soil P budget deficits or surpluses and soil loss due to erosion (see Section 5.2.2). This is because most soil P is absorbed by soil minerals, since P is retained in soil components with a continuum of bonding energies with varying degrees of reversibility. In contrast, most soil N is in soil organic matter, which can build-up in case of a positive budget (surplus), and be lost by soil organic matter decomposition and mineralization. The soil N budget ignores soil organic N changes, because modeling these processes would require complex soil process models. Therefore we assume that with no accumulation, N surpluses represent a potential loss (denitrification, surface runoff and leaching).

S5.5   Soil N leaching

For positive values of the soil N budget (equation S5.4), leaching from the top 1 m of soil (or less for shallow soils) is calculated as a fraction $f_{\text{leach,soil}}$ (Van Drecht et al. 2003):

$$N_{\text{leach,soil}} = f_{\text{leach,soil}} \left(N_{\text{budget}} - N_{\text{sro}} \right) \tag{S5.5}$$

$$f_{\text{leach,soil}} = \left(1 - \min\left[(f_{\text{climate}} + f_{\text{text}} + f_{\text{drain}} + f_{\text{soc}}), 1 \right] \right) f_{\text{landuse}} \tag{S5.6}$$

where N_{sro} is the erosion of soil and organic matter containing N by surface runoff; f_{climate} (-) represents the effect of climate on denitrification rates, combining the

effects of temperature and residence time of water and NO_3^- in the root zone; f_{text}, f_{drain}, and f_{soc} (-) (Table S5.2) are factors representing the effects of soil texture, soil drainage, and soil organic C content, respectively. The factor f_{climate} is calculated as:

$$f_{\text{climate}} = T_{\text{r,so}} f_K \qquad (S5.7)$$

where f_K (-) is the temperature effect on denitrification, $T_{\text{r,so}}$ (yr) is the mean annual residence time of water and NO_3^- in the root zone. The temperature effect f_K is calculated according to the Arrhenius equation (Firestone 1982, Shaffer et al. 1991, Kragt et al. 1990):

$$f_K = 7.94 \cdot 10^{12} \exp\left(\frac{-E_{\text{a,d}}}{R\,K}\right) \qquad (S5.8)$$

where $E_{\text{a,d}}$ is the activation energy (74830 J mol^{-1}), K the mean annual temperature (Kelvin) and R is the molar gas constant (8.3144 J mol^{-1} K^{-1}). The mean annual residence time of water in the root zone is given by:

$$T_{\text{r,so}} = \frac{tawc}{q_{\text{eff}}} \qquad (S5.9)$$

where $tawc$ (m) is the soil total available water capacity for the top 1 m (or less if soils are shallower) and q_{eff} is excess water flow (equation S5.1). We assume that the residence time of NO_3^- equals that of water based on the high mobility of NO_3^- in soils. For agricultural soils under crops in dry regions we assume a minimum value for $T_{\text{r,so}}$ of 1.0; in dry regions agricultural crops can not grow without irrigation, and this is represented by assuming a total water supply equal to the soil water capacity.

This formulation implies that in arid regions residence time is long, resulting in values of f_{climate} and $f_{\text{den,soil}}$ equal to one, suggesting that 100% of the N surplus is removed by denitrification. In arid regions this is not realistic, since there are various fates of N, including accumulation of nitrate in the vases zone below the root zone (Walvoord et al. 2003), surface runoff, ammonia-N volatilization, nitrification, denitrification (Peterjohn and Schlesinger 1990). It is not possible to quantify the relative contribution of each process (Peterjohn and Schlesinger 1990), but it is clear that only a negligible part of N surpluses in arid climates is lost by denitrification. We therefore assume that the fate of the N surplus is determined by other processes than denitrification in soils under natural vegetation and grassland and with annual precipitation < 3 mm. The global amount of this N surplus in the 3100 Mha of arid lands was 20 Tg in the year 2000.

The factors for f_{text}, f_{drain}, and f_{soc} account for the soil water and O_2 status (Table S5.2). Anaerobic conditions favoring denitrification may be more easily reached and maintained for longer periods in fine-textured soils than in coarse-textured ones. This is because fine-textured soils have more capillary pores and hold water more tightly than sandy soils do. The factor f_{drain} accounts for soil aeration, and denitrification rates are generally higher in poorly drained than in well-drained soils (Bouwman et al. 1993). The soil O_2 status is also influenced by

root respiration and microbial activity. Oxygen consumption by microorganisms is driven by temperature, supply of C, and water availability. Temperature and soil water are represented in f_{climate}; we therefore use soil organic C content as a proxy for the C supply.

Finally, the coefficient f_{landuse} is the land use effect on leaching, where arable land has a value of 1, and grassland and natural vegetation a value of 0.36 (Keuskamp et al. 2012).

S5.6   Groundwater transport and denitrification

Here, denitrification is used to denote denitrification and anammox. The NO_3^- concentration in the excess water leaching from the root zone is calculated from the leached N and the excess water flow (q_{eff}, equation S5.1):

$$C_{\text{in}}(0) \quad = \quad \frac{N_{\text{leach}}}{q_{\text{eff}}} \tag{S5.10}$$

After infiltration, groundwater flows laterally to ditches and streams or vertically to deeper groundwater layers. Two groundwater subsystems are distinguished, similar to Van Drecht et al. (2003), De Wit and Pebesma (2001) and De Wit (2001). The shallow groundwater system represents the upper meters of the saturated zone (typically 5 m) and is characterized by short residence times before water enters local surface water at short distances or infiltrates the deep groundwater system.

The excess water flow q_{eff} (equation S5.1) is divided into interflow (shallow system) and groundwater runoff (deep system):

$$q_{\text{eff}} \quad = \quad (1 - f_{\text{qsro}})\, q_{\text{tot}} \quad = \quad q_{\text{int}} + q_{\text{gwb}} \tag{S5.11}$$

where q_{int} is interflow through the shallow system (m yr^{-1}), and q_{gwb} is the groundwater runoff through the deep system (m yr^{-1}). The fraction f_{qgwb} of q_{eff} that flows towards the deep system is obtained from:

$$f_{\text{qgwb}} \quad = \quad f_{\text{qgwb}}(p) \tag{S5.12}$$

where p is the effective porosity (-) (Table S5.1). We assume that the deep layer (if present) has the same characteristics as the surface layer.

We assume that no denitrification occurs in the deep groundwater system. We note that some denitrification could be expected with sedimentary organic matter and pyrite, but also that a bias exists in the literature for sites with rapid denitrification (Green et al. 2008), which makes assessment at the global scale difficult.

The NO_3^- concentration in groundwater depends on the historical year of infiltration into the saturated zone and the denitrification loss during its transport (Böhlke et al. 2002, Van Drecht et al. 2003). Outflow concentrations of N compounds depend on reaction progress. Therefore the time available for denitrification needs to be known. Since we use a time step of one year, seasonal changes

in groundwater level are ignored, and mean travel time $T_{\mathrm{r,aq}}$ depends on the ratio between specific groundwater volume and water recharge:

$$T_{\mathrm{r,aq}}(t) \;=\; \min\left[\frac{p\,D}{q_{\mathrm{inflow}}(t)}, 1000\right] \tag{S5.13}$$

where p is the effective porosity ($\mathrm{m^3\ m^{-3}}$), D is aquifer depth (m) (Table S5.1) and q_{inflow} is the water recharge of shallow groundwater, q_{int}, or recharge of deep groundwater, q_{gwb} ($\mathrm{m\ y^{-1}}$). Effective porosity is estimated based on the lithological class (Table S5.1). The deep system is fed by a vertically draining of the shallow system (Figure 5.1). The travel time distribution for vertical flow in the shallow system is uniform so travel time equals mean travel time. For lateral flow to surface water, travel times are highly variable. Meinardi (1994) describes travel time distribution for lateral flow in a vertical cross section as follows:

$$g_{\mathrm{age}}(z) \;=\; -T_{\mathrm{r,aq}} \ln\left(1 - \frac{z}{D}\right) \tag{S5.14}$$

where z is the depth (m; $z = 0$ at the top and and $z = D$ at the bottom of the aquifer), g_{age} is the age of groundwater at depth z (yr), and $T_{\mathrm{r,aq}}$ is the mean travel time over the thickness of the aquifer (yr). For shallow groundwater (sgrw) we assume $D_{\mathrm{sgrw}} = 5$ m, and for the deep groundwater (dgrw) layer (if present) $D_{\mathrm{dgrw}} = 50$ m (Meinardi 1994).

Denitrification during transport in the shallow system along each flow path in a homogeneous and isotropic aquifer, drained by parallel rivers or streams, is described by a first order degradation process. At time t and at depth z the outflow concentration is:

$$C(t,z) \;=\; C_0(t - g_{\mathrm{age}}(z))\,e^{-k\,g_{\mathrm{age}}(z)} \tag{S5.15}$$

where the decay rate k is:

$$k \;=\; \frac{\ln(2)}{dt50_{\mathrm{den}}} \tag{S5.16}$$

The $\mathrm{NO_3^-}$ concentration in the inflow to deep groundwater ($C_0(t)$) is the outflow from the shallow groundwater system. The half-life of $\mathrm{NO_3^-}$ in the shallow system $dt50_{\mathrm{den}}$ depends on the lithological class (Dürr et al. 2005), with low values (1 year) for silici-clastic material, 2 years for alluvial material, and 5 years for all other lithological classes. For $dt50_{\mathrm{den}} = 2$ and a travel time of 50 years, the $\mathrm{NO_3^-}$ concentration will be reduced by $e^{-k(t-50)}$, which is close to $3 \cdot 10^{-8}$.

Nitrogen transported through submarine groundwater discharge (SGD) is excluded from the delivery to rivers and other water bodies using the approach presented recently (Beusen et al. 2013). We use the groundwater and nitrate outflow for all coastal land, considering those aquifers within a strip of 5 km, i.e., only 10% of each $0.5°$ grid box contributes to SGD. The aquifers in the complement of the grid box are assumed to discharge towards streams and rivers.

The role of urbanized areas is neglected, because the total area of urbanized land is about 0.3% of the total land area of countries (Angel et al. 2005). We note that loss of N to the environment can be substantial in urbanized areas, where

sewerage systems are either well-developed or absent (e.g., Foppen 2002, Wakida and Lerner 2005, Van Den Brink et al. 2007, Nyenje et al. 2010). The role of natural NH_4^+ in groundwater is also neglected, which is justified by the observation that the median NH_4^+ concentration in groundwater of 25 European aquifers is 0.15 mg l^{-1} (Shand and Edmunds 2008), which is low (0.7–1.2%) compared to present-day agricultural contamination of groundwater with nitrate, for example in Europe (EEA 2013).

S5.7   Denitrification in riparian areas

Modelling riparian processes requires very detailed spatial information on hydrogeological conditions. It is impossible to know the location of riparian areas at the 0.5° by 0.5° resolution of this study, and even a 0.1 km resolution would not be adequate to determine the topography of riparian areas (Vidon and Hill 2006). We therefore used a conceptual approach.

For riparian areas, pH is one of the key parameters controlling denitrification rates (Simek and Cooper 2002, Knowles 1982), next to temperature, water saturation, NO_3^- availability and soil organic carbon availability. Under controlled conditions using pure cultures, denitrification activities have been shown to have an optimum at pH 6.5 to 7.5, and decrease at both low (below 4) and high (above 10) pH values.

The denitrification potential in riparian zones is based on the characteristics of the groundwater flow, soil and climate. Denitrification in riparian zones is calculated using the same approach as discussed for soil denitrification; in addition, we assume that heterotrophic denitrification is dominant and is highest at pH > 7 (Van Den Heuvel et al. 2010). A dimensionless denitrification pH reduction factor $f_{\text{denpH,rip}}$ is commonly included in denitrification models. This factor assumes a value of 1 at pH > 7 and values of 0 at pH < 3.

$$N_{\text{den,rip}} \;=\; f_{\text{den,rip}}\, N_{\text{in}} \tag{S5.17}$$

$$f_{\text{den,rip}} \;=\; \min[(f_{\text{climate}} + f_{\text{text}} + f_{\text{drain}} + f_{\text{soc}}), 1]\, f_{\text{denpH,rip}} \tag{S5.18}$$

The N_{in} entering the riparian zone is the residual in the shallow groundwater layer after denitrification has been accounted for. The factor f_{climate} includes the temperature effect f_{K} (equation S5.8) and the travel time $T_{\text{r,rip}}$ of water and NO_3^- through the riparian zone. $T_{\text{r,rip}}$ is calculated as follows:

$$T_{\text{r,rip}} \;=\; \frac{D_{\text{rip}}\, tawc}{q_{\text{int}}} \tag{S5.19}$$

where *tawc* is the available water capacity for the top 1 m, D_{rip} is the thickness of the riparian zone ($D_{\text{rip}} = 0.3$ m of soil, or less for shallow soils), and q_{int} is the interflow leaving the shallow groundwater system and flowing through riparian areas. Thus, $T_{\text{r,rip}}$ is short where the water flux is large or where the soil layer is thin.

S5.8   Other sources of nutrient delivery to surface water

The calculation of P release from weathering to rivers, P_{RLW}, is based on a recent study (Hartmann et al. 2014) which uses the lithological classes distinguished by Dürr et al. (2005). The lithological classes are available on a 5 by 5 minute resolution, hence the weighted average P concentration within each 0.5° by 0.5° grid cell is calculated, and the P_{RLW} (kg P yr^{-1}) is computed as follows:

$$P_{\mathrm{RLW}} \;=\; 0.001 \cdot C_{\mathrm{PWeath}} \cdot q_{\mathrm{tot}} \cdot A_{\mathrm{g}} \cdot SS_{\mathrm{corr}} \cdot \exp\left(\frac{-E_{\mathrm{a,w}}}{R}\left(\frac{1}{K} - \frac{1}{284} \right) \right) \quad \text{(S5.20)}$$

where C_{PWeath} (g m^{-3}) is the background concentration specified for each lithological class (Table S5.1) and derived from river runoff data, q_{tot} is the total runoff (m yr^{-1}), A_{g} is the land area (m^2) in the grid cell considered, SS_{corr} is a correction factor for soil shielding, $E_{\mathrm{a,w}}$ is the activation energy (J mol^{-1}), K the local mean annual air temperature (Kelvin), and R the molar gas constant (8.3144 J mol^{-1} K^{-1}). The soil shielding correction SS_{corr} is a correction factor of 0.1 leading to a 90% reduction for FAO soil units (FAO/UNESCO 1988), Ferralsols, Acrisols, Nitosols, Lixisols, Gleysols (soils with hydromorphic properties) and Histosols (organic soils). For all other soils $SS_{\mathrm{corr}} = 1$ (no reduction). With this approach, regions with the same lithology but with more precipitation have higher P weathering losses than regions in dry climates.

N and P inputs from wastewater for the 20$^{\mathrm{th}}$ century are from Morée et al. (2013), and those from freshwater aquaculture are calculated using the country-scale model estimates of Bouwman et al. (2013b) for finfish and Bouwman et al. (2011b) for shellfish using data for the period 1950–2000 from FAO (2013b); data indicate that prior to 1950 aquaculture production was negligible.

N and P emissions from aquaculture are allocated within countries using three weighing factors, i.e., population density, presence of surface water bodies, and mean annual air temperature. For population density, all grid cells with no inhabitants and those with more than 10,000 inhabitants km^{-2} are excluded; around an optimum density of 1000 inhabitants km^{-2}, a steep parabolic function on the left and less steep on the right are used to calculate the weighing. Lakes, reservoirs, rivers and wetlands have the maximum weight for water bodies, and floodplains and intermittent lakes only half of that; all other types have a weight of zero. Grid cells with mean annual air temperature < 0 °C are excluded for aquaculture. The three weighing factors are combined by multiplication to obtain the overall weight $[0, 1]$. Then all grid cells with overall probability < 10% are excluded for aquaculture, yielding the map for allocation for all years. Subsequently, the country production for shellfish and finfish are allocated separately. Grid cells with fish production less than a threshold are excluded for that particular year, and the remaining grid cells are used to allocate the N and P emissions from shellfish and finfish based on the weighing map.

Atmospheric N deposition to water bodies is from ensemble of chemistry-transport models for the year 2000 (Dentener et al. 2006), and the years before

that were made by scaling the deposition with grid-based emissions of ammonia (Bouwman et al. 2013d). The deposition in floodplains, wetlands and river channels is ignored, because it is already part of the soil N budget, and does not need to be accounted for in periods of flooding.

S5.9   Sensitivity analysis

Table S5.3: Model parameters included in the sensitivity analysis, their symbol and description, for which nutrient it is used, and the standard, minimum, mode and maximum value considered for the sampling procedure. Parameters are listed in alphabetical order of their symbol

Symbol	Description	Nut-rient	Dist.[a]	Stan-dard	Min.	Max.
A	Width factor	N/P	U3	8.3	7.5	9.1
A_1	Drainage area first order stream	N/P	U3	2.6	2.3	2.9
A_{flooding}	Area of flooding areas	N/P	U1	1.0	0.9	1.1
B	Width exponent	N/P	U3	0.52	0.47	0.57
B_{soil}	Bulk density of the soil	N/P	U1	1.0	0.9	1.1
CN_{gnpp}	C : N weight ratio of gnpp in flooding areas	N	U3	100	90	110
$CN_{\mathrm{soil,crop}}$	C : N weight ratio of soil loss under crops	N	U3	12	11	13
$CN_{\mathrm{soil,grass}}$	C : N weight ratio of soil loss under grassland	N	U3	14	12.5	15.5
$CN_{\mathrm{soil,nat}}$	C : N weight ratio of soil loss under natural ecosystems	N	U3	14	12.5	15.5
CP_{aomi}	C : P weight ratio of gnpp in flooding areas	P	U3	1200	1080	1320
$C_{\mathrm{sro,N}}$	Calibration constant for N in surface runoff	N	U3	0.3	0.27	0.33
$C_{\mathrm{sro,P}}$	Calibration constant for P in surface runoff	P	U3	0.3	0.27	0.33
D_{dgrw}	Thickness of deep groundwater system	N	U3	50.0	45	55
D_{flooding}	Depth of flooding areas	N/P	U1	1.0	0.9	1.1
D_{rip}	Thickness of riparian zone	N	U3	0.3	0.27	0.33
D_{sgrw}	Thickness of shallow groundwater system	N	U3	5.0	4.5	5.5
$dt50_{\mathrm{den,dgrw}}$	Half-life of nitrate in deep groundwater	N	U3		50.0	100.0
$dt50_{\mathrm{den,sgrw}}$	Half-life of nitrate in shallow groundwater	N	U1	1.0	0.9	1.1
F_{aomi}	Reduction factor for litter load to surface water	N/P	U1	0.5	0.45	0.55
$F_{\mathrm{leach,crop}}$	Reduction fraction of N towards the shallow groundwater system	N	U3	1.0	0.9	1.0
$F_{\mathrm{leach,grass}}$	Reduction fraction of N towards the shallow groundwater system	N	U3	0.36	0.32	0.4
$F_{\mathrm{leach,nat}}$	Reduction fraction of N towards the shallow groundwater system	N	U3	0.36	0.32	0.4
f_{qgwb}	Fraction of q_{eff} that flows towards the deep system	N	U1	1.0	0.9	1.1

Continued on next page . . .

Table S5.3: (Continued)

Symbol	Description	Nut-rient	Dist.[a]	Stan-dard	Min.	Max.
f_{qsro}	Overall runoff fraction	N/P	U1	1.0	0.9	1.1
$f_{\text{qsro}}(crops)$	Land-use effect on surface runoff for soils under crops	N/P	T2	1.0	0.75	1.0
$f_{\text{qsro}}(grass)$	Land-use effect on surface runoff for soils under grassland	N/P	T1	0.25	0.125	0.5
$f_{\text{qsro}}(nat)$	Land-use effect on surface runoff for soils in natural ecosystems	N/P	T3	0.125	0.1	0.3
$AOMI$	Litterfall in flooding areas	N/P	U1	1.0	0.9	1.1
L_1	Mean length first order stream	N/P	U3	1.6	1.4	1.8
N_{aqua}	N load from aquaculture	N	U1	1.0	0.9	1.1
$N_{\text{budget,crops}}$	N budgets in croplands	N	U1	1.0	0.9	1.1
$N_{\text{budget,grass}}$	N budget in grasslands	N	U1	1.0	0.9	1.1
$N_{\text{budget,nat}}$	N budget in natural ecosystems	N	U1	1.0	0.9	1.1
$N_{\text{conc,high}}$	Retention multiplier for retention at high N concentrations.	N	U3	0.3	0.2	0.4
$N_{\text{conc,low}}$	Retention multiplier for retention at low N concentrations.	N	U3	7	6	9
N_{depo}	N deposition on surface water	N	U1	1.0	0.9	1.1
N_{point}	N from point sources	N	U1	1.0	0.9	1.1
$N_{\text{uptake,crops}}$	N uptake in croplands	N	U1	1.0	0.9	1.1
$N_{\text{uptake,grass}}$	N uptake in grasslands	N	U1	1.0	0.9	1.1
P_{aqua}	P load from aquaculture	P	U1	1.0	0.9	1.1
$P_{\text{budget,crops}}$	P budgets in croplands	P	U1	1.0	0.9	1.1
$P_{\text{budget,grass}}$	P budget in grasslands	P	U1	1.0	0.9	1.1
$P_{\text{budget,nat}}$	P budget in natural ecosystems	P	U1	1.0	0.9	1.1
$Poros$	Porosity of aquifer material	N	U1	1.0	0.9	1.1
P_{point}	P from point sources	P	U1	1.0	0.9	1.1
P_{soil}	P content of the soil	P	U1	1.0	0.9	1.1
$P_{\text{uptake,crops}}$	P uptake in croplands	P	U1	1.0	0.9	1.1
$P_{\text{uptake,grass}}$	P uptake in grasslands	P	U1	1.0	0.9	1.1
$P_{\text{weathering}}$	P content of per lithology class	P	U1	1.0	0.9	1.1
q_{tot}	Runoff (total)	N/P	U1	1.0	0.9	1.1
R_{a}	Drainage area ratio	N/P	U3	4.7	4.2	5.2
R_{b}	Stream number ratio	N/P	U3	4.5	4.05	4.95
R_{L}	Mean length ratio	N/P	U3	2.3	2.0	2.6
$Temp$	Mean annual air temperature	N/P	U2	0.0	−1.0	1.0
$v_{\text{f,lake}}$	Net uptake velocity for lakes	N	U3	35	32	38
$v_{\text{f,lake}}$	Net uptake velocity for lakes	P	U3	44.5	40	49
$v_{\text{f,reservoir}}$	Net uptake velocity for reservoirs	N	U3	35	32	38
$v_{\text{f,reservoir}}$	Net uptake velocity for reservoirs	P	U3	44.5	40	49
$v_{\text{f,river}}$	Net uptake velocity for rivers	N	U3	35	32	38
$v_{\text{f,river}}$	Net uptake velocity for rivers	P	U3	44.5	40	49

Table S5.3: (Continued)

Symbol	Description	Nut-rient	Dist.[a]	Stan-dard	Min.	Max.
$v_{f,wetland}$	Net uptake velocity for wetlands	N	U3	35	32	38
$v_{f,wetland}$	Net uptake velocity for wetlands	P	U3	44.5	40	49
V_{water}	Water volume of all water bodies	N/P	U1	1.0	0.9	1.1

The sensitivity of the modeled delivery, retention and river export to variation of 48 and 34 model parameters for N and P, respectively, is based on parameter-specific distributions between a minimum and maximum value around the standard parameter values (Table S5.3). In order to limit computational load in the sensitivity analysis, the Latin Hypercube Sampling (LHS) technique (Saltelli et al. 2000) is used. LHS offers a stratified sampling method for the separate input parameters, based on subdividing the range of each of the k parameters into disjunct equiprobable intervals based on a uniform distribution. By sampling one value in each of the *Num* intervals according to the associated distribution in this interval, we obtain *Num* sampled values for each parameter. The number of runs (*Num*) was 500 for P and 750 for N.

The sampled values for the first model parameter are randomly paired to the samples of the second parameter, and these pairs are subsequently randomly combined with the samples of the third source, etc. This results in an LHS consisting of *Num* combinations of k parameters. The parameter space is thus representatively sampled with a limited number of samples.

LHS can be used in combination with linear regression to quantify the uncertainty contributions of the input parameters to the model outputs (Saltelli et al. 2000, 2004). The output Y considered (see columns in Tables S5.4 and S5.5) is approximated by a linear function of the parameters X_i expressed by

$$Y = \beta_0 + \beta_1 X_1 + \beta_2 X_2 + \cdots + \beta_n X_n + \epsilon \qquad \text{(S5.21)}$$

[a]Distribution: Samples values are applied to all grid cells. For sampling, either uniform of triangular distributions are used. A triangular distribution is a continuous probability distribution with lower limit a, upper limit b and mode c, where $a \leq c \leq b$. The probability to sample a point depends on the skewness of the triangle. In the case of $dt50_{den,dgrw}$, $a\,c = b\,c$, and probability to sample a point on the left and right hand side of c is the same. In other cases, for example $f_{Qsro}(crops)$ is a fraction $[0,1]$, with standard value of 1.0. To achieve a high probability to sample close to 1.0, the triangle is designed with $b = 1$ and c is close to 1. For some of the above distributions the expected value is not equal to the standard. Since the calculated R^2 for all output parameters exceeds 0.99, this approach for analyzing the sensitivity is still valid. The distributions used are:
U1. Uniform; values are multipliers for standard values on a grid cell basis.
U2. Uniform; values are added to the standard values on a grid cell basis.
U3. Uniform; values are used as such.
T1. Triangular; values between 0.125 and 0.5 with an expected value of 0.25.
T2. Triangular; values between 0.75 and 1.0 with an expected value of 0.995.
T3. Triangular; values between 0.1 and 0.3 with an expected value of 0.125.

where β_i is the so-called ordinary regression coefficient and ϵ is the error of the approximation. The quality of the regression model is expressed by the coefficient of determination (R^2), representing the amount of variation Y explained by $Y - \epsilon$. Since β_i depends on the scale and dimension of X_i, we used the standardized regression coefficient (SRC_i), which is a relative sensitivity measure obtained by rescaling the regression equation on the basis of the standard deviations σ_Y and σ_{X_i}:

$$SRC_i \;=\; \beta_i \, \frac{\sigma_{X_i}}{\sigma_Y} \tag{S5.22}$$

SRC_i can take values in the interval $[-1, 1]$. SRC is the relative change $\Delta Y / \sigma_Y$ of Y due to the relative change $\Delta X_i / \sigma_{X_i}$ of the parameter X_i considered (both with respect to their standard deviation σ). Hence, SRC_i is independent of the units, scale and size of the parameters, and thus sensitivity analysis comes close to an uncertainty analysis. A positive SRC_i value indicates that increasing a parameter value will cause an increase in the calculated model output, while a negative value indicates a decrease in the output considered caused by a parameter increase.

The sum of squares of SRC_i values of all parameters equals the coefficient of determination (R^2), which for a perfect fit equals 1. Hence, SRC_i^2 / R^2 yields the contribution of parameter X_i to Y. For example, a parameter X_i with $SRC_i = 0.1$ adds 0.01 or 1% to Y in case R^2 equals 1.

Table S5.4: Standardized regression coefficient $(SRC)^a$ representing the relative sensitivity of N delivery, N retention and river N export representing global model results (columns) to variation in 48 parameters (see Table S5.3)

Year Process Parameter	1900	1950	2000	1900	1950	2000	1900	1950	2000
		N delivery			N retention			River N export	
A				0.15	0.15	0.16	−0.12	−0.12	−0.12
A_1				−0.03	−0.03	−0.04	0.02	0.02	0.03
A_{flooding}	**0.37**	**0.39**	**0.30**	−0.16	−0.15	−0.10	**0.27**	**0.28**	**0.22**
B				0.08	0.08	0.09	−0.06	−0.07	−0.06
B_{soil}									
CN_{gnpp}	**−0.38**	**−0.41**	**−0.31**	0.16	0.15	0.10	**−0.28**	**−0.28**	**−0.23**
$CN_{\text{soil,crop}}$	−0.06	−0.09	−0.11	0.01	0.01		−0.03	−0.04	−0.05
$CN_{\text{soil,grass}}$	−0.01	−0.02	−0.02					−0.01	−0.01
$CN_{\text{soil,nat}}$	−0.05	−0.05	−0.03	0.01	0.01		−0.03	−0.03	−0.02
$C_{\text{sro,N}}$	0.05	0.07	0.14	−0.01	−0.01	−0.01	0.02	0.03	0.07
D_{dgrw}	−0.01	−0.01	−0.02	0.01	0.01	0.01	−0.01	−0.01	−0.02
D_{flooding}				−0.01	−0.01	−0.01	0.01	0.01	0.01
D_{rip}	−0.01	−0.01	−0.02	0.01	0.01	0.01	−0.01	−0.01	−0.02
D_{sgrw}	−0.07	−0.06	−0.12	0.01	0.01	0.01	−0.04	−0.03	−0.07
$dt50_{\text{den,dgrw}}$	0.02	0.02	0.02						
$dt50_{\text{den,sgrw}}$	0.07	0.07	0.13	−0.02	−0.01	−0.01	0.04	0.04	0.07

Table S5.4: (Continued)

Year	1900	1950	2000	1900	1950	2000	1900	1950	2000
Process	N delivery			N retention			River N export		
Parameter									
F_{aomi}	**0.38**	**0.40**	**0.31**	−0.16	−0.15	−0.10	**0.27**	**0.28**	**0.22**
$F_{\mathrm{leach,crop}}$	0.03	0.04	0.16			−0.03	0.01	0.02	0.10
$F_{\mathrm{leach,grass}}$	0.03	0.04	0.06	−0.01	−0.01	−0.01	0.02	0.03	0.04
$F_{\mathrm{leach,nat}}$	**0.40**	**0.31**	**0.26**	−0.09	−0.05	−0.03	**0.23**	0.17	0.14
f_{qgwb}	−0.01	−0.05	−0.08		0.02	0.02	−0.01	−0.04	−0.05
f_{qsro}	0.03	0.05	0.11	−0.01	−0.01		0.02	0.03	0.06
$f_{\mathrm{qsro}}(crops)$	0.02	0.03	0.08		−0.01	−0.01	0.01	0.02	0.05
$f_{\mathrm{qsro}}(grass)$	0.06	0.10	0.13	−0.01	−0.01		0.03	0.04	0.06
$f_{\mathrm{qsro}}(nat)$	0.06	0.07	0.06	−0.01			0.03	0.03	0.03
$AOMI$	**0.38**	**0.40**	**0.31**	−0.16	−0.15	−0.10	**0.27**	**0.28**	**0.22**
L_1				0.19	0.20	**0.21**	−0.15	−0.15	−0.15
N_{aqua}			0.02			−0.01			0.02
$N_{\mathrm{budget,crops}}$	0.04	0.07	**0.36**	−0.02	−0.02	−0.08	0.03	0.05	**0.23**
$N_{\mathrm{budget,grass}}$	0.03	0.04	0.07	−0.01			0.02	0.02	0.03
$N_{\mathrm{budget,nat}}$	**0.38**	**0.30**	**0.25**	−0.09	−0.05	−0.03	**0.21**	0.16	0.14
$N_{\mathrm{conc,high}}$				0.11	0.12	0.16	−0.09	−0.09	−0.12
$N_{\mathrm{conc,low}}$				**0.49**	**0.50**	**0.40**	**−0.38**	**−0.39**	**−0.30**
N_{depo}	0.02	0.02	0.03			0.01			
N_{point}	0.05	0.11	0.20	−0.03	−0.04	−0.06	0.04	0.08	0.14
$N_{\mathrm{uptake,crops}}$	0.01	0.01	0.04						0.02
$N_{\mathrm{uptake,grass}}$	0.01	0.02	0.02					0.01	0.01
$Poros$	−0.07	−0.07	−0.15	0.02	0.01	0.01	−0.04	−0.04	−0.08
q_{tot}	0.15	0.15	**0.26**	−0.10	−0.12	**−0.23**	0.14	0.15	**0.29**
R_{a}				−0.06	−0.06	−0.08	0.04	0.04	0.05
R_{b}				0.07	0.07	0.08	−0.06	−0.06	−0.06
R_{L}				**0.50**	**0.51**	**0.53**	**−0.38**	**−0.40**	**−0.38**
$Temp$	−0.09	−0.08	−0.14	**0.34**	**0.34**	**0.41**	**−0.30**	**−0.31**	**−0.37**
$v_{\mathrm{f,lake}}$				0.03	0.04	0.06	−0.02	−0.03	−0.04
$v_{\mathrm{f,reservoir}}$						0.07			−0.05
$v_{\mathrm{f,river}}$				**0.38**	**0.38**	**0.38**	**−0.30**	**−0.30**	**−0.28**
$v_{\mathrm{f,wetland}}$									
V_{water}				0.01	0.01	0.01			

---

[a]Cells with no values represent insignificant SRC values; all cells with values have significant SRC, cells with light grey color indicate values $-0.2 < SRC < 0.2$; dark grey colors indicate values exceeding $+0.2$ and -0.2, respectively. An SRC value of 0.2 indicates that the parameter concerned has an influence of $0.2^2 = 0.04$ (4%) on the model variable considered.

Table S5.5: Standardized regression coefficient $(SRC)^a$ representing the relative sensitivity of P delivery, P retention and river P export representing global model results (columns) to variation in 34 parameters (see Table S5.3)

Year Process Parameter	1900	1950	2000	1900	1950	2000	1900	1950	2000
		P delivery			P retention			River P export	
A				**0.24**	**0.24**	**0.22**	−0.19	−0.19	−0.17
A_1				−0.14	−0.14	−0.13	0.11	0.11	0.10
A_{flooding}	**0.22**	0.19	0.13	−0.02	−0.02	−0.02	0.16	0.14	0.11
B				−0.01	−0.02		0.01	0.02	0.01
B_{soil}	**−0.55**	**−0.59**	**−0.62**	−0.10	−0.10	−0.13	**−0.28**	**−0.32**	**−0.35**
CP_{aomi}	**−0.23**	**−0.20**	−0.14	0.02	0.02	0.02	−0.16	−0.14	−0.11
$C_{\text{sro,P}}$	0.02	0.04	0.14				0.01	0.03	0.10
D_{flooding}				−0.01	−0.01	−0.01			
F_{aomi}	**0.23**	**0.20**	0.14	−0.02	−0.02	−0.02	0.17	0.15	0.12
$F_{\text{leach,crop}}$									
$F_{\text{leach,grass}}$									
$F_{\text{leach,nat}}$									
f_{qsro}	0.02	0.04	0.13				0.02	0.03	0.10
$AOMI$	**0.23**	**0.20**	0.14	−0.02	−0.02	−0.02	0.16	0.15	0.12
L_1				**0.31**	**0.31**	**0.28**	**−0.25**	**−0.24**	**−0.22**
P_{aqua}			0.01						0.02
$P_{\text{budget,crops}}$		0.01	0.07					0.01	0.05
$P_{\text{budget,grass}}$									
$P_{\text{budget,nat}}$									
P_{point}	0.04	0.07	0.14	−0.02	−0.03	−0.06	0.04	0.07	0.16
P_{soil}	**0.56**	**0.60**	**0.63**	0.09	0.10	0.13	**0.29**	**0.33**	**0.36**
$P_{\text{uptake,crops}}$	0.02	0.02	0.06				0.01	0.02	0.05
$P_{\text{uptake,grass}}$	0.01	0.01	0.01					0.01	0.01
$P_{\text{weathering}}$	**0.27**	**0.23**	0.17	−0.05	−0.05	−0.04	**0.21**	0.19	0.15
q_{tot}	**0.27**	**0.23**	0.17	**−0.39**	**−0.40**	**−0.47**	**0.48**	**0.46**	**0.48**
R_a				**−0.27**	**−0.26**	**−0.24**	**0.21**	**0.20**	0.19
R_b				0.17	0.17	0.16	−0.13	−0.13	−0.12
R_L				**0.53**	**0.53**	**0.49**	**−0.42**	**−0.42**	**−0.38**
$Temp$	0.19	0.16	0.12	**0.21**	**0.22**	**0.27**	−0.05	−0.07	−0.12
$v_{\text{f,lake}}$				0.05	0.05	0.06	−0.03	−0.03	−0.04
$v_{\text{f,reservoir}}$					0.02	0.10		−0.01	−0.08
$v_{\text{f,river}}$				**0.43**	**0.43**	**0.40**	**−0.33**	**−0.33**	**−0.30**
$v_{\text{f,wetland}}$									
V_{water}				0.01	0.01	0.01			

---

^{a}See Table S5.4.

S5.10   Soil N and P budgets

Global soil N budget (natural ecosystems and agriculture) increased from 95 to 170 Tg N yr^{-1} (increase by 80%) and that of P from negligible amounts to 11 Tg P yr^{-1}. The change in the N budget is the result of decreasing N cycling in natural ecosystems due to conversion of forest to agriculture, and an increase in the N inputs in agriculture, particularly after 1950. In some regions this increase has been much faster than in others. For example, in river basins draining into the Pacific, the N soil budget increased by more than a factor of 3, and for the river basins debouching in the Mediterranean Sea and Black Sea by more than a factor of two. For P the changes are even more rapid, with shifts from negative in early 20$^{\text{th}}$ century to positive budgets for the Mediterranean Sea and Black Sea and the Pacific Ocean from the 1940s.

The N : P ratios in fertilizers applied to agricultural soils are gradually increasing, since the 1970s in all industrialized countries, and in more recent years also in developing countries (FAO 2013a). Livestock production is an internal nutrient cycle in agricultural systems, with manure production with high P contents as a result of feeding characteristics and also due to ammonia losses from manure causing a relative P enrichment. Hence, while fertilizer use shows increasing N : P ratios, the soil budgets have lower ratios, and with a decreasing trend.

It should be noted, that soil P surpluses are actually stored as residual soil P in many regions where it may contribute to future crop and grass production as it increases the amount of plant-available P. A small part of the soil P surplus is lost through surplus runoff. The increase in soil P is substantial in many industrialized countries and also China and India (Figure S5.1).

S5.11   Description of the measurement data

Rhine   Measurements biweekly from 1 January 1970 to present at station Lobith at the Dutch-German border (light grey line, Figure 5.2). The discharge is available from 1989 onwards. The average yearly concentration is weighted with discharge (dark grey line in Figure 5.2) (Ministry of Infrastructure and Environment 2013).

Meuse   Measurements bi-weekly from 1 January 1970 to 2012 (light grey line, Figure 5.2) at station Eijsden at the Dutch-Belgian border. The average yearly concentration is weighted with discharge (dark grey line in Figure 5.2) (Ministry of Infrastructure and Environment 2013).

Mississippi   Measurements (p00600 for N and p00665 for P) monthly from October 1974 up till 2013 at USGS station number 07373420 (MISSISSIPPI R NR ST. FRANCISVILLE, LA) (light grey line, Figure 5.2) (United States Geological Survey 2013). The average yearly concentration is weighted with discharge (dark grey line in Figure 5.2).
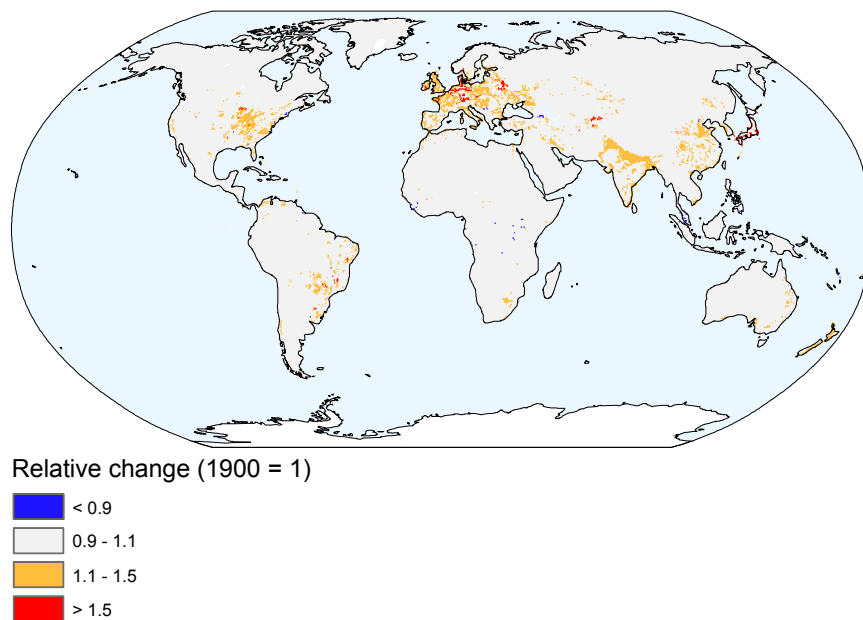
Relative change (1900 = 1)

■ (blue)	< 0.9
□ (grey)	0.9 - 1.1
□ (orange)	1.1 - 1.5
■ (red)	> 1.5

Figure S5.1: Relative change in residual soil P since 1990 for the top 30 cm.

European rivers   The full database for European rivers is from European Environment Agency (2013) (http://www.eea.europa.eu/data-and-maps/data/water base-rivers-9; version 13, dd. 11 October 2013). We selected measurements data for total N and total P concentrations for stations in rivers with an upstream catchment area > 10000 km². Each entry in the database contains information on the measurement station (id, name, location, longitude, latitude and river name) and year, minimum, maximum, median and mean of the concentration. We used 1809 measurements for years prior to the year 2001.

The location of the station (longitude, latitude) and year is used to collect the simulated annual N and P concentrations from $0.5°$ by $0.5°$ grid cells of the model.

A first comparison is made and the residues of the difference between simulated and measured concentration re-examined. Some rivers could not be matched with the model schematization, others were removed as outliers based on Cooks distance, qqplot and linear regression. A total of 11 stations were thus removed (in the order they are given) from the dataset (Table S5.6).

The location of the first and second river which has been excluded (SE_RV_SE 649673-151838 and HU_RV_04FV12) do not match the model schematization. The Motala Ström drains lake Vättern into Baltic Sea, but in the hydrological schematization this river starts at this location without the water from lake Vättern. The same holds for the Csaszarviz, which is located next to the main stream of the Danube, but has no water import from other grid cells. Furthermore, 8 Spanish
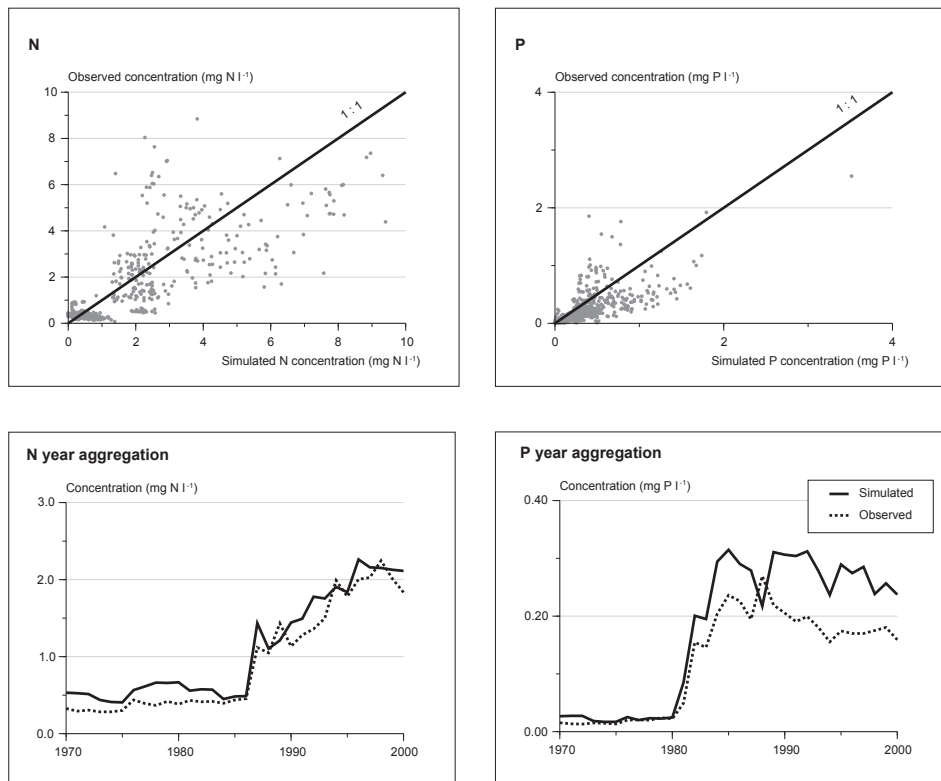
Figure S5.2: Comparison of simulated total N and P concentration with the EEA dataset for the period 1970–2000. Please note that the European coverage is not constant and the trend is not representative of European rivers, because the number and location of stations has changed in time, causing changes in the trend.

Table S5.6: Measurement stations from the EEA database that were removed based on Cooks distance, qqplot and lineair regression

Id	Rivername	Nutrients	Years	# of measurements
SE_RV_SE649673-151838	Motala Ström	N/P	1970–2000	62
HU_RV_04FV12	Csaszarviz	N/P	1987–2000	28
ES_RV_ES08120	Tuejar	P	1994–1996	3
ES_RV_ES02046	Adaja	P	1994	1
ES_RV_ES08067	Canoles	P	1994	1
ES_RV_ES08202	Turia	P	1994	1
ES_RV_ES01186	Agüera	P	1995–1996	2
ES_RV_ES01346	Nalon	P	1995–1996	2
DE_RV_BE01	Spree	N/P	1994–2000	14
ES_RV_ES08036	Jucar	P	1994, 1996	2
ES_RV_ES08112	Cabriel	P	1994–1996	3

and one German rivers are outliers. The resulting database contains 1690 measurements, including 49 stations for N with 709 N concentration measurements and 76 stations with 981 measurements for P concentrations.

The model results are collected by taking the same year as the measurement and the simulated concentration from the grid cell where the station is located on the basis of the reported longitude–latitude coordinates. The first step is to plot the data in one scatterplot for N and P (Figure S5.2). The average of all N or P observations is compared with the average of the simulated concentrations. Both models simulate slightly higher concentrations. For N ($n = 709$) the correlation coefficient (R^2) is 0.63 with a slope of 0.71 and an intercept of 0.26. For P ($n = 981$) the R^2 is 0.58 with a slope of 0.60 and an intercept of 0.02. Both models have a small intercept and a slope smaller than one, which confirms the higher simulated averages.

We also compared the model performance for different stations by calculating the mean of observations and model values over the monitoring period for each station. For N the correlation coefficient has not improved ($R^2 = 0.59$), but for P this comparison yields a $R^2 = 0.80$. The high value of the regression coefficient is mainly due to one station with a high total P concentration (see Figure 5.2). We also calculated the average of all observations for each year to test the agreement of simulated and observed trend over the last three decades. For N there is a good agreement between the simulated trend and the observed trend ($R^2 = 0.96$). For P the simulated trend follows the monitoring trend ($R^2 = 0.92$) but after a sharp increase of P concentration, the simulated P concentrations exceed observations by about 0.1 mg P l^{-1} (see Figure S5.2). Please note that the European coverage is not constant and the trend is not representative of European rivers, because the number and location of stations has changed in time, causing changes in the trend.

Observed TN (mg N l^{-1})
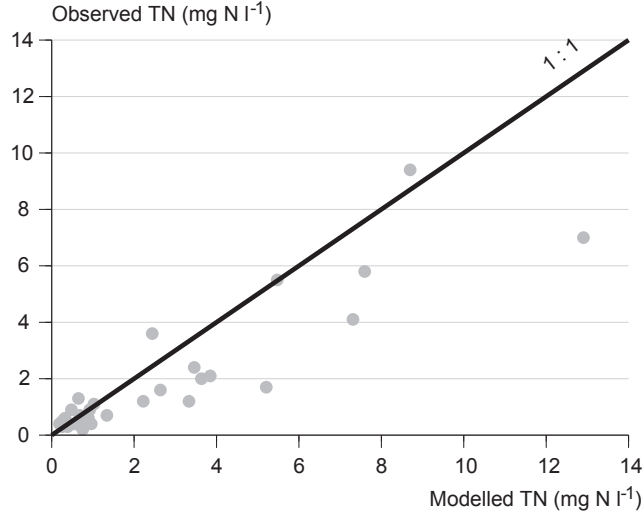
Figure S5.3: Comparison of simulated discharge weighted average over the 1980–1990 period of the total N concentration with the validation dataset for the early 1990's for total N collected by Van Drecht et al. (2003).

S5.12   Parameterization of lower order streams

The drainage network of PCR-GLOBWB represents streams and rivers of Strahler order (Strahler 1957) six and higher. The parameterization of lower order streams follows the approach presented by Wollheim et al. (2008a). A globally uniform subgrid river network is included for all cells without lakes or reservoirs. It is assumed that PCR-GLOBWB has one river of order 6 in each grid cell, and all lower order rivers are lacking. The river network is then defined on the basis of stream length and basin area of the first order river. The mean length ratio (R_L) is used to calculate the stream length of the next higher order the river according to:

$$L_n \;=\; L_1 \, R_L{}^{(n-1)} \tag{S5.23}$$

with L_n being the stream length of order n (km); $L_1 = 1.6$ km. The drainage area ratio (R_a) is used to calculate the basin area for higher order stream as follows:

$$A_n \;=\; A_1 \, R_a{}^{(n-1)} \tag{S5.24}$$

where A_n is basin area of order n in km^2; $A_1 = 2.6$ km^2. With the stream number ratio (R_b) the number of lower order streams is calculated as:

$$R_n \;=\; R_b{}^{(6-n)} \tag{S5.25}$$

with R_n being the number of streams of order n in this grid cell and $R_b = 4.5$. The discharge for each stream is calculated with the runoff (q):

$$Q_n = q\,A_n\,C_Q \tag{S5.26}$$

with the discharge of stream order n (Q_n) in m^3 s^{-1} and runoff in mm yr^{-1} and C_Q the unit conversion ($C_Q = 1000/(3600 \cdot 24 \cdot 365)$). The midpoint discharge of a stream length of order n is calculated as:

$$Q_{\mathrm{mid},n} = Q_n + 0.5\,Q_{n-1} \tag{S5.27}$$

The width of the stream of order n is calculated as:

$$W_n = A\,(Q_{\mathrm{mid},n})^B \tag{S5.28}$$

where W_n = width (m), A is constant (8.3 m) and coefficient $B = 0.52$. It is now possible to calculate the hydrologic load (H_L) and thus the retention of the stream with according to:

$$H_L = \frac{C_{Q1}\,Q_{\mathrm{mid},n}}{W_n\,L_n\,C_{Q2}} \tag{S5.29}$$

with C_{Q1} being the conversion from seconds to years ($C_{Q1} = 3600 \cdot 24 \cdot 365$) and C_{Q2} the conversion from km to m (1000) and H_L in m yr^{-1}. The local diffuse load in a grid cell is spatially uniformly distributed over the streams. Here, the fraction of the total stream length per order is used to calculate the distribution of the load. The direct load is allocated to stream order n as follows:

$$F_{d,n} = \frac{R_n\,L_n}{\sum_{i=1}^{6} R_i\,L_i} \tag{S5.30}$$

where $F_{d,n}$ is the fraction of the total load which is direct input for streams of order n. The pathway of the outflow of the streams is determined according to a matrix $T_{i,j}$ representing the fraction of the outflow of stream order i to stream order j, whereby $T_{i,j} = 0.0$ for $i \geq j$. For $i < j$, $T_{i,j}$ is calculated as follows:

$$T_{i,j} = \frac{R_j\,L_j}{\sum_{k=i+1}^{6} R_k\,L_k} \tag{S5.31}$$

The calculation of the retention is performed for each stream order, starting with order $n = 1$, and is identical to the calculation of the PCR-GLOBWB schematization. The load of a stream is the sum of the direct load and the sum of the outflow from lower order streams.

References

AAPFCO/TFI (2006). Commercial fertilizers 2005. Technical report, Association of American Plant Food Control Officials / The Fertilizer Institute (www.aapfco.org), Washington, D.C.

Adam, J. C. and Lettenmaier, D. P. (2008). Application of new precipitation and reconstructed streamflow products to streamflow trend attribution in Northern Eurasia. *Journal of Climate*, 21(8): 1807–1828.

Akaike, H. (1974). A new look at statistical model identification. *IEEE Transactions on Automatic Control*, 19: 716–722.

Alcamo, J., Van Vuuren, D., and Cramer, W. (2006). Changes in ecosystem services and their drivers across the scenarios. In: Carpenter, S. R., Pingali, P. L., Bennett, E. M., and Zurek, M. B. (eds.), *Ecosystems and human well-being: scenarios*, volume 2, pages 279–354. Island Press, Washington, D.C.

Alexander, R. B., Smith, R. A., and Schwarz, G. E. (2000). Effect of stream channel size on the delivery of nitrogen to the Gulf of Mexico. *Nature*, 403: 758–761.

Alexander, R. B., Smith, R. A., Schwarz, G. E., Boyer, E. W., Nolan, J. V., and Brakebill, J. W. (2008). Differences in phosphorus and nitrogen delivery to the Gulf of Mexico from the Mississippi river basin. *Environmental Science and Technology*, 42(3): 822–830.

Alexander, R. B., Smith, R. A., Schwarz, G. E., Preston, S. D., Brakebill, J. W., Srinivasan, R., and Pacheco, P. A. (2001). Atmospheric nitrogen flux from the watersheds of major estuaries of the United States: an application of the SPARROW watershed model. In: Valigura, R., Alexander, R., Castro, M., Meyers, T., Paerl, H., Stacey, P., and Turner, R. E. (eds.), *Nitrogen loading in coastal water bodies: an atmospheric perspective*, volume Monograph 57, pages 119–170. American Geophysical Union.

Allen, R. G., Pereira, L. S., Raes, D., and Smith, M. (1998). Crop evapotranspiration - guidelines for computing crop water requirements. Technical Report FAO Irrigation and Drainage Paper 56, Food and Agriculture Organization of the United Nations, Rome.

Allison, F. E. (1973). *Soil organic matter and its role in crop production. Developments in Soil Science 3*. Elsevier, Amsterdam.

Alluvione, F., Bertora, C., Zavattaro, L., and Grignani, C. (2010). Nitrous oxide and carbon dioxide emissions following green manure and compost fertilization in corn. *Soil Science Society of America Journal*, 74(2): 384–395.

Amiotte Suchet, P., Probst, J.-L., and Ludwig, W. (2003). Worldwide distribution of continental rock lithology: Implications for the atmospheric/soil CO_2 uptake by conti-

nental weathering and alkalinity river transport to the oceans. *Global Biogeochemical Cycles*, 17(2), doi: 10.1029/2002GB001891.

Angel, S., Sheppard, S., and Civco, D. (2005). The dynamics of global urban expansion. Technical report, The Word Bank, Transport and Urban Developemnt Department, Washington, D.C.

Asman, W. A. H., Sutton, M. A., and Schjorring, J. K. (1998). Ammonia: emission, atmospheric transport and deposition. *New Phytologist*, 139: 27–48.

Bartoli, F. (1983). The biogeochemical cycle of silicon in two temperate forest ecosystems. *Ecological Bulletins*, 35: 469–476.

Batjes, N. H. (1996). Total carbon and nitrogen in the soils of the world. *European Journal of Soil Science*, 47: 151–163.

Batjes, N. H. (1997). A world dataset of derived soil properties by FAO-UNESCO soil unit for global modelling. *Soil Use and Management*, 13: 9–16.

Batjes, N. H. (2002). Revised soil parameter estimates for the soil types of the world. *Soil Use and Management*, 18: 232–235.

Beaulieu, J. J., Tank, J. L., Hamilton, S. K., Wollheim, W. M., Hall, R. O., Jr., Mulholland, P. J., Peterson, B. J., Ashkenas, L. R., Cooper, L. W., Dahm, C. N., Dodds, W. K., Grimm, N. B., Johnson, S. L., McDowell, W. H., Poole, G. C., Valett, H. M., Arango, C. P., Bernot, M. J., Burgin, A. J., Crenshaw, C. L., Helton, A. M., Johnson, L. T., O'Brien, J. M., Potter, J. D., Sheibley, R. W., Sobota, D. J., and Thomas, S. M. (2011). Nitrous oxide emission from denitrification in stream and river networks. *Proceedings of the National Academy of Sciences of the United States of America*, 108(1): 214–219.

Berdanier, A. B. and Conant, R. T. (2011). Regionally differentiated estimates of cropland N_2O emissions reduce uncertainty in global calculations. *Global Change Biology*, doi: 10.1111/j.1365-2486.2011.02554.x.

Berner, E. K. and Berner, R. A. (1996). *Global environment: water, air, and geochemical cycles.* Prentice Hall, Upper Saddle River, N.J.

Beusen, A., Dekkers, A., Bouwman, A., Ludwig, W., and Harrison, J. (2005). Estimation of global river transport of sediments and associated particulate C, N, and P. *Global Biogeochemical Cycles*, 19(4), doi: 10.1029/2005GB002453.

Beusen, A. H. W., Bouwman, A. F., Dürr, H. H., Dekkers, A. L. M., and Hartmann, J. (2009). Global patterns of dissolved silica export to the coastal zone: results from a spatially explicit global model. *Global Biogeochemical Cycles*, 23, doi: 10.1029/2008GB003281.

Beusen, A. H. W., Bouwman, A. F., Heuberger, P. S. C., Van Drecht, G., and Van Der Hoek, K. W. (2008). Bottom-up uncertainty estimates of global ammonia emissions from global agricultural production systems. *Atmospheric Environment*, 42(24): 6067–6077.

Beusen, A. H. W., Slomp, C. P., and Bouwman, A. F. (2013). Global land-ocean linkage: direct inputs of nitrogen to coastal waters via submarine groundwater discharge. *Environmental Research Letters*, 8(3): 034035, doi: 10.1088/1748-9326/8/3/034035.

Billen, G. and Garnier, J. (2000). Nitrogen transfers through the Seine drainage network: a budget based on the application of the 'Riverstrahler' model. *Hydrobiologia*, 410: 139–150.

Billen, G. and Garnier, J. (2007). River basin nutrient delivery to the coastal sea: Assess-

ing its potential to sustain new production of non-siliceous algae. *Marine Chemistry*, 106: 148–160, doi:10.1016.j.marchem.2006.12.017.

Billen, G., Garnier, J., and Rousseau, V. (2005). Nutrient fluxes and water quality in the drainage network of the Scheldt basin over the last 50 years. *Hydrobiologia*, 540: 47–67.

Billen, G., Lancelot, C., and Meybeck, M. (1991). N, P, and Si retention along the aquatic continuum from land to ocean. In: Mantoura, R. F. C., Martin, J. M., and Wollast, R. (eds.), *Ocean margin processes in global change*, pages 19–44. John Wiley and Sons, New York.

Bland, J. M. and Altman, D. G. (1996). Statistical methods for assessing agreement between two methods of clinical measurements. *The Lancet*, I: 307–310.

Blicher-Mathiesen, G., McCarty, G. W., and Nielsen, L. P. (1998). Denitrification and degassing in groundwater estimated from dissolved dinitrogen and argon. *Journal of Hydrology*, 208(1-2): 16–24.

Bodirsky, B. L., Popp, A., Weindl, I., Dietrich, J. P., Rolinski, S., Scheiffele, L., Schmitz, C., and Lotze-Campen, H. (2012). N_2O emissions from the global agricultural nitrogen cycle - current state and future scenarios. *Biogeosciences*, 9(10): 4169–4197, doi: 10.5194/bg-9-4169-2012.

Bogena, H., Kunkel, R., Schobel, T., Schrey, H. P., and Wendland, F. (2005). Distributed modeling of groundwater recharge at the macroscale. *Ecological Modelling*, 187(1): 15–26.

Böhlke, J.-K., Wanty, R., Tuttle, M., Delin, G., and Landon, M. (2002). Denitrification in the recharge area and discharge area of a transient agricultural nitrate plume in a glacial outwash sand aquifer, Minnesota. *Water Resources Research*, 38(7), doi: 10.1029/2001WR000663.

Bollmann, A. and Conrad, R. (1997). Enhancement by acetylene of the decomposition of nitric oxide in soil. *Soil Biology and Biochemistry*, 29(7): 1057–1066.

Bolt, G. H. and Bruggenwert, M. G. M. (eds.) (1976). *Soil chemistry. A. Basic elements.* Elsevier Scienctific Publishing Company, Amsterdam.

Bouwman, A. F. (1999). *Approaches to scaling of trace gas fluxes in ecosystems.* Elsevier Science, Amsterdam.

Bouwman, A. F. and Asman, W. A. H. (1997). Scaling of nitrogen gas fluxes from grasslands. In: Jarvis, S. C. and Pain, B. F. (eds.), *Gaseous nitrogen emissions from grasslands*, pages 311–330. CAB International, Wallingford, New York.

Bouwman, A. F., Beusen, A. H. W., and Billen, G. (2009). Human alteration of the global nitrogen and phosphorus soil balances for the period 1970-2050. *Global Biogeochemical Cycles*, 23, doi: 10.1029/2009GB003576.

Bouwman, A. F., Beusen, A. H. W., Griffioen, J., Groenigen, J. W. V., Hefting, M. M., Oenema, O., Van Puijenbroek, P. J. T. M., Seitzinger, S., Slomp, C. P., and Stehfest, E. (2013a). Global trends and uncertainties in terrestrial denitrification and N_2O emissions. *Philosophical Transactions of the Royal Society B: Biological Sciences*, 368(1621), doi: 10.1098/rstb.2013.0112.

Bouwman, A. F., Beusen, A. H. W., Overbeek, C. C., Bureau, D. P., Pawlowski, M., and Glibert, P. M. (2013b). Hindcasts and future projections of global inland and coastal nitrogen and phosphorus loads due to finfish aquaculture. *Reviews in Fisheries Science*, 21(2): 112–156.

Bouwman, A. F., Bierkens, M. F. P., Griffioen, J., Hefting, M. M., Middelburg, J. J.,

Middelkoop, H., and Slomp, C. P. (2013c). Nutrient dynamics, transfer and retention along the aquatic continuum from land to ocean: towards integration of ecological and biogeochemical models. *Biogeosciences*, 10(1): 1–22, doi: 10.5194/bg-10-1-2013.

Bouwman, A. F., Boumans, L. J. M., and Batjes, N. H. (2002a). Estimation of global NH₃ volatilization loss from synthetic fertilizers and animal manure applied to arable lands and grasslands. *Global Biogeochemical Cycles*, 16(2), doi: 10.1029/2000GB001389.

Bouwman, A. F., Boumans, L. J. M., and Batjes, N. H. (2002b). Modeling global annual N₂O and NO emissions from fertilized fields. *Global Biogeochemical Cycles*, 16(4), doi: 10.1029/2001GB001812.

Bouwman, A. F., Fung, I., Matthews, E., and John, J. (1993). Global analysis of the potential for N₂O production in natural soils. *Global Biogeochemical Cycles*, 7: 557–597.

Bouwman, A. F., Klein Goldewijk, K., Van Der Hoek, K. W., Beusen, A. H. W., Van Vuuren, D. P., Willems, W. J., Rufino, M. C., and Stehfest, E. (2011a). Exploring global changes in nitrogen and phosphorus cycles in agriculture induced by livestock production over the 1900-2050 period. *Proceedings of the National Academy of Sciences of the United States of America*, doi: 10.1073/pnas.1012878108.

Bouwman, A. F., Klein Goldewijk, K., Van Der Hoek, K. W., Beusen, A. H. W., Van Vuuren, D. P., Willems, W. J., Rufino, M. C., and Stehfest, E. (2013d). Exploring global changes in nitrogen and phosphorus cycles in agriculture induced by livestock production over the 1900-2050 period. *Proceedings of the National Academy of Sciences of the United States of America*, 110(52): 20882–20887, doi: 10.1073/pnas.1012878108.

Bouwman, A. F., Kram, T., and Klein Goldewijk, K. (eds.) (2006). *Integrated modelling of global environmental change. An overview of IMAGE 2.4*. Publication 500110002/2006, Netherlands Environmental Assessment Agency, Bilthoven.

Bouwman, A. F., Lee, D. S., Asman, W. A. H., Dentener, F. J., Van Der Hoek, K. W., and Olivier, J. G. J. (1997). A global high-resolution emission inventory for ammonia. *Global Biogeochemical Cycles*, 11: 561–587.

Bouwman, A. F., Pawlowski, M., Liu, C., Beusen, A. H. W., Shumway, S. E., Glibert, P. M., and Overbeek, C. C. (2011b). Global hindcasts and future projections of coastal nitrogen and phosphorus loads due to shellfish and seaweed aquaculture. *Reviews in Fisheries Science*, 19(4): 331–357, doi: 10.1080/10641262.2011.603849.

Bouwman, A. F., Van Der Hoek, K. W., Eickhout, B., and Soenario, I. (2005a). Exploring changes in world ruminant production systems. *Agricultural Systems*, 84(2): 121–153, doi: 10.1016/j.agsy.2004.05.006.

Bouwman, A. F., Van Drecht, G., Knoop, J. M., Beusen, A. H. W., and Meinardi, C. R. (2005b). Exploring changes in river nitrogen export the the world's oceans. *Global Biogeochemical Cycles*, 19: GB1002, doi: 10.1029/2004GB002314.

Bouwman, A. F., Van Drecht, G., and Van Der Hoek, K. W. (2005c). Nitrogen surface balances in intensive agricultural production systems in different world regions for the period 1970–2030. *Pedosphere*, 15(2): 137–155.

Bouwman, A. F., Van Drecht, G., and Van Der Hoek, K. W. (2005d). Surface N balances and reactive N loss to the environment from intensive agricultural production systems for the period 1970-2030. *Science in China Series C. Life Sciences*, 48 Supp.: 1–13.

Bouwman, A. F., Van Vuuren, D. P., Derwent, R. G., and Posch, M. (2002c). A global analysis of acidification and eutrophication of terrestrial ecosystems. *Water, Air and*

Soil Pollution, 141: 349–382.

Box, G. E. P. and Cox, D. R. (1964). An analysis of transformations. *Journal of Royal Statistical Society Series B*, 26: 211–246.

Boyer, E. W., Alexander, R. B., Parton, W. J., Li, C., Butterbach-Bahl, K., Donner, S. D., Skaggs, R. W., and Grosso, S. J. D. (2006a). Modeling denitrification in terrestrial and aquatic ecosystems at regional scales. *Ecological Applications*, 16(6): 2123–2142.

Boyer, E. W., Howarth, R. W., Galloway, J. N., Dentener, F. J., Green, P. A., and Vörösmarty, C. J. (2006b). Riverine nitrogen export from the continents to the coasts. *Global Biogeochemical Cycles*, 20(1), doi: 10.1029/2005GB002537.

Brady, N. C. (1990). *The nature and properties of soils.* Macmillan Publishing Company, New York, 10th edition.

Bruinsma, J. E. (2003). *World agriculture: towards 2015/2030. An FAO perspective.* Earthscan, London.

Bussink, D. W. and Oenema, O. (1998). Ammonia volatilization from dairy farming systems in temperate areas: a review. *Nutrient Cycling in Agroecosystems*, 51: 19–33.

Butcher, R. W. (1947). Studies in the ecology of rivers: VII. The algae of organically enriched waters. *Journal of Ecology*, 35: 186–191.

Canadell, J., Jackson, R. B., Ehleringer, J. R., Mooney, H. A., Sala, O. E., and Schulze, E. D. (1996). Maximum rooting depth of vegetation types at the global scale. *Oecologia*, 108(4): 583–595.

Canfield, D. E., Glazer, A. N., and Falkowski, P. G. (2010). The evolution and future of earth's nitrogen cycle. *Science*, 330(6001): 192–196.

Cerdan, O., Govers, G., Bissonnais, Y. L., Van Oost, K., Poesen, J., Saby, N., Gobin, A., Vacca, A., Quinton, J., Auerswald, K., Klik, A., Kwaad, F. J. P. M., Raclot, D., Ionita, I., Rejman, J., Rousseva, S., Muxart, T., Roxo, M. J., and Dostal, T. (2010). Rates and spatial variations of soil erosion in Europe: a study based on erosion plot data. *Geomorphology*, 122(1-2): 167–177, doi: 10.1016/j.geomorph.2010.06.011.

China National Bureau of Statistics (2006a). China agricultural statistics. Technical report, Beijing.

China National Bureau of Statistics (2006b). China statistical yearbook. Technical report, Beijing.

Clarke, F. W. (1924). The composition of the river and lake waters of the United States. Technical report, United States Geological Survey.

Cleveland, C. C., Townsend, A. R., Schimel, D. S., Fisher, H., Howarth, R. W., Hedin, L. O., Perakis, S. S., Latty, E. F., Fisher, J. C. V., Elserod, A., and Wasson, M. F. (1999). Global patterns of terrestrial biological nitrogen (N_2) fixation in natural ecosystems. *Global Biogeochemical Cycles*, 13: 623–645.

Cloern, J. E. (1996). Phytoplankton bloom dynamics in coastal ecosystems: a review with some general lessons from sustained investigation of San Fransisco Bay, California. *Review of Geophysics*, 34: 127–168.

Codispoti, L. A., Brandes, J. A., Christensen, J. P., Devol, A. H., Naqvi, S. W. A., Pearl, H. W., and Yoshinari, T. (2001). The oceanic fixed nitrogen and nitrous oxide budgets: moving targets as we enter the anthropocene. *Scientia Marina*, 65: 85–105.

Cole, J. J., Prairie, Y. T., Caraco, N. F., McDowell, W. H., Tranvik, L. J., Striegl, R. G., Duarte, C. M., Kortelainen, P., Downing, J. A., Middelburg, J. J., and Melack, J.

(2007). Plumbing the global carbon cycle: integrating inland waters into the terrestrial carbon budget. *Ecosystems*, 10(1): 172–185, doi: 10.1007/s10021-006-9013-8.

Conley, D. (1997). Riverine contribution of biogenic silica to the oceanic silica budget. *Limnology and Oceanography*, 42: 774–777.

Conley, D. (2002). Terrestrial ecosystems and the global biogeochemical silica cycle. *Global Biogeochemical Cycles*, 16, doi: 10.1029/2002GB001894.

Conley, D. J. (2000). Biogeochemical nutrient cycles and nutrient management strategies. *Hydrobiologia*, 410: 87–96.

Conley, D. J., Likens, G. E., Buso, D. C., Saccone, L., Bailey, S. W., and Johnson, C. E. (2008). Deforestation causes increased dissolved silicate losses in the Hubbard Brook Experimental Forest. *Global Change Biology*, 14(11): 2548–2554, doi: 10.1111/j.1365-2486.2008.01667.x.

Conley, D. J., Schelske, C. L., and Stoermer, E. F. (1993). Modification of the biogeochemical cycle of silica with eutrophication. *Marine Ecology Progress Series*, 101(1-2): 179–192.

Cook, R. D. (1977). Detection of influential observations in linear regression. *Technometrics*, 19: 15–18.

Corazza, M., Bergamaschi, P., Vermeulen, A. T., Aalto, T., Haszpra, L., Meinhardt, F., O'Doherty, S., Thompson, R., Moncrieff, J., Popa, E., Steinbacher, M., Jordan, A., Dlugokencky, E., Brühl, C., Krol, M., and Dentener, F. (2011). Inverse modelling of European N_2O emissions: assimilating observations from different networks. *Atmospheric Chemistry and Physics*, 11(5): 2381–2398.

De Pauw, E., Nachtergaele, F. O., Antoine, J., Fisher, G., and Velthuizen, H. T. V. (1996). A provisional world climatic resource inventory based on the length-of-growing-period concept. In: Batjes, N. H., Kauffman, J. H., and Spaargaren, O. C. (eds.), *National soil reference collections and databases (NASREC)*, pages 30–43. International Soil Reference and Information Centre (ISRIC), Wageningen.

De Wit, M. and Pebesma, E. (2001). Nutrient fluxes at the river basin scale. II: the balance between data availability and model complexity. *Hydrological Processes*, 15(5): 761–775.

De Wit, M. J. M. (2001). Nutrient fluxes at the river basin scale. I: the PolFlow model. *Hydrological Processes*, 15(5): 743–759.

Dentener, F., Stevenson, D., Ellingsen, K., Van Noije, T., Schultz, M., Amann, M., Atherton, C., Bell, N., Bergmann, D., Bey, I., Bouwman, L., Butler, T., Cofala, J., Collins, B., Drevet, J., Doherty, R., Eickhout, B., Eskes, H., Fiore, A., Gauss, M., Hauglustaine, D., Horowitz, L., Isaksen, I. S. A., Josse, B., Lawrence, M., Krol, M., Lamarque, J. F., Montanaro, V., Müller, J. F., Peuch, V. H., Pitari, G., Pyle, J., Rast, S., Rodriguez, J., Sanderson, M., Savage, N. H., Shindell, D., Strahan, S., Szopa, S., Sudo, K., Dingenen, R. V., Wild, O., and Zeng, G. (2006). The global atmospheric environment for the next generation. *Environment Science and Technology*, 40: 3586–3594.

Derry, L. A., Kurtz, A. C., Ziegler, K., and Chadwick, O. A. (2005). Biological control of terrestrial silica cycling and export fluxes to watersheds. *Nature*, 433(7027): 728–731, doi: 10.1038/nature03299.

DeSimone, J., Macrae, M. L., and Bourbonniere, R. A. (2010). Spatial variability in surface N(2)O fluxes across a riparian zone and relationships with soil environmental

conditions and nutrient supply. *Agriculture Ecosystems & Environment*, 138(1-2): 1–9.

Dhondt, K., Boeckx, P., Hofman, G., and Van Cleemput, O. (2004). Temporal and spatial patterns of denitrification enzyme activity and nitrous oxide fluxes in three adjacent vegetated riparian buffer zones. *Biology and Fertility of Soils*, 40(4): 243–251.

Diaz, R. J. and Rosenberg, R. (2008). Spreading dead zones and consequences for marine ecosystems. *Science*, 321: 926–929, doi: 10.1126/science.1156401.

Dobermann, A. and Cassman, K. G. (2005). Cereal area and nitrogen use efficiency are drivers of future nitrogen fertilizer consumption. *Science in China Ser. C Life Sciences*, 48 Supp 1-14.

Dodds, W. K. (2002). *Freshwater ecology: concepts and environmental applications*. Academic Press, San Diego.

Döll, P. and Lehner, B. (2002). Validation of a new global 30-min drainage direction map. *Journal of Hydrology*, 258(1-4): 214–231.

Dragosits, U., Theobald, M. R., Place, C. J., Lord, E., Webb, J. A., Hill, J., ApSimon, H. M., and Sutton, M. A. (2002). Ammonia emission, deposition and impact assessment at the field scale: a case study of sub-grid spatial variability. *Environmental Pollution*, 117: 147–158.

Driessen, P. M. and Dudal, R. (1990). *Lecture notes on the geography, formation, properties and use of the major soil of the world*. Agricultural University Wageningen, Katholieke Universiteit Leuven, Leuven.

Duce, R. A., LaRoche, J., Altieri, K., Arrigo, K. R., Baker, A. R., Capone, D. G., Cornell, S., Dentener, F., Galloway, J., Ganeshram, R. S., Geider, R. J., Jickells, T., Kuypers, M. M., Langlois, R., Liss, P. S., Liu, S. M., Middelburg, J. J., Moore, C. M., Nickovic, S., Oschlies, A., Pedersen, T., Prospero, J., Schlitzer, R., Seitzinger, S., Sorensen, L. L., Uematsu, M., Ulloa, O., Voss, M., Ward, B., and Zamora, L. (2008). Impacts of atmospheric anthropogenic nitrogen on the open ocean. *Science*, 320(5878): 893–897, doi: 10.1126/science.1150369.

Ducharne, A., Baubion, C., Beaudoin, N., Benoit, M., Billen, G., Brisson, N., Garnier, J., Kieken, H., Lebonvallet, S., Ledoux, E., Mary, B., Mignolet, C., Poux, X., Sauboua, E., Schott, C., Thery, S., and Viennot, P. (2007). Long term prospective of the Seine river system: confronting climatic and direct anthropogenic changes. *Science of the Total Environment*, 375: 292–311.

Dumont, E., Harrison, J. A., Kroeze, C., Baker, E. J., and Seitzinger, S. P. (2005). Global distribution and sources of dissolved inorganic nitrogen export to the coastal zone: results from a spatially explicit, global model. *Global Biogeochemical Cycles*, 19, GB4S02, doi:10.1029/2005GB002488.

Dupré, B., Dessert, C., Oliva, P., Goddéris, Y., Viers, J., Francois, L., Millot, R., and Gaillardet, J. (2003). Rivers, chemical weathering and earth's climate. *Comptes Rendus Geoscience*, 335: 1141–1160.

Dürr, H., Meybeck, M., Hartmann, J., Laruelle, G. G., and Roubeix, V. (2009). Global spatial distribution of natural river silica inputs to the coastal zone. *EGU-Biogeosciences (special issue Si-WEBS)*, page (in press).

Dürr, H. H., Meybeck, M., and Dürr, S. (2005). Lithologic composition of the earth's continental surfaces derived from a new digital map emphasizing riverine material transfer. *Global Biogeochemical Cycles*, 19, GB4S10, doi:10.1029/2005GB002515.

Dürr, H. H., Meybeck, M., Hartmann, J., Laruelle, G. G., and Roubeix, V. (2011). Global

spatial distribution of natural riverine silica inputs to the coastal zone. *Biogeosciences*, 8(3): 597–620, doi: 10.5194/bg-8-597-2011.

EEA (2013). Nitrate concentrations in groundwater between 1992 and 2010 in different geographical regions of Europe (http://www.eea.europa.eu/data-and-maps/figures/nitrate-concentrations-in-groundwater-between-1992-and-2005-in-different-regions-of-europe-3).

Emery, K. O., Orr, W. L., and Rittenberg, S. C. (1955). Nutrient budgets in the ocean. In: *Essays in the natural sciences in honor of Captain Alan Hancock*, pages 299–310. University of Southern California Press, Los Angeles, California, USA.

Ensign, S. H. and Doyle, M. W. (2006). Nutrient spiraling in streams and river networks. *J. Geophys. Res.*, 111(G4): G04009, doi: 10.1029/2005jg000114.

European Environment Agency (2013). Waterbase rivers version 13 (http://www.eea.europa.eu/data-and-maps/data/waterbase-rivers-9). Technical report, Copenhagen.

FAO (1991). The digitized soil map of the world (release 1.0). Technical report, Food and Agriculture Organization of the United Nations, Rome.

FAO (2007). FAOSTAT database collections. Technical report, Food and Agriculture Organization of the United Nations (http://faostat.fao.org), Rome.

FAO (2008). FAOSTAT database collections. Technical report, Food and Agriculture Organization of the United Nations (http://faostat.fao.org), Rome.

FAO (2013a). FAOSTAT database collections. Technical report, Food and Agriculture Organization of the United Nations (http://faostat.fao.org), Rome.

FAO (2013b). FishStatJ - software for fishery statistical time series [online http://www.fao.org/fi/statist/fisoft/fishplus.asp](release data March 2013).

FAO/IIASA (2000a). Global Agro-Ecological Zones (Global AEZ). Technical report, Food and Agriculture Organization (FAO) / International Insitute for Applied Systems Analysis (IIASA), Rome.

FAO/IIASA (2000b). Joined Global Agro-Ecological Zones Project (Global-AEZ), FAO-IIASA, Laxenburg, Austria (http://www.fao.org/ag/agl/agll/gaez/index.htm).

FAO/UNESCO (1988). Soil map of the world. Revised legend. World Resources Report 60, FAO, Rome, Italy.

Farquharson, R. and Baldock, J. (2008). Concepts in modelling N_2O emissions from land use. *Plant and Soil*, 309(1-2): 147–167.

Fekete, B. M., Vörösmarty, C. J., and Grabs, W. (2002). High-resolution fields of global runoff combining observed river discharge and simulated water balances. *Global Biogeochemical Cycles*, 16(3), doi: 10.1029/1999GB001254.

Fekete, B. M., Wisser, D., Kroeze, C., Mayorga, E., Bouwman, A. F., Wollheim, W. M., and Vörösmarty, C. J. (2011). Millennium ecosystem assessment scenario drivers (1970-2050): climate and hydrological alterations. *Global Biogeochemical Cycles*, 24, GB0A12, doi: 10.1029/2009GB003593.

Firestone, M. K. (1982). Biological denitrification. In: Stevenson, F. J. (ed.), *Nitrogen in agricultural soils*, volume Agronomy Monograph 22, pages 280–326. American Society of Agronomy, Crop Science Society of America, Soil Science Society of America, Madison, Wisconsin.

Foppen, J. W. A. (2002). Impact of high-strength wastewater infiltration on groundwater quality and drinking water supply: the case of Sanaá, Yemen. *Journal of Hydrology*,

263: 198–216.

Forsberg, B. R., Devol, A. H., Richey, J. E., Martinelli, L. A., and Santos, H. D. (1988). Factors controlling nutrient concentrations in Amazon floodplain lakes. *Limnology and Oceanography*, 33(1): 41–56.

Gaillardet, J., Dupré, B., Louvat, P., and Allègre, C. J. (1999). Global silicate weathering and CO_2 consumption rates deduced from the chemistry of large rivers. *Chemical Geology*, 159: 3–30.

Galloway, J. N., Dentener, F. J., Capone, D. G., Boyer, E. W., Howarth, R. W., Seitzinger, S. P., Asner, G. P., Cleveland, C. C., Green, P. A., Holland, E. A., Karl, D. M., Michaels, A. F., Porter, J. H., Townsend, A. R., and Vörösmarty, C. J. (2004). Nitrogen cycles: past, present, and future. *Biogeochemistry*, 70: 153–226.

Galloway, J. N., Schlesinger, W. H., Levy III, H., Michaels, A., and Schnoor, J. L. (1995). Nitrogen fixation: anthropogenic enhancement-environmental response. *Global Biogeochemical Cycles*, 9: 235–252.

Garnier, J., Beusen, A. H. W., Thieu, V., Billen, G., and Bouwman, A. F. (2010). N:P:Si nutrient export ratios and ecological consequences in coastal seas evaluated by the ICEP approach. *Global Biogeochemical Cycles*, 24, doi: 10.1029/2009GB003583.

Garnier, J., Billen, G., Hannon, E., Fonbonne, S., Videnina, Y., and Soulie, M. (2002). Modelling the transfer and retention of nutrients in the drainage network of the Danube river. *Estuarine, Coastal and Shelf Science*, 54(3): 285–308.

Garnier, J., Billen, G., and Palfner, L. (2000). Understanding the oxygen budget and related ecological processes in the river Mosel: the Riverstrahler approach. *Hydrobiologia*, 410: 151–166.

Garnier, J., Sferratore, A., Meybeck, M., Billen, G., and Dürr, H. (2006). Modeling silicon transfer processes in river catchments. In: Ittekot, V., Unger, D., Humborg, C., and Nguyen, N. T. (eds.), *The silicon cycle. Human perturbations and impacts on aquatic systems*, pages 139–162. Island Press, Washington, D.C.

Ghassemi, F. and White, I. (2007). *Inter-basin water transfer: case studies from Australia, United States, Canada, China, and India. International Hydrology Series*. Cambridge University Press, Cambridge, U.K.

Graedel, T. E. and Crutzen, P. J. (1993). *Atmospheric change. An earth system perspective*. W.H. Freeman and Company, New York.

Green, C. T., Puckett, L. J., Bohlke, J. K., Bekins, B. A., Phillips, S. P., Kaufman, L. J., Denver, J. M., and Johnson, H. M. (2008). Limited occurrence of denitrification in four shallow aquifers in agricultural areas in the United States. *Journal of Environmental Quality*, 37: 994–1009, doi: 10.2134/jeq2006.0419.

Green, P., Vörösmarty, C. J., Meybeck, M., Galloway, J. N., Petersen, B. J., and Boyer, E. W. (2004). Pre-industrial and contemporary fluxes of nitrogen through rivers: a global assessment based on typology. *Biogeochemistry*, 68: 71–105.

Griffioen, J., Brunt, R., Vasak, S., and der Gun, J. V. (2005). *A global inventory of groundwater quality: first results*, pages 3–10. Number 297. International Association of Hydrolical. Sciences (IAHS), Centre for Ecology and Hydrology, Wallingford, Oxfordshire OX10 8BB, UK.

Groffman, P. M., Altabet, M. A., Böhlke, J. K., Butterbach-Bahl, K., David, M. B., Firestone, M. K., Giblin, A. E., Kana, T. M., Nielsen, L. P., and Voytek, M. A. (2006). Methods for measuring denitrification: diverse approaches to a difficult problem. *Eco-*

logical Applications, 16(6): 2091–2122.

Groffman, P. M., Gold, A. J., and Jacinthe, P.-A. (1998). Nitrous oxide production in riparian zones and groundwater. *Nutrient Cycling in Agroecosystems*, 52: 179–186.

Gruber, N. and Sarmiento, J. L. (1997). Global patterns of marine nitrogen fixation and denitrification. *Global Biogeochemical Cycles*, 11: 235–266.

Guo, L. B. and Gifford, R. M. (2002). Soil carbon stocks and land use change: a meta analysis. *Global Change Biology*, 8(4): 345–360, doi: 10.1046/j.1354-1013.2002.00486.x.

Haddeland, I., Skaugen, T., and Lettenmaier, D. P. (2006). Anthropogenic impacts on continental surface water fluxes. *Geophysical Research Letters*, 33(8).

Hageman, S. and Gates, L. D. (2003). Improving a sub-grid runoff parameterization scheme for climate models by the use of high-resolution data derived from satellite observations. *Climate Dynamics*, 21: 349–359.

Hagemann, S., Botzet, M., Dümenil, L., and Machenhauer, B. (1999). Derivation of global GCM boundary conditions from 1 km land use satellite data. Technical Report 289, Max Planck Institute for Meteorology, Hamburg, Germany.

Hallegraeff, G. M. (1993). A review of harmful algal blooms and their apparent global increase. *Phycologia*, 32: 79–99.

Harrison, J. A., Seitzinger, S. P., Bouwman, A. F., Caraco, N. F., Beusen, A. H. W., and Vörösmarty, C. J. (2005). Dissolved inorganic phosphorus export to the coastal zone: results from a spatially explicit, global model. *Global Biogeochemical Cycles*, 19, GB4S03, doi: 10.1029/2004GB002357.

Hart, M. R., Quin, B. F., and Nguyen, M. L. (2004). Phosphorus runoff from agricultural land and direct fertilizer effects: a review. *Journal of Environmental Quality*, 33(6): 1954–1972.

Hartmann, J., Jansen, N., Dürr, H., Harashima, A., Okubo, K., and Kempe, S. (2008). Predicting riverine dissolved silica fluxes into coastal zones from a hyperactive region and analysis of their first order controls. *International Journal of Earth Sciences*, doi: 10.1007/s00531-008-0381-5.

Hartmann, J., Moosdorf, N., Lauerwald, R., Hinderer, M., and West, A. J. (2014). Global chemical weathering and associated P-release - The role of lithology, temperature and soil properties. *Chemical Geology*, 363: 145–163, doi: 10.1016/j.chemgeo.2013.10.025.

Hefting, M., Beltman, B., Karssenberg, D., Rebel, K., Van Riessen, M., and Spijker, M. (2006a). Water quality dynamics and hydrology in nitrate loaded riparian zones in the Netherlands. *Environmental Pollution*, 139(1): 143–156.

Hefting, M. M., Bobbink, R., and Caluwe, H. D. (2003). Nitrous oxide emission and denitrification in chronically nitrate-loaded riparian buffer zones. *Journal of Environmental Quality*, 32(4): 1194–1203.

Hefting, M. M., Bobbink, R., and Janssens, M. P. (2006b). Spatial variation in denitrification and N_2O emission in relation to nitrate removal efficiency in a N-stressed riparian buffer zone. *Ecosystems*, 9(4): 550–563.

Heinen, M. (2006). Simplified denitrification models: overview and properties. *Geoderma*, 133: 444–463.

Heisler, J., Glibert, P. M., Burkholder, J. M., Anderson, D. M., Cochlan, W., Dennison, W. C., Dortch, Q., Gobler, C. J., Heil, C. A., Humphries, E., Lewitus, A., Magnien, R., Marshall, H. G., Sellner, K., Stockwell, D. A., Stoecker, D. K., and Suddleson, M. (2008). Eutrophication and harmful algal blooms: a scientific consensus. *Harmful*

Algae, 8(1): 3–13, doi: 10.1016/j.hal.2008.08.006.

Hejzlar, J., Anthony, S., Arheimer, B., Behrendt, H., Bouraoui, F., Grizzetti, B., Groenendijk, P., Jeuken, M. H. J. L., Johnsson, H., Porto, A. L., Kronvang, B., Panagopoulos, Y., Siderius, C., Silgram, M., Venohr, M., and Zaloudík, J. (2009). Nitrogen and phosphorus retention in surface waters: an inter-comparison of predictions by catchment models of different complexity. *Journal of Environmental Monitoring*, 11: 584–593.

Hill, A. R. (1996). Nitrate removal in stream riparian zones. *Journal of Environmental Quality*, 25: 743–755.

Hilley, G. E. and Porder, S. (2008). A framework for predicting global silicate weathering and CO_2 drawdown rates over geologic time-scales. *Proceedings of the National Academy of Sciences*, 105(44): 16855–16859, doi: 10.1073/pnas.0801462105.

Hofstra, N. and Bouwman, A. F. (2005). Denitrification in agricultural soils: summarizing published data and estimating global annual rates. *Nutrient Cycling in Agroecosystems*, 72: 267–278, doi: 10.1007/s10705-005-3109-y.

Holdridge, L. R. (1967). *Life Zone Ecology*. Tropical Science Center, San Jose, Costa Rica.

Hopfensperger, K. N., Gault, C. M., and Groffman, P. M. (2009). Influence of plant communities and soil properties on trace gas fluxes in riparian northern hardwood forests. *Forest Ecology and Management*, 258(9): 2076–2082.

Howarth, R., Billen, G., Swaney, D., Townsend, A., Jaworski, N., Lajtha, K., Downing, J., Elmgren, R., Caraco, N., Jordan, T., Berendse, F., Freney, J., Kudeyarov, V., Murdoch, P., and Zhao-Liang, Z. (1996). Regional nitrogen budgets and riverine N & P fluxes for the drainages to the North Atlantic Ocean: natural and human influences. *Biogeochemistry*, 35(1): 75–139, doi: 10.1007/bf02179825.

Humborg, C., Conley, D. J., Rahm, L., Wulff, F., Cociasu, A., and Ittekkot, V. (2000). Silicon retention in river basins: far-reaching effects on biogeochemistry and aquatic food webs in coastal marine environments. *Ambio*, 29(1): 45–50.

Humborg, C., Rahm, L., Smedberg, E., Mörth, C.-M., and Danielson, A. (2006). Dissolved silica dynamics in boreal and arctic rivers: vegetation control over temperature? In: Ittekot, V., Unger, D., Humborg, C., and Tac An, N. (eds.), *The silicon cycle*, volume SCOPE 66, pages 53–69. Island Press, Washington.

Hutchinson, G. L. and Livingston, G. P. (2001). Vents and seals in non-steadystate chambers used for measuring gas exchange between soil and the atmosphere. *European Journal of Soil Science*, 52: 675–682.

IFA (2003). IFADATA statistics from 1973/74-1973 to 2001-2001/02, production, imports, exports and consumption statistics for nitrogen, phosphate and potash fertilizers. Data on CD-ROM (http://www.fertilizer.org/ifa/statis-tics/ifadata/dataline.asp). Technical report, International Fertilizer Industry Association, Paris.

IFA/IFDC/FAO (2003). Fertilizer use by crop. 5th edition. Technical report, Food and Agriculture Organization of the United Nations, Rome.

IMAGE-team (2001). The IMAGE 2.2 implementation of the SRES scenarios. A comprehensive analysis of emissions, climate change and impacts in the 21st century. Technical Report 481508018, National Institute for Public Health and the Environment, Bilthoven.

Iman, R. L. and Helton, J. C. (1985). A comparison of uncertainty and sensitivity analysis

techniques for computer models. Technical Report NUREGICR-3904, SAND 84-1461, Sandia National Laboratories, Albuquerque, New Mexico.

Insightful (2005). *S-PLUS 7.0 Guide to statistics*. Volume 1&2. Insightful Corporation, Seattle, WA.

IPCC (2006). 2006 IPCC guidelines for national greenhouse gas inventories. Technical report, IPCC NGGIP Programme, IPCC-TSU/IGES. Published by the Institute for Global Environmental Strategies (IGES), Hayama, Japan on behalf of the IPCC, Hayama, Japan.

Ittekot, V., Unger, D., Humborg, C., and Tac An, N. (2006). The perturbed silicon cycle. In: Ittekot, V., Unger, D., Humborg, C., and Tac An, N. (eds.), *The silicon cycle*, volume SCOPE 66, pages 245–252. Island Press, Washington.

Jacinthe, P. A., Groffman, P. M., Gold, A. J., and Mosier, A. (1998). Patchiness in microbial nitrogen transformations in groundwater in a riparian forest. *Journal of Environmental Quality*, 27(1): 156–164.

Jennerjahn, T. C., Knoppers, B. A., De Souze, W. F. L., Brunskill, G. J., Silva, E. I. L., and Adi, S. (2006). Factors controlling dissolved silica in tropical rivers. In: Ittekot, V., Unger, D., Humborg, C., and Tac An, N. (eds.), *The silicon cycle*, volume SCOPE 66, pages 29–51. Island Press, Washington.

Jordan, T. E., Weller, D. E., and Correll, D. L. (1998). Denitrification in surface soils of a riparian forest: effects of water, nitrate and sucrose additions. *Soil Biology and Biochemistry*, 30(7): 833–843.

Ju, X., Liu, X., Zhang, F., and Roelcke, M. (2004). Nitrogen fertilization, soil nitrate accumulation, and policy recommendations. *Ambio*, 33: 300–305.

Keuskamp, J. A., Van Drecht, G., and Bouwman, A. F. (2012). European-scale modelling of groundwater denitrification and associated N_2O production. *Environmental Pollution*, 165(0): 67–76, doi: 10.1016/j.envpol.2012.02.008.

Klein Goldewijk, K., Beusen, A., and Janssen, P. (2010). Long-term dynamic modeling of global population and built-up area in a spatially explicit way: HYDE 3.1. *Holocene*, 20(4): 565–573.

Klein Goldewijk, K., Beusen, A., Van Drecht, G., and De Vos, M. (2011). The HYDE 3.1 spatially explicit database of human induced land use change over the past 12,000 years. *Global Ecology and Biogeography*, 20: 73–83, doi: 10.1111/j.1466-8238.2010.00587.x.

Klein Goldewijk, K. and Van Drecht, G. (2006). HYDE 3: current and historical population and land cover. In: Bouwman, A. F., Kram, T., and Klein Goldewijk, K. (eds.), *Integrated modelling of global environmental change. An overview of IMAGE 2.4*, pages 93–111. Netherlands Environmental Assessment Agency, Bilthoven.

Klein Goldewijk, K., Van Drecht, G., and Bouwman, A. F. (2006). Contemporary global cropland and grassland distributions on a 5 by 5 minute resolution. *Journal of Land Use Science*, 2: 167 – 190, doi: 10.1080/17474230701622940.

Knowles, R. (1982). Denitrification. *Microbiological Reviews*, 46: 43–70.

Kragt, J. F., De Vries, W., and Breeuwsma, A. (1990). Modelling nitrate leaching on a regional scale. In: Merckx, R. H., Vereecken, H., and Vlassak, K. (eds.), *Fertilization and the environment*, pages 340–347. Leuven University Press, Leuven, Belgium.

Kristiansen, S. and Hoell, E. (2002). The importance of silicon for marine production. *Hydrobiologia*, 484: 21–31.

Kruska, R. L., Reid, R. S., Thornton, P. K., Henninger, N., and Kristjanson, P. M.

(2003). Mapping livestock-oriented agricultural production systems for the developing world. *Agricultural Systems*, 77: 39–63.

Kump, L. R., Brantley, S. L., and Arthur, M. A. (2000). Chemical weathering, atmospheric CO_2 and climate. *Annual Review of Earth and Planetary Sciences*, 28: 611–667.

Kurtz, A. C. and Derry, L. A. (2004). Tracing silicate weathering and terrestrial silica cycling with Ge/Si ratios. In: Wanty, R. B. and Seal, R. R. (eds.), *Proceedings of the 11th international symposium on water rock interaction*, pages 833–836. A.A. Balkema Publishers, Dordrecht.

Leemans, R. (1989). World map of Holdridge Life Zones (digital data set). 0.5 Degree resolution map, presenting the 38 Holdridge Life Zones. Technical report, IIASA, Laxenburg, Austria.

Leemans, R. (1990). Global data sets collected and compiled by the Biosphere Project. Technical report, IIASA, Laxenburg, Austria.

Lehner, B. and Döll, P. (2004). Development and validation of a global database of lakes, reservoirs and wetlands. *Journal of Hydrology*, 296(1-4): 1–22.

Lehner, B., Liermann, C. R., Revenga, C., Vörösmarty, C., Fekete, B., Crouzet, P., Döll, P., Endejan, M., Frenken, K., Magome, J., Nilsson, C., Robertson, J. C., Rödel, R., Sindorf, N., and Wisser, D. (2011). High-resolution mapping of the world's reservoirs and dams for sustainable river-flow management. *Frontiers in Ecology and the Environment*, 9(9): 494–502, doi: 10.1890/100125.

Levy, P. E., Gray, A., Leeson, S. R., Gaiawyn, J., Kelly, M. P. C., Cooper, M. D. A., Dinsmore, K. J., Jones, S. K., and Sheppard, L. J. (2011). Quantification of uncertainty in trace gas fluxes measured by the static chamber method. *European Journal of Soil Science*, 62: 811–821.

Livingstone, D. A. (1963). Chemical composition of rivers and lakes. Technical report, U.S. Geol. Survey.

Mander, U., Lohmus, K., Teiter, S., Uri, V., and Augustin, J. (2008). Gaseous nitrogen and carbon fluxes in riparian alder stands. *Boreal Environment Research*, 13(3): 231–241.

Marcé, R. and Armengol, J. (2009). Modeling nutrient in-stream processes at the watershed scale using nutrient spiralling metrics. *Hydrol. Earth Syst. Sci.*, 13(7): 953–967.

Mayer, P. M., Jr, S. K. R., McCutchen, M. D., and Canfield, T. J. (2007). Meta-analysis of nitrogen removal in riparian buffers. *Journal of Environmental Quality*, 36(4): 1172–1180.

Mayorga, E., Seitzinger, S. P., Harrison, J. A., Dumont, E., Beusen, A. H. W., Bouwman, A. F., Fekete, B. M., Kroeze, C., and Van Drecht, G. (2010). Global Nutrient Export from WaterSheds 2 (NEWS 2): model development and implementation. *Environmental Modelling and Software*, 25(7): 837–853.

McBride, G. B., Alexander, R. B., Elliot, A. H., and Shankar, U. (2000). Regional scale modelling of water quality. Technical report, National Institute of Water and Atmospheric Research (NIWA), Auckland, New Zealand.

McClain, M. E., Boyer, E. W., Dent, C. L., Gergel, S. E., Grimm, N. B., Groffman, P. M., Hart, S. C., Harvey, J. W., Johnston, C. A., Mayorga, E., McDowell, W. H., and Pinay, G. (2003). Biogeochemical hot spots and hot moments at the interface of terrestrial and aquatic ecosystems. *Ecosystems*, 6(4): 301–312, doi: 10.1007/s10021-003-0161-9.

McDowell, R. W. and Sharpley, A. N. (2001). Approximating phosphorus release from

soils to surface runoff and subsurface drainage. *Journal of Environmental Quality*, 30(2): 508–520.

McLauchlan, K. (2006). The nature and longevity of agricultural impacts on soil carbon and nutrients: a review. *Ecosystems*, 9(8): 1364–1382.

Meinardi, C. R. (1994). Groundwater recharge and travel times in the sandy regions of the Netherlands. Technical Report 715501004, National Institute for Public Health and the Environment, Bilthoven.

Meybeck, M. (1979). Concentrations des eaux fluviales en éléments majeurs et apports en solution aux océans. *Revue de Géologie Dynamique et de Géographie Physique*, 21: 215–246.

Meybeck, M. (1982). Carbon, nitrogen and phosphorous transport by world rivers. *American Journal of Science*, 282: 401–450.

Meybeck, M. and Ragu, A. (1995). River discharges to oceans: an assessment of suspended solids, major ions and nutrients. Technical report, United Nations Environment Programme (UNEP), Nairobi.

Millennium Ecosystem Assessment (ed.) (2006). *Ecosystems and human well-being: scenarios*, volume 2. Edited by Carpenter S.R., Pingali P.L., Bennett, E.M. and Zurek, M.B., Island Press, Washington, D.C.

Ministry of Infrastructure and Environment (2013). http://live.waterbase.nl/waterbase_wns.cfm?taal=nl (in Dutch). Website. Accessed 1 March 2013.

Moatar, F. and Meybeck, M. (2007). Riverine fluxes of pollutants: towards predictions of uncertainties by flux duration indicators. *C. R. Geosci.*, 339: 367–382, doi: 10.1016/j.crte.2007.05.001.

Morée, A. L., Beusen, A. H. W., Bouwman, A. F., and Willems, W. J. (2013). Exploring global nitrogen and phosphorus flows in urban wastes during the twentieth century. *Global Biogeochemical Cycles*, 27: 1–11, doi: 10.1002/gbc.20072.

Mortatti, J. and Probst, J.-L. (2003). Silicate rock weathering and atmospheric/soil CO_2 uptake in the Amazon basin estimated from river water geochemistry: seasonal and spatial variations. *Chemical Geology*, 197: 177–196.

Mosier, A. R., Kroeze, C., Nevison, C., Oenema, O., Seitzinger, S., and Van Cleemput, O. (1998). Closing the global atmospheric N_2O budget: nitrous oxide emissions through the agricultural nitrogen cycle. *Nutrient Cycling in Agroecosystems*, 52: 225–248.

Mulholland, P. J., Helton, A. M., Poole, G. C., Hall, R. O., Hamilton, S. K., Peterson, B. J., Tank, J. L., Ashkenas, L. R., Cooper, L. W., Dahm, C. N., Dodds, W. K., Findlay, S. E. G., Gregory, S. V., Grimm, N. B., Johnson, S. L., McDowell, W. H., Meyer, J. L., Valett, H. M., Webster, J. R., Arango, C. P., Beaulieu, J. J., Bernot, M. J., Burgin, A. J., Crenshaw, C. L., Johnson, L. T., Niederlehner, B. R., O'Brien, J. M., Potter, J. D., Sheibley, R. W., Sobota, D. J., and Thomas, S. M. (2008). Stream denitrification across biomes and its response to anthropogenic nitrate loading. *Nature*, 452(7184): 202–205, doi: 10.1038/nature06686.

National Geophysical Data Center (2002). NDGC 5 minute gridded elevation data (ETOPO5). Technical report, National Geophysical Data Center, NOAA Satellites and Information (http://www.ngdc.noaa.gov).

National Land and Water Resources Audit (2001). Rangelands: and overview. Technical report, National Land and Water Resources Audit, The National Heritage Trust, Commonwealth of Australia, Canberra.

New, M., Hulme, M., and Jones, P. (1999). Representing twentieth century space-time climate variability. Part I: development of a 1961-90 mean monthly terrestrial climatology. *Journal of Climate*, 12: 829–856.

New, M., Hulme, M., and Jones, P. (2000). Representing twentieth-century space-time climate variability. Part II: development of 1901-96 monthly grids of terrestrial surface climate. *Journal of Climate*, 13: 2217–2238.

Newbold, J. D., Elwood, J. W., O'Neill, R. V., and Winkle, W. V. (1981). Measuring nutrient spiraling in streams. *Canadian Journal of Fisheries and Aquatic Sciences*, 38: 860–863.

Nyenje, P. M., Foppen, J. W., Uhlenbrook, S., Kulabako, R., and Muwanga, A. (2010). Eutrophication and nutrient release in urban areas of sub-Saharan Africa – A review. *Science of the Total Environment*, 408: 447–455, doi: 10.1016/j.scitotenv.2009.10.020.

Oehler, F., Bordenave, P., and Durand, P. (2007). Variations in denitrification in a farming catchment area. *Agriculture, Ecosystems and Environment*, 120: 313–324, doi: 10.1016/j.agee.10.007.

Paul, B. K., Lubbers, I. M., and Groenigen, J. W. V. (2012). Residue incorporation depth is a controlling factor of earthworm-induced nitrous oxide emissions. *Global Change Biology*, 18(3): 1141–1151.

Peierls, B. L., Caraco, N. F., Pace, M. L., and Cole, J. C. (1991). Human influence on river nitrogen. *Nature*, 350: 386–387.

Peterjohn, W. T. and Schlesinger, W. H. (1990). Nitrogen loss from deserts in the southwestern United States. *Biogeochemistry*, 10: 67–79.

Postma, D., Boesen, C., Kristiansen, H., and Larsen, F. (1991). Nitrate reduction in an unconfined sandy aquifer: water chemistry, reduction processes, and geochemical modeling. *Water Resources Research*, 27(8): 2027–2045.

Preston, S. D. and Brakebill, J. W. (1999). Application of spatially referenced regression modeling for the evaluation of total nitrogen loading in the Chesapeake Bay watershed. Technical report, U.S. Geological Survey.

Qin, S., Hu, C., and Oenema, O. (2012). Quantifying the underestimation of soil denitrification potential as determined by the acetylene inhibition method. *Soil Biology and Biochemistry*, 47: 14–17.

Quynh, L. T. P., Billen, G., Garnier, J., Théry, S., and Fézard, C. (2005). Nutrient (N, P) budgets for the Red River basin (Vietnam and China). *Global Biogeochemical Cycles*, 19, GB2022, doi: 101029/2004GB002405.

Rabalais, N. N. (2002). Nitrogen in aquatic ecosystems. *Ambio*, 31: 102–112.

Ragueneau, O., Conley, D., Leynaert, A., Ni Longphuirt, S., and Slomp, C. P. (2006). Role of diatoms in silicon cycling and coastal marine foodwebs. In: Ittekot, V., Unger, D., Humborg, C., and Tac An, N. (eds.), *The silicon cycle*, volume SCOPE 66, pages 163–195. Island Press, Washington.

Reddy, K. R., Kadlec, R. H., Flaig, E., and Gale, P. M. (1999). Phosphorus retention in streams and wetlands: a review. *Critical Reviews in Environmental Science and Technology*, 29(1): 83–146.

Reynolds, C. S. (1984). *The ecology of freshwater phytoplankton.* Cambridge University Press, New York.

Richardson, C. J. and Qian, S. S. (1999). Long-term phosphorus assimilative capacity in freshwater wetlands: a new paradigm for sustaining ecosystem structure and function.

Environmental Science and Technology, 33(10): 1545–1551, doi: 10.1021/es980924a.

Rivett, M. O., Buss, S. R., Morgan, P., Smith, J. W. N., and Bemment, C. D. (2008). Nitrate attenuation in groundwater: a review of biogeochemical controlling processes. *Water Research*, 42(16): 4215–4232.

Ryan, M., Müller, C., Di, H. J., and Cameron, K. C. (2004). The use of artificial neural networks (ANNs) to simulate N_2O emissions from a temperate grassland ecosystem. *Ecological Modelling*, 175(2): 189–194, doi: 10.1016/j.ecolmodel.2003.10.010.

Ryden, J. C., Lund, L. J., and Focht, D. D. (1978). Direct in-field measurement of nitrous oxide flux from soils. *Soil Science Society of America Journal*, 42: 731–737.

Saad, A. L. O. and Conrad, R. (1993). Temperature dependence of nitrification, denitrification and turnover of nitric oxide in different soils. *Biology and Fertility of Soils*, 15: 21–27.

Saltelli, A., Chan, K., and Scott, E. M. (2000). *Sensitivity analysis*. Wiley and Sons, Chichester.

Saltelli, A., Tarantola, S., Campolongo, F., and Ratto, M. (2004). *Sensitivity analysis in practice. A guide to assessing scientific models*. Wiley and Sons, Chichester.

Saunders, D. L. and Kalff, J. (2001). Nitrogen retention in wetlands, lakes and rivers. *Hydrobiologia*, 443: 205–212, doi: 10.1023/a:1017506914063.

Schipper, L. A., Cooper, A. B., Harfoot, C. G., and Dyck, W. J. (1993). Regulators of denitrification in an organic riparian soil. *Soil Biology and Biochemistry*, 25(7): 925–933.

Schmidt, I., Bock, E., and Jetten, M. S. M. (2001). Ammonia oxidation by Nitrosomonas eutropha with NO(2) as oxidant is not inhibited by acetylene. *Microbiology*, 147: 2247–2253.

Schumm, S. A. (1977). *The fluvial system*. Wiley-Interscience, New York.

Seitzinger, S. P., Harrison, J. A., Böhlke, J. K., Bouwman, A. F., Lowrance, R., Peterson, B., Tobias, C., and Van Drecht, G. (2006). Denitrification across landscapes and waterscapes: a synthesis. *Ecological Applications*, 16: 2064–2090.

Seitzinger, S. P., Harrison, J. A., Dumont, E., Beusen, A. H. W., and Bouwman, A. F. (2005). Sources and delivery of carbon, nitrogen, and phosphorus to the coastal zone: an overview of global NEWS models and their application. *Global Biogeochemical Cycles*, 19, GB4S01, doi: 10.1029/2004GB002606.

Seitzinger, S. P., Mayorga, E., Bouwman, A. F., Kroeze, C., Beusen, A. H. W., Billen, G., Van Drecht, G., Dumont, E., Fekete, B. M., Garnier, J., Harrison, J., Wisser, D., and Wollheim, W. M. (2010). Global river nutrient export: a scenario analysis of past and future trends. *Global Biogeochemical Cycles*, 24, GB0A08, doi: 10.1029/2009GB003587.

Seré, C. and Steinfeld, H. (1996). World livestock production systems. Current status, issues and trends. Technical Report Animal Production and Health Paper 127, Food and Agriculture Organization of the United Nations, Rome.

Sferratore, A., Billen, G., Garnier, J., and Théry, S. (2005). Modeling nutrient (N, P, Si) budget in the Seine watershed: application of the Riverstrahler model using data from local to global scale. *Global Biogeochemical Cycles*, 19, GB4S07, doi: 10.1029/2005GB002496.

Sferratore, A., Garnier, J., Billen, G., Conley, D. J., and Pinault, S. (2006). Diffuse and point sources of silica in the Seine river watershed. *Environmental Science and Technology*, 40(21): 6630–6635, doi: 10.1021/es060710q.

Shaffer, M. J., Halvorson, A. D., and Pierce, F. J. (1991). Nitrate leaching and economic analysis package (NLEAP): model description and application. In: Follet, R. F., Keeney, D. R., and Cruse, R. M. (eds.), *Managing nitrogen for groundwater quality and farm profitability*, pages 285–322. Soil Science Society of America, Madison, Wisconsin, USA.

Shand, P. and Edmunds, W. M. (2008). The baseline inorganic chemistry of European groundwater. In: Edmunds, W. M. and Shand, P. (eds.), *Natural groundwater quality*, pages 22–58. Blackwell, Oxford.

Sheppard, S. C., Bittman, S., Tait, J., Sommer, S. G., and Webb, J. A. (2007). Sensitivity analysis of alternative model structures for an indicator of ammonia emissions from agriculture. *Canadian Journal of Soil Science*, 87: 129–139.

Siebert, S. and Döll, P. (2001). A digital global map of irrigated areas. An update for Latin America and Europe. Technical Report Kassel World Water Series No. 4, Center for Environmental Systems Research, University of Kassel, Kassel.

Simek, M. and Cooper, J. E. (2002). The influence of soil pH on denitrification: progress towards the understanding of this interaction over the last 50 years. *European Journal of Soil Science*, 53: 345–354.

Smil, V. (2001). *Enriching the earth: Fritz Haber, Carl Bosch, and the transformation of world food*. MIT Press, Cambridge.

Smith, R. A., Schwarz, G. E. G., and Alexander, R. B. (1997). Regional interpretation of water-quality monitoring data. *Water Resources Research*, 33: 2781–2798.

Smith, S. V., Swaney, D. P., Talaue-McManus, L., Bartley, D. D., Sandhei, P. T., McLaughlin, C. J., Dupra, V. C., Crossland, C. J., Buddemeier, R. W., Maxwell, B. A., and Wulff, F. (2003). Humans, hydrology, and the distribution of inorganic nutrient loading to the ocean. *BioScience*, 53: 235–245.

Soderlund, R. and Svensson, B. H. (1976). The global nitrogen cycle. In: Svensson, B. H. and Soderlund, R. (eds.), *Nitrogen, Phosphorus and Sulphur - Global cycles*, volume SCOPE 7, pages 23–73. Ecological Bulletin, Stockholm.

Soetaert, K., Middelburg, J. J., Heip, C., Meire, P., Van Damme, S., and Maris, T. (2006). Long-term change in dissolved inorganic nutrients in the heterotrophic Scheldt estuary (Belgium, The Netherlands). *Limnology and Oceanography*, 51(1, part 2): 409–423.

Sommer, M., Kaczorek, D., Kuzyakov, Y., and Breuer, J. (2006). Silicon pools and fluxes in soils and landscapes -a review. *Journal of Plant Nutrition and Soil Science*, 169(3): 310–329.

Soosaar, K., Mander, U., Maddison, M., Kanal, A., Kull, A., Lohmus, K., Truu, J., and Augustin, J. (2011). Dynamics of gaseous nitrogen and carbon fluxes in riparian alder forests. *Ecological Engineering*, 37(1): 40–53.

Stanley, E. H., Powers, S. M., and Lottig, N. R. (2010). The evolving legacy of disturbance in stream ecology: concepts, contributions, and coming challenges. *Journal of the North American Benthological Society*, 29(1): 67–83, doi: 10.1899/08-027.1.

Stehfest, E. (2006). *Modelling of global crop production and resulting N_2O emissions*. PhD thesis. Universität Kassel, Kassel, Germany.

Stehfest, E. and Bouwman, A. F. (2006). N_2O and NO emission from agricultural fields and soils under natural vegetation: summarizing available measurement data and modeling of global annual emissions. *Nutrient Cycling in Agroecosystems*, 74: 207–228, doi: 10.1007/s10705-006-9000-7.

Stehfest, E., Van Vuuren, D., Kram, T., Bouwman, L., Alkemade, R., Bakkenes, M., Biemans, H., Bouwman, A., Den Elzen, M., Janse, J., Lucas, P., Van Minnen, J., Müller, C., and Prins, A. (2014). *Integrated Assessment of Global Environmental Change with IMAGE 3.0. Model description and policy applications.* PBL Netherlands Environmental Assessment Agency, The Hague, The Netherlands.

Stelzer, R. S. and Likens, G. E. (2006). Effects of sampling frequency on estimates of dissolved silica export by streams: the role of hydrological variability and concentration-discharge relationships. *Water Resources Research*, 42, W07415, doi: 10.1029/2005WR004615.

Strahler, A. N. (1957). Quantitative analysis of watershed geomorphology. *Transactions of the American Geophysical Union*, 38: 913–920.

Stream Solute Workshop (1990). Concepts and methods for assessing solute dynamics in stream ecosystems. *Journal of the North American Benthological Society*, 9: 95–119.

Stumm, W. (1973). The acceleration of the hydrogeochemical cycling of phosphorus. *Water Research*, 7: 131–144, doi: 10.1016/0043-1354(73)90158-9.

Syvitski, J. P. M., Peckham, S. D., Hilberman, R., and Mulder, T. (2003). Predicting the terrestrial flux of sediment to the global ocean: a planetary perspective. *Sedimentary Geology*, 162: 5–24.

Tarkalson, D. D. and Mikkelsen, R. L. (2004). Runoff phosphorus losses as related to soil test phosphorus and degree of phosphorus saturation on Piedmont soils under conventional and no-tillage. *Communications in Soil Science and Plant Analysis*, 35(19-20): 2987–3007.

Tiedje, J. M. (1988). Ecology of denitrification and dissimilatory nitrate reduction to ammonium. In: Zehnder, A. J. B. (ed.), *Biology of Anaerobic microorganisms*, pages 179–244. Wiley and Sons, New York.

Todini, E. (1996). The ARNO rainfall-runoff model. *Journal of Hydrology*, 175: 339–382.

Treguer, P., Nelson, D. M., Van Bennekom, A. J., DeMaster, D. J., Leynaert, A., and Queguiner, B. (1995). The silica balance in the world ocean: a reestimate. *Science*, 268(5209): 375–379, doi: 10.1126/science.268.5209.375.

Treguer, P. and Pondaven, P. (2000). Global change: silica control of carbon dioxide. *Nature*, 406(6794): 358–359, doi: 10.1038/35019236.

Trumbore, S. E., Davidson, E. A., De Camarge, P. B., Nepstad, D. C., and Martinelli, L. A. (1995). Belowground cycling of carbon in forests and pastures of eastern Amazonia. *Global Biogeochemical Cycles*, 9(4): 515–528, doi: 10.1029/95GB02148.

Turner, R. E. and Rabalais, N. N. (1994). Coastal eutrophication near the Mississippi river delta. *Nature*, 368: 619–621.

Turner, R. E., Rabalais, N. N., Justic, D., and Dortch, Q. (2003). Global patterns of dissolved N, P and Si in large rivers. *Biogeochemistry*, 64: 297–317.

UN-ECE (1999). Draft protocol to the 1979 convention on long range transboundary air pollution to abate acidification, eutrophication and ground-level ozone. Technical report, United Nations-Economic Commision for Europe (UN-ECE), Geneva.

UNECE (2003). Present state of emission data. Technical report, United Nations Economic Commission for Europe (UNECE), Geneva.

United States Geological Survey (2013). Water quality samples for the nation (http://waterdata.usgs.gov/nwis/qwdata). Website.

Uppala, S. M., Kållberg, P. W., Simmons, A. J., Andrae, U., Da Costa Bechtold, V.,

Fiorino, M., Gibson, J. K., Haseler, J., Hernandez, A., Kelly, G. A., Li, X., Onogi, K., Saarinen, S., Sokka, N., Allan, R. P., Andersson, E., Arpe, K., Balmaseda, M. A., Beljaars, A. C. M., Van De Berg, L., Bidlot, J., Bormann, N., Caires, S., Chevallier, F., Dethof, A., Dragosavac, M., Fisher, M., Fuentes, M., Hagemann, S., Hólm, E., Hoskins, B. J., Isaksen, L., Janssen, P. A. E. M., Jenne, R., McNally, A. P., Mahfouf, J. F., Morcrette, J. J., Rayner, N. A., Saunders, R. W., Simon, P., Sterl, A., Trenberth, K. E., Untch, A., Vasiljevic, D., Viterbo, P., and Woollen, J. (2005). The ERA-40 re-analysis. *Quarterly Journal of the Royal Meteorological Society*, 131(612): 2961–3012, doi: 10.1256/qj.04.176.

US-EPA (2006). Inventory of U.S. greenhouse gas emissions and sinks 1990-2004. Technical report, United States Environmental Protection Agency, Washington, D.C.

USDA (2006). China agricultural and economic data: provincial data. Technical report, United States Department of Agriculture. Economic Research Service (www.ers.usda.gov).

USEPA (2005). *National emission inventory. Ammonia emissions from animal agricultural operations.* United States Environmental Protection Agency.

Van Beek, L. P. H. and Bierkens, M. F. P. (2009). The global hydrological model PCR-GLOBWB: conceptualization, parameterization and verification. Technical Report (http://vanbeek.geo.uu.nl/suppinfo/vanbeekbierkens2009.pdf), Utrecht.

Van Beek, L. P. H., Wada, Y., and Bierkens, M. F. P. (2011). Global monthly water stress: 1. Water balance and water availability. *Water Resources Research*, 47(7): W07517, doi: 10.1029/2010wr009791.

Van Breemen, N., Burrough, P. A., Velthorst, E. J., Van Dobben, H. F., De Wit, T., Ridder, T. B., and Reijnders, H. F. R. (1982). Soil acidification from atmospheric ammonium sulphate in forest canopy throughfall. *Nature*, 299: 548–550.

Van Cappellen, P. (2003). Biomineralization and global biogeochemical cycles. *Rev Mineral Geochem*, 54: 357–381.

Van Cleemput, O. (1998). Subsoils: chemo- and biological denitrification, N_2O and N_2 emissions. *Nutrient Cycling in Agroecosystems*, 52(2-3): 187–194.

Van Den Brink, C., Frapporti, G., Griffioen, J., and Zaadnoordijk, W. J. (2007). Statistical analysis of anthropogenic versus geochemical-controlled differences in groundwater composition in the Netherlands. *Journal of Hydrology*, 336: 470–480.

Van Den Heuvel, R. N., Bakker, S. E., Jetten, M. S. M., and Hefting, M. M. (2011). Decreased N(2)O reduction by low soil pH causes high N(2)O emissions in a riparian ecosystem. *Geobiology*, 9(3): 294–300.

Van Den Heuvel, R. N., Van Der Biezen, E., Jetten, M. S. M., Hefting, M. M., and Kartal, B. (2010). Denitrification at pH 4 by a soil-derived Rhodanobacter-dominated community. *Environmental Microbiology*, 12(12): 3264–3271.

Van Der Hoek, K. W. (1998). Nitrogen efficiency in global animal production. In: Van Der Hoek, K. W., Erisman, J. W., Smeulders, S., Wisniewski, J. R., and Wisniewski, J. (eds.), *Nitrogen, the Confer-N-s*, pages 127–132. First International Nitrogen Conference 1998, Elsevier, Amsterdam.

Van Dokkum, H., Hulskotte, J., Kramer, K., and Wilmot, J. (2004). Emission,fate and effects of soluble silicates (waterglass) in the aquatic environment. *Environ. Sci. Technol.*, 38: 515–521, doi: 10.1021/es0264697.

Van Drecht, G., Bouwman, A. F., Boyer, E. W., Green, P., and Siebert, S. (2005).

A comparison of global spatial distributions of nitrogen inputs for nonpoint sources and effects on river nitrogen export. *Global Biogeochemical Cycles*, 19, GB4S06, doi: 10.1029/2005GB002454.

Van Drecht, G., Bouwman, A. F., Harrison, J., and Knoop, J. M. (2009). Global nitrogen and phosphate in urban waste water for the period 1970-2050. *Global Biogeochemical Cycles*, 23, GB0A03, doi: 10.1029/2009GB003458.

Van Drecht, G., Bouwman, A. F., Knoop, J. M., Beusen, A. H. W., and Meinardi, C. R. (2003). Global modeling of the fate of nitrogen from point and nonpoint sources in soils, groundwater and surface water. *Global Biogeochemical Cycles*, 17(4), doi: 10.129/2003GB002060.

Van Egmond, K., Bresser, T., and Bouwman, L. (2002). The European nitrogen case. *Ambio*, 31: 72–78.

Van Vuuren, D. P., Bouwman, A. F., and Beusen, A. H. W. (2010). Phosphorus demand for the 1970–2100 period: a scenario analysis of resource depletion. *Global Environmental Change*, 20(3): 428–439, doi: 10.1016/j.gloenvcha.2010.04.004.

Van Vuuren, D. P., Van Ruijven, B., Hoogwijk, M. M., Isaac, M., and De Vries, H. J. M. (2006). TIMER 2: model description and application. In: Bouwman, A. F., Kram, T., and Klein Goldewijk, K. (eds.), *Integrated modelling of global environmental change*, pages 39–59. Netherlands Environmental Assessment Agency, Bilthoven.

Velthof, G. L., Brader, A. B., and Oenema, O. (1996). Seasonal variations in nitrous oxide losses from managed grasslands in The Netherlands. *Plant and Soil*, 181: 263–274.

Velthof, G. L., Oudendag, D., Witzke, H. P., Asman, W. A. H., Klimont, Z., and Oenema, O. (2009). Integrated assessment of nitrogen losses from agriculture in EU-27 using MITERRA-EUROPE. *Journal of Environmental Quality*, 38(2): 402–417.

Velthof, G. L., Oudendag, D. A., and Oenema, O. (2007). Development and application of the integrated nitrogen model MITERRA-EUROPE. Technical report, Alterra, Wageningen UR, The Netherlands; EuroCare, University of Bonn, Germany; ASG, Wageningen UR, The Netherlands, Wageningen.

Verdin, K. L. and Greenlee, S. K. (1996). Development of continental scale digital elevation models and extraction of hydrographic features. Paper presented at 3rd international conference/workshop on integrating GIS and environmental modeling. National Center for Geographical Information and Analysis. Santa Barbara, California.

Vestreng, V. (2003). EMEP/MSC-W Technical report. Review and Revision. Emission data reported to CLRTAP. MSC-W Status Report 2003. Technical report, EMEP-Meteorological Synthesizing centre West (MSC-W), Oslo, Norway.

Vestreng, V., Breivik, K., Adams, M., Wagener, A., Goodwin, J., Rozovskkaya, O., and Pacyna, J. M. (2005). Inventory review 2005, emission data reported to LRTAP convention and NEC directive, initial review of HMs and POPs. Technical report, EMEP-Meteorological Synthesizing Centre West (MSC-W), Oslo, Norway.

Vidon, P. G. and Hill, A. R. (2006). A landscape-based approach to estimate riparian hydrological and nitrate removal functions. *Journal of the American Water Resources Association*, 42: 1099–1112, doi: 10.1111/j.1752-1688.2006.tb04516.x.

Vilain, G., Garnier, J., Tallec, G., and Tournebize, J. (2011). Indirect N_2O emissions from shallow groundwater in an agricultural catchment (Seine basin, France). *Biogeochemistry*, 111: 253–271, doi: 10.1007/s10533-011-9642-7.

Vitousek, P. M. (1984). Litterfall, nutrient cycling, and nutrient limitation in tropical

forests. *Ecology*, 65: 285–298.

Vitousek, P. M., Fahey, T., Johnson, D. W., and Swift, M. J. (1988). Element interactions in forest ecosystems: succession, allometry and input-output budgets. *Biogeochemistry*, 5: 7–34.

Vitousek, P. M., Menge, D. N. L., Reed, S. C., and Cleveland, C. C. (2013). Biological nitrogen fixation: rates, patterns and ecological controls in terrestrial ecosystems. *Philosophical Transactions of the Royal Society B: Biological Sciences*, 368(1621), doi: 10.1098/rstb.2013.0119.

Vogt, K. A., Grier, C. C., and Vogt, D. J. (1986). Production, turnover, and nutrient dynamics of above- and belowground detritus of world forests. *Advances in Ecological Research*, 15: 303–377.

Vollenweider, R. A., Marchetti, R., and Viviani, R. (eds.) (1992). *Marine coastal eutrophication*. Elsevier, Amsterdam.

Vörösmarty, C. J. and Fekete, B. M. (2000). Global system of rivers: its role in organizing continental land mass and defining land-to-ocean linkages. *Global Biogeochemical Cycles*, 14: 599–621.

Vörösmarty, C. J., Green, P., Salisbury, J., and Lammers, R. B. (2000). Global water resources: vulnerability from climate change and population growth. *Science*, 289: 284–288.

Vörösmarty, C. J., McIntyre, P. B., Gessner, M. O., Dudgeon, D., Prusevich, A., Green, P., Glidden, S., Bunn, S. E., Sullivan, C. A., Liermann, C. R., and Davies, P. M. (2010). Global threats to human water security and river biodiversity. *Nature*, 467(7315): 555–561, doi: 10.1038/nature09440.

Vörösmarty, C. J., Meybeck, M., Fekete, B., Sharma, K., Green, P., and Syvitski, J. P. M. (2003). Anthropogenic sediment retention: major global impact from registered river impoundments. *Global and Planetary Change*, 39: 169–190.

Vörösmarty, C. J., Sharma, K. P., Fekete, B. M., Copeland, A. H., Holden, J., Marble, J., and Lough, J. A. (1997). The storage and ageing of continental runoff in large reservoir systems of the world. *Ambio*, 26: 210–219.

Wakida, F. T. and Lerner, D. N. (2005). Non agricultural sources of groundwater nitrate: a review and a case study. *Water Resources*, 39: 3–16.

Walker, J. T., Geron, C. D., Vose, J. M., and Swank, W. T. (2002). Nitrogen trace gas emissions from a riparian ecosystem in southern Appalachia. *Chemosphere*, 49(10): 1389–1398.

Walvoord, M. A., Phillips, F. M., Stonestrom, D. A., Evans, R. D., Hartsough, P. C., Newman, B. D., and Striegl, R. G. (2003). A reservoir of nitrate beneath desert soils. *Science*, 302: 1021–1024.

Webb, J. and Misselbrook, T. H. (2004). A mass-flow model of ammonia emissions from UK livestock production. *Atmospheric Environment*, 38: 2163–2176.

Weller, D. E., Correll, D. L., and Jordan, T. E. (1994). Denitrification in riparian forests receiving agricultural discharges. In: Mitsch, W. J. (ed.), *Global wetlands: old world and new*, pages 117–131. Elsevier, Amsterdam.

Winsemius, H. C., Van Beek, L. P. H., Jongman, B., Ward, P. J., and Bouwman, A. (2013). A framework for global river flood risk assessments. *Hydrology and Earth System Sciences*, 17(5): 1871–1892, doi: 10.5194/hess-17-1871-2013.

Wisser, D., Fekete, B. M., Vörösmarty, C. J., and Schumann, A. H. (2010). Re-

constructing 20th century global hydrography: a contribution to the global terrestrial network- hydrology (GTN-H). *Hydrology and Earth System Sciences*, 14: 1–24, doi: 10.5194/hess-14-1-2010.

Wollheim, W., Vörösmarty, C. J., Bouwman, A. F., Green, P., Harrison, J., Meybeck, M., Peterson, B. J., Seitzinger, S. P., and Syvitski, J. (2008a). Global N removal by freshwater aquatic systems using a spatially distributed, within-basin approach. *Global Biogeochemical Cycles*, 22, GB2026, doi: 10.1029/2007GB002963.

Wollheim, W. M., Peterson, B. J., Thomas, S. M., Hopkinson, C. H., and Vörösmarty, C. J. (2008b). Dynamics of N removal over annual time periods in a suburban river network. *J. Geophys. Res.*, 113, doi: 10.1029/2007JG000660.

Wollheim, W. M., Vörösmarty, C. J., Peterson, B. J., Seitzinger, S. P., and Hopkinson, C. S. (2006). Relationship between river size and nutrient removal. *Geophysical Research Letters*, 33(6).

Wrage, N., Velthof, G. L., Oenema, O., and Laanbroek, H. J. (2004). Acetylene and oxygen as inhibitors of nitrous oxide production in Nitrosomonas europaea and Nitrosospira briensis: a cautionary tale. *Fems Microbiology Ecology*, 47(1): 13–18.

Wrage, N., Velthof, G. L., Van Beusichem, M. L., and Oenema, O. (2001). Role of nitrifier denitrification in the production of nitrous oxide. *Soil Biology and Biochemistry*, 33(12-13): 1723–1732.

Yamulki, S., Harrison, R. M., Goulding, K. W. T., and Webster, C. P. (1997). N_2O, NO and NO_2 fluxes from a grassland: effect of soil pH. *Soil Biology and Biochemistry*, 29: 1199–1208.

Yang, Z., Post, W. M., Thornton, P. E., and Jain, A. (2010). The distribution of soil phosphorus for global biogeochemical modeling. *Biogeosciences*, 10: 2525–2537, doi: 10.5194/bg-10-2525-2013.

Zhang, Y.-C., Slomp, C. P., Broers, H. P., Passier, H. F., and Van Cappellen, P. (2009). Denitrification coupled to pyrite oxidation and changes in groundwater quality in a shallow sandy aquifer. *Geochimica et Cosmochimica Acta*, 73: 6716–6726.

Summary

This thesis presents four examples of global models developed as part of the framework of the Integrated Model to Assess the Global Environment (IMAGE). They describe different components of global biogeochemical cycles of nitrogen (N), phosphorus (P) and silicon (Si), with a focus on approaches to analyze model sensitivity and uncertainty. These models range from a lumped model at the scale of river basins to spatially explicit flow-path approaches, and are ultimately developed to analyze sources and transport of nutrients in rivers, and biogeochemistry in the land-river continuum.

Chapter 2

Chapter 2 establishes a global river export model for dissolved silica (SiO_2) (DSi), a compound which was not covered in the Global Nutrient Export from WaterSheds (NEWS) family of models (Seitzinger et al. 2005). Although process-based models describing DSi in rivers are available (e.g., Sferratore et al. 2005, Garnier et al. 2002, Billen and Garnier 2000), such models require data on processes and their controls in the Si cycle that are currently not available for global-scale application. Other attempts to globally estimate river export of DSi were merely based on extrapolation of data and expert knowledge for a number of rivers (e.g., Dürr et al. 2011, Garnier et al. 2010).

Therefore, a multiple linear regression model was developed for describing the current global annual river export of DSi to the ocean at the river mouth, i.e., at the river basin scale. Aggregated river basin-scale values were calculated from a range of variables with potential relevance to Si weathering and transport. Results revealed that four variables have a significant influence on DSi yields for the situation prior to dam construction: soil bulk density, precipitation, slope, and the fraction of the river basin area covered by volcanic rocks. The overall importance of precipitation and occurrence of volcanic rocks points to the role of weathering as the ultimate source of DSi. The bulk density (indicator for soil and ecosystem development) supports the important biological control of the global silicon cycle. Precipitation and slope probably influence erosion, transport, and dissolution of DSi from both the mineral and biological components.

Cross validation showed that the model is robust with respect to the selected

model variables and coefficients. Multiple linear regression was also used to develop the NEWS model of the particulate forms of carbon (C), N and P (Mayorga et al. 2010, Beusen et al. 2005). For the DSi model, the development was extended with a Box-Cox transformation and a cross validation as well as an extensive uncertainty analysis.

During the DSi model development it turned out that extrapolation can lead to serious overestimations when applying the model at the global scale. This problem is not merely limited to the DSi model but may also lead to errors in other regression models such as those from the NEWS family. In addition, there are multiple scale problems related to lumped model approaches, for example when applying the model to single river basins with limited areal extent. The DSi model is therefore not appropriate for predicting the DSi load for individual rivers, and regional, continental or global aggregations of model results are more opportune than local applications.

Chapter 3

Given the limitations of lumped regression models discussed in Chapter 1, a logical next step was toward a distributed model. The components at the beginning of the modeling chain in the distributed model presented in further chapters (4, 5) are based on the soil nutrient budget approach. These distributed and spatially explicit IMAGE models to calculate soil N and P budgets are presented in detail elsewhere (e.g., Bouwman et al. 2009, 2013d); Chapter 3 presents the uncertainty analysis of one of the main components of the soil N budget, i.e., ammonia (NH_3) volatilization.

Uncertainty ranges were established for 16 model parameters on the basis of expert knowledge. Using Latin Hypercube Sampling in combination with a linear regression, the uncertainty contributions of the input parameters to the model outputs were quantified. The standardized regression coefficient (SRC) was used as a relative sensitivity measure. SRC is independent of the units, scale and size of the parameters, and thus the sensitivity analysis comes close to an uncertainty analysis.

Five parameters with an important contribution to the global NH_3 emission were identified. Four of them relate to mixed and landless production systems (N excretion rates, NH_3 emission rates from animal houses and storage, the grazing fraction and the fraction of manure ending outside the agricultural system). The fifth parameter is the total animal stock. The N excretion rate in mixed and landless livestock production systems consistently remains the dominant parameter in large parts of the world. However, in countries where landless white meat and confined milk and beef production systems are dominant, the contribution of animal houses and storage systems to the uncertainty in the total agricultural NH_3 emission exceeds that of animal N excretion.

This uncertainty analysis allows for identifying and improving the input parameters which mostly influence the results. Future updates of emission inventories

and soil nutrient budget approaches of this type, both on the global and country scales, should focus on these factors.

Chapter 4

In Chapter 4, the soil N budgets presented in Chapter 3 are used as input for the second step in the development of a distributed global model for describing N delivery to streams. Soil N budgets are used in a global, distributed flow-path model with $0.5°$ by $0.5°$ resolution which accounts for denitrification and N_2O emissions from soils, and includes groundwater and riparian zones. This model is used to simulate the time period of 1900 to 2000 and implements the Millennium Ecosystem Assessment scenarios for the period of 2000 to 2050.

In close collaboration with Peter Vitousek, the model included an improved computation of biological N_2 fixation in natural ecosystems. This led to a drastic reduction of the estimated global natural N_2 fixation, and to the insight that human acceleration of the global N cycle is even more important than previously believed.

Despite large uncertainties in our model approach, Chapter 4 concludes that N removal by denitrification as a fraction of the N inflow has not changed in the continuum formed by soil-groundwater-riparian zones during the 20th century, and that the removal of reactive N via denitrification in terrestrial ecosystems has not kept pace with accelerated N inputs into agriculture. This implies that the transfer of N from land to surface water has increased roughly at the same rate as the increase in the N budget. In terrestrial systems, denitrification in soils is the primary N removal process, followed by denitrification in groundwater and riparian zones.

Our approach to simulate riparian denitrification and N_2O emission at the global scale in a spatially explicit manner is the first ever published, and indicates that riparian zones may be an important landscape element for N removal at the global level. Given the conditions in many riparian areas, with incomplete denitrification accompanied by high fractional N_2O production, global N_2O emissions from riparian areas may exceed those from groundwater. Conversely, soils are key sites for denitrification and are much more important than groundwater and riparian zones in controlling the N flow to rivers and the oceans.

The scenarios indicate that the gradual increase of reactive N transfer to surface waters and the atmosphere will continue in the coming decades, unless drastic improvements in agricultural management occur. This may have important consequences for the biogeochemistry in river networks and coastal seas, inducing a series of processes, such as stimulation of plant growth, algal blooms, decomposition, burial, and hypoxia.

Model sensitivity was performed for the year 2000. In contrast to Chapter 2 and Chapter 3, where the sensitivity was investigated within uncertainty bounds, this is a pure sensitivity analysis, because the uncertainty ranges of many parameters could not be established. Temperature, net precipitation (or runoff) and the

soil N budget for natural ecosystems, cropland and grassland proved to be important determinants for almost all global model variables, including the N delivery to streams and rivers. The direction of the effect is variable, e.g., precipitation increase reduces soil denitrification, while temperature has a positive effect. N in surface runoff is most strongly determined by the various parameters that determine runoff and the N therein, with a strong effect of land use. Global soil denitrification is most sensitive to the N budget in cropland and in natural ecosystems, and N leaching is sensitive to the same group of parameters. A temperature increase leads to more denitrification, but leaching (and subsequent groundwater transport and delivery to streams) is reduced.

The outflow from shallow groundwater is most sensitive to variation of the thickness of the shallow layer, the N budget in natural ecosystems, net precipitation, and the N budget of cropland. The outflow from the deep groundwater system is sensitive to the half-life of nitrate, the thickness of the deep layer, and the water partitioning to the deep layer.

Two important remarks on these results need to be made. Firstly, the sensitivity of the model to the thickness of the shallow and deep groundwater layers is a logical consequence of the model formulation. Lacking better information, the current model defines a shallow groundwater layer with a thickness of 5 meters in each grid cell, and a deep groundwater layer of 50 meters thick where applicable. Major improvements can be achieved by incorporating improved spatially explicit geohydrological information to more accurately describe the physical and environmental conditions in aquifers. Secondly, denitrification was assumed not to occur in the deep groundwater system, and the modelled NO_3^- outflow from deep groundwater is thus a maximum estimate. This assumption may be incorrect if NO_3^- moves to deep groundwater in sedimentary deposits containing reactive organic matter and pyrite. However, NO_3^- outflow from deep groundwater is much less important than that from shallow groundwater, and the sensitivity of modelled river loading due to variation of the half-life of nitrate in deep groundwater is relatively small.

Chapter 5

Chapter 5 presents a global, spatially explicit model of N and P delivery to surface water and in-stream retention. This model couples submodels for hydrology, spatial explicit nutrient delivery patterns and in-stream retention, each of which has been parameterized independently.

Apart from the transport pathways in the model of Chapter 4, this coupled model distinguishes direct N and P sources to surface water, i.e., weathering, allochtonous organic matter input to streams and wetlands, direct atmospheric deposition to surface water, N and P release from aquaculture and N and P discharge of urban wastewater. The model accounts for the role of accumulation of residual P in soils due to long-term surpluses in agriculture, which is transported through erosion of soil particles, and for the N contained in the organic matter

present in soils. Separate uncoupled models can be used for in-stream processing of N and P, as different processes are responsible for N and P retention, i.e., denitrification and chemical sorption. Only in the case of plant uptake, decomposition and mineralization, is there a close coupling of N and P (and C and Si).

Particularly small streams are known to play an important role in nutrient retention. Since the hydrological model lacks first to fifth order streams it was necessary to describe the biogeochemistry with a simple a priori parameterization of sub-grid spiraling.

The model was deliberately not calibrated, since that would not lead to a better understanding of the behavior of the model or identification of lacunae in the data used. The uncalibrated model results are in fair agreement with time series of concentration measurements for a selection of rivers. Unlike empirical models which mainly estimate river nutrient export, this model can also be used to explore changes in various processes and interactions between them.

Dramatic changes occurred during the 20th century in both delivery and in-stream retention due to expanding agriculture, increasing wastewater discharge, and dam construction and reservoir development. Model results indicate a rapid increase of nutrient retention in reservoirs and a concomitant reduction in the monthly variation in river discharge, with less flooding and a decrease of the retention downstream of the dam. However, the model results also suggest that there has been a world-wide increase of nutrient delivery to streams during the 20th century that is much larger than the increase in retention induced by reservoir development; the balance of these two changes has been a net increase of river transport of nutrients. Ultimately, P delivery to streams and transport to coastal seas showed to be much less than the estimates found in literature based on expert knowledge.

Over the 20th century the model results indicate an increasing anthropogenic influence and diminishing contribution of natural sources to river nutrient delivery and export to the ocean. Allochtonous organic matter input into streams is an important but uncertain nutrient source. The factors determining the allochtonous organic matter input of N and P to streams and rivers (flooded area, litterfall, and its C : N and C : P ratios) are similarly important for the simulated delivery and river export of N in 1900, 1950 and 2000. The influence of these factors on the modeled P delivery to stream and rivers is important in 1900 and decreases during the 20th century due to the increasing role of agricultural P surface runoff.

A sensitivity analysis of the modeled river retention shows that net uptake velocity and mean length ratio (ratio of mean length of nth order river divided by the mean length of $(n-1)^{th}$ order river) are important for the simulated retention and river export for both N and P. The assumed decrease of denitrification at high levels of N concentration has a significant effect on overall N retention and river export. For all years, temperature is an important factor for N and P retention and for river N export. A temperature increase leads to a lower N delivery, a higher N retention and a lower N export to the coastal zone. Higher temperatures lead to an increase of both P delivery and retention, together resulting in a small decrease of P export to the coastal ocean.

The sensitivity analysis in Chapter 5 shows that the transport of N and P are influenced by different processes. For example, the soil N budget in natural ecosystems, primarily due to biological N fixation, is an important factor but is decreasing in time due to deforestation and expansion and intensification of agricultural production. In contrast, we assumed that natural ecosystems have no external P inputs. Leaching of P is not considered in the model. Weathering occurs in both natural and agricultural landscapes and is determined by the lithology and total water flow (runoff). Finally, surface runoff is the second loss pathway for P, and depends on fertilizer and manure inputs and soil erosion with a memory due to soil residual P in fertilized areas. Total water flow (runoff) is therefore more important for delivery, retention and river export of P than of N.

Future research directions

The models presented in this thesis describe the development of global models for nutrient transport from land to sea. These models improve our understanding of the evolution during the past century of nutrients processes and interactions.

Improvements are possible in both data and model components. In discussing future research directions, the focus is on the model presented in Chapter 5, which includes all elements presented in Chapters 3 and 4. Many components and data are ignored in this discussion, including all the data stemming from the Integrated Model to Assess the Global Environment (IMAGE) on soils, lithology, land use, vegetation distribution, nutrient cycles in agriculture and natural ecosystems, climate, and the water balance model PCR-GLOBWB used in Chapter 5.

Short-term improvements which maintain the balance of the scale and detail of process descriptions of the current model include: 1) The addition of P saturation of sediments and desorption in case of decreasing river P loads. 2) The incorporation of DSi release and amorphous silicon. As rock weathering is the dominant source of DSi, this requires an approach similar to the weathering of P. 3) The improvement of the geohydrological information in order to better describe global aquifers, their thickness and their denitrification potential.

Long-term improvements center on the incorporation of a mechanistic model for describing in-stream biogeochemical processes. This allows further analysis of individual processes and their interplay (plant uptake, sedimentation, benthic processes, denitrification). This will involve a change to a temporal resolution that matches the requirements of the description of the biogeochemical processes (day, week, month). Also, such mechanistic models require a delivery model that distinguishes different nutrient forms, which is important when studying impacts such as harmful algal blooms, blue-green algae and hypoxia. Regarding spatial scale, the current $0.5°$ by $0.5°$ resolution is large enough to assume that there are no interactions between grid cells. Future models at finer resolutions need to consider the fact that transport and processes may cross boundaries of grid cells.

An interesting application of the N and P transport and biogeochemistry model would be an analysis of the C exchange between rivers and the atmosphere. Recent

studies indicate that rivers act as sources of C. A more in-depth analysis is possible now, including not only the carbon dioxide release by fresh water but also the sources of the carbon. In addition, a coupling of the processes of C with the nutrients N, P and Si may lead to better understanding of the C fluxes to and from river basins.

Another important application is to study the impacts of increasing river export, i.e., eutrophication of coastal marine ecosystems leading to phenomena such as increased production and hypoxia. Furthermore, the changing nutrient stoichiometry in freshwater and coastal systems may lead to phenomena such as harmful algal blooms. These analyses require coupling our model to coastal biogeochemistry models.

Samenvatting

Dit proefschrift behandelt vier voorbeelden van mondiale modellen die zijn ontwikkeld als onderdeel van het Integrated Model to Assess the Global Environment (IMAGE). Het doel van deze modellen is om verschillende componenten van mondiale biogeochemische kringlopen van stikstof (N), fosfor (P) en silicium (Si) te beschrijven, met speciale aandacht voor modelgevoeligheid en -onzekerheid. Het proefschrift laat een ontwikkeling van een model zien waarin alle gegevens en processen zijn geaggregeerd op de schaal van het stroomgebied, naar een ruimtelijk bepaald stroombaan model voor het analyseren van bronnen van nutriënten en hun transport en biogeochemische processen in het land-rivier continuüm.

Hoofdstuk 2

Hoofdstuk 2 beschrijft een mondiaal model om de export van opgelost silicaat (SiO_2) (DSi) door rivieren naar de monding te berekenen. DSi is een nutriënt dat nog ontbrak in de Global Nutrient Export from WaterSheds (NEWS) familie van modellen (Seitzinger et al. 2005). Er bestaan mechanistische modellen om DSi in rivieren te beschrijven (bijv. Sferratore et al. 2005, Garnier et al. 2002, Billen and Garnier 2000), maar zulke modellen hebben gegevens nodig over processen en regulerende factoren die nog niet beschikbaar zijn voor mondiale toepassingen. Naast mechanistische modellen zijn er schattingen van DSi export door rivieren op basis van extrapolatie van data en expertkennis van een selectie van rivieren (bijv. Dürr et al. 2011, Garnier et al. 2010).

Om een betere schatting te kunnen maken van de huidige mondiale jaarlijkse export van DSi door rivieren naar de oceaan, is een multipel lineair regressiemodel op de schaal van het stroomgebied ontwikkeld. Hiertoe werden een reeks van variabelen gebruikt op de schaal van stroomgebieden met een potentiële relevantie voor verwering en transport van DSi. Regressieanalyse toonde aan dat vier variabelen de DSi vracht per oppervlakte-eenheid stroomgebied significant bepalen in de situatie vóór damconstructie, namelijk bodemdichtheid, neerslag, reliëf, en de fractie van areaal met vulkanisch gesteente binnen het stroomgebied. Het feit dat neerslag en het voorkomen van vulkanisch gesteente als belangrijke variabelen naar voren komen duidt op de rol van verwering als de uiteindelijke bron van DSi in rivieren. De bodemdichtheid is een indicator voor bodem- en ecosysteem

ontwikkeling en dit bevestigt het belang van biologische processen in de mondiale silicium kringloop. Neerslag en reliëf beïnvloeden erosie, transport en het oplossen van DSi uit minerale en biologische bestanddelen.

Kruisvalidatie laat zien dat het model robuust is met betrekking tot de geselecteerde modelvariabelen en -coëfficiënten. Multipel lineaire regressie is ook toegepast om het NEWS model voor koolstof (C), N en P partikels (Mayorga et al. 2010, Beusen et al. 2005) te ontwikkelen. Naast regressie en kruisvalidatie, is de ontwikkeling van het DSi model uitgebreid met een Box-Cox transformatie en een uitgebreide onzekerheidsanalyse.

Tijdens de ontwikkeling van het DSi model werd duidelijk dat extrapolatie kan leiden tot forse overschattingen bij een mondiale toepassing van het model. Dit probleem beperkt zich niet tot het DSi model, maar geldt waarschijnlijk ook voor andere regressiemodellen zoals de Global NEWS modellen. Behalve overschattingen ten gevolge van extrapolatie, zijn er andere schaalproblemen bij toepassing van geaggregeerde stroomgebied modellen, bijvoorbeeld bij modeltoepassing voor kleine stroomgebieden. Het DSi model is derhalve niet geschikt voor toepassing voor individuele rivieren. Regionale, continentale en mondiale toepassingen liggen meer voor de hand.

Hoofdstuk 3

Gegeven alle beperkingen van regressiemodellen met het stroomgebied als ruimtelijke schaal zoals in Hoofdstuk 1 beschreven, was de ontwikkeling van een ruimtelijk bepaald, gedistribueerd model een logische volgende stap.

De componenten aan het begin van de modelketen van het gedistribueerde model dat in latere hoofdstukken (4, 5) wordt beschreven zijn gebaseerd op bodem nutriënten budgetten. De ruimtelijk bepaalde IMAGE modellen om bodem N en P budgetten te berekenen zijn in de literatuur uitvoerig beschreven (bijv. Bouwman et al. 2009, 2013d); Hoofdstuk 3 beschrijft de onzekerheidsanalyse van één van de belangrijkste componenten van het bodem N budget, namelijk ammoniak (NH_3) vervluchtiging.

De eerste stap was het schatten van het onzekerheidsbereik van 16 model parameters op basis van expertkennis. De bijdragen van 16 model parameters aan de onzekerheid van de modeluitvoer (NH_3 emissie) zijn berekend met Latin Hypercube Sampling in combinatie met lineaire regressie. De gestandaardiseerde regressie coëfficiënt (SRC) is gebruikt als een relatieve maat voor de gevoeligheid. Omdat de SRC onafhankelijk is van de eenheden, schaal en grootte van de parameters, kan de gevoeligheidsanalyse ook worden beschouwd als een onzekerheidsanalyse.

Op deze manier zijn vijf parameters geïdentificeerd die een belangrijk aandeel in de onzekerheid van de mondiale NH_3 emissie hebben. Vier hiervan zijn gerelateerd aan gemengde en landloze veeteeltsystemen (jaarlijkse N excretie per dier, NH_3 emissie uit stallen en mestopslagsystemen, de fractie van de tijd dat dieren op stal staan of grazen, en de fractie van de mest die niet binnen de landbouw wordt gebruikt). De vijfde parameter is de dierpopulatie. Jaarlijkse N excretie per dier

in gemengde en landloze veeteelt was steeds de dominante parameter in grote delen van de wereld. Echter, in landen waar industriële varkens- en kippenproductie en stal-gebaseerde melk en rundvlees productiesystemen dominant zijn, is de bijdrage van NH_3 emissies uit stallen en mestopslag aan de onzekerheid groter dan die van dierlijke excretie.

Op basis van deze onzekerheidsanalyse zijn de input parameters met de grootste invloed op de onzekerheid van gemodelleerde NH_3 emissies geïdentificeerd. Verbetering van emissieberekeningen en bodem nutriënten budgetten zou zich vooraleerst op deze parameters moeten richten.

Hoofdstuk 4

De bodem budget methode voor stikstof zoals besproken in Hoofdstuk 3, wordt in Hoofdstuk 4 gebruikt als input voor de volgende stap in de ontwikkeling van een gedistribueerd model voor het berekenen van de stikstofaanvoer naar beken en rivieren. Bodem N budgetten worden in een mondiaal gedistribueerd stroombaan model met een resolutie van $0.5°$ bij $0.5°$ gebruikt om denitrificatie en lachgas (N_2O) emissies uit bodems, grondwater en oeverzones te berekenen. Dit model is gebruikt om veranderingen gedurende de periode 1900 tot 2000 te simuleren, alsmede Millennium Ecosystem Assessment scenario's voor de periode 2000–2050.

In samenwerking met Peter Vitousek is het model voor biologische stikstofbinding in natuurlijke ecosystemen verbeterd. Deze nieuwe schattingen suggereren een veel kleinere mondiale input van atmosferische stikstof in natuurlijke ecosystemen, waardoor geconcludeerd mag worden dat de acceleratie van de mondiale stikstofkringloop door de mens wezenlijker is dan tot dan toe werd verondersteld.

Ondanks de grote onzekerheid in ons model, is de conclusie van Hoofdstuk 4 dat denitrificatie als fractie van de N inputs in het continuüm van bodem-grondwater-oeverzone niet is veranderd gedurende de 20^e eeuw, en dat de verwijdering van stikstof uit het systeem door denitrificatie niet in dezelfde mate is toegenomen als het kunstmest N gebruik in de landbouw. Dit heeft tot gevolg dat de toevoer van stikstof van het land naar oppervlaktewater in ongeveer dezelfde mate is toegenomen als het N surplus. In terrestrische ecosystemen is bodemdenitrificatie het belangrijkste N verwijderingsproces, gevolgd door denitrificatie in grondwater en vervolgens denitrificatie in oeverzones.

Onze methode voor het ruimtelijk expliciet simuleren van denitrificatie en N_2O emissies in oeverzones op mondiale schaal is de eerste die is gepubliceerd. De resultaten laten zien dat oeverzones belangrijke landschapselementen zijn voor N verwijdering op mondiale schaal. Door de omstandigheden in oeverzones die gunstig zijn voor incomplete denitrificatie en daardoor verantwoordelijk voor een grotere fractie N_2O in de totale denitrificatieproductie, is het mogelijk dat N_2O emissie door oeverzones belangrijker is op mondiale schaal dan N_2O emissies uit grondwater. Echter, bodemdenitrificatie is veel belangrijker voor het bepalen van de N stroom van land naar beken en rivieren en uiteindelijk naar de oceaan dan denitrificatie in oeverzones en grondwater.

De scenarioanalyse toont dat de geleidelijke toename van het transport van N naar oppervlaktewater en emissies naar de atmosfeer in de komende tientallen jaren zich zal voortzetten, tenzij drastische verbeteringen in landbouwmanagementsystemen worden doorgevoerd. Dit heeft mogelijk belangrijke gevolgen voor de biogeochemie in rivieren en kustzeeën, zoals stimulering van plantengroei, schadelijke algenbloei, decompositie, bezinken van organisch materiaal, en zuurstofloosheid.

De gevoeligheid van het model is onderzocht voor de situatie in het jaar 2000. In tegenstelling tot Hoofdstukken 2 en 3, waar de gevoeligheid was onderzocht binnen een onzekerheidsbereik, kon hier alleen de modelgevoeligheid worden onderzocht, omdat het onzekerheidsbereik van een groot aantal modelparameters niet kon worden vastgesteld. De belangrijkste parameters voor bijna alle modelvariabelen (waaronder de N aanvoer naar beken en rivieren) zijn temperatuur, netto neerslag en het bodem N budget in natuurlijke ecosystemen. De richting van het effect is verschillend. Bijvoorbeeld, meer neerslag leidt tot een afname van denitrificatie en toename van N uitspoeling uit bodems, terwijl een hogere temperatuur leidt tot meer denitrificatie en minder uitspoeling. De belangrijkste factor voor N verlies via oppervlakkige afstroming is landgebruik, dat belangrijk is voor zowel runoff en bodem N budget. De mondiale bodemdenitrificatie en N uitspoeling uit de bodem zijn het meest gevoelig voor veranderingen in het bodem N budget in akkerland en in natuurlijke ecosystemen. Een hogere temperatuur leidt tot meer denitrificatie, en minder uitspoeling en vervolgens minder grondwatertransport naar beken en rivieren.

De N die via ondiep grondwater uitstroomt naar oeverzones of direct naar oppervlaktewater, is het meest gevoelig voor de dikte van de ondiepe grondwaterlaag, het bodem N budget in natuurlijke ecosystemen, netto neerslag, en het bodem N budget in akkerland. De N uitstroom uit diep grondwater is gevoelig voor de halfwaarde tijd van nitraat, de dikte van de diepe grondwaterlaag en de partitionering van water van de ondiepe naar de diepe grondwaterlaag.

Twee belangrijke kanttekeningen zijn hier op zijn plaats. Ten eerste is de modelgevoeligheid voor de dikte van de ondiepe en diepe grondwaterlaag een logisch gevolg van modelformulering. Het huidige model definieert ondiep grondwater als een laag van 5 meter dik, en waar diep grondwater voorkomt, is deze 50 meter dik. Een belangrijke verbetering kan worden bereikt door het gebruiken van ruimtelijk bepaalde geohydrologische informatie over de fysische en omgevingsfactoren in aquifers. Ten tweede is de gemodelleerde stroom van nitraat uit diep grondwater naar oppervlaktewater een maximum schatting, omdat aangenomen is dat denitrificatie niet optreedt in diep grondwater. Deze veronderstelling is niet juist op plaatsen waar nitraat stroomt naar diep grondwater in sedimentaire afzettingen met afbreekbaar organisch materiaal en pyriet. De N stroom via diep grondwater naar oppervlaktewater is echter veel minder belangrijk dan die via ondiep grondwater, en de gevoeligheid van de gemodelleerde N toevoer naar beken en rivieren voor veranderingen in de halfwaardetijd van nitraat in diep grondwater is daardoor betrekkelijk klein.

Hoofdstuk 5

Hoofdstuk 5 behandelt een mondiaal, ruimtelijk bepaald model van N en P transport naar oppervlaktewater en retentie van N en P in de waterkolom. Dit model gebruikt een koppeling van modellen voor de hydrologie, ruimtelijk bepaalde nutriënten toevoer processen en retentie van nutriënten in het water. De parametrisatie van ieder van deze onderdelen is onafhankelijk.

Het model in Hoofdstuk 5 is gebaseerd op de N transportroutes in het model van Hoofdstuk 4, en is uitgebreid met verwering als bron van P, de aanvoer van N en P in allochtoon organisch materiaal in uiterwaarden van beken en rivieren, directe atmosferische N depositie in oppervlaktewater, N en P emissies door visproductie in aquacultuur systemen, en N en P aanvoer via afvalwater in stedelijk gebied. Het model houdt rekening met de P accumulatie of verlies in bodems door P overschotten of tekorten in de landbouw gedurende de 20^e eeuw, transport van aldus verrijkt of verarmd bodemmateriaal door erosie naar het oppervlaktewater, samen met de N in bodemmateriaal. Aparte, niet-gekoppelde modellen worden gebruikt voor biogeochemische processen voor N en P in het watersysteem, omdat verschillende processen verantwoordelijk zijn voor N en P retentie, namelijk denitrificatie voor N en chemische sorptie door sediment voor P. Alleen in geval van plantopname, afbraak van organisch materiaal en mineralisatie is er sprake van gekoppelde processen van N en P (en koolstof en Si).

Vooral kleine beken spelen een belangrijke rol in retentie van nutriënten. Omdat rivieren van eerste tot vijfde orde niet kunnen worden onderscheiden door het hydrologische model, wordt gebruik gemaakt van een simpele parametrisatie van retentieprocessen binnen iedere gridcel.

Het model is bewust niet gekalibreerd, omdat kalibratie niet leidt tot een beter begrip van het modelgedrag en ook niet tot het identificeren van lacunes in de gebruikte data. De resultaten van het ongekalibreerde model komen redelijk goed overeen met tijdseries van concentratiemetingen in een aantal geselecteerde rivieren. Terwijl statistische modellen met de ruimtelijke schaal van het stroomgebied slechts de export naar de oceaan schatten, kan dit ruimtelijk bepaalde en gedistribueerde model ook worden gebruikt om veranderingen in verschillende processen en de interacties tussen processen te bestuderen.

De veranderingen in zowel de aanvoer van nutriënten als de retentie in het watersysteem gedurende de 20^e eeuw zijn groot geweest, met als voornaamste oorzaken uitbreiding en intensivering van de landbouw, toenemende N en P aanvoer via afvalwater, en de bouw van dammen en reservoirs. Het model beschrijft een snelle toename van N en P retentie in reservoirs. Dammen zorgen tevens voor afname van de maandelijkse en seizoenschommeling van de waterafvoer in de rivier stroomafwaarts, waardoor uiterwaarden van rivieren minder vaak onder water staan en waardoor de retentie in deze gebieden afneemt. Echter, het model geeft daarnaast aan dat de wereldwijde aanvoer van nutriënten naar het oppervlaktewater veel meer is toegenomen dan de retentie in het watersysteem als gevolg van toename van de mondiale reservoirinhoud. Deze twee gelijktijdige veranderingen resulteren in een netto toename van het mondiale riviertransport van nutriënten

naar de oceaan. Op basis van dit model blijkt dat de P aanvoer naar rivieren en P transport door rivieren naar de oceaan veel kleiner is dan vaak in de literatuur wordt gemeld op basis van expertkennis.

De modelresultaten voor de 20^e eeuw tonen dat de menselijk invloed steeds meer toeneemt, terwijl de absolute en relatieve bijdrage van natuurlijke ecosystemen aan de nutriënten aanvoer in rivieren langzaam aan het afnemen is. De aanvoer van allochtoon organisch materiaal in beken en rivieren is een belangrijke maar onzekere bron van nutriënten. Het belang van de factoren die bepalen hoeveel N en P met allochtoon organisch materiaal in het water terecht komt (oppervlakte van overstroomde gebied, de hoeveelheid organisch materiaal en de $C:N$ en $C:P$ verhoudingen) voor de berekende N aanvoer naar de rivier en transport naar de oceaan is gelijk voor de jaren 1900, 1950 en 2000; echter, de invloed van deze factoren op de gesimuleerde P aanvoer is groot in het jaar 1900, en neemt langzaam af gedurende de 20^e eeuw door de steeds belangrijkere rol van aanvoer van P via erosie in landbouwgebieden.

Analyse van de gevoeligheid van de gesimuleerde retentie in het watersysteem toont aan dat de netto opnamesnelheid en de gemiddelde lengte verhouding (verhouding tussen de gemiddelde lengte van een riviersegment van orde n tot dat van orde $n - 1$) belangrijk zijn voor de berekende retentie en riviertransport naar de oceaan voor zowel N als P. De veronderstelling dat denitrificatie in relatieve zin afneemt bij hoge N concentraties in het water, heeft een significant effect op de N retentie in de rivier als geheel en op het N transport naar de oceaan. Temperatuur is een belangrijke factor voor de gevoeligheid van N en P retentie en transport naar de oceaan voor alle jaren. Een hogere temperatuur leidt tot minder N aanvoer (door meer denitrificatie), en meer retentie in de rivier en minder transport naar de oceaan. Voor P ligt dit anders. Een hogere temperatuur leidt tot een toename van P aanvoer naar oppervlaktewater en retentie in het watersysteem, en samen geeft dit een kleine afname van P transport naar de oceaan.

De gevoeligheidsanalyse in Hoofdstuk 5 laat zien dat N en P transport in rivieren wordt beïnvloed door verschillende processen. Bijvoorbeeld, het bodem N budget in natuurlijke ecosystemen, hoofdzakelijk bepaald door biologische N fixatie, is een belangrijke factor, die echter tijdens de 20^e eeuw in belang is afgenomen door ontbossing en uitbreiding en intensivering van landbouw. Voor natuurlijke ecosystemen is verondersteld dat er geen aanvoer van P is van buiten het systeem, terwijl het proces van uitspoeling van P wordt verwaarloosd. Verwering van gesteente vindt plaats in natuurlijke en gecultiveerde landschappen, en wordt bepaald door de lithologie en de totale waterstroom (runoff). Tenslotte is de oppervlakkige afstroming van water het tweede transportmedium voor P en dit hangt in landbouwgebieden af van P in kunstmest en dierlijke mest, erosiegevoeligheid met een geheugeneffect door langjarige verandering van de bodem P voorraad (accumulatie in surplus gebieden, en afname in gebieden met een netto afname van bodem P). Als gevolg van al deze verschillen tussen N en P processen, is de totale waterstroom (runoff) belangrijker voor de aanvoer, retentie en transport naar de oceaan van P dan van N.

Toekomstige onderzoeksrichtingen

Dit proefschrift beschrijft de ontwikkeling van mondiale modellen voor het simuleren van nutriëntentransport van land naar zee. Deze modellen dragen bij tot het vergroten van ons begrip van de veranderingen die in de afgelopen eeuw zijn opgetreden in nutriëntenprocessen en hun interacties.

Zowel de gegevens als de verschillende modelcomponenten kunnen worden verbeterd. Hier beperk ik mij tot het model dat in Hoofdstuk 5 is beschreven, dat alle elementen heeft van Hoofdstukken 3 en 4. Een aantal modelonderdelen wordt niet besproken, waaronder alle data afkomstig van het Integrated Model to Assess the Global Environment (IMAGE) over bodems, lithologie, landgebruik, vegetatie, nutriëntenkringlopen in landbouwsystemen en natuurlijke ecosystemen, klimaat, en het waterbalansmodel PCR-GLOBWB dat in Hoofdstuk 5 is gebruikt.

Er is een aantal verbeteringen die op korte termijn kan worden aangebracht, waarbij de schaal en detail van procesbeschrijvingen wordt gehandhaafd, zoals: 1) Het beschrijven van P accumulatie in sedimenten in rivieren, meren en reservoirs, en desorptie bij lage P concentraties. 2) Het modelleren van DSi aanvoer en amorf silicium in rivieren. Verwering van gesteenten is de dominante bron van DSi, en dit kan worden beschreven met een methode analoog aan die van P verwering. 3). Het gebruik van geohydrologische data om mondiale aquifers beter te beschrijven, zoals dikte en denitrificatievermogen.

Een aantal verbeteringen dat op langere termijn aan bod komt is gerelateerd aan het inbouwen van een mechanistisch model om de biogeochemische processen in het watersysteem te beschrijven. Zo'n procesmodel zal ons in staat stellen om individuele processen en hun interacties te bestuderen, zoals plantopname, sedimentatie, benthale processen, denitrificatie. Hiertoe is een tijdschaal van het model nodig die past bij de beschrijving van de biogeochemische processen (dag, week, maand). Daarnaast zullen de verschillende nutriëntenvormen moeten worden onderscheiden in de nutriëntenaanvoer, en dit vergroot de mogelijkheden om effecten van nutriënten op het voorkomen van algenbloei, blauwgroene algen en zuurstofloosheid te analyseren. Bij de huidige ruimtelijke modelschaal van $0.5°$ bij $0.5°$ kan worden aangenomen dat er geen interacties optreden tussen gridcellen. Bij grotere resoluties moet rekening worden gehouden met het feit dat grondwater transport plaatsvindt tussen gridcellen.

Naast modelverbetering zijn er interessante toepassingen van het N en P transport en biogeochemisch model denkbaar, waaronder een mondiale analyse van de koolstofuitwisseling tussen rivieren en de atmosfeer. Recente studies tonen aan dat rivieren een bron zijn van C. Het model beschreven in Hoofdstuk 5 maakt het mogelijk om de veranderingen in de aanvoer van organisch materiaal en de emissie van CO_2 te analyseren. Tevens kan het koppelen van de processen van C omzettingen en uitwisseling met de nutriënten N, P en Si meer inzicht geven in de C kringloop in rivieren.

Een tweede toepassing betreft de invloed van toenemend nutriëntentransport naar de oceaan, zoals eutrofiëring van kustwateren, toenemende biologische productie en zuurstofloosheid. Veranderingen in de stoichiometrie (verhoudingen tus-

sen nutriënten) in zoetwater en kustwateren kunnen leiden tot symptomen als schadelijke algenbloei. Om zulke processen te analyseren, is het nodig om ons model voor rivieren te koppelen met een biogeochemisch model voor mariene kust-ecosystemen.

Dankwoord

Een proefschrift schrijf je wel en niet alleen – vele uren werk zitten er in, naast het gewone werk en dit was nooit mogelijk geweest zonder steun van iedereen om me heen. Daarom dit dankwoord.

Laat ik beginnen bij het instituut waar ik werkzaam ben: zonder deze werkkring en alle kansen om me daar te ontwikkelen als onderzoeker en beleidsondersteuner, had dit werk er nooit gelegen. In 1991 begon ik als net afgestudeerd wiskundige te werken bij het RIVM (Rijksinstituut voor Volksgezondheid en Milieu). Uit één sector van het RIVM werd het MNP (Milieu en Natuur Planbureau) opgericht en op papier verhuisde ik naar het MNP. Een aantal jaren geleden fuseerde MNP met het RPB (Ruimtelijk Planbureau) en verhuisde ik wederom op papier naar het PBL (Planbureau voor de Leefomgeving). In de tussenliggende jaren heb ik vele verschillende projecten mogen uitvoeren, in diverse rollen en met heel gevarieerde werkzaamheden. Met talloze collegae heb ik samengewerkt aan projecten, met verschillende middelen en methoden. Dankzij jullie allemaal sta ik nu hier, ligt dit boekje nu hier. Samen deden we spannende, interessante, boeiende dingen, ontdekten en schreven daarover notities en artikelen. Ik zou graag iedereen bij naam noemen, maar ben ook benauwd dat ik iemand vergeet ... vandaar een algemeen bedankje voor alle RIVM/MNP/PBL collegae: DANK JULLIE WEL voor inspiratie, kameraadschap en samenwerking.

Een paar namen wil ik toch noemen: allereerst dank aan Anton van der Giessen. Anton, jij bent al bijna mijn gehele loopbaan mijn direct leidinggevende. Een betere kan ik me niet wensen. Dank dat je mij altijd het vertrouwen en ruimte gegeven hebt om mijn werkzaamheden uit te voeren. Daarmee gaf jij mij een kans en groeimogelijkheden, waarvoor ik je echt heel erg dankbaar ben. Daarnaast past een woord van dank aan directe en oud-collegae. Ferd Sauter, mijn mentor, die mij (mede) heeft aangenomen en de basisbeginselen van modelleren heeft bijgebracht: dankjewel Ferd. Samen werkten we binnen CWM als wiskundigen aan modellen en modelmatige aanpak van milieuproblemen – daarbij gaat mijn dank ook uit naar Jan van Eijkeren, Ed Veling, Arnold Dekkers, Peter Heuberger en Peter Janssen. De laatste is nog steeds een directe collega en een onmisbare kan ik wel stellen: Peter, jij bent een wandelend lexicon. Daar kan wikipedia of welke zoekmachine dan ook niet tegenop. Daarnaast is geen enkel wiskundig vraagstuk jou te moeilijk. Het is geweldig om altijd bij jou te rade te kunnen gaan en altijd met een antwoord weer te mogen vertrekken. Dank voor het zo open en grootmoedig delen van je

kennis en inzichten!

Chronologisch gezien kom ik na alle collega's van het eerste uur ook bij de collega's van latere tijden: TARGETS werden gezet ten tijde van de GLOBO's onder leiding van Jan Rotmans. Hard werken maar we hadden ook veel plezier! De meesten vlogen uit en doen in andere wetenschappelijke gremia hun werk. Ik denk met veel plezier terug aan deze tijd.

In het PBL werd het anders, de organisatie wijzigde, de banden met Den Haag werden en worden aangehaald. Een verhuizing gaat er komen. Mijn eerste fysieke verhuizing binnen deze werkkring. Ook met de PBL collega's is het prima toeven: en ik wil jullie allemaal, stuk voor stuk bedanken voor alle steun die ik heb gekregen. Het is fantastisch om met jullie te werken. Het wetenschappelijk klimaat in het PBL is grotendeels te danken aan de Chief Scientist, Arthur Petersen, die ik leerde kennen als kamergenoot en altijd een luisterend oor had. Arthur heeft mij uitgedaagd om wetenschappelijk te groeien en gezorgd dat de ruimte voor onderzoek geborgd werd. Dank!

Het IMAGE team heeft voor mij een bijzonder plekje omdat het model een goed bruikbare consistente set resultaten produceert die goed te gebruiken is bij de ontwikkeling van andere modellen. Daarnaast is het internationale karakter van het model een leuke bijkomstigheid. In het bijzonder dank ik Kees Klein Goldewijk voor de vele figuren in onze publicaties en de leuke 'historische' samenwerking: dankjewel Kees. Daarnaast heb ik ook erg genoten van de participatie in internationale werkgroepen zoals GlobalNews (workgroup of UNESCO's Intergovernmental Oceanographic Commission (IOC)) and the SCOR/LOICZ WG 132 (Land-based Nutrient Pollution and the Relationship to Harmful Algal Blooms in Coastal Marine Systems). I learned a lot from all members of these working groups. I owe you all a lot for companionship and inspiration and look forward to continue the collaborative work!

Last but not least: zonder jou Lex, had dit er niet gelegen. Jij bent een fantastische collega en ik vind het geweldig om met jou samen te werken. Zonder jou had ik hier nu niet gestaan en was deze promotie nooit van de grond gekomen. Dankzij jou werd ik gedetacheerd op de Universiteit Utrecht en kon ik nog dieper de materie in gaan. Ik ben blij jouw promovendus te zijn! Ik hoop dat wij nog lang mogen samenwerken. Dan komen er vast nog meer mooie dingen uit onze handen. Lex bedankt! Natuurlijk wil ik ook mijn tweede promotor Jack Middelburg bedanken: Jack, wij kennen elkaar nog niet zo lang maar ik heb veel van je geleerd en wil je bedanken voor al jouw input en alles dat ik in die korte tijd van je heb mogen leren. Dankjewel Jack.

Paranimf word je niet zomaar: Sido Mylius, collega, vriend EN nu mijn paranimf – je bent mijn technisch maatje en sparring partner – het is een genot met jou samen te mogen werken. Dit boek ziet er vooral door jou zo mooi uit: dankjewel. Bram, onze oudste zoon en ook paranimf, van jou geen inhoudelijke bijdrage maar jouw studiekeuze ligt vooralsnog in de lijn van dit werk. Wie weet komt er ooit nog een moment dat we echt de degens inhoudelijk kruisen. Dat zou ik erg leuk vinden!

Sara en Simon, middelste en jongste van onze kinderen – er zijn maar twee

paranimfen mogelijk en jullie zijn nog te jong, dus geen rol tijdens de promotie voor jullie. Wel voor jullie een apart woord van dank: dat jullie me met rust lieten als ik weer 'even' in de computer verzonken was of geen tijd had. Ik zal proberen in de toekomst mijn leven te beteren en meer tijd vrij te maken!

Anneke, ik heb in de vorige eeuw verzucht dat onze relatie geen tweede promotie zou verdragen, maar gelukkig is er voortschrijdend inzicht en zijn er nieuwe tijden: ook dit kunnen we samen! Of onze kinderen twee gepromoveerde ouders verdragen is een ander verhaal. De tijd zal dat leren. Anneke, we studeerden beiden tegelijk af in Nijmegen in 1991, we promoveren allebei in Utrecht – met een tussenpoos van 15 jaar. Dat we nog lang samen mogen blijven – met twee promoties op zak gaan we een nieuw evenwicht vinden. Daarbij prijs ik me gelukkig dat we allebei een eigen vak hebben waar we van houden en dat ook dagelijks uit mogen oefenen. Ik hoop dat we dat nog lang kunnen doen.

Mam, dank voor wie je bent en voor alle ruimte die jij geeft en hulp die je biedt in drukke tijden! Dankjewel!! Twee mensen had ik heel graag hier bij aanwezig gezien: mijn vader, die tijdens mijn wiskunde studie overleed en mijn studievriend Edwin, collega wiskundige. Ik had dit resultaat van vele jaren werken heel erg graag ook met jullie gedeeld!

Om ons heen staan verder nog vele vrienden, familie en kennissen. Iedereen heeft op zijn of haar eigen wijze bijgedragen aan de ruimte die ik gevoeld heb en gekregen heb om dit werk te doen en te publiceren. Dank!

Dank dus aan alles en iedereen – fijn om zo rijk te zijn met allemaal betrokken collegae, gezin, vrienden en familie om me heen. Dank jullie wel.

Arthur

Curriculum Vitae

Arthur H.W. Beusen holds a degree in applied and numerical mathematics. Born on September 30th 1965 in Heerlen, he went to secondary school in Schimmert and Meerssen, where he obtained his VWO diploma in 1985. That year, he left Limburg to take his first steps on the academic road by studying mathematics (minor and major) and computerscience (minor) in Nijmegen. After his graduation in 1991 Arthur started to work in the field of environmental studies as a mathematical hydrologist at the RIVM (Public Health and Environmental Protection Agency) in Bilthoven.

Initially his focus was on development of local and national models, but over the years the focus broadened to European and worldwide models concerning environmental issues in relation to population, energy, land use, water and nutrient cycles. Gradually he became an expert in designing, integrating, calibrating and evaluating complex environmental models, both on a national, European and global scale, which is shown in an extensive publication list in peer reviewed journals.

He is currently working as senior advisor modeling for the PBL (Department of Information, Data and Methodology). Next to this work he is employed for one day a week at the Utrecht University, Department of Earth Sciences - Geochemistry for a period of three years. There he works for the Global Environment Facility (GEF) project on Global Foundations for reducing nutrient enrichment and oxygen depletion from land based pollution in support of global nutrient cycle.

Published articles

Beusen, A., De Vink, P., and Petersen, A. (2011). The dynamic simulation and visualization software MyM. *Environmental Modelling and Software*, 26(2): 238–240.

Beusen, A., Dekkers, A., Bouwman, A., Ludwig, W., and Harrison, J. (2005). Estimation of global river transport of sediments and associated particulate C, N, and P. *Global Biogeochemical Cycles*, 19(4), doi: 10.1029/2005GB002453.

Beusen, A., Klepper, O., and Meinardi, C. (1995). Modelling the flow of nitrogen and phosphorus in Europe: from loads to coastal seas. *Water Science and Technology*, 31(8): 141–145.

Beusen, A. H. W., Bouwman, A. F., Dürr, H. H., Dekkers, A. L. M., and Hartmann, J. (2009). Global patterns of dissolved silica export to the coastal zone: results from a spatially explicit global model. *Global Biogeochemical Cycles*, 23, doi: 10.1029/2008GB003281.

Beusen, A. H. W., Bouwman, A. F., Heuberger, P. S. C., Van Drecht, G., and Van Der Hoek, K. W. (2008). Bottom-up uncertainty estimates of global ammonia emissions from global agricultural production systems. *Atmospheric Environment*, 42(24): 6067–6077.

Beusen, A. H. W., Slomp, C. P., and Bouwman, A. F. (2013). Global land-ocean linkage: direct inputs of nitrogen to coastal waters via submarine groundwater discharge. *Environmental Research Letters*, 8(3): 034035, doi: 10.1088/1748-9326/8/3/034035.

Billen, G., Beusen, A. H. W., Bouwman, A. F., and Garnier, J. (2010). Anthropogenic nitrogen autotrophy and heterotrophy of the world's watersheds: past, present, and future trends. *Global Biogeochemical Cycles*, 23, doi: 10.1029/2009GB003702.

Bouwman, A. F., Beusen, A. H. W., and Billen, G. (2009). Human alteration of the global nitrogen and phosphorus soil balances for the period 1970–2050. *Global Biogeochemical Cycles*, 23, doi: 10.1029/2009GB003576.

Bouwman, A. F., Beusen, A. H. W., Griffioen, J., Groenigen, J. W. V., Hefting, M. M., Oenema, O., Van Puijenbroek, P. J. T. M., Seitzinger, S., Slomp, C. P., and Stehfest, E. (2013a). Global trends and uncertainties in terrestrial denitrification and N_2O emissions. *Philosophical Transactions of the Royal Society B: Biological Sciences*, 368(1621), doi: 10.1098/rstb.2013.0112.

Bouwman, A. F., Beusen, A. H. W., Overbeek, C. C., Bureau, D. P., Pawlowski, M., and Glibert, P. M. (2013b). Hindcasts and future projections of global inland and coastal nitrogen and phosphorus loads due to finfish aquaculture. *Reviews in Fisheries Science*, 21(2): 112–156.

Bouwman, A. F., Klein Goldewijk, K., Van Der Hoek, K. W., Beusen, A. H. W., Van Vuuren, D. P., Willems, W. J., Rufino, M. C., and Stehfest, E. (2013c). Exploring global changes in nitrogen and phosphorus cycles in agriculture induced by livestock production over the 1900–2050 period. *Proceedings of the National Academy of Sciences of the United States of America*, 110(52): 20882–20887, doi: 10.1073/pnas.1012878108.

Bouwman, A. F., Pawlowski, M., Liu, C., Beusen, A. H. W., Shumway, S. E., Glibert, P. M., and Overbeek, C. C. (2011). Global hindcasts and future projections of coastal nitrogen and phosphorus loads due to shellfish and seaweed aquaculture. *Reviews in Fisheries Science*, 19(4): 331–357, doi: 10.1080/10641262.2011.603849.

Bouwman, A. F., Van Drecht, G., Knoop, J. M., Beusen, A. H. W., and Meinardi, C. R. (2005). Exploring changes in river nitrogen export the the world's oceans. *Global Biogeochemical Cycles*, 19: GB1002, doi: 10.1029/2004GB002314.

Bouwman, L., Beusen, A., Glibert, P., Overbeek, C., Pawlowski, M., Herrera, J., Mulsow, S., Yu, R., and Zhou, M. (2013d). Mariculture: significant and expanding cause of coastal nutrient enrichment. *Environmental Research Letters*, 8(4): 044026, doi: 10.1088/1748-9326/8/4/044026.

De Vries, B., Janssen, M., and Beusen, A. (1999). Perspectives on global energy futures: Simulations with the TIME model. *Energy Policy*, 27(8): 477–494.

Den Elzen, M. G. J., Beusen, A. H. W., and Rotmans, J. (1997). An integrated modeling approach to global carbon and nitrogen cycles: balancing their budgets. *Global Biogeochemical Cycles*, 11: 191–215.

Garnier, J., Beusen, A. H. W., Thieu, V., Billen, G., and Bouwman, A. F. (2010). N:P:Si nutrient export ratios and ecological consequences in coastal seas evaluated by the ICEP approach. *Global Biogeochemical Cycles*, 24, doi: 10.1029/2009GB003583.

Harrison, J., Frings, P., Beusen, A., Conley, D., and McCrackin, M. (2012). Global importance, patterns, and controls of dissolved silica retention in lakes and reservoirs. *Global Biogeochemical Cycles*, 26(2), doi: 10.1029/2011GB004228.

Harrison, J. A., Seitzinger, S. P., Bouwman, A. F., Caraco, N. F., Beusen, A. H. W., and Vörösmarty, C. J. (2005). Dissolved inorganic phosphorus export to the coastal zone: results from a spatially explicit, global model. *Global Biogeochemical Cycles*, 19, GB4S03, doi: 10.1029/2004GB002357.

Hofstra, N., Bouwman, A. F., Beusen, A. H. W., and Medema, G. J. (2013). Exploring global Cryptosporidium emissions to surface water. *Science of the Total Environment*, 442(0): 10–19, doi: http://dx.doi.org/10.1016/j.scitotenv.2012.10.013.

Klein Goldewijk, K., Beusen, A., and Janssen, P. (2010). Long-term dynamic modeling of global population and built-up area in a spatially explicit way: HYDE 3.1. *Holocene*, 20(4): 565–573.

Klein Goldewijk, K., Beusen, A., Van Drecht, G., and De Vos, M. (2011). The HYDE 3.1 spatially explicit database of human-induced global land-use change over the past 12,000 years. *Global Ecology and Biogeography*, 20(1): 73–86.

Mayorga, E., Seitzinger, S. P., Harrison, J. A., Dumont, E., Beusen, A. H. W., Bouwman, A. F., Fekete, B. M., Kroeze, C., and Van Drecht, G. (2010). Global Nutrient Export from WaterSheds 2 (NEWS 2): model development and implementation. *Environmental Modelling and Software*, 25(7): 837–853.

Meinardi, C. R., Beusen, A. H. W., Bollen, M. J. S., Klepper, O., and Willems, W. J. (1995). Vulnerability to diffuse pollution and average nitrate contamination of European soils and groundwater. *Water Science and Technology*, 31: 159–165.

Morée, A., Beusen, A., Bouwman, A., and Willems, W. (2013). Exploring global nitrogen and phosphorus flows in urban wastes during the twentieth century. *Global Biogeochemical Cycles*, 27, doi: 10.1002/gbc.20072.

Overbeek, G., Tiktak, A., Beusen, A., and Van Puijenbroek, P. (2001). Partial validation of the Dutch model for emission and transport of nutrients (STONE). *TheScientificWorldJournal [electronic resource]*, 1 Suppl 2: 194–199.

Sauter, F. and Beusen, A. (1994). Streamline calculations using continuous and discontinuous velocity fields and several time integration methods. *Groundwater Quality Management (Proceedings of the GQM 1993, Conference held at Tallinn, September 1993*, IAHS publ. 220: 347–355.

Seitzinger, S. P., Harrison, J. A., Dumont, E., Beusen, A. H. W., and Bouwman, A. F. (2005). Sources and delivery of carbon, nitrogen, and phosphorus to the coastal zone: an overview of global NEWS models and their application. *Global Biogeochemical Cycles*, 19, GB4S01, doi: 10.1029/2004GB002606.

Seitzinger, S. P., Mayorga, E., Bouwman, A. F., Kroeze, C., Beusen, A. H. W., Billen, G., Van Drecht, G., Dumont, E., Fekete, B. M., Garnier, J., Harrison, J., Wisser, D., and Wollheim, W. M. (2010). Global river nutrient export: a scenario analysis of past and future trends. *Global Biogeochemical Cycles*, 24, GB0A08, doi: 10.1029/2009GB003587.

Struijs, J., Beusen, A., De Zwart, D., and Huijbregts, M. (2011). Characterization factors for inland water eutrophication at the damage level in life cycle impact assessment. *International Journal of Life Cycle Assessment*, 16(1): 59–64.

Van Asselt, M., Beusen, A., and Hilderink, H. (1996). Uncertainty in integrated assessment, a social scientific perspective. *Environmental Modeling and Assessment*, 1: 71–90.

Van Der Sluijs, J. P., Potting, J., Risbey, J., Van Vuuren, D., De Vries, B., Beusen, A., Heuberger, P., Quintana, S. C., Funtowicz, S., Kloprogge, P., Nuijten, D., Petersen, A., and Ravetz, J. (2002). Uncertainty assessment of the IMAGE/TIMER B1 CO_2 emissions scenario, using the NUSAP method. Technical report, Dutch National Research Program on Climate Change, Bilthoven, The Netherlands.

Van Drecht, G., Bouwman, A., Knoop, J., Meinardi, C., and Beusen, A. (2001). Global pollution of surface waters from point and nonpoint sources of nitrogen. *TheScientificWorldJournal [electronic resource]*, 1 Suppl 2: 632–641, doi: 10.1100/tsw.2001.326.

Van Drecht, G., Bouwman, A. F., Knoop, J. M., Beusen, A. H. W., and Meinardi, C. R. (2003). Global modeling of the fate of nitrogen from point and nonpoint sources in soils, groundwater and surface water. *Global Biogeochemical Cycles*, 17(4), doi: 10.129/2003GB002060.

Van Vuuren, D., De Vries, B., Beusen, A., and Heuberger, P. (2008). Conditional probabilistic estimates of 21st century greenhouse gas emissions based on the storylines of the IPCC-SRES scenarios. *Global Environmental Change*, 18(4): 635–654.

Van Vuuren, D. P., Bouwman, A. F., and Beusen, A. H. W. (2010). Phosphorus demand for the 1970–2100 period: a scenario analysis of resource depletion. *Global Environmental Change*, 20(3): 428–439, doi: 10.1016/j.gloenvcha.2010.04.004.

Wolf, J., Beusen, A., Groenendijk, P., Kroon, T., Rötter, R., and Van Zeijts, H. (2003). The integrated modeling system STONE for calculating nutrient emissions from agriculture in the Netherlands. *Environmental Modelling and Software*, 18(7): 597–617.

Published book chapters

Billen, G., Silvestre, M., Grizzetti, B., Leip, A., Bouraoui, F., Behrendt, H., Garnier, J., Humborg, C., Smedberg, E., Johnes, P., Kaste, O., Curtis, C., Lepisto, A., Kortelainen, P., Ganeshram, R., Beusen, A., and Voss, M. (2011). Nitrogen flows from European regional watersheds to coastal marine waters. In: Sutton, M. A., Howard, C. M., Erisman, J. W., Billen, G., Bleeker, A., Grennfelt, P., Van Grinsven, H., and Grizzetti, B. (eds.), *European Nitrogen Assessment*, pages 271–297. Cambrigde University Press, Cambridge, UK.

Bouwman, A., Beusen, A., Van Der Hoek, K., and Van Drecht, G. (2006). Modelling the fate of nutrients through the soil and hydrological sytem. In: Bouwman, A., Kram, T., and Klein Goldewijk, K. (eds.), *Integrated modelling of global environmental change. An overview of IMAGE 2.4*. RIVM, Report no. 500110002, Bilthoven, the Netherlands.

De Vries, H., Beusen, A., and Janssen, M. (1997a). Energy systems in transition. In: Rotmans, J. and De Vries, H. (eds.), *Perspectives on global change: the TARGETS approach*. Cambrigde University Press, Cambridge, UK.

De Vries, H., Hilderink, H., Den Elzen, M., Beusen, A., Hoekstra, A., Rotmans, J., and Strengers, B. (1997b). Uncertainty and risk: dystopian futures. In: Rotmans, J. and De Vries, H. (eds.), *Perspectives on global change: the TARGETS approach*. Cambrigde University Press, Cambridge, UK.

De Vries, H., Rotmans, J., Van Asselt, M., Beusen, A., Den Elzen, M., Hilderink, H., Hoekstra, A., and Strengers, B. (1997c). Towards an integrated assessment of global change. In: Rotmans, J. and De Vries, H. (eds.), *Perspectives on global change: the TARGETS approach*. Cambrigde University Press, Cambridge, UK.

De Vries, H., Rotmans, J., Van Asselt, M., Beusen, A., Hilderink, H., Den Elzen, M., Hoekstra, A., and Strengers, B. (1997d). The larger picture: utopian worlds. In: Rotmans, J. and De Vries, H. (eds.), *Perspectives on global change: the TARGETS approach*. Cambrigde University Press, Cambridge, UK.

Den Elzen, M., Beusen, A., Rotmans, J., and Köster, H. (1997a). The biogeochemical submodel: Cycles. In: Rotmans, J. and De Vries, H. (eds.), *Perspectives on global change: the TARGETS approach*. Cambrigde University Press, Cambridge, UK.

Den Elzen, M., Beusen, A., Rotmans, J., and Van Asselt, M. (1997b). Human disturbance of the global element cycles. In: Rotmans, J. and De Vries, H. (eds.), *Perspectives on global change: the TARGETS approach*. Cambrigde University Press, Cambridge, UK.

Hoekstra, A., Beusen, A., and Hilderink, H. (1997). Water in crisis? In: Rotmans, J. and De Vries, H. (eds.), *Perspectives on global change: the TARGETS approach*. Cambrigde University Press, Cambridge, UK.

Rotmans, J., Van Asselt, M., Beusen, A., Den Elzen, M., Hilderink, H., Hoekstra, A., Niessen, L., Strengers, B., and De Vries, H. (1996). The integrated assessment model for global change: TARGETS. In: Chen, R., Tuttle, D., and Linville, C. (eds.), *Integrated assessment of global change: science and policy*. Springer Verlag, Berlin.